Optical Spectroscopy of Quantum Spin Systems

Reproduced on the front cover is the first direct observation of a pair of strongly-coupled giant quantum spins, embedded in a quasi one-dimensional tulip system. This incredible snap-shot was taken by Markus Grüninger in the countryside of Leiden, The Netherlands, in March 1996.

Printed by: PrintPartners Ipskamp B.V., Enschede, The Netherlands

ISBN 90-367-1032-4

The work described in this thesis was performed at the Solid State Physics Laboratory of the University of Groningen. The project was supported by the Dutch Foundation for Fundamental Research on Matter (FOM) with financial support from the Dutch Organization for the Advancement of Pure Research (NWO).

Rijksuniversiteit Groningen

Optical Spectroscopy of Quantum Spin Systems

Proefschrift

ter verkrijging van het doctoraat in de
Wiskunde en Natuurwetenschappen
aan de Rijksuniversiteit Groningen
op gezag van de
Rector Magnificus, dr. D.F.J. Bosscher,
in het openbaar te verdedigen op
vrijdag 19 maart 1999
om 16.00 uur

door

Andrea Damascelli

geboren op 24 oktober 1967
te Milaan (Italië)

Promotor: Prof. dr. D. van der Marel

Saranno le stelle più luminose
a guidare il tuo cammino.
A te, il trovarle.

Contents

1 Introduction **3**
- 1.1 Strongly Correlated Electron Systems . . . 3
- 1.2 Optical Conductivity . . . 4
- 1.3 Scope of this Thesis . . . 5

2 Optical Spectroscopy of Transition-Metal Mono-Silicides **9**
- 2.1 Structural Properties of TM Mono-Silicides . . . 10
  - 2.1.1 Group Theoretical Analysis . . . 12
- 2.2 Experimental . . . 13
- 2.3 Optical Spectroscopy of TM Mono-Silicides . . . 15
  - 2.3.1 Optical Spectroscopy of FeSi . . . 15
  - 2.3.2 Optical Spectroscopy of CoSi . . . 24
  - 2.3.3 Optical Spectroscopy of MnSi . . . 26
- 2.4 The Electronic Properties of TM Mono-Silicides . . . 26
  - 2.4.1 Magnetic Properties . . . 26
  - 2.4.2 Optical Properties . . . 28
  - 2.4.3 Activation Energies . . . 30
  - 2.4.4 Transport Properties . . . 31
  - 2.4.5 Resonating Bonds Coupled to Phonons . . . 34
- 2.5 The Electronic Structure of TM Mono-Silicides . . . 35
- 2.6 Discussion . . . 38
- 2.7 Conclusions . . . 39

3 Optical Spectroscopy of $CuGeO_3$ **43**
- 3.1 Group Theoretical Analysis . . . 44
- 3.2 Experimental . . . 47
- 3.3 Pure $CuGeO_3$ . . . 48
  - 3.3.1 Phonon Spectrum and Lattice Distortion . . . 50
  - 3.3.2 Phonon Parameters and Soft-Mode Issue . . . 56
  - 3.3.3 Magnetic Excitations . . . 59
- 3.4 Doped $CuGeO_3$ . . . 61
  - 3.4.1 Far-Infrared Reflection . . . 62
  - 3.4.2 Mid-Infrared Transmission . . . 71

3.5 Discussion . . . 73
3.6 Conclusions . . . 75

4 Charged Magnon Model **79**
4.1 Single Two-Leg Ladder . . . 79
4.1.1 Model Hamiltonian . . . 79
4.1.2 Interaction Hamiltonians and Effective Charges . . . 83
4.1.3 Spectral Weights . . . 84
4.2 Conclusions . . . 88

5 Optical Spectroscopy of α'-NaV_2O_5 **91**
5.1 Room-Temperature Crystal Structure . . . 92
5.1.1 X-Ray Diffraction Analysis . . . 94
5.1.2 Group Theoretical Analysis . . . 98
5.2 Optical Spectroscopy: Experimental . . . 99
5.3 Optical Spectroscopy: Results . . . 99
5.3.1 Phonon Spectrum of the High Temperature Phase . . . 101
5.3.2 Phonon Spectrum of the Low Temperature Phase . . . 105
5.3.3 Symmetry of the Lattice Distortion . . . 108
5.3.4 Optical Conductivity . . . 111
5.4 Charged Bi-Magnons . . . 116
5.5 Discussion . . . 120
5.6 Conclusions . . . 122

Summary **125**

Samenvatting **129**

Acknowledgements **133**

List of Publications **137**

Happy End **139**

Chapter 1

Introduction

1.1 Strongly Correlated Electron Systems

One of the most challenging branches of solid state physics, from the intellectual point of view, is represented by the investigation of *strongly correlated electron systems*, i.e., compounds whose properties are dominated by strong electron-electron correlations. This is the case when the on-site electron-electron repulsion U is much larger than the energies associated with the overlap of atomic orbitals belonging to different atoms. Because these energies are characterized, in a solid, by the width W of the energy band under consideration, a large U/W ratio is expected in systems involving well-localized electrons like the $4f$ and $5f$ electrons of the rare earths and the actinides, respectively, but also the d electrons of the transition metals (TM) [1].

The importance of electron-electron correlations in influencing the basic properties of a compound can be understood considering the case of CoO which, although not discussed further on in this thesis, represents a very typical example. This oxide, if treated within the independent-electron approximation (i.e., writing the total wavefunction of the N-electron system in the form of an antisymmetrized product of single-electron wavefunctions), is expected to be metallic, with an odd number of electrons per unit cell and a partially filled d band. In reality, as a consequence of strong correlations, which are suppressing charge fluctuations and therefore the electrical conductivity, CoO is a rather good insulator at all temperatures, with an optical gap of about 6 eV [1, 2].

More in general, strong electron-electron correlations can give rise to a large variety of peculiar phenomena, the most famous being probably high-temperature superconductivity, heavy-fermion and Kondo-insulating behavior, spin-Peierls phase transition, spin-gap phenomena, and colossal magnetoresistance. For the description of these collective phenomena, and for the development of appropriate microscopic models, it is useful to investigate the elementary excitations of these materials. In fact, the excitations from the ground state to the lowest excited states reflect the interplay between quantum magnetism and low energy charge degrees of freedom, a fingerprint of strong electron-electron correlations.

1.2 Optical Conductivity

A powerful tool to study the elementary excitations of an N-particle system is optical spectroscopy. This technique consists of shining light of different frequencies onto the sample under investigation, and of observing which frequencies are absorbed by the material itself. In the course of this thesis we will present transmission and reflectivity data obtained in the frequency range extending from the far infrared to the ultra violet (i.e., from 4 meV to 4 eV). Additional information was obtained by performing the optical experiments with linearly polarized light, in order to probe the possible anisotropy of the crystals, and varying the temperature of the samples between 4 and 300 K. The optical conductivity was then obtained by Kramers-Kronig transformations [3], in the regions where only reflectivity spectra were measurable, and by direct inversion of the Fresnel equations [4], wherever both reflection and transmission data were available.

For the analysis of the conductivity spectra presented in the course of the thesis, it is useful to derive a functional expression for the optical conductivity of a system of N electrons, in the presence of an externally applied time-dependent electric field. From the fluctuation-dissipation theorem, which relates the fluctuations of a system described by a correlation function to the dissipations described by the imaginary part of a susceptibility, it follows that the dynamical conductivity is related to the equilibrium current-current correlation function $\chi(\omega)$ [5–7]:

$$\sigma(\omega) = \frac{1}{i\omega}\left[\chi(\omega) - \frac{nq_e^2}{m}\right] \ , \tag{1.1}$$

where n is the density of electrons, and q_e and m are the electronic charge and mass, respectively. The retarded correlation function $\chi(\omega)$ is defined as:

$$\chi(\omega) = \frac{i}{V}\int_0^\infty dt\, e^{i\omega t}\langle[\hat{\mathbf{j}}(t), \hat{\mathbf{j}}(0)]\rangle \ , \tag{1.2}$$

where V is the volume of the system, and $\hat{\mathbf{j}} = \partial\hat{\mathbf{P}}/\partial t = i[\hat{H}, \hat{\mathbf{P}}]$ is the current operator (being $\hat{\mathbf{P}}$ the polarization operator and $\hat{H}$ the Hamiltonian describing the system in presence of the external electric field). If we denote by $|n\rangle$ and E_n the eigenstates and eigenvalues, respectively, of the many-body Hamiltonian of the system, the current-current correlation function can be written as:

$$\chi(\omega) = \frac{1}{V}\sum_{n\neq g} |\langle n|\,\hat{\mathbf{j}}\,|g\rangle|^2 \left(\frac{1}{\omega + E_n - E_g - i\eta} - \frac{1}{\omega - E_n + E_g + i\eta}\right) \ , \tag{1.3}$$

where g refers to the ground state of the N-electron system. From eq. 1.1 and 1.3 , the real part of the optical conductivity, $\sigma_1(\omega)$, becomes:

$$\sigma_1(\omega) = \frac{\pi}{V}\sum_{n\neq g} |\langle n|\,\hat{\mathbf{j}}\,|g\rangle|^2 \ \frac{\delta(\omega - E_n + E_g)}{E_n - E_g} \ , \tag{1.4}$$

which defines the excitation spectrum of the system. It consists of a series of sharp lines (corresponding to the excitation between the ground state $|g\rangle$ and the excited states $|n\rangle$), which will merge into a continuum upon increasing the number of electrons, making $\sigma_1(\omega)$ a continuous function of frequency.

For the quantitative analysis of the conductivity spectra obtained in the experiments, we will in particular make use of the integral, with respect to the frequency, of the real part of the dynamical conductivity $\sigma_1(\omega)$, which is give by:

$$\int_0^\infty \sigma_1(\omega)d\omega = \frac{\pi q_e^2}{\hbar^2 V} \sum_{n\neq g} (E_n - E_g) \, |\langle n|\hat{\mathbf{x}}|g\rangle|^2 \ , \tag{1.5}$$

where $\hat{\mathbf{x}} = \sum_i \hat{\mathbf{x}}_i$ is the sum of the position operators of the electrons.

1.3 Scope of this Thesis

In the course of this thesis we will present optical data obtained on a number of different compounds, whose common feature is that they all belong to the class of strongly correlated electron systems. We will discuss in detail the detected lattice vibrational modes and the electronic and/or magnetic excitation spectra, in order to learn about the crystal structure of the different systems, and their electronic and magnetic properties like, e.g., ground state configuration, electron-phonon coupling, and spin-charge interplay.

In chapter 2 we will present the optical spectra of several transition-metal (TM) mono-silicides (FeSi, CoSi, and MnSi), with particular emphasis on FeSi, which shows Kondo-insulating behavior at low temperature [8]: Total compensation of the local magnetic moment on the Fe sites together with the opening of a narrow electronic gap. Based on the discussion of our infrared spectra (in particular, of the coupling between vibrational degrees of freedom and low energy electron-hole excitations [9, 10]), and of published transport data [11, 12], we will develop a qualitative model for the electronic structure of the TM mono-silicides [13]. This framework provides a basis for understanding the observed range of chemical stability of these compounds (from CrSi to NiSi), and the properties of FeSi.

In chapter 3 we will concentrate on $CuGeO_3$ which can be described as a quasi one-dimensional (1D) system due to the presence of weakly-coupled 1D CuO_2 chains, running parallel to each other. Because each Cu^{2+} ion has spin 1/2 and the exchange between these local moments is antiferromagnetic (AF), the CuO_2 chains can be regarded as 1D AF $S = 1/2$-Heisenberg-spin chains. In $CuGeO_3$, for temperatures lower than 14 K, electron-electron correlations and the low dimensionality give rise to a fascinating phenomenon, namely, the spin-Peierls (SP) phase transition [14, 15]: A lattice distortion that occurs together with the formation of a nonmagnetic ground state ($S = 0$), and the opening of a finite energy gap in the magnetic excitation spectrum. We will discuss the temperature dependent optical data for pure and doped $CuGeO_3$ and, in particular, the phonon spectra, seeking for optical vibrational modes activated by the SP phase transition [16,17]. We will show that, following the temperature dependence of these modes, we can determine the second order character of the phase transition and study the effect of doping on T_{SP}: The

substitution of Ge with Si will turn out to be three times more efficient, than the one of Cu with Mg, in reducing T_{SP}. This result will be discussed in relation to the difference, between Mg and Si doping, in affecting the magnetism of the system [18].

In chapter 4 and 5 we will devote our attention to α'-NaV_2O_5, another quasi 1D inorganic compound which, after $CuGeO_3$, has been attracting the attention of the scientific community working on low-dimensional spin systems, in general, and on the SP phenomenon, in particular. In fact, in 1996 the SP picture was proposed to explain the low temperature properties of α'-NaV_2O_5, with a transition temperature $T_{SP} = 34$ K [19]. As in the case of $CuGeO_3$, by analyzing the optically allowed phonons at various temperatures below and above the phase transition [20], we will show that, consistently with the proposed SP picture, a second-order change to a larger unit cell takes place below 34 K (chapter 5). On the other hand, on the basis of recently reported specific heat measurements in high magnetic field [21], the interpretation of the phase transition in α'-NaV_2O_5 is still controversial. We will see that an even more basic problem is the determination of crystal structure and symmetry of the electronic configuration, for α'-NaV_2O_5 in the high temperature phase. In fact, the analysis of x-ray diffraction measurements [22] and optical phonon spectra suggests that the symmetry of this compound, at room temperature, is better described by the centrosymmetric space group $Pmmn$ than by the noncentrosymmetric $P2_1mn$ proposed in the 1970's [23]. On the other hand, the intensities and polarization dependence of the electronic excitations detected in the optical spectra are not understandable in terms of the centrosymmetric space group (chapter 5). We will show that a consistent interpretation of both x-ray diffraction results and optical conductivity data requires a charge disproportionated electronic ground-state at least on a local scale, i.e., without any long range order [24]. It will than be possible to interpret the optical conductivity on the basis of the *Charged Magnon Model* developed in chapter 4, and show that the presence of only one d electron per two V ions, along with the broken symmetry of the ground-state, gives rise to a fascinating behavior of the spin flips in α'-NaV_2O_5: Spin-flip excitations carry a finite electric dipole moment, which is responsible for the detection of *charged bi-magnons* in the optical spectra, i.e., direct two-magnon optical absorption processes [20].

References

[1] For a detailed description, see C.N.R. Rao, and B. Raveau, *Transition Metal Oxides* (VCH Publishers, New York, 1995).

[2] R.J. Powell, and W.E. Spicer, Phys. Rev. B **2**, 2182 (1970).

[3] F. Wooten, *Optical Properties of Solids* (Academic Press, New York, 1972).

[4] M.V. Klein, and T.E. Furtak, *Optics* (John Wiley & Sons, New York, 1983).

[5] P.F. Maldague, Phys. Rev. B **16**, 2437 (1977).

[6] G.D. Mahan, *Many-Particle Physics* (Plenum Press, New York, 1990).

[7] P. Fulde, *Electron Correlations in Molecules and Solids* (Springer-Verlag, Berlin, 1995).

[8] Z. Schlesinger, Z. Fisk, Hai-Tao Zhang, M.B. Maple, J.F. DiTusa, and G. Aeppli, Phys. Rev. Lett. **71**, 1748 (1993).

[9] A. Damascelli, K. Schulte, D. van der Marel, and A.A. Menovsky, Phys. Rev. B **55**, R4863 (1997).

[10] A. Damascelli, K. Schulte, D. van der Marel, M. Fäth, and A.A. Menovsky, Physica B **230-232**, 787 (1997).

[11] S. Paschen, E. Felder, M.A. Chernikov, L. Degiorgi, H. Schwer, H.R. Ott, D.P. Young, J.L. Sarrao, and Z. Fisk, Phys. Rev. B **56**, 12 916 (1997).

[12] M. Fäth, J. Aarts, A.A. Menovsky, G.J. Nieuwenhuys, and J.A. Mydosh, Phys. Rev. B **58**, 15 483 (1998).

[13] D. van der Marel, A. Damascelli, K. Schulte, and A.A. Menovsky, Physica B **244**, 138 (1998).

[14] M. Hase, I. Terasaki, and K. Uchinokura, Phys. Rev. Lett. **70**, 3651 (1993).

[15] For a review, see J.P. Boucher, and L.P. Regnault, J. Phys. I **6**, 1939 (1996).

[16] A. Damascelli, D. van der Marel, F. Parmigiani, G. Dhalenne, and A. Revcolevschi, Phys. Rev. B **56**, R11 373 (1997).

[17] A. Damascelli, D. van der Marel, F. Parmigiani, G. Dhalenne, and A. Revcolevschi, Physica B **244**, 114 (1998).

[18] W. Geertsma, and D. Khomskii, Phys. Rev. B **54**, 3011 (1996).

[19] M. Isobe, and Y. Ueda, J. Phys. Soc. Jpn. **65**, 1178 (1996).

[20] A. Damascelli, D. van der Marel, M. Grüninger, C. Presura, T.T.M. Palstra, J. Jegoudez, and A. Revcolevschi, Phys. Rev. Lett. **81**, 918 (1998).

[21] W. Schnelle, Yu. Grin, and R.K. Kremer, Phys. Rev. B **59**, 73 (1999).

[22] A. Meetsma, J.L. de Boer, A. Damascelli, J. Jegoudez, A. Revcolevschi, and T.T.M. Palstra, Acta Cryst. C **54**, 1558 (1998).

[23] P.A. Carpy, and J. Galy, Acta Cryst. B **31**, 1481 (1975).

[24] A. Damascelli, D. van der Marel, J. Jegoudez, G. Dhalenne, and A. Revcolevschi, Physica B, in press (1999).

Chapter 2

Optical Spectroscopy of Transition-Metal Mono-Silicides

FeSi is a fascinating material which has been studied already many years ago for its unusual magnetic and thermal properties [1]. Nowadays, this system is object of renewed interest. In fact, during the last five years many theoretical and experimental investigations, of the magnetic and electronic properties, have been reported. At low temperature, FeSi shows an insulating behavior characterized by a nonmagnetic ground state whereas, at room temperature, it behaves as a paramagnetic 'dirty' metal.

The magnetic susceptibility exhibits a broad maximum at approximately 500 K and, for higher temperatures, decreases following a Curie-Weiss law [1]. On the other hand, upon reducing the temperature below 500 K, the susceptibility drops nearly exponentially and vanishes below 50 K, once the extrinsic paramagnetic Curie tail, due to the presence of impurities, has been subtracted from the experimental data [1]. Neutron diffraction [2], ^{29}Si nuclear magnetic resonance [3], and Mössbauer [3] studies excluded, however, the onset of an antiferromagnetic order below 500 K.

Optical reflectivity [4–6], transport [7–10], tunneling [10, 11], and photoemission [12] measurements all revealed the existence of an energy gap (with values ranging from 40 to 100 meV) in the electronic excitation spectrum, at low temperatures. In contrast with what is expected within a semiconductor-like picture, the gap disappears at a temperature which is about 1/4 of its size. Moreover, in an angle resolved photoemission experiment one narrow band was detected near the gap edge [13]. Similarly, with tunneling spectroscopy, two distinct peaks, with a remarkable temperature dependence below 200 K, were observed on both sides of the Fermi energy E_F [10]. These findings supports a theoretical picture characterized by two narrow bands at the edges of a narrow gap, to account for the temperature dependence of the magnetic susceptibility and of the optical conductivity.

Moreover, while band structure calculations predict a gap of the correct order of magnitude, they fail to account for the temperature dependence of both magnetic and electronic properties [14–16]. On the basis of these results, it has been suggested that FeSi is a strongly correlated insulator [14–17], possibly belonging to the class of materials called Kondo insulators [18, 19].

In the course of this chapter we will present our result obtained with optical spectroscopy on FeSi. In particular we will concentrate on:

- The electronic gap in the optical conductivity and its temperature dependence.
- The transfer of the spectral weight from low to high frequencies, once the gap is open, in order to address the relevant energy scales for this compound.
- The unusual oscillator strength observed for the optical phonons in FeSi which was previously interpreted as an indication of highly ionic character for FeSi [4].

Furthermore, we will also present our optical spectroscopy results on other transition-metal (TM) mono-silicides, namely CoSi and MnSi, in order to find possible differences and similarities with the case of FeSi. Finally, we will discuss the wider class of TM mono-silicides (CrSi, MnSi, FeSi, CoSi, NiSi, etc.) with the FeSi structure, we will review the structural and physical data of this class of compounds, and explore the relation between their structural characteristics and the electronic properties.

2.1 Structural Properties of TM Mono-Silicides

In table 2.1 we summarize the lattice structures of the mono-silicides for the various d-transition elements [20]. For the 3d series the $P2_13 - T^4$ space group has been observed from CrSi to NiSi. For NiSi, in addition, the NiAs structure has been reported. The $P2_13 - T^4$ space group has also been reported for RuSi, RhSi, ReSi and OsSi. TiSi, VSi, PdSi, IrSi, and PtSi all have the MnP structure.

In this chapter we restrict the discussion to the mono-silicides with the $P2_13 - T^4$ space group (displayed in fig. 2.1). This simple cubic structure contains four TM atoms in the positions $(x, x, x; x+\frac{1}{2}, \frac{1}{2}-x, 1-x$; et cycl.) and four Si atoms in an equivalent set.

In table 2.1 we summarize the cell parameters and the interatomic distances [20]. The four transition metal and silicon atoms occupy equivalent sites. The site symmetry has only a three-fold rotation axis, which we indicate throughout this chapter as the local z-axis. The TM-atom has a 7-fold coordination by Si atoms and vice versa: A single bond pointing toward the Si-atom along the z-axis (type 1), and two groups of three identical bonds (types 2 and 3), with azimuthal angles relative to the z-axis of 0 (type 1) 74 (type 2) and 141 degrees (type 3). The two groups of type 2 and 3 are rotated around the local z-axis with an angle of 24 ± 2 degree relative to each other. The four equivalent sites within the unit cell have the same sense of rotation, hence two isomeric structures (left handed and right handed) exist. As a result phase/anti-phase boundaries of the two isomers can occur (also in single crystals) which may will considerable influence on the transport properties. Single domain crystals should exhibit optical activity. These aspects of the transition metal mono silicides still await further scrutiny.

Within an accuracy of 2% the average distance between the TM-atom and its 7 Si neighbors (d) follows the rule $d = r_{\mathrm{TM}} + r_{\mathrm{Si}}$, where r_{TM} is the atomic radius of the TM atom in 12-coordinated metals [21], and $r_{\mathrm{Si}} = 1.173$Å is the single bond radius of Si (fig. 2.2 and

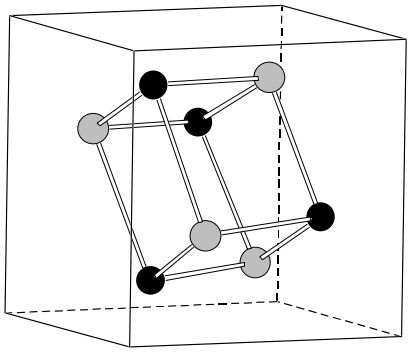

$P2_13$ - T^4

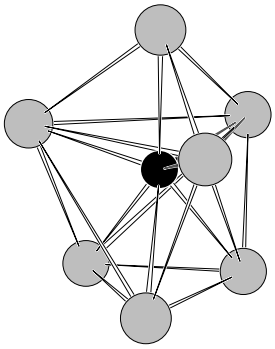

$TMSi_7$ cluster

Figure 2.1: *Unit cell of the TMSi compounds described by the space group $P2_13$-T^4 (top), and $TMSi_7$ cluster representing the site symmetry of individual atoms (bottom).*

TMSi	a (Å)	x_{TM} (a)	$1-x_{Si}$ (a)	d_1 (Å)	d_2 (Å)	d_3 (Å)	d (Å)	d_{sum} (Å)
ReSi	4.775	0.140	0.160	2.500	2.500	2.700	2.56	2.55
OsSi	4.728	0.128	0.161	2.364	2.429	2.715	2.54	2.52
RuSi	4.701	0.128	0.164	2.383	2.395	2.706	2.53	2.51
RhSi	4.676	0.147	0.155	2.451	2.480	2.548	2.51	2.52
CrSi	4.629	0.136	0.154	2.325	2.435	2.589	2.49	2.45
MnSi	4.558	0.138	0.154	2.305	2.402	2.537	2.45	2.43
FeSi	4.493	0.136	0.156	2.271	2.352	2.519	2.41	2.44
CoSi	4.447	0.14?	0.16?	2.2?	2.3?	2.5?	2.4?	2.42
NiSi	4.437	0.14?	0.16?	2.2?	2.3?	2.5?	2.4?	2.42

Table 2.1: *Lattice parameter (a), displacement vectors x (units of lattice constant a), interatomic distances between TM and Si atoms (d_1, d_2, d_3), weighted average of the latter (d), and the sum of the atomic radii for 12-coordinated metals and the single bond radius of Si (d_{sum}). For CoSi and NiSi no published values of x could be found.*

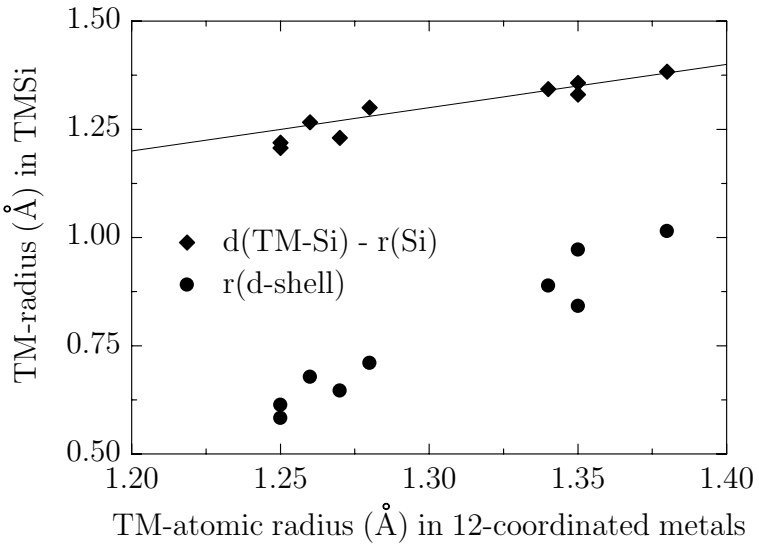

Figure 2.2: *TM radius in TMSi (TM-Si bond length minus radius of Si, diamonds) and d-shell radii (circles) versus the TM radius in 12-coordinated metals. The solid line represents the relation:* $d - r_{\mathrm{Si}} = r_{\mathrm{TM}}$.

table 2.1), indicating that almost no charge transfer takes place between Si and the TM atom. The absence of charge transfer between TM and Si can be anticipated from the fact that the Pauling electronegativities are almost the same.

For $x(\mathrm{TM}) = 0.1545$ and $x(\mathrm{Si}) = -0.1545$ all seven neighbors have the same bond length. As we can see in table 2.1 the structure of the TM mono-silicides is rather close to this situation, but the deviations are significant. The variation of the bond length within the group of 7 nearest neighbors has been discussed by Pauling *et al.* [22, 23] for CrSi to NiSi in terms of valence bond sums, which lead to the following bond numbers: one full bond (type 1), three 2/3 bonds (type 2) and three 1/3 bonds (type 3).

2.1.1 Group Theoretical Analysis

At this point, while discussing the structural properties of the TM silicides with $P2_13$ symmetry, it is useful to perform a group theoretical analysis of the lattice vibrations for this space group. In fact, prominent absorption lines were detected below the gap, in FeSi, in reflectivity experiments [4–6]. In the early optical investigations [4, 5], no agreement was achieved about the nature of these excitations which were attributed to phonons and partly to excitons, on the basis of a group theoretical analysis suggesting only three optically allowed phonon modes for the space group $P2_13$ [5] (i.e., number which is smaller than the one of the lines experimentally observed in the far-infrared region, as we will see later in section 2.3.1).

On the basis of a group theoretical analysis it is possible to calculate the number and the symmetry of the lattice vibrational modes and then to determine how many optical active

phonons can be expected in the experiment. FeSi has a cubic structure $B20$ (space-group $P2_13$, factor-group $T(23)$ and site group C_3), with four Si and four Fe atoms at equivalent positions per unit cell . This corresponds to 24 degrees of freedom, and subtracting the three degrees of freedom related to the acoustic modes, we have 21 degrees of freedom associated to optical modes. Using the correlation method [24] we found for the irreducible representation of FeSi optical vibrations [25]:

$$\Gamma = 2A + 2E + 5T \ . \tag{2.1}$$

As the A, E and T symmetry modes are single, doubly and triply degenerate, respectively, this irreducible representation accounts for the correct number of degrees of freedom. From the lack of inversion symmetry it follows that all these modes are Raman active. But the most important conclusion is that all the five triply degenerate T symmetry modes are infrared active, and not only three as was obtained in ref. 5. The A and E modes are instead infrared forbidden. We will see later, in section 2.3.1, that the results we obtained for the optical vibrations allowed by symmetry, for the TM silicides described by the space group $P2_13$, are in rather good agreement with the Raman and infrared experimental data. Moreover, no indication of excitonic absorptions was found.

2.2 Experimental

We investigated the optical properties of FeSi, CoSi, and MnSi in the frequency range going from 30 to 34 000 cm^{-1}. High-quality single crystals were grown from the stoichiometric melt either by the floating zone method using a light image furnace in a purified argon atmosphere, or by a modified tri-arc Czochralski method [26]. The cubic symmetry of the crystals was confirmed by x-ray diffraction analysis. Electron-probe microanalysis showed a stoichiometric and homogeneous single phase. The crystals, with dimensions of approximately $3 \times 3 \times 1$ mm were mounted in a liquid He flow cryostat to study the temperature dependence of the optical properties between 4 and 300 K. Reflectivity measurements, in near normal incidence configuration ($\theta = 11°$), were performed on two different Fourier transform spectrometers: A Bruker IFS 113v, in the frequency range going 20 - 5000 cm^{-1}, and a Bomem DA3, between 1000 and 32 000 cm^{-1}. The absolute reflectivity was obtained by calibrating the data acquired on the samples against a gold mirror, from low frequencies up to 15 000 cm^{-1}, and an aluminum mirror for higher frequencies. The optical conductivity was calculated from the reflectivity data using Kramers-Kronig (KK) relations [27]. However, because of the intrinsic difficulties in obtaining reliable estimates of the optical conductivity, via KK transformations, in materials characterized by a high value of reflectivity over the entire frequency range experimentally investigated, also reflection ellipsometry was performed for frequencies higher than 6000 cm^{-1} on a Woollam (VASE) ellipsometer. In this way, it was possible to obtain a very accurate and direct estimate of the optical conductivity, over a very broad frequency range. Moreover, we could also use this result to improve the KK analysis yet necessary in order to calculate the optical conductivity for the low frequency region.

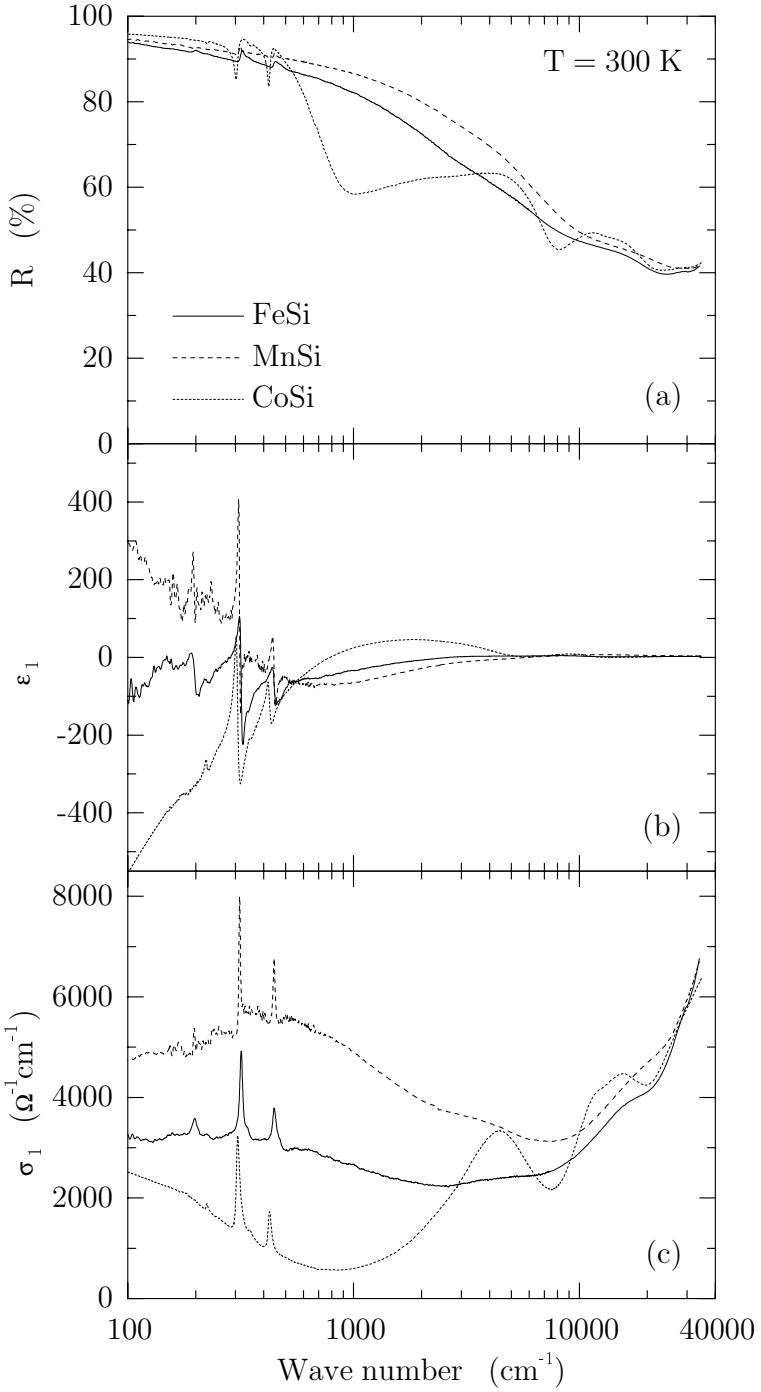

Figure 2.3: *Room temperature optical spectra of FeSi, CoSi, and MnSi in the frequency range going from 100 to 34 000 cm^{-1}. Panel (a), (b), and (c) show the results for the reflectivity, the real part of the dielectric constant ϵ_1, and the real part of the optical conductivity σ_1, respectively, versus frequency.*

2.3 Optical Spectroscopy of TM Mono-Silicides

In this section, as a introduction to what will be discussed in detail in the course of the chapter, we will present the room temperature optical spectra of FeSi, CoSi, and MnSi in the frequency range going from 100 to 34 000 cm^{-1}.

As we can see in fig. 2.3a, all samples show a reflectivity which, for a metal, is relatively low, indicating a small number of free carriers (semimetal like behavior, i.e., CoSi) or a large value of the scattering rate (dirty-metal like behavior, i.e., FeSi and MnSi). on the other hand, at 34 000 cm^{-1}, the reflectivity has a value of $\sim 40\%$, which makes the KK analysis on these data rather delicate [27]. In panel (c), where the optical conductivity obtained by combining KK analysis and ellipsometric measurements is shown, we can observe, for CoSi, the very narrow Drude peak typical for a semimetal. Different is the situation of FeSi and MnSi, which exhibit a more intense, however strongly damped and non-Drude like, metallic response. Moreover, for these two compounds, from approximately 700 to 2000 cm^{-1}, an additional band is present which is responsible, in particular in MnSi, for the downturn of the conductivity at very low frequency (see fig. 2.3c), and for the upturn of the dielectric constant (see fig. 2.3b). The latter, contrary to a typical metallic case which is characterized by a large negative value of ϵ_1 due to the free carrier contribution (see, e.g., CoSi), is becoming positive below ~ 300 cm^{-1}.

In the far-infrared region, sharp absorption lines are present for all the three samples, with approximately the same frequency. These excitations, as we will discuss later, can all be ascribed to optical phonon modes.

At high frequencies, the optical response of FeSi, CoSi, and MnSi tends to become very similar (see in particular fig. 2.3a and c). Two more electronic bands are present on all the compounds at approximately 4000 and 13 500 cm^{-1} (particularly pronounced on CoSi where the Drude peak is extremely narrow). Above 28 000 cm^{-1} the experimental data for the three compounds are, basically, undistinguishable. However, we have to stress that, contrary to what has been previously reported [5], the optical conductivity is not decreasing for frequencies higher than 15000 cm^{-1}, but is still raising considerably. This discrepancy is only due to the large uncertainty of the KK analysis: In fact, the optical conductivity data presented in ref. 5 were obtained from the experimental reflectivity via KK transformation, whereas we took advantage of ellipsometric measurements.

2.3.1 Optical Spectroscopy of FeSi

In this section we will investigate in detail the temperature dependent optical response of FeSi. In fig. 2.4 the reflectivity data (R), the real part of the dielectric function (ϵ_1), and the dynamical conductivity (σ_1) are shown up to 10 000 cm^{-1}, for five different temperatures.

Electronic Gap

In fig. 2.4 we can see that there is a strong temperature dependence in the optical data for frequency up to 6 000 cm^{-1}. Using the f-sum rule [27] we estimate that at room temper-

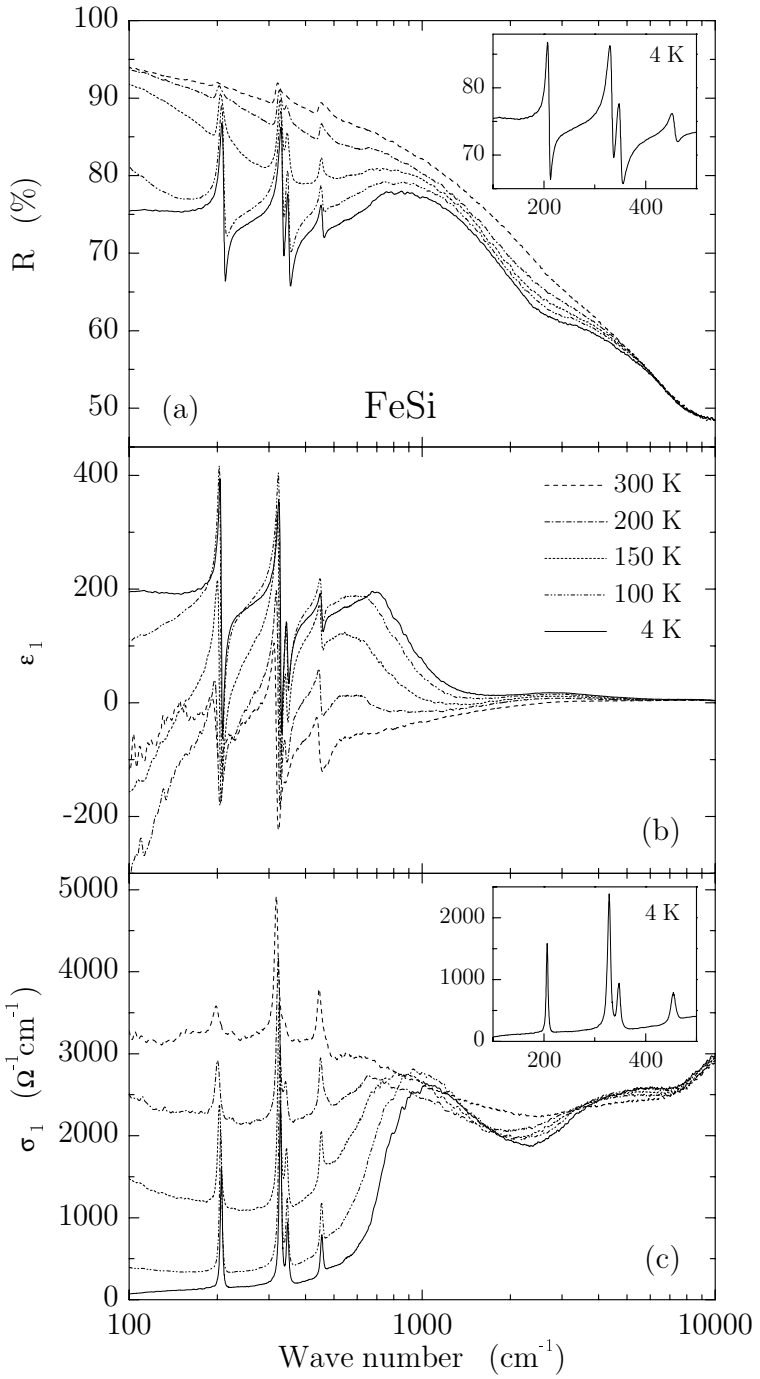

Figure 2.4: *Reflectivity, real part of the dielectric function and optical conductivity of FeSi, for several temperatures between 4 and 300 K. The insets of panel (a) and (c) show an expanded view of the 4 K data for reflectivity and optical conductivity, respectively.*

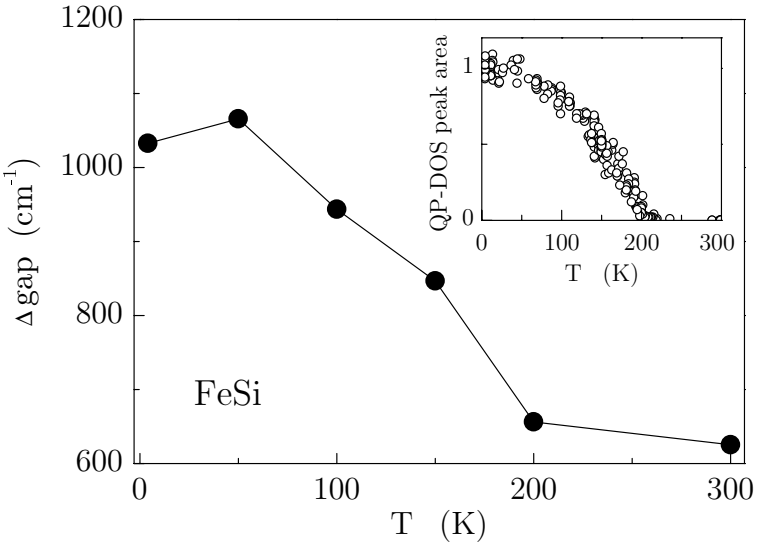

Figure 2.5: *Peak position of the shoulder marking the onset of electronic absorption above the gap, in the optical conductivity of FeSi, plotted versus temperature. Inset: Temperature dependence of the quasiparticle DOS area under the tunneling conductance curves, measured on the same samples used for the optical measurements (from ref. 10).*

ature the free carrier contribution corresponds to a charge carrier density of the order of 10^{21} to 10^{22} cm^{-3} with a life-time of 5 fs or less, which is rather untypical for clean semiconductors. The free carrier contribution drops rapidly upon reducing the temperature. This results in a strong depletion of the optical conductivity at low frequencies and in the onset of absorption at 570 cm^{-1} (70 meV), which we identify as a semiconducting gap in the particle-hole continuum, thus confirming earlier reports on the infrared properties [4, 5]. With respect to the debate on the energy scale characteristic for the complete recovery of the spectral weight lost in the low frequency region [4, 5], a detailed discussion will be presented in section 2.4.

In order to estimate the temperature dependence of the gap, we can follow the frequency shift of the peak position of the shoulder marking the onset of electronic absorption above the gap itself, in the optical conductivity (see fig. 2.4c). The temperature dependence of this quantity is plotted in fig. 2.5, where we can see that the 'closing in' of the gap can be followed up to 200 K, whereas between 200 and 300 K no difference is detectable any more. In this temperature range, only an additional 'filling in' of the optical conductivity, in the low frequency region, is observable. In our opinion, these results suggest that at approximately 200 K, at least for certain k points in the Brillouin zone, the gap is already closed. At higher temperatures, only the further overlap of valence and conduction bands over larger portions of the Brillouin zone is taking place.

It is interesting to compare these findings with the results obtained in tunneling spectroscopy measurements, performed on the same samples used for the our optical experiments, and reported in ref. 10. Fäth *et al.* observed in the tunneling spectra a strong

Schlesinger *et al.* [4]	—	205	—	332	—	466
Degiorgi *et al.* [5]	140	200	—	330	—	460
Nyhus *et al.* [28]	—	193	260	311	333	436
Our data (300K)	—	198	—	318	338	445
Our data (4K)	—	207	—	329	347	454

Table 2.2: *Resonant frequencies (in cm^{-1}) of the T-symmetry absorption peaks observed on FeSi in the far-infrared region, with Raman (Nyhus et al.), and infrared spectroscopy (others).*

temperature dependence below about 200 K [10]: Two narrow conductance peaks on either side of E_F were detected below 200 K, and became progressively more pronounced, with a well defined minimum at E_F, upon further reducing the temperature. These results were interpreted as a manifestation of the interacting d-electrons quasiparticle density of states (DOS) [10], which was previously shown to dominate the angle-resolved photoemission spectra [13]. In order to give an approximate description of the gap evolution with temperature, Fäth *et al.* [10] adopted the integrated area under the quasiparticle DOS peaks detected in the tunneling conductance curves. The results of this analysis are here shown in the inset of fig. 2.5.

We see that the trend of optical and tunneling data sets is very similar, indicating that the gap can be considered closed at approximately 200 K. Therefore, contrary to what is expected for usual semiconductors where carriers are thermally excited across the gap, in FeSi the gap is closed at a temperature which is a factor of four lower than the size of the gap itself ($\sim$800 K).

Phonon Spectrum

Below the gap (see fig. 2.4), we observe a number of prominent absorption lines which were previously attributed to phonons [4] and partly to excitons [5]. In our far-infrared spectra four peaks are clearly visible (see insets of fig. 2.4), with $\omega_{\mathrm{TO}} \approx$ 198, 318, 338, and 445 cm^{-1}, at $T = 300$ K. The resonant frequencies of all the far-infrared absorption peaks detected in different optical experiments have been summarized in table 2.2. So far, the 338 cm^{-1} mode had escaped detection in infrared spectroscopy [4, 5], possibly due to inhomogeneous broadening of the lines. There is no evidence in our data for an optical absorption at 140 cm^{-1} [5] or at 820 cm^{-1} [4].

On the basis of the group theoretical analysis presented in section 2.1.1, we should expect, in FeSi, five optical phonon modes with T symmetry (see eq. 2.1). Therefore, the four resonances we detected can all be interpreted as infrared active phonons. An additional confirmation of our group theory analysis, and of the interpretation of the prominent absorption lines in the gap region as infrared active phonons is given by Raman scattering experiments done by Nyhus *et al.* [28]. They were able to measure and identify

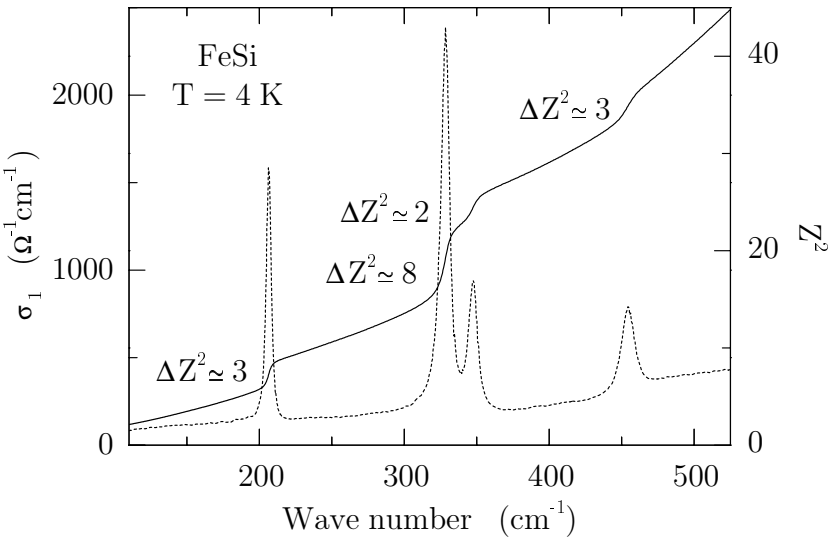

Figure 2.6: *Optical conductivity of FeSi at $T = 4$ K (dotted curve, left axis), together with the function $Z^2(\omega) = 8\mu(4\pi n_i e^2)^{-1} \int_0^\omega \sigma(\omega')d\omega'$ (solid curve, right axis).*

two E modes at 180 and 315 cm^{-1}, an A mode at 219 cm^{-1} and five T modes at 193, 260, 311, 333 and 436 cm^{-1} (see table 2.2). They could resolve all the expected Raman active modes except one A mode. In particular, they were able to measure all the five T modes which are expected to be both Raman and infrared active. The correspondence between Raman and infrared lines is rather good, except for the one observed by Nyhus *et al.* [28] at 260 cm^{-1}, which is completely absent in our infrared reflectivity spectra.

Later in the course of this chapter, while discussing the optical data we obtained on CoSi and MnSi (see fig. 2.9 and 2.10), and those reported in the literature for RuSi [29], we will see that all the TM mono-silicides investigated with optical spectroscopy show very similar phonon spectra. In particular, of the five lattice vibrational modes expected to be optically active on the basis of the group theoretical analysis (see eq. 2.1), only four have been detected on all these compounds. It is very plausible that the missing T symmetry mode, which corresponds to the 260 cm^{-1} line observed in Raman spectroscopy [28], did escape detection in infrared reflectivity measurements simply because of its very small oscillator strength. On the other hand, an alternative explanation could be a hidden symmetry of the system, producing a net vanishing dipole moment for that lattice vibrational mode, in infrared spectroscopy. In this case, it would be understandable why the optically inactivity of this particular phonon seems to be a general feature of this class of compounds.

Phonon Effective Charge

At low temperature, the value $\epsilon_\infty \approx 200$ (i.e., the dielectric constant at frequencies just above the last phonon resonance) indicates a high electronic polarizability for FeSi, mainly due to virtual transitions in a band from 700 to 1500 cm^{-1}, which becomes progressively masked by the negative free carrier contribution, upon increasing the temperature (see

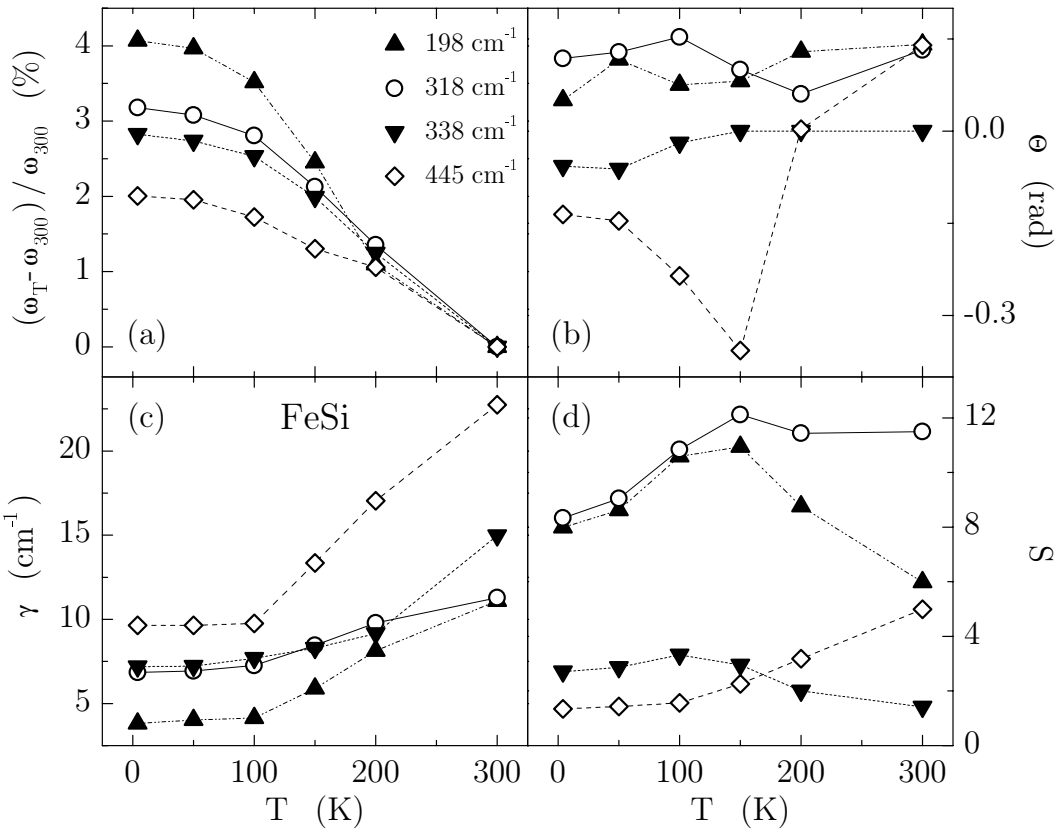

Figure 2.7: *Temperature dependence of the frequency shift* $[\Delta\omega_j(T) = \omega_j(T) - \omega_j(300)]$*, decay rate* ($\gamma_j$)*, Fano asymmetry parameter* (Θ_j)*, and oscillator strength* (S_j) *of the 4 transverse optical phonons detected in the reflectivity spectra of FeSi.*

fig. 2.4b). We will discuss below that the optical phonons in the infrared region derive their optical oscillator strength from a coupling of the atomic coordinates to these charge degrees of freedom.

Previously, the high intensity of these phonon lines has been indicated as evidence for a strong ionicity in this compound [4]. The transverse effective charge e_T^* of the ions [30] can be calculated directly by applying the f-sum rule to the vibrational component of $\sigma_1(\omega)$:

$$8\int_0^\infty \sigma_1(\omega')d\omega' = 4\pi\mu^{-1}n_i e_T^{*2} = \sum_j S_j\omega_j^2 \ , \tag{2.2}$$

where μ is the reduced mass of an Fe-Si pair, n_i is the number of Fe-Si pairs per unit volume (i.e., 4 per unit cell), S_j is the phonon strength, ω_j is the resonant frequency, and j is the index identifying the j th phonon. Throughout this chapter, we will use the dimensionless number $Z = e_T^*/e$ to indicate the total transverse effective charge summed over all phonons.

In fig. 2.6 we display for $T = 4$ K, together with the optical conductivity, the quantity $Z^2(\omega)$, obtained by integrating σ_1 in eq. 2.2 up to a frequency ω. We observe, superimposed

on a smooth remnant electronic background, four steps ΔZ^2, one for each optical phonon. Adding up these steps we estimate, for the total transverse effective charge at 4 K, a value $Z^2 \approx 16$. However, because Fe and Si have practically the same electronegativity and electron affinity, strong ionicity is not expected from a chemical point of view, nor has it been inferred from *ab initio* calculations of the electron density distribution [14,31]. This situation is reminiscent of the IV-VI narrow-gap semiconductors PbS, PbSe, PbTe and SnTe where Z values between 5 and 8 were found. For the latter systems this has been attributed to a resonance (or mesomeric) bonding effect [30]. With this model, the empirically found relation $Z^2 \sim (\epsilon_\infty - 1)$ was explained by the resonance aspect of the chemical bond in these compounds [22,23,30]. Based on a similar concept, a theory of infrared/optical spectra of coupled vibrational and charge transfer excitations was developed by Rice, Strässler and Lipari in the context of dimerized organic linear-chain conductors [32].

The next step is the analysis of the phonon parameters for the different modes. Some of them exhibit an asymmetric line shape, probably deriving from an interaction between lattice vibrations and the electronic background. We were successful in fitting the phonon lines with a Fano profile. Fano theory describes the interaction of one or more discrete levels with a continuum of states resulting in asymmetric optical absorption peaks [33]. After subtraction of the continuous electronic background the Fano profile, expressed in a form which guarantees that $\sigma^*(\omega) = \sigma(-\omega)$, is given by:

$$\sigma(\omega) = i\sigma_0 \left[\frac{(q-i)^2}{i+x} + \frac{\gamma q^2 \omega}{\omega_{\mathrm{T}}^2} \right] \ , \tag{2.3}$$

where σ_0 is the background, $x = (\omega^2 - \omega_{\mathrm{T}}^2)/\gamma\omega$ (γ and ω_{T} are the line-width and the resonant frequency of the unperturbed vibrational state), and $q(\omega) = \omega_q/\omega$ is the dimensionless Fano parameter reflecting the degree of asymmetry of the peak (for $|q| \to \infty$ a Lorentz line shape is recovered). When a fit over a sufficiently limited frequency range is performed, as in the case of sharp phonon peaks, the Fano asymmetry parameter can be rewritten as $q \simeq \omega_q/\omega_{\mathrm{T}} = -1/\tan(\Theta/2)$. In this case, a lorentzian line shape is recovered for $\Theta = 0$.

The functional expression of the oscillator strength in terms of the Fano parameters, which is of fundamental importance for our analysis, can be obtained from the usual definition of oscillator strength by integrating the optical conductivity:

$$S \equiv \frac{8}{\omega_{\mathrm{T}}^2} \int_0^\infty \sigma_1(\omega)\, d\omega = \frac{4\pi\sigma_0\gamma}{\omega_{\mathrm{T}}^2} \left(\frac{\omega_q^2}{\omega_{\mathrm{T}}^2} - 1 \right) \ . \tag{2.4}$$

The Fano parameters obtained for all the peaks are summarized in fig. 2.7, where we have plotted the phonon frequency shift $\Delta\omega(T)$, the line-width γ, the phonon strength S and the asymmetry parameter Θ. We can see that $\Delta\omega(T)$ and γ show a very strong temperature dependence, in particular for $T > 100$ K. Clearly there is a strong decrease of the line-width γ upon reducing the temperature. This dramatic loss of electronic relaxational channels, which comes with the opening of a gap in the electronic spectrum, suggests the presence of a coupling between electronic states and the lattice vibrations in FeSi.

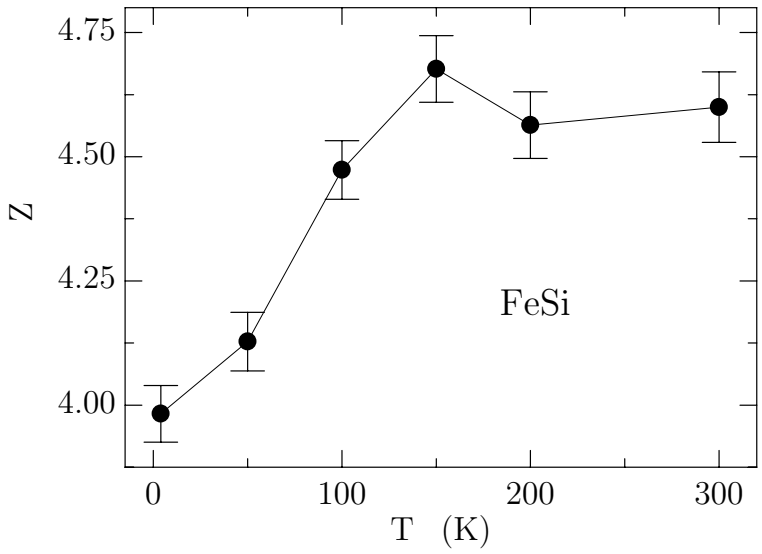

Figure 2.8: *Temperature dependence of the transverse effective charge Z, summed over all phonons, obtained from the parameters of the fit of the optical modes with Fano line shapes.*

The behavior of the parameter Θ is also very important in establishing whether or not such a coupling exists, and whether it reflects the temperature dependence of the gap itself. While the 338 cm^{-1} line shows a slight asymmetry only at low temperature, and this mode is well described by a classical Lorentz oscillator ($|\Theta| \approx 0$) for $T > 100$ K, the situation is rather different for the other phonons. All of them are characterized by considerable asymmetry, especially the one at 445 cm^{-1}. Significant in this analysis is also the sign of the parameter Θ. For the lines at 198 and 318 cm^{-1} we found $\Theta > 0$ at all temperatures, indicating a predominant interaction between these modes and electronic states higher in energy. On the other hand, the 445 cm^{-1} peak exhibits a negative value of Θ (interaction with electronic states lower in energy), with a maximal degree of asymmetry (maximum in $|\Theta|$) at $T = 150$ K. One has to notice (see fig. 2.4c) that it is approximately at this temperature that the gap edge crosses the phonon resonance frequency of 445 cm^{-1}. Moreover, for $T > 150$ K the asymmetry of this mode changes sign, i.e., $\Theta > 0$. At $T = 300$ K, having the gap already closed, the value of Θ is the same for all the three phonons characterized by a considerable asymmetry.

These differences in the behavior of Θ can possibly be related to the way the gap disappears (see fig. 2.4 and 2.5). Increasing the temperature, the conductivity increases within the gap as a result of two different processes. First the 'closing in' of the gap: The movement of the gap edge from high to low frequency. Secondly the 'filling in' of the gap: The increase with temperature of the background conductivity within the gap. Probably the 445 cm^{-1} phonon, as it is the closest one to the gap edge, is more strongly influenced by the 'closing in' than by the 'filling in'. In fact, as we pointed out, the asymmetry of the mode at 445 cm^{-1} changes sign when the gap edge has moved below the resonant frequency. The other phonons, whose Θ does not show such a strong temperature dependence, seem

to be influenced predominantly by the 'filling in' of the gap, a process smoother than the movement of the gap edge.

By summing over the contributions of the four phonons, using the values for S_j and ω_j displayed in fig. 2.7, the temperature dependence of e_T^*/e was calculated. The total transverse charge, shown in fig. 2.8, increases with rising temperature and saturates at a value of $Z \approx 4.6$ for $T > 150$ K.

Charged Phonon Model

The value for Z which, as mentioned, cannot be due to a real ionicity of the system, can be explained if we assume a coupling between the vibrational degrees of freedom and electron-hole excitations across the gap of 70 meV. These charge excitations have a large contribution of $E+T$ character and a weak contribution of A character, as measured in Raman spectroscopy [28]. Because of the lack of inversion symmetry, for this crystal structure there are no charge or vibrational excitations of pure even/odd character. Therefore a coupling is allowed between the infrared-active T modes and the charge excitations of T character.

Within this approach it is possible, considering a linear coupling between lattice vibrations and electronic oscillators, to account for the strong oscillator strength observed for the infrared-active phonons. For a phonon coupled to an electronic resonance the optical conductivity is [32, 34]:

$$\sigma_j(\omega) = \frac{-i\omega n_e \mu^{-1} e_{T,j}^{*2}}{(1-\lambda_j)\omega_j^2 - \omega(\omega + i\gamma_j)} \ . \tag{2.5}$$

Here $\lambda_j = g^2 m_e^{-1} \mu^{-1} \omega_j^{-2} \omega_{p,e}^{-2} \epsilon_e$ is a dimensionless electron-phonon coupling parameter and $\epsilon_e = \omega_{p,e}^2 \left[\omega_e^2 - \omega(\omega + i\gamma_e)\right]^{-1}$ is the contribution to the dielectric function due to an electronic oscillator coupled to the phonons. The indices e and j refer to the electronic oscillator and to the j th phonon, respectively. The transverse effective charge in this model is:

$$e_{T,j}^{*2} = \lambda_j \epsilon_e n_e^{-1} n_i (Z_i e)^2 \omega_j^2 \Omega_{ph}^{-2} \ . \tag{2.6}$$

The quantity $\Omega_{ph}^2 = 4\pi n_i \mu^{-1} Z_i^2 e^2$ is the square plasma frequency of the lattice, where Z_i is the formal valence of the ions. Using these experimental quantities of FeSi we obtain $\Omega_{ph}/(2\pi c Z_i) = 341$ cm^{-1}. From a detailed fit of our data to the generalization of eq. 2.5 to several phonons coupled to the charge, which reproduces the intensities and the Fano-line shapes of the four phonons, we obtained the coupling constants $\lambda_j = 0.063, 0.080, 0.096$ and 0.036 for the four phonons at 198, 318, 338, and 445 cm^{-1}, respectively, at 4 K. The Fano asymmetry parameter Θ in this model is $\Theta_j = 2\mathrm{Arg}\left[\epsilon_e(\omega_j)\right]$. To reproduce the positive and negative values of Θ for all phonons, we had to introduce in the model an electronic oscillator with a resonant frequency $\omega_e = 900$ cm^{-1} as well as a Drude peak, both of them coupled to the phonons. If we insert these values of λ_j in eq. 2.6, using the transverse effective charges of fig. 2.6, we obtain $\epsilon_e \approx 80$ for the electronic resonance coupled to the phonons. This implies that about 1/3 of the oscillator strength associated with the high

electronic dielectric constant ($\epsilon_\infty \approx 200$) is coupled to the phonons. We conclude from this analysis, that the high transverse effective charge results from a moderate coupling of the optical phonons to an electronic resonance with a large oscillator strength.

An important question concerns the relation of this resonance to the unusual magnetic properties in FeSi. Each Si atom is coordinated by six Si neighbors at a distance of 2.78 Å, while the transition-metal atom has seven Si neighbors with distances varying from 2.27 to 2.52 Å. As the same structure is formed for CrSi, MnSi, FeSi, CoSi, NiSi, RuSi, RhSi, ReSi, and OsSi, it appears that the backbone of these compounds is formed by the Si and transition-metal outer shells. The localized $3d$ electrons on the transition-metal sites would have a magnetic moment (e.g., $S=1$ for Fe [22,23]). These local moments can then be compensated by the conduction electrons of the backbone. The many-body ground state built from a superposition of such singlets centered at every Fe site then corresponds to a state which could be described as a Kondo-insulator [18, 19]. Alternatively one can postulate that an even number of $3d$ electrons resides on every Fe atom in a singlet ground state [17], while thermal excitations to a high spin (e.g., triplet) state would be responsible for the Curie-like magnetic susceptibility at elevated temperatures. However, neither of these two scenario's results in a resonance hybrid [22, 23] of bonds between Fe and Si. Hence our experimental evidence for such resonant behavior may indicate that a different theoretical approach is required. In this respect, a more detailed discussion of the electronic structure of TM mono-silicides will be the subject of section 2.5.

2.3.2 Optical Spectroscopy of CoSi

In this section we present the results of temperature dependent optical measurements performed on CoSi. In fig. 2.9, where reflectivity, real part of the dielectric function, and optical conductivity of CoSi are plotted, for several temperatures between 4 and 300 K, we can see that not much is happening upon cooling down the sample. The material remains a semimetal at any temperatures, with a Drude peak which becomes more pronounced the more the temperature is reduced. This effect is shown not only, directly, by the optical conductivity spectra (fig. 2.9c), but also by the increase, upon lowering the temperature, of the absolute reflectivity (fig. 2.9a), and of the negative free-carrier contribution to the dielectric constant (fig. 2.9b), at low frequencies.

The change in spectral weight below 200 cm^{-1}, is immediately compensated in the frequency range between 200 and 700 cm^{-1}. Therefore, contrary to the case of FeSi [4], no transfer of spectral weight from low to high frequencies takes place in CoSi. However, this particular point will be discussed in more detail, for the three different TM mono-silicides we investigated with optical spectroscopy, in section 2.4.

In the far-infrared region, as on FeSi, only four optically active phonon modes are detected on CoSi, with resonance frequencies $\omega_{TO} \approx 227, 309, 350$, and 427 cm^{-1}, at 4 K. The remarkable result is that also in the case of CoSi the phonon absorption lines are characterized by a certain asymmetry and, in particular, by a large oscillator strength. For FeSi we have been discussing this finding on the basis of a charged phonon model [32], i.e., as a consequence of the coupling between lattice degrees of freedom and an electronic

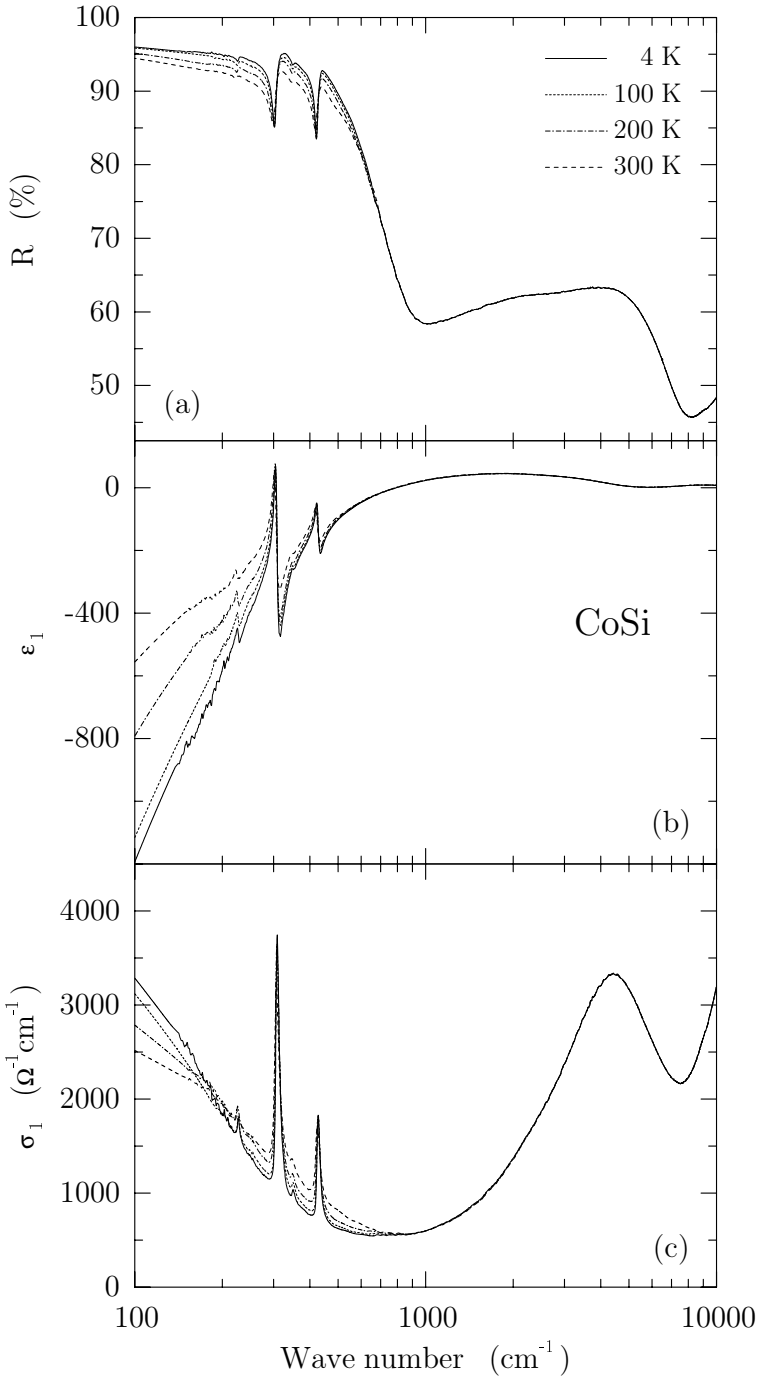

Figure 2.9: *Reflectivity, real part of the dielectric function and optical conductivity of CoSi, for several temperatures between 4 and 300 K.*

resonance with a large oscillator strength. The observation of the same effect on CoSi strongly suggests that this has to be an intrinsic feature of the TM mono-silicides described by the space group $P2_13$. In particular, it has to be related to an electronic configuration, similar for all the compounds of this class, which favors a resonant hybrid of bonds between the TM and Si atoms [22,23]. A more extensive discussion and a possible microscopic model will be presented in sections 2.4 and 2.5.

2.3.3 Optical Spectroscopy of MnSi

In this section we present the results of temperature dependent optical measurements performed on MnSi. Reflectivity, real part of the dielectric function and optical conductivity of MnSi are plotted, for several temperatures between 4 and 300 K, in fig. 2.10. As in the case of CoSi, MnSi is a metal at all temperatures. On the other hand, in fig. 2.10 we can see that MnSi shows, in particular at low frequency, a rather strong temperature dependence. As we already discuss in section 2.3, at 300 K we can observe a strongly damped and non-Drude like metallic behavior. Cooling down the material, we can observe the sharpening and the increase in intensity of the low frequency metallic response. A strong effect, as shown in the inset of fig. 2.10c, is noticeable in going from 50 to 4 K: The absolute conductivity extrapolated to zero frequency, at 4 K, shoots up to the value of $\sim 52\,000\ \Omega^{-1}\mathrm{cm}^{-1}$, in agreement with DC resistivity data [35] (see fig. 2.13). This effect is related to the magnetic ordering phase transition taking place in the system for $T < T_c = 29$ K [36,37]: Below T_c, MnSi has an helical (ferro)magnetic structure with a wavelength, for the helical modulation, of 180 Å in the (111) direction [36,37]. The magnetic ordering results in a reduction of spin fluctuations and, in its turn, in a decrease of the scattering rate for free electrons.

In the far-infrared frequency range, as on FeSi and on CoSi, only four optically active phonon modes are detected on MnSi, with resonance frequencies $\omega_{\mathrm{TO}} \approx 200, 317, 346$, and 449 cm^{-1}, at 4 K. Also on MnSi the large oscillator strength of the modes has been observed, which will be subject of further discussion in sections 2.4 and 2.5. These results confirm that a resonant hybrid of bonds, between the TM and Si atoms [22,23], is indeed a characteristic feature of the TM mono-silicides with the FeSi structure, and has to be taken into account in trying to develop a microscopic model for the electronic structure of this class of compounds.

2.4 The Electronic Properties of TM Mono-Silicides

2.4.1 Magnetic Properties

The best studied materials in the class of TM mono-silicides with space group $P2_13$ are MnSi and FeSi. MnSi has a helical spin structure at low fields below the critical temperature of 29 K, and is paramagnetic above T_c. CrSi and NiSi are either weakly paramagnetic or diamagnetic. Estimates of the local moment on Mn based on magnetic susceptibilities vary

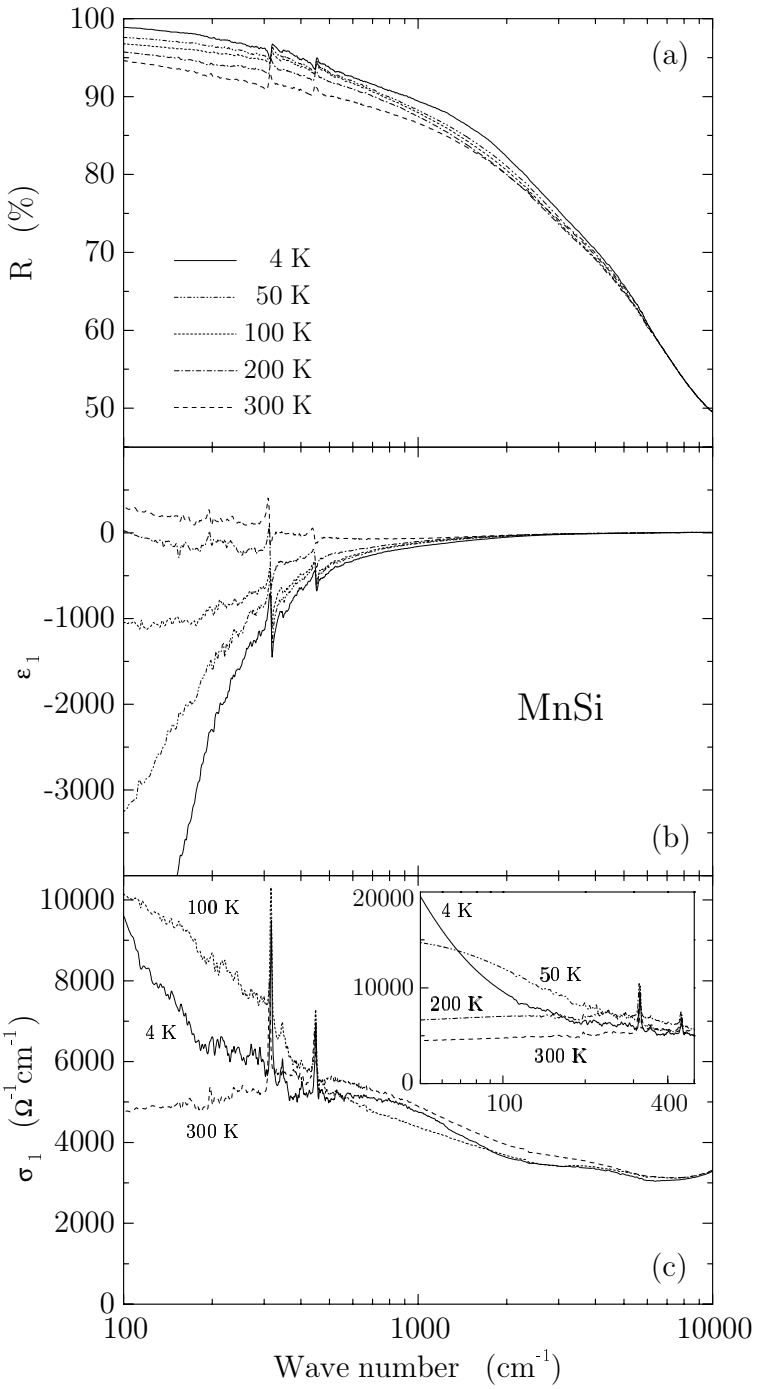

Figure 2.10: *Reflectivity, real part of the dielectric function and optical conductivity of MnSi, for several temperatures between 4 and 300 K. The inset of panel (c) shows an expanded view of the optical conductivity in the frequency range 50-500 cm^{-1}.*

from $\mu_{eff} = 2.12\mu_B$ with $g = 2$, below 300 K, to $3.3\mu_B$ above 600 K [38]. For FeSi [1] the high temperature limiting behavior of the susceptibility gives $\mu_{eff} = 1.7$ with $g = 3.9$, but good fits to thermally activated Curie-Weiss behavior were also obtained with $\mu_{eff} = 2.8$ and $g = 2$.

2.4.2 Optical Properties

We already presented, in the previous sections, the optical spectra of FeSi, CoSi, and MnSi. We now concentrate on the transfer of spectral weight from low to high frequencies in the optical conductivity, for different temperatures, issue which has been subject of intense debate in the previous studies of the optical response of FeSi [4, 5].

In fact, Schlesinger *et al.* [4] found that the increase in conductivity above the gap, observed upon raising the temperature, does not compensate for the depletion of conductivity in the gap region, at low temperature (see fig. 2.4c). Moreover, because the real part of the dielectric function ϵ_1 has a large positive value at low frequency, for T=4 K (see fig. 2.4b), one can exclude a shifting of the 'missing area' to low frequency (as, e.g., observed on superconductors). Therefore, Schlesinger *et al.* [4] pointed out that, because one needs to go to extremely high frequency (i.e., ~ 1 eV), with respect to the gap size, in order to satisfy the conductivity sum rule, strong electron-electron interactions play a major role in the physics of FeSi.

On the other hand, these observations were questioned in a later investigation of the optical conductivity of FeSi [5]. Degiorgi *et al.* [5], from the analysis of their optical data, concluded that the spectral weight is essentially recovered at $\sim$0.4 eV ($\sim$3000 cm^{-1}). This claim was based on the fact that, on the one hand, they did not observed a particular temperature dependence in the optical conductivity above this frequency while, on the other hand, the integrals of the optical conductivity, for different temperatures, were not distinguishable any more within the accuracy of the Kramers-Kronig analysis [5].

In fig. 2.11 we display the function $Nm_e/m^*(\omega) = 2m_e\pi^{-1}q_e^{-2}n_{TMSi}^{-1}\int_0^\omega \sigma(\omega')d\omega'$ for the three compounds we investigated experimentally. The high frequency limit corresponds to the total number of electrons per TMSi pair (i.e., 40 electrons for FeSi). Here we neglected the contribution of the nuclei, which is justified due to the large ratio of the nuclear mass compared to the electron mass. We see (inset of fig. 2.11b), that for CoSi the $Nm_e/m^*(\omega)$-curves, for different temperatures, merge above 1000 cm^{-1}, indicating that no transfer of spectral weight from high to low frequencies takes place.

For FeSi (inset of fig. 2.11a), we see a considerable difference in the $Nm_e/m^*(\omega)$-curves for 300 and 4 K, just above the gap region (~ 700 cm^{-1}). A partial recovery of spectral weight can be followed up to approximately 4000 cm^{-1}. Above this frequency no further evolution is observable and the $Nm_e/m^*(\omega)$-curves remain parallel to each other, indicating no recovery of spectral weight in this frequency region. However, we have to keep in mind that above 4000 cm^{-1} the experimental error bars become rather large as a result of uncertainties in the KK analysis, mainly induced by the extrapolations at high frequency [4, 5]. In fact, we could improve our KK analysis on the reflectivity data using the optical conductivity obtained from ellipsometric measurements which were, however, performed

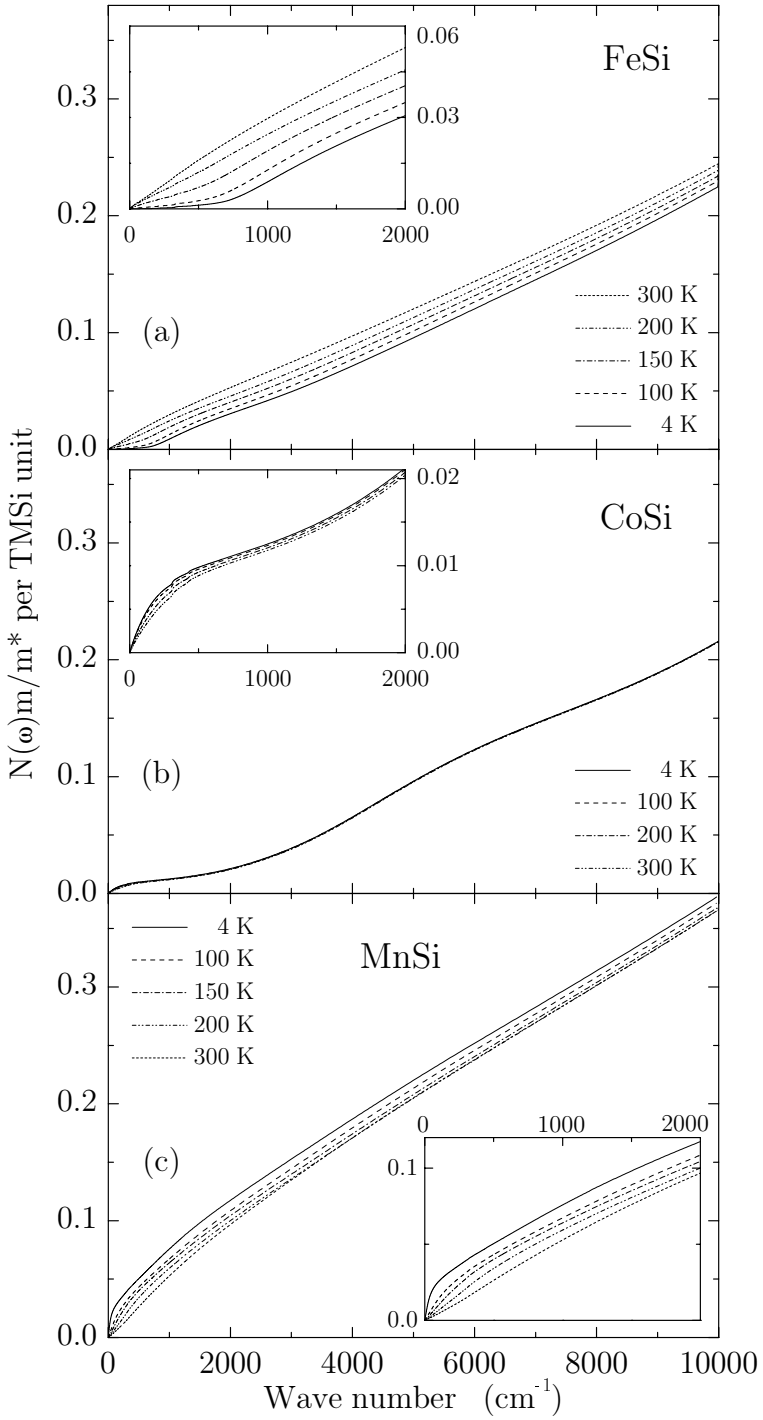

Figure 2.11: *Number of carriers per TMSi versus the frequency ω, obtained from partial integration of the optical conductivity up to ω, for FeSi (a), CoSi (b), and MnSi(c).*

only at room temperature. The high frequency ($\omega > 15\,000$ cm^{-1}) room temperature conductivity data were then used to fix the KK analysis also at low temperature (implicitly assuming no particular temperature dependence above 15 000 cm^{-1}, as suggested by the reflectivity measurements shown in fig. 2.4a). As a consequence, whereas at 300 K the conductivity is accurately determined over the all the frequency range, at low temperature the results are completely reliable only up to 4000 cm^{-1} (in particular, as far as the exact absolute value of conductivity is concerned).

We can then conclude that at $\sim$4000 cm^{-1} only a partial recovery of the spectral weight, lost at low frequencies as a consequence of the opening of the gap, has been observed. The missing fraction must, eventually, reappear at energies higher that $\sim$0.5 eV, an energy scale which is a factor of seven larger than the size of the gap itself. On the basis of this results we believe that, in agreement with Schlesinger *et al.* [4], electron-electron correlations play a relevant role in determining the electric and/or magnetic properties of FeSi, and their temperature dependence. However, for a more precise estimate of the energy scale needed to satisfy the optical sum rule, low temperature ellipsometric measurements are necessary and are, as a matter of fact, currently in progress in our group.

In the case of MnSi (see fig. 2.11c), we can observe a trend 'opposite' to the one shown by FeSi. The $Nm_e/m^*(\omega)$-curve for 4 K is higher than all the others, because of the large increase of spectral weight observed, in the optical conductivity, in the low frequency metallic response at 4 K (see fig. 2.10c). As for FeSi, above 4000 cm^{-1} no further evolution is observable and the $Nm_e/m^*(\omega)$-curves remain parallel to each other. However, for MnSi, the tendency of the different curves to merge at high frequency is more pronounced than for FeSi. Within the accuracy of our Kramers-Kronig analysis, we cannot exclude that a transfer of spectral weight from low to high frequencies takes place, in this material. However, if this were the case, the portion of this spectral weight (and, therefore, the corresponding energy scale), would be smaller than in FeSi.

For FeSi, it seems plausible to associate the temperature dependence of the section between 1000 and 2000 cm^{-1} with the optical conductivity due to thermally induced charge carriers. In fig. 2.12 this number is displayed versus temperature, along with the Hall number of Paschen *et al.* [8]. We display $Nm_e/m^*(\omega)$ for 3 different values of the cutoff frequency ($\omega = 100, 800$ and 2000 cm^{-1}) to demonstrate that the activation energy is independent of frequency. We observe that the Hall number and Nm_e/m^* have approximately the same activation energy of about $200-250$ K.

2.4.3 Activation Energies

In table 2.3 we collect the activation energies and gap values, for FeSi, determined from various spectroscopic data and transport properties. For the tunneling data the gap-value corresponds to the peak-to peak value in the dI/dV versus V curves. In a single particle band picture this value should match the optical and Raman gap. Clearly there is a rather large spread of activation energies. When different temperature ranges are considered, different are also the activation energies obtained. This indicates that the thermal evolution involves a distribution of activation energies.

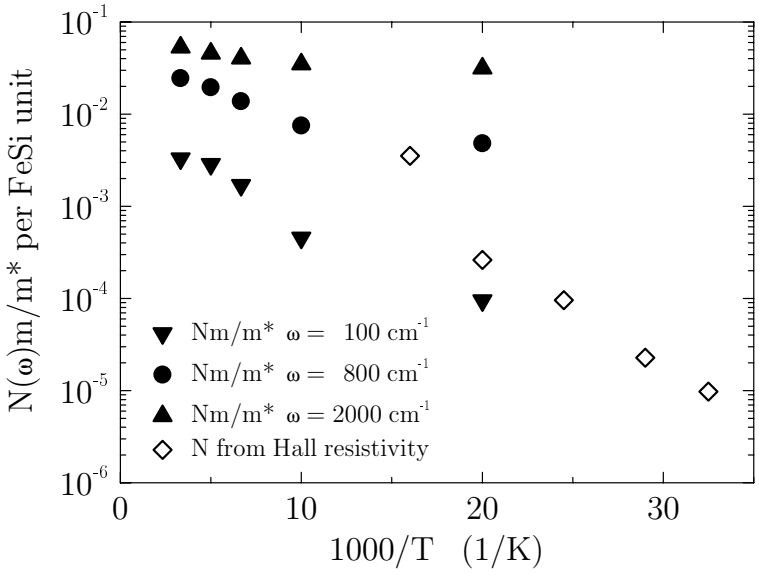

Figure 2.12: *Number of carriers per unit of FeSi from integrating our optical conductivity data (closed symbols), and the Hall conductivity data reported in ref. 8 (open diamonds).*

2.4.4 Transport Properties

The behavior of the electrical resistivity of FeSi, CoSi, and MnSi is quite different (see fig. 2.13 where the DC resistivity data taken from ref. 10 and 35 are plotted). CoSi has a high residual resistance and conventional Bloch-Grüneisen behavior.

For MnSi, the DC resistivity drops monotonically by approximately two orders of magnitude upon cooling the sample from 300 to 4 K. At $T_c = 29$ K a shoulder appears marking the onset of magnetic order, which results in a loss of electronic scattering channels and, therefore, in a stronger decrease of the resistivity.

FeSi shows insulating behavior at low temperature. The DC resistivity $\rho = m^*/(ne^2\tau)$ varies from 2500 to 300 $\mu\Omega cm$ between 100 and 300 K. When combined with the carrier densities of fig. 2.12, we see that τ varies from 4.6 to 10 fs between 100 and 300 K. Note that the same ratio n/m^* appears in the Drude expression as in the expression of the optical carrier density. Hence our result for τ does not depend on assumptions for the effective mass. An estimate of the carrier life-time τ is also obtained from direct inspection of $\sigma(\omega, T)$. As there are no thermally excited carriers at 4K we proceed by subtracting $\sigma(\omega, 4K)$ from the conductivity spectra at higher temperature. In zero th approximation the increase in conductivity upon raising temperature is a Drude-Lorentzian one, due to the thermally excited carriers. At the gap and at the optical phonons frequencies the difference spectra contain quirks due to the shifting of the gap, and to the thermal broadening of the phonons (not shown). Otherwise, the different curves have a half-width of $500 < (2\pi c\tau)^{-1} < 1000$ cm^{-1}, or $10\,\text{fs} > \tau > 5\,\text{fs}$, in good agreement with the lifetime calculated from the DC resistivity.

Let us first explore the possibility that the excited carriers can be described in the

Exp. Method	Source	T (K)	E_a (meV)
Tunneling	Ref. [10]	4	43
IR spectr.	This work	4	35
Raman	Ref. [28]	4	47
K(Si)	Ref. [3]	<800	41
χ(T)	Ref. [1]	<800	68
Q(Fe)	Ref. [3]	<800	46
n(Hall)	Ref. [8]	<100	22
n(IR)	This work	>100	22
$\rho_{\rm DC}$	This work	>100	30

Table 2.3: *Compilation of activation energies observed for FeSi. For tunneling, Raman spectroscopy, and infrared spectroscopy, the indicated value corresponds to the gap divided by two. K(Si) is the activation energy of the Knight shift at the Si nucleus, Q(Fe) of the nuclear quadrupole splitting of Fe observed with Mössbauer spectroscopy.*

same way as in conventional doped semiconductors. The carrier density and k_F are related through $n_e = gk_F^3/(6\pi^2)$, where g is the overall degeneracy factor (valley and spin). Band theory predicts a 12-fold degeneracy of the electron pockets, and an 8-fold degeneracy of the hole pockets [14, 17]. To simplify matters we will ignore possible differences in mass and mobility for electrons and holes. Hence the degeneracy factor entering the optical carrier density is $g = 2\times(8+12) = 40$. The observed density n_e varies from 0.3 to 1.3×10^{21} cm^{-3} ($100-300$ K), implying that k_F varies from 4.9 to 7.5×10^6 cm^{-1}, v_F varies from 5.6 to 8.7×10^4 m/s and E_F varies from 9 to 21 meV. Hence the electrons and holes are approximately nondegenerate throughout this temperature range, as expected for thermal excitation across a semiconductor gap. Using our estimate of v_F we calculate a mean free path of $2.6-9.0$ Å for temperatures in the range $100-300$ K. This mean free path is sufficiently short to smear the momentum of the charge carriers on the scale of the size of the electron and hole pockets ($0.02 < k_F l/(2\pi) < 0.1$), and even sufficient to smear the momentum over the entire Brillouin zone ($0.5 < l/a < 2$). This implies that the conduction of the charge carriers is essentially of the hopping type. However, this small value of l implies that the fine details of the band structure become irrelevant, and the multi-valley character of electron and hole pockets is scrambled, thus invalidating the assumption made on input that $g = 40$.

Let us now compare the absolute values of the carrier density in fig. 2.12 obtained from the Hall effect [8] and from the optical conductivity. If we extrapolate the Hall number to the region between 100 and 300 K, where we have reliable estimates of the optical carrier density(Nm_e/m^*), the Hall number seems to overshoot Nm_e/m^* with a factor of $5-10$. In a semiconductor model with equal electron and hole masses and mobilities, the optical carrier density corresponds to $n_{opt} = n_e + n_h$, whereas $1/n_{Hall} = 1/n_e - 1/n_h$. There is a compensation between electron and hole contributions to the Hall constant, leading to an

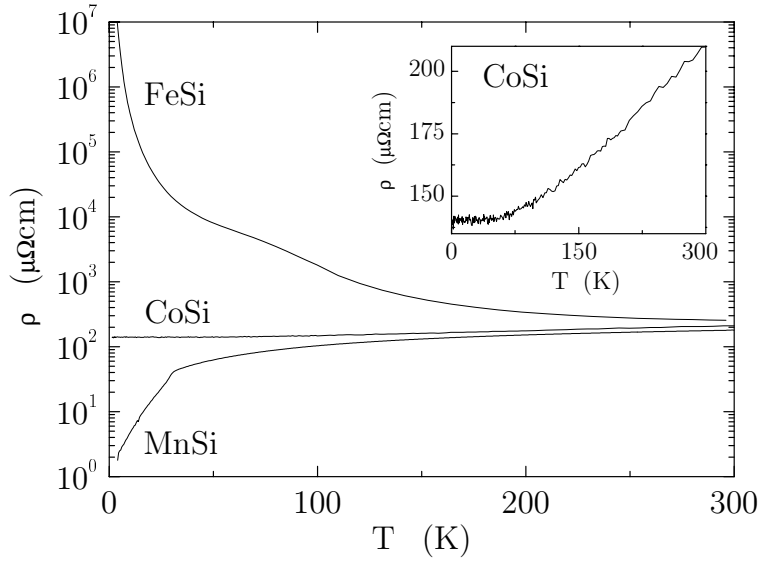

Figure 2.13: *DC resistivity of FeSi, CoSi, and MnSi (all data from ref. 10 and 35).*

experimental Hall number which is always larger than the optical carrier density.

The combination of electron-like Hall conductivity, and short mean free path of the carriers, motivates us to propose a different scenario from the semiconductor picture which we explored above: The effect of raising temperature is to excite electrons to a wide band above the Fermi energy. The holes which are left behind move within a narrow band of (almost) localized states. From the perspective of the effect of doping, the latter states behave in the same way as donor states in a conventional semiconductor, but should be really understood as a narrow band of quasi-atomic states of the transition metal atoms. As we may now ignore the contribution to the charge response of the hole channel (due to the low mobility), the smaller value of the optical carrier density Nm_e/m^* compared to the (extrapolated) Hall number in the $100-300$ K range indicates a moderate effective mass of the mobile charge carriers $m^*/m_e \approx 5-10$. An explicit realization of this situation is the pairing of itinerant electrons with local moments at low temperature to form a lattice of Kondo-singlets [4]. At sufficiently high temperatures, these singlets will be broken into their constituents, i.e., itinerant electrons and local moments. As no mobile charges are associated with the local moments, these moments add a negligible contribution both to the Hall conductivity and the infrared conductivity, so that the dominant contribution comes from the thermally excited itinerant electrons. A natural consequence of having unpaired local moments at higher temperatures is spin-flip scattering of the itinerant electrons, leading to a reduction of the mean free path. This scattering mechanism will be suppressed if the local moments are aligned by the external application of a magnetic field (positive magneto-conductivity).

Motivated by these arguments, we recalculate the carrier properties, with a degeneracy factor $g = 2$ (only spin): k_F now varies from 1.3 to 2.0×10^7 cm^{-1}, v_F varies from 1.5 to 2.4×10^5 m/s, E_F from 66 to 160 meV, l from 7.0 to 25.0 Å, and $k_F l/2\pi$ from 0.15 to 0.8.

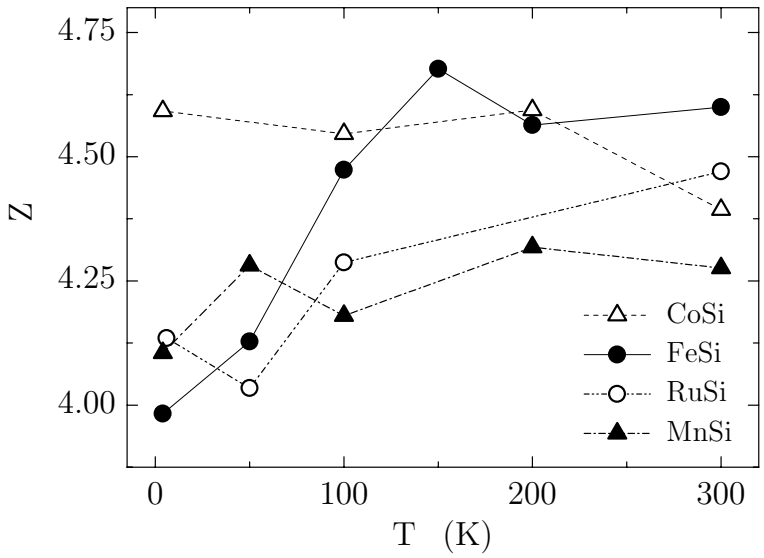

Figure 2.14: *Temperature dependence of the transverse effective charge of Co-Si, Fe-Si, Ru-Si, and Mn-Si pairs, calculated from the oscillator strength of the optical phonons. The points for RuSi were obtained by fitting the optical conductivity data reported in ref. 29.*

2.4.5 Resonating Bonds Coupled to Phonons

In section 2.3.1, we saw that, for FeSi, the steps in the Z^2 curve in fig. 2.6, at frequencies below 1000 cm^{-1}, are due to optical phonons [6]. From the parameters obtained by fitting the phonon peaks to Fano line shapes, we could determine the dynamical (or transverse effective) charge of Fe and Si, for each temperature. For a purely ionic insulator this is also the actual charge of the ions. For a covalent compound with resonating bonds a finite value of the transverse effective charge results from a dynamical charge redistribution associated with the ionic motion of an optical phonon.

For the TM mono-silicides, Pauling has argued that a resonance occurs between the partial bonds of types 2 and 3 (2/3 and 1/3 bonds) [22, 23]. Lucovsky and White have shown (for the IV-VI narrow gap semiconductors) that this phenomenon leads to a high value of the transverse effective charge [30]. Rice, Lipari and Strässler developed the theory for the infrared spectra for phonons coupled to charge excitations [32] (see section 2.3.1).

Experimentally we observed that CoSi and MnSi have phonon spectra very close to the one of FeSi: Not only in terms of number of phonons (the compounds have the same symmetry $P2_13$) and resonant frequencies (the TM elements have comparable atomic weights), but also in terms of the large oscillator strengths. Furthermore, similar results were obtained by Vescoli *et al.* also on RuSi [29]. The resonant frequencies of the four T-symmetry optical modes detected on FeSi, CoSi, MnSi (for $T = 4$ K), and on RuSi (for $T = 6$ K) are summarized in table 2.4.

Repeating the fitting procedure, with Fano line shapes, on the spectra we obtained on CoSi and MnSi, and on those reported in ref. 29 for RuSi, we could calculate the

FeSi	This work	207	329	347	454
CoSi	This work	227	309	350	427
MnSi	This work	200	317	346	449
RuSi	Ref. [29]	203	305	324	449

Table 2.4: *Resonant frequencies (in cm^{-1}) of the infrared phonon modes observed on FeSi, CoSi, and MnSi, at 4 K (from the optical spectra presented in this chapter). For RuSi, the values were obtained by fitting the optical data reported in ref. 29, for T=6 K.*

temperature dependent effective charge Z for all these materials. The results are displayed all together in fig. 2.14, where we can see that a large value of more than 4 is found, for Z, on all these TM mono-silicides. Based on the electronegativities and from the observed atomic radii (see table 2.1 and fig. 2.2), there can be almost no charge transfer between the transition metal atom and Si in these compounds. Hence, we attribute the large value of the transverse effective charge to a dynamical coupling of the optical phonons to electronic resonances. This requires that at least some of the bonds between the TM and the Si ions are incomplete. The enhancement of transverse effective charge is then due to a coupling of the ionic displacement to charge flow between the unsaturated bonds.

2.5 The Electronic Structure of TM Mono-Silicides

From ab initio band structure calculations for FeSi it is known that, in these materials, the Si $3s$ states are fully occupied and have a binding energy of about 10 eV. The Si $3p$ states are partially occupied and form with the TM-states a complex manifold of bands.

According to a famous rule from the theory of Mott-Hubbard metal-insulator transitions, the atomic description of the TM atom becomes the appropriate ansatz if the on-site correlation energy exceeds the bandwidth. For the TM silicides the bandwidth is of order 6 eV, and U^{eff} is of the same order of magnitude. The silicides, therefore, seem to provide a border case. A band description, where the correlation effects are taken into account perturbatively, has been used by several investigators [15–17, 39, 40]. In this section, we want to explore a more intuitive approach based on an atomistic picture.

In their elemental metallic phase the TM atoms have approximately a $d^{n-2}s^2$ configuration, with n the number of valence electrons per atom. From the d-shell radii displayed in fig. 2.2, we can see that in the whole series the d-shell radius [41] falls well below the atomic radius, which implies that the d-shells exhibit quasi atomic characteristics due to shielding by the outer s and p-shells. Due to the low site symmetry of the TM atoms, mixing of s, p and d-character occurs in the eigenstates. For the purpose of compactness of notation we will label the TM valence bands as d-states. We will assume that these states have quasi-atomic characteristics, so that we can use a ligand field description to describe the influence of the Si-matrix. For the purpose of bookkeeping of the actual d-

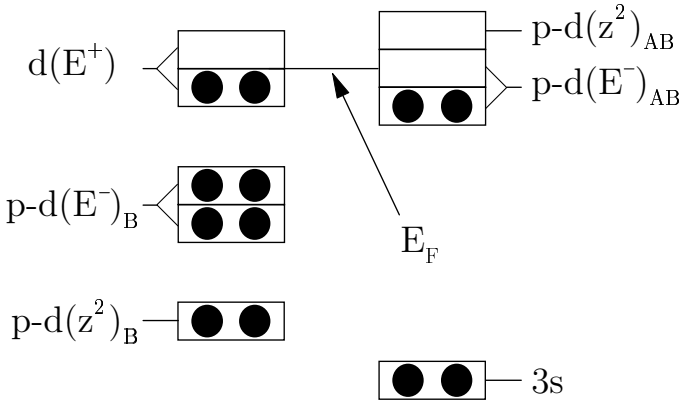

Figure 2.15: *Schematic diagram of the energy levels in TMSi. The situation with two electrons in the d(E$^+$) level, which is displayed here, corresponds to FeSi.*

and *sp*-count of the atoms, it is important to take into account the relative contribution of s and p character to the d-states.

With this approach, we arrive to the following scenario: Each TM atom contributes five d-states and n electrons. In the case of FeSi: $n=8$. Each Si contributes three $3p$ states and four electrons. Due to the 3-fold rotation symmetry the five d-states are grouped in a single degenerate $d_0(z^2)$ state, and two groups of doubly degenerate levels (E^+ and E^-) corresponding to linear combinations of d_{-2}, d_{-1}, d_1, and d_2. Here we adopted a local reference frame with the z-axis oriented along the 3-fold rotation axis which pierces the TM atom. Of the surrounding shell of seven Si atoms, only the $3p$ orbitals with their lobes pointing toward the transition metal atom couple to the TM states. Thus seven ligand orbitals are engaged in bonds with the TM-atom. We indicate the ligand of type 1 as $|L_{0,1}\rangle$. Taking into account the hopping τ between the Si atoms at relative angles $\phi = 0, \pi/3$ and $2\pi/3$, we obtain the ligand-states of types $j=2,3$ [42]:

$$\begin{aligned}
|L_{0,j}\rangle &= |p_0\rangle + |p_{+\pi/3}\rangle + |p_{-\pi/3}\rangle \ , & E_0 &= \epsilon_p - 2\tau \ ; \\
|L_{+,j}\rangle &= |p_0\rangle + e^{2\pi i/3}|p_{+\pi/3}\rangle + e^{-2\pi i/3}|p_{-\pi/3}\rangle \ , & E_+ &= \epsilon_p + \tau \ ; \\
|L_{-,j}\rangle &= |p_0\rangle + e^{-2\pi i/3}|p_{+\pi/3}\rangle + e^{2\pi i/3}|p_{-\pi/3}\rangle \ , & E_- &= \epsilon_p + \tau \ .
\end{aligned} \tag{2.7}$$

The degeneracy between the ligand states $|L_{\pm,j}\rangle$ with j=2 and j=3 is lifted due to a finite hopping probability between these groups: $\langle L_{\pm 2}|H|L_{\pm,3}\rangle = \tau'$.

The dependence on the angular coordinate ϕ of the hopping integral, between the $d_{\pm 2}$ ($d_{\pm 1}$) and the ligand $3p$ orbital, is $e^{\pm 2i\phi}$ ($e^{\pm i\phi}$). The angle η_j identifies the orientation of the two rings of ligand Si atoms: $\eta_j = 0°, 24°$ for type $j=2,3$, respectively. The resulting (nonzero) hopping matrix elements between the ligand orbitals and the central TM atom are, with this choice of local reference frame [42]:

$$\begin{aligned}
\langle d_0|H|L_{0,j}\rangle &= t_{0,j} \ , \\
\langle d_{\pm 1}|H|L_{\pm,j}\rangle &= t_{1,j} e^{\mp i\eta_j} \ , \\
\langle d_{\pm 2}|H|L_{\pm,j}\rangle &= t_{2,j} e^{\pm 2i\eta_j} \ .
\end{aligned} \tag{2.8}$$

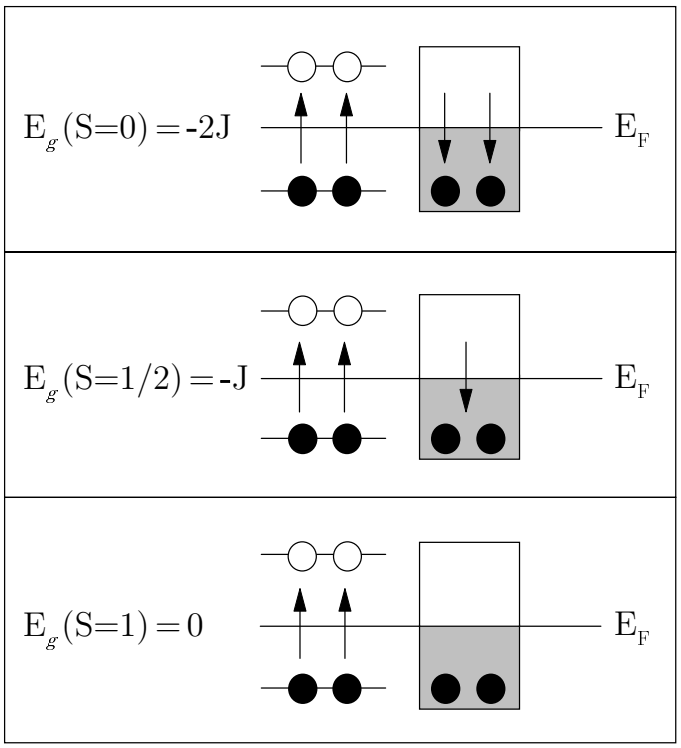

Figure 2.16: *Schematic diagram of the relevant low energy degrees of freedom of FeSi. The top panel corresponds to the singlet low temperature phase, the bottom panel to the high temperature S=1 phase, and the middle panel represents an intermediate situation with a partial compensation of the local moment.*

All other matrix elements are zero. In principle, all ligand combinations of the $TMSi_7$ cluster are shared between neighboring TM-sites and form bands. Due to the angle of $\simeq 70^\circ$ between the bonds of types 2 and 3, we anticipate that a linear combination of $d_{\pm 1}$ and $d_{\pm 2}$ exists, which has a strongly reduced hopping matrix element to the cluster of ligand orbitals, resulting in a (doubly degenerate) non-bonding orbital of a quasi-atomic character. The resulting level scheme of hybrid TM-ligand character is sketched in fig. 2.15. The single (per TM atom) axial bonding orbitals of $d_0 - L(1)$ character have the highest binding energy, followed by a band containing the two states of bonding $d(E^-) - L_\pm(2,3)$ character. Around E_F we find a combined partially occupied anti-bonding band, containing three states in total. Finally two non-bonding $d(E^+)$ states are located at E_F. With a finite value for the hopping parameter of these states to the ligand orbitals taken into account, the latter states form a narrow band. Provided that the width of this band is sufficiently small, it behaves as a lattice of quasi-atomic open shells obeying Hund's rules. The observation that two quasi-atomic d-states with two electrons per Fe atom should exist in FeSi was originally made by Pauling, using a different line of arguing based on his analysis of the valence bond sums [22, 23].

We conjecture, that these sub-shells are filled step by step in the series CrSi (zero

electrons/atom) up to NiSi (four electrons/atom). This leaves two electrons per Si atom to populate the more itinerant anti-bonding band at E_F. This partly filled anti-bonding band corresponds to partial bonds of type 2 and 3, and is responsible for the strong enhancement of the transverse dynamical charge in CoSi and FeSi [6, 42].

This scenario provides a qualitative argument why the same crystal structure is observed from CrSi up to NiSi: only if electrons are added to -or removed from- the itinerant anti-bonding band, chemical bonds are affected, and the FeSi structure is de-stabilized. Addition or removal of electrons from this wide band will not take place unless the $d(E^+)$ sub-shell is either completely full or empty, e.g., for VSi or CuSi.

In fig. 2.16 the relevant elements for the low energy scale are sketched: One local moment with $S=1$ at every site, exchange-coupled to a band with two conduction electrons per site. It is now possible to understand the high spin state of FeSi at elevated temperatures: The electrons in the itinerant band contribute a Pauli-paramagnetic susceptibility, which is small. According to Hund's rules the two electrons in the $d(E^+)$ sub-shell are in a triplet configuration (see fig. 2.16, bottom panel), thus providing the Curie-susceptibility with $S=1$ and $g=2$, which has been observed at high temperatures [1]. At low temperature, the local moment ($S=1$) on the Fe site is completely compensate by the itinerant electrons of the anti-bonding band, and a Kondo singlet is formed (see fig. 2.16, top panel). At intermediate temperatures, only a partial compensation of the local moment is present (see fig. 2.16, middle panel).

2.6 Discussion

In the course of this chapter, we showed that several experimental results obtained on FeSi indicate that electron-electron correlations play an important role in the physics of this compound [1,4–13]. However, whereas band-structure calculations failed in describing the temperature dependence of the electronic and magnetic properties, they could at least reproduced a gap of the correct order of magnitude [14–17]. In this respect, as on-site correlations are of the order of the bandwidth, FeSi seems to provide a border case in between classical band insulators and Mott-Hubbard insulators. A direct evidence for this situation came from the investigation of the metal-insulator transition in Al-doped FeSi [43,44]. In fact, DiTusa *et al.* [43,44] could observe such a transition on FeSi with the chemical substitution of Al at the Si site: They showed that, for Al concentrations ≥ 0.01, the properties of the system are very similar to those of classical doped semiconductors, the major difference being a considerably enhanced value of the carrier effective mass [43, 44].

On the basis of the discussion of the electronic properties of the TM mono-silicides and, in particular, of the enhanced transverse effective charge suggesting a coupling of ionic displacements to the charge flow between unsaturated bonds, we proposed an atomistic description for the electronic configuration of this class of materials. In our opinion this framework, which shows the fundamental role of a doubly degenerate quasi-atomic d-state located at E_F, provides a basis for understanding the observed range of chemical stability of these compounds (from CrSi to NiSi), and the physical properties of FeSi.

On the other hand, within our simplified approach based on the $TMSi_7$ cluster, it is not possible to fully understand all the experimental features: In particular, the different evolution of the low frequency optical weight observed, upon reducing the temperature, for FeSi (i.e., decrease), MnSi (i.e., increase), and CoSi (i.e., weak increase). In order to address this specific point, a treatment beyond the single $TMSi_7$ cluster should be performed.

In this respect, very interesting are the results obtained by Rozenberg *et al.* by considering the Hubbard model and the periodic Anderson model, within the local impurity self-consistent approximation [45]. Working in the limit of large U^{eff}, in order to model correlated electron systems where the low frequency optical response is dominated by orbitals of localized character, they obtained that a noticeable temperature dependence affects the optical conductivity for both the Hubbard and the Anderson lattice model [45]. In particular, in the case of the Hubbard model the low frequency spectral weight increases upon reducing the temperature and the system becomes more metallic (e.g., as observed on MnSi). In the case of the periodic Anderson model, it decreases as a consequence of the system opening a gap and becoming insulating (e.g., as observed on FeSi) [45]. Rozenberg *et al.* showed that the unusual transfer of spectral weight results from the emergence of a small Kondo energy scale in both Hubbard and periodic Anderson model [45].

2.7 Conclusions

We have investigated the optical response of FeSi, CoSi, and MnSi. Whereas on CoSi and MnSi we observed a metallic behavior at any temperature, on FeSi we could follow the opening of a gap of the order of 70 meV, upon reducing the temperature below 100 K.

On the basis of a group theoretical analysis, all the sharp absorption peaks detected in the far-infrared region have been assigned to optically active lattice excitations. The position, oscillator strength and asymmetry of the phonons were analyzed using the Fano model. The large value of the transverse effective charge ($e_T^* \approx 4e$) obtained on all compounds, along with the resonance behavior of the phonon parameters, observed on FeSi when the gap sweeps through the phonon-frequency, provides strong evidence for a moderate coupling between the vibrational degrees of freedom and low energy electron-hole excitations in these compounds ($\lambda \approx 0.1$, in FeSi).

Based on the discussion of the infrared spectra presented in this chapter and of published transport data, we provided a qualitative model for the electronic structure of the TM mono-silicides. The main conclusion is that six electrons per transition metal atom are engaged in chemical bonds to the Si sublattice. The remaining electrons of the TM atoms (e.g., two for FeSi) occupy a doubly degenerate quasi-atomic d-state, and obey Hund's rules. The conduction band supports two weakly bound itinerant electrons (mainly Si $3p$ character) which, in the case of FeSi, compensate the local moment at low temperatures by forming a Kondo singlet. This framework provides a basis for understanding the observed range of chemical stability of these compounds (from CrSi to NiSi), and the physical properties of FeSi.

References

[1] V. Jaccarino, G.K. Wertheim, J.H. Wernick, L.R. Walker, and S. Arajs, Phys. Rev. **160**, 476 (1967).

[2] H. Watanabe, H. Yamamoto, and K. Ito, J. Phys. Soc. Jpn. **18**, 995 (1963).

[3] G.K. Wertheim, V. Jaccarino, J.H. Wernick, J.A. Seitchik, H.J. Williams, and R.C. Sherwood, Phys. Lett. **18**, 89 (1965).

[4] Z. Schlesinger, Z. Fisk, Hai-Tao Zhang, M.B. Maple, J.F. DiTusa, and G. Aeppli, Phys. Rev. Lett. **71**, 1748 (1993).

[5] L. Degiorgi, M.B. Hunt, H.R. Ott, M. Dressel, B.J. Feenstra, G. Grüner, Z. Fisk, and P. Canfield, Europhys. Lett. **28**, 341 (1994).

[6] A. Damascelli, K. Schulte, D. van der Marel, and A.A. Menovsky, Phys. Rev. B **55**, R4863 (1997).

[7] A. Lacerda, H. Zhang, P.C. Canfield, M.F. Hundley, Z. Fisk, J.D. Thompson, C.L. Seaman, M.B. Maple, and G. Aeppli, Physica B **186-188**, 1043 (1993).

[8] S. Paschen, E. Felder, M.A. Chernikov, L. Degiorgi, H. Schwer, H.R. Ott, D.P. Young, J.L. Sarrao, and Z. Fisk, Phys. Rev. B **56**, 12 916 (1997).

[9] M.A. Chernikov, E. Felder, S. Paschen, A.D. Bianchi, H.R. Ott, J.L. Sarrao, D. Mandrus, and Z. Fisk, Physica B **230**, 790 (1997).

[10] M. Fäth, J. Aarts, A.A. Menovsky, G.J. Nieuwenhuys, and J.A. Mydosh, Phys. Rev. B **58**, 15 483 (1998).

[11] P. Samuely, P. Sazabó, M. Mihalik, N. Hudáková, and A.A. Menovsky, Physica B **218**, 185 (1996).

[12] K. Breuer, S. Messerli, D. Purdie, M. Garnier, M. Hengsberger, Y. Baer, and M. Mihalik, Phys. Rev. B **56**, R7061 (1997).

[13] C.-H. Park, Z.-X. Shen, A.G. Loeser, D.S. Dessau, D.G. Mandrus, A. Migliori, J. Sarrao, and Z. Fisk, Phys. Rev. B **52**, R16 981 (1995).

[14] L.F. Mattheiss, and D.R. Hamann, Phys. Rev. B **47**, 13 114 (1993).

[15] C. Fu, M.P.C.M. Krijn, and S. Doniach, Phys. Rev. B **49**, 2219 (1994).

[16] C. Fu, and S. Doniach, Phys. Rev. B **51**, 17 439 (1995).

[17] V.I.Anisimov, S.Yu. Ezhov, I.S. Elfimov, I.V. Solovyev, and T.M. Rice, Phys. Rev. Lett. **76**, 1735 (1996).

[18] G. Aeppli, and Z. Fisk, Comments Condens. Matter Phys. **16**, 155 (1992).

[19] G. Aeppli, in *Strongly Correlated Electron Materials*, edited by K. S. Bedell *et al.* (Addison-Wesley, Reading, MA, 1994), p. 3.

[20] Ru, Os, RhSi: K. Göransson, I. Engström, and B. Noläng, J. Alloys and Compounds **210**, 107 (1995); ReSi: R.A. Mc Nees, and A.W. Searcy, J. Am. Chem. Soc. **77**, 4290 (1955); Cr, Mn, Fe, Co, NiSi: B. Borén, Ark. Kemi Min. Geol. **11A**, 1 (1933).

[21] W.B. Pearson, *Crystal Chemistry and Physics of Metals and Alloys* (Wiley, 1972).

[22] L. Pauling, and A.M. Soldate, Acta Cryst. **1**, 212 (1948).

[23] L. Pauling, *The Nature of the Chemical Bond* (Cornell U.P., Ithaca, New York, 1960).

[24] W. G. Fately, F.R. Dollish, N.T. McDevit, and F.F. Bentley, *Infrared and Raman Selection Rules for Molecular and Lattice Vibrations: The Correlation Method* (Wiley-Interscience, New York, 1972).

[25] A. Damascelli, K. Schulte, D. van der Marel, M. Fäth, and A.A. Menovsky, Physica B **230-232**, 787 (1997).

[26] A.A. Menovsky, and J.J.M. Franse, J. Cryst. Growth **65**, 286 (1983).

[27] F. Wooten, *Optical Properties of Solids* (Academic Press, New York, 1972).

[28] P. Nyhus, S.L. Cooper, and Z. Fisk, Phys. Rev. B **51**, 15 626 (1995).

[29] V. Vescoli, L. Degiorgi, B. Buschinger, W. Guth, C. Geibel, and F. Steglich, Solid State Comm. **105**, 367 (1998).

[30] G. Lucovsky, and R.M. White, Phys. Rev. B **8**, 660 (1973).

[31] R.A. de Groot, private communication.

[32] M.J. Rice, N.O. Lipari, and S. Strässler, Phys. Rev. Lett. **39**, 1359 (1977).

[33] U. Fano, Phys. Rev. **124**, 1866 (1961).

[34] M.J. Rice, private communication.

[35] M. Fäth, Ph.D. Thesis, University of Leiden, in preparation (1999).

[36] Y. Ishikawa, K. Tajima, D. Bloch, and M. Roth, Solid State Comm. **19**, 525 (1976).

[37] K. Motoya, H. Yasuoka, Y. Nakamura, and J.H. Wernick, Solid State Comm. **19**, 529 (1976).

[38] F.A.Sidorenko *et al.*, Soviet Phys. J. **12**, 329 (1969); Z.Radovskii *et al.*, Soviet Phys. J. **8**, 98 (1965); G. Ofëx, J. Phys. Radium **9**, 37 (1938).

[39] Y. Takahashi, and T. Moriya, J. Phys. Soc. Japan **46**, 1451 (1979).

[40] S.N. Evangelou, and D.M. Edwards, J. Phys. C **16**, 2121 (1983).

[41] D. van der Marel, and G.A. Sawatzky, Phys. Rev. B **37**, 10 674 (1988).

[42] D. van der Marel, A. Damascelli, K. Schulte, and A.A. Menovsky, Physica B **244**, 138 (1998).

[43] J.F. DiTusa, K. Friemelt, E. Bucher, G. Aeppli, and A.P. Ramirez, Phys. Rev. Lett. **78**, 2831 (1997).

[44] J.F. DiTusa, K. Friemelt, E. Bucher, G. Aeppli, and A.P. Ramirez, Phys. Rev. B **58**, 10 288 (1998).

[45] M.J. Rozenberg, G. Kotliar, and H. Kajueter, Phys. Rev. B **54**, 8452 (1996).

Chapter 3

Optical Spectroscopy of $CuGeO_3$

In 1993 $CuGeO_3$ was recognized, on the basis of magnetic susceptibility measurements [1], as the first inorganic compound showing a spin-Peierls (SP) phase transition, i.e., a lattice distortion (due to the magneto-elastic coupling between the one-dimensional spin system and the three-dimensional phonon system) that occurs together with the formation of a spin-singlet ground state and the opening of a finite energy gap in the magnetic excitation spectrum. This magneto-elastic transition is driven by the magnetic energy gain due to dimerization of the antiferromagnetic (AF) exchange between the spin 1/2 moments of the Cu^{2+} ions (arranged in weakly coupled one-dimensional (1D) CuO_2 chains in this material [2]), which overcompensates the elastic energy loss resulting from the deformation of the lattice [3, 4]. In the SP ordered phase, the Cu^{2+} magnetic moments form singlet dimers along the chains and spin triplet excitations are gapped [1].

The SP nature of the phase transition in $CuGeO_3$ was inferred from the isotropic drop in the magnetic susceptibility at the transition temperature T_{SP}=14 K, and from the reduction of T_{SP} upon increasing the intensity of an applied magnetic field [1], as theoretically expected for SP systems [3–6]. This initial claim was later confirmed by an impressive variety of experimental results [7]. The gap in the magnetic excitation spectrum was directly observed with inelastic neutron scattering [8], and the singlet-triplet nature of the gap was established with the same technique under application of a magnetic field: A splitting of the single gap into three distinct excitation branches was clearly detected [9]. The dimerization of the Cu^{2+} ions was observed and the lattice distortion very carefully investigated with both neutron and x-ray scattering [10–12]. Finally, the phase transition from the dimerized to the incommensurate phase, expected in magnetic fields higher than a certain critical value [5,6], was found with field-dependent magnetization measurements at $H_c \approx 12$ T [13], and the H-T phase diagram was studied in great detail [14].

The discovery of the SP phase transition in $CuGeO_3$ has renewed the interest in this phenomenon, observed previously in organic materials in the 1970's [15–17], because the availability of large high-quality pure and doped single crystals of $CuGeO_3$ made it possible to investigate this magneto-elastic transition by a very broad variety of experimental techniques. This way, the traditional SP theory [3–5] based on 1D AF chains with only nearest-neighbor (nn) magnetic couplings and a mean-field treatment of the 3D phonon

system, could be tested in all its expectations for a deeper understanding of the problem.

Also optical techniques, like Raman and infrared spectroscopy, are very useful in investigating magnetic and/or structural phase transitions. Information on the nature of the electronic (magnetic) ground state, lattice distortion and interplay of electronic (magnetic) and lattice degrees of freedom can be obtained studying in detail the electronic (magnetic) excitations and the phonon spectrum, as a function of temperature. The aim of our experimental investigation of $CuGeO_3$ with optical spectroscopy was, of course, to detect all possible 'infrared signatures' of the SP phase transition in this material. However, we were in particular interested in a number of issues which could help us in understanding how far the classical SP picture [3,4] is appropriate for the case of $CuGeO_3$, namely:

- Analysis of the phonon spectrum in order to study the lattice distortion and to verify the proposed crystal structures for both the high and the low temperature phase.

- Verify the presence of a soft mode in the phonon spectrum, upon passing through the SP transition. In fact, a well-defined soft mode is expected in those theoretical models describing a SP system in terms of a linear coupling between lattice and magnetic degrees of freedom [4,5].

- Detect possible magnetic bound states and/or a magnetic continuum in the excitation spectrum which could tell us about the symmetry and the order (nnn versus nn) of the magnetic interactions.

- Study the influence of doping on the vibrational and electronic properties.

Before proceeding to the experimental results [18, 19], we will present, in the next section, the outcome of a group theoretical analysis [19], which will be useful in the discussion of the phonon spectrum. In fact, the number and the symmetry of the infrared and Raman active phonons expected for the proposed high-temperature undistorted phase [2] and the low-temperature SP phase [11,12] of $CuGeO_3$ can be obtained from a group theoretical analysis of the lattice vibrational modes. The results of this calculation will later be compared to the experimental data.

3.1 Group Theoretical Analysis

At room temperature the orthorhombic crystal structure with lattice parameters a=4.81 Å, b=8.47 Å, and c=2.941 Å and space group $Pbmm$ ($x\|a$, $y\|b$, $z\|c$) or, equivalently, $Pmma$ ($x\|b$, $y\|c$, $z\|a$) in standard setting, was proposed for $CuGeO_3$ [2]. The building blocks of the structure are edge-sharing CuO_6 octahedra and corner-sharing GeO_4 tetrahedra stacked along the c axis of the crystal and resulting in Cu^{2+} and Ge^{4+} chains parallel to the c axis. These chains are linked together via the O atoms, and form layers parallel to the b-c plane weakly coupled along the a axis (fig. 3.1). The unit cell contains 2 formula units of $CuGeO_3$ (fig. 3.2), with site group C_{2h}^y for the 2 Cu atoms, C_{2v}^z for the 2 Ge and the 2 O(1) atoms, and C_s^{xz} for the 4 O(2) atoms [where O(2) denotes the O atoms linking

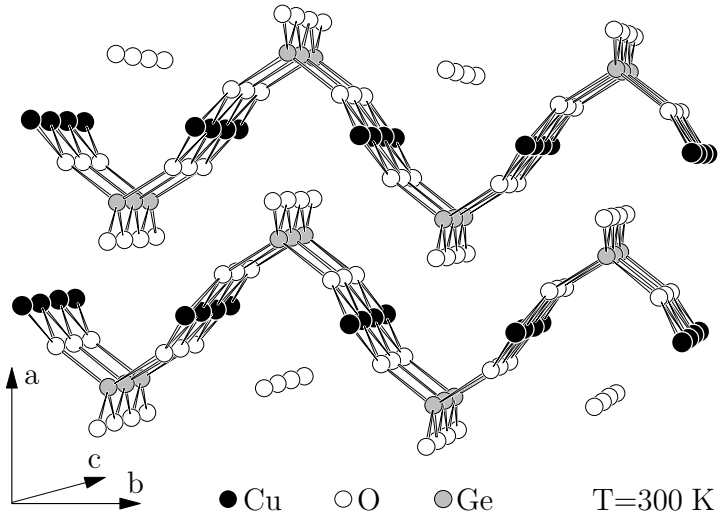

Figure 3.1: *Crystal structure of $CuGeO_3$ in the high temperature (T=300 K) undistorted phase.*

the chains together] [11, 12]. A group theoretical analysis can be performed, working in standard orientation, to obtain the number and the symmetry of the lattice vibrational modes. Following the nuclear site group analysis method extended to crystals [20], the contribution of each occupied site to the total irreducible representation of the crystal is:

$$\begin{aligned}
\Gamma_{\mathrm{Cu}} &= A_u + 2B_{1u} + B_{2u} + 2B_{3u} \ , \\
\Gamma_{\mathrm{Ge+O(1)}} &= 2[A_g + B_{1u} + B_{2g} + B_{2u} + B_{3g} + B_{3u}] \ , \\
\Gamma_{\mathrm{O(2)}} &= 2A_g + A_u + B_{1g} + 2B_{1u} + 2B_{2g} + B_{2u} + B_{3g} + 2B_{3u} \ .
\end{aligned} \tag{3.1}$$

Subtracting the silent modes ($2A_u$) and the acoustic modes (B_{1u}+B_{2u}+B_{3u}), the irreducible representation of the optical vibrations in standard setting ($Pmma$), is:

$$\begin{aligned}
\Gamma = &\, 4A_g(aa, bb, cc) + B_{1g}(bc) + 4B_{2g}(ab) + 3B_{3g}(ac) \\
&+ 5B_{1u}(E\|a) + 3B_{2u}(E\|c) + 5B_{3u}(E\|b) \ .
\end{aligned} \tag{3.2}$$

This corresponds to an expectation of 12 Raman active modes ($4A_g + B_{1g} + 4B_{2g} + 3B_{3g}$) and 13 infrared active modes ($5B_{1u} + 3B_{2u} + 5B_{3u}$) for $CuGeO_3$, in agreement with the calculation done by Popović *et al.* [21].

At temperatures lower than T_{SP} the proposed crystal structure is still orthorhombic, but with lattice parameters $a' = 2 \times a$, $b' = b$ and $c' = 2 \times c$ and space group $Bbcm$ ($x\|a$, $y\|b$, $z\|c$) or , equivalently, $Cmca$ ($x\|c$, $y\|a$, $z\|b$) in standard setting [11, 12]. The distortion of the lattice taking place at the phase transition (fig. 3.2) is characterized by the dimerization of Cu-Cu pairs along the c axis (dimerization out of phase in neighboring chains), together with a rotation of the GeO_4 tetrahedra around the axis defined by the O(1) sites (rotation opposite in sense for neighboring tetrahedra). Moreover, the O(2) sites of the undistorted structure split in an equal number of O(2a) and O(2b) sites, distinguished by the distances

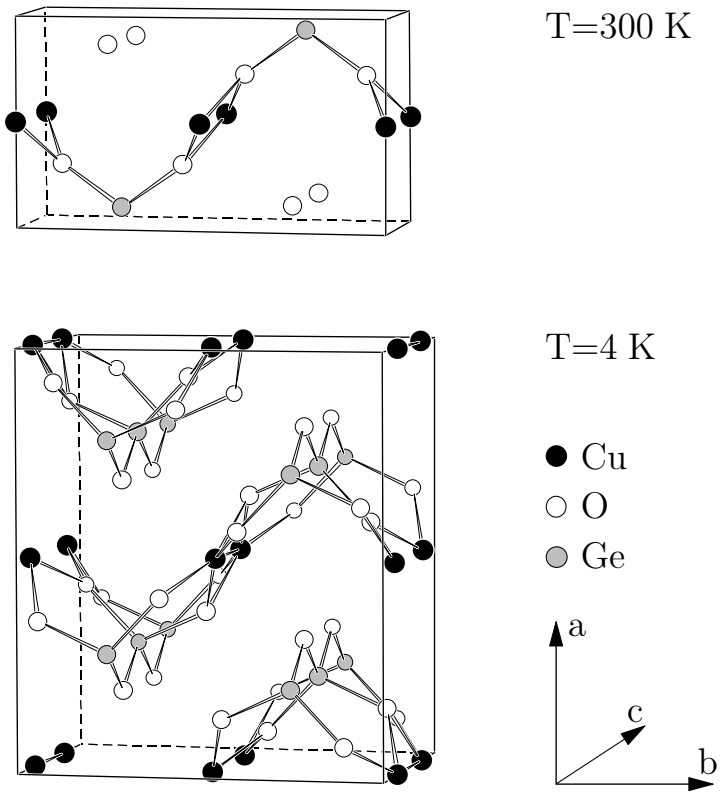

Figure 3.2: *Conventional unit cell of $CuGeO_3$ in the undistorted (top) and SP phase (bottom). For clarity purpose, the ion displacements due to the SP transition have been enlarged by a factor of 30.*

O(2a)-O(2a) and O(2b)-O(2b) shorter and larger than O(2)-O(2) [12], respectively. The SP transition is also characterized (fig. 3.2) by a doubling of the unit cell (corresponding to a doubling of the degrees of freedom from 30 to 60); the site groups in the new unit cell are: C_2^x for Cu, C_2^y for O(1), and C_s^{yz} for Ge, O(2a) and O(2b) [12]. Repeating the group theoretical analysis we obtain for the contributions to the total irreducible representation:

$$\begin{aligned}
\Gamma_{\mathrm{Cu}} &= A_g + A_u + 2B_{1g} + 2B_{1u} + 2B_{2g} + 2B_{2u} + B_{3g} + B_{3u} \ , \\
\Gamma_{\mathrm{Ge+O(2a)+O(2b)}} &= 3[2A_g + A_u + B_{1g} + 2B_{1u} + B_{2g} + 2B_{2u} + 2B_{3g} + B_{3u}] \ , \\
\Gamma_{\mathrm{O(1)}} &= A_g + A_u + 2B_{1g} + 2B_{1u} + B_{2g} + B_{2u} + 2B_{3g} + 2B_{3u} \ .
\end{aligned} \tag{3.3}$$

The irreducible representation of the optical vibrations of $CuGeO_3$ in the SP phase in standard setting (*Cmca*), is:

$$\begin{aligned}
\Gamma_{\mathrm{SP}} = &\, 8A_g(aa,bb,cc) + 7B_{1g}(ac) + 6B_{2g}(bc) + 9B_{3g}(ab) \\
&+ 9B_{1u}(E\|b) + 8B_{2u}(E\|a) + 5B_{3u}(E\|c) \ .
\end{aligned} \tag{3.4}$$

Therefore 30 Raman active modes ($8A_g+7B_{1g}+6B_{2g}+9B_{3g}$) and 22 infrared active modes ($9B_{1u}+8B_{2u}+5B_{3u}$) are expected for $CuGeO_3$ in the SP phase, all the additional vibrations being zone boundary modes activated by the folding of the Brillouin zone.

In order to compare the results obtained for the undistorted and the SP phase of $CuGeO_3$, it is better to rewrite the irreducible representations Γ and Γ_{SP} into *Pbmm* and *Bbcm* settings, respectively, because both groups are characterized by: $x\|a$, $y\|b$ and $z\|c$. This can be done by permuting the $(1g, 2g, 3g)$ and $(1u, 2u, 3u)$ indices in such a way that it corresponds to the permutations of the axis relating *Pmma* to *Pbmm* and *Cmca* to *Bbcm*. Therefore, the irreducible representations of the optical vibrations of $CuGeO_3$, for $T > T_{SP}$ (*Pbmm*) and $T < T_{SP}$ (*Bbcm*), respectively, are:

$$\begin{aligned}\Gamma' = &\, 4A_g(aa, bb, cc) + 4B_{1g}(ab) + 3B_{2g}(ac) + B_{3g}(bc) \\ &+ 3B_{1u}(E\|c) + 5B_{2u}(E\|b) + 5B_{3u}(E\|a) \ ,\end{aligned} \tag{3.5}$$

$$\begin{aligned}\Gamma'_{SP} = &\, 8A_g(aa, bb, cc) + 9B_{1g}(ab) + 7B_{2g}(ac) + 6B_{3g}(bc) \\ &+ 5B_{1u}(E\|c) + 9B_{2u}(E\|b) + 8B_{3u}(E\|a) \ .\end{aligned} \tag{3.6}$$

It is now evident that the number of infrared active phonons is expected to increase from 5 to 8, 5 to 9 and 3 to 5 for light polarized along the a, b and c axes, respectively.

3.2 Experimental

We investigated the optical properties of several $Cu_{1-\delta}Mg_\delta GeO_3$ (with $\delta = 0, 0.01$), and $CuGe_{1-x}B_xO_3$ [with B=Si ($x = 0, 0.007, 0.05, 0.1$), and Al ($x = 0, 0.01$)] single crystals, in the frequency range 20 - 32 000 cm^{-1}. These high-quality single crystals, several centimeters long in the a direction, were grown from the melt by a floating zone technique [22]. Plate-like samples were easily cleaved perpendicularly to the a axis. Typical dimensions were about 2 and 6 mm parallel to the b and c axis, respectively. The thickness was chosen in dependence of the experiment to be performed. In reflectivity measurements, when enough material was available, several millimeters thick samples were used in order to avoid interference fringes in the spectra, due to Fabry-Perot resonances [23]. Particular attention had to be paid when measuring reflectivity in frequency regions characterized by weak excitations (i.e., from 1000 to 25 000 cm^{-1}): Because of the multiple reflections within the sample these excitations, which would not be directly detectable in reflectivity, would be observable as an absorption with respect to the background dominated by the interference fringes. If a Kramers-Kronig transformation is performed on such a pathological data in order to obtain the optical conductivity, unphysical results would be produced. As a matter of fact, it is precisely for this reason that a charge-transfer excitation at 1.25 eV (10 000 cm^{-1}) was erroneously reported in one of the early optical papers on $CuGeO_3$ [24]. On the other hand, in transmission measurements, where interference fringes cannot be avoided, the thickness of the sample was chosen in dependence of the strength of the particular excitation under investigation.

The samples were aligned by conventional Laue diffraction and mounted in a liquid He flow cryostat to study the temperature dependence of the optical properties between 4 and

300 K. Reflectivity and transmission measurements in the frequency range going from 20 - 7000 cm^{-1} were performed with a Fourier transform spectrometer (Bruker IFS 113v), with polarized light, in order to probe the optical response of the crystals along the b and the c axes. In reflectivity a near normal incidence configuration ($\theta = 11°$) was used. The absolute reflectivity and transmission values were obtained by calibrating the data acquired on the samples against a gold mirror and an empty sample holder, respectively. For frequencies higher than 6000 cm^{-1} a Woollam (VASE) ellipsometer was used in both transmission and reflection operational modes. Unfortunately, on this last system it was not (yet) possible to perform temperature dependent measurements. The optical conductivity spectra were obtain by Kramers-Kronig transformations in the regions were only reflectivity spectra were measurable, and by direct inversion of the Fresnel equations [23] wherever both reflection and transmission data were available.

3.3 Pure $CuGeO_3$

Let us now, as an introduction to what we will discuss in detail in the following sections, describe briefly the main features of the optical spectra of pure $CuGeO_3$ over the entire frequency range we covered with our experimental systems. In fig. 3.3 we present reflectivity, transmission, and conductivity spectra of $CuGeO_3$ at 300 K, for $E \parallel b$ (i.e., $\perp$ to the chain direction), and $E \parallel c$ (i.e., $\parallel$ the chain direction), in the frequency range going from 30 to 34 000 cm^{-1}. The results are typical of an ionic insulator. The far-infrared region ($\omega <$1000 cm^{-1}) is characterized by strong optical phonon modes showing the expected anisotropy for the b and c axes, as one can see from reflectivity and conductivity (the detail discussion of the phonon spectra will be subject of the next section). Besides the phonon lines, no background conductivity is observable (fig. 3.3c). Transmission spectra for $\omega <$400 cm^{-1} are not shown. In fact, transmission is not a particularly useful tool in investigating such a rich phonon spectrum because of the overall absorption. However, infrared transmission measurements carried out at low temperature, in order to investigate very weak magnetic and lattice excitations, will be shown later in the course of the chapter. At frequencies larger than 1000 cm^{-1}, reflectivity is low and almost completely featureless. More information can be gained from transmission in this case. In fig. 3.3b we can see (in addition to the strong phonons in the far infrared) absorption processes at 1330 and 1580 cm^{-1} along the c and b axes, respectively, and at $\sim$14 000 and $\sim$27 000 cm^{-1}, with approximately the same frequency for the two different axes. Having both reflectivity and transmission data in this region, we could calculate the dynamical conductivity by direct inversion of the Fresnel formula [23]. As shown by fig. 3.3c and in particular by the enlarged view given in the inset (note the very low absolute value of conductivity), extremely weak excitations are present, in the region going from 1000 to 30 000 cm^{-1}, on top of a zero background. Let us now briefly discuss the nature of these excitations. At 1000 cm^{-1} we can see the vanishing tail of the highest b-axis phonon (inset of fig. 3.3c). Above that, we find the two peaks at 1330 and 1580 cm^{-1} along the c and b axes, respectively. On the basis of the energy position and of the temperature dependence, these features can be ascribed to mul-

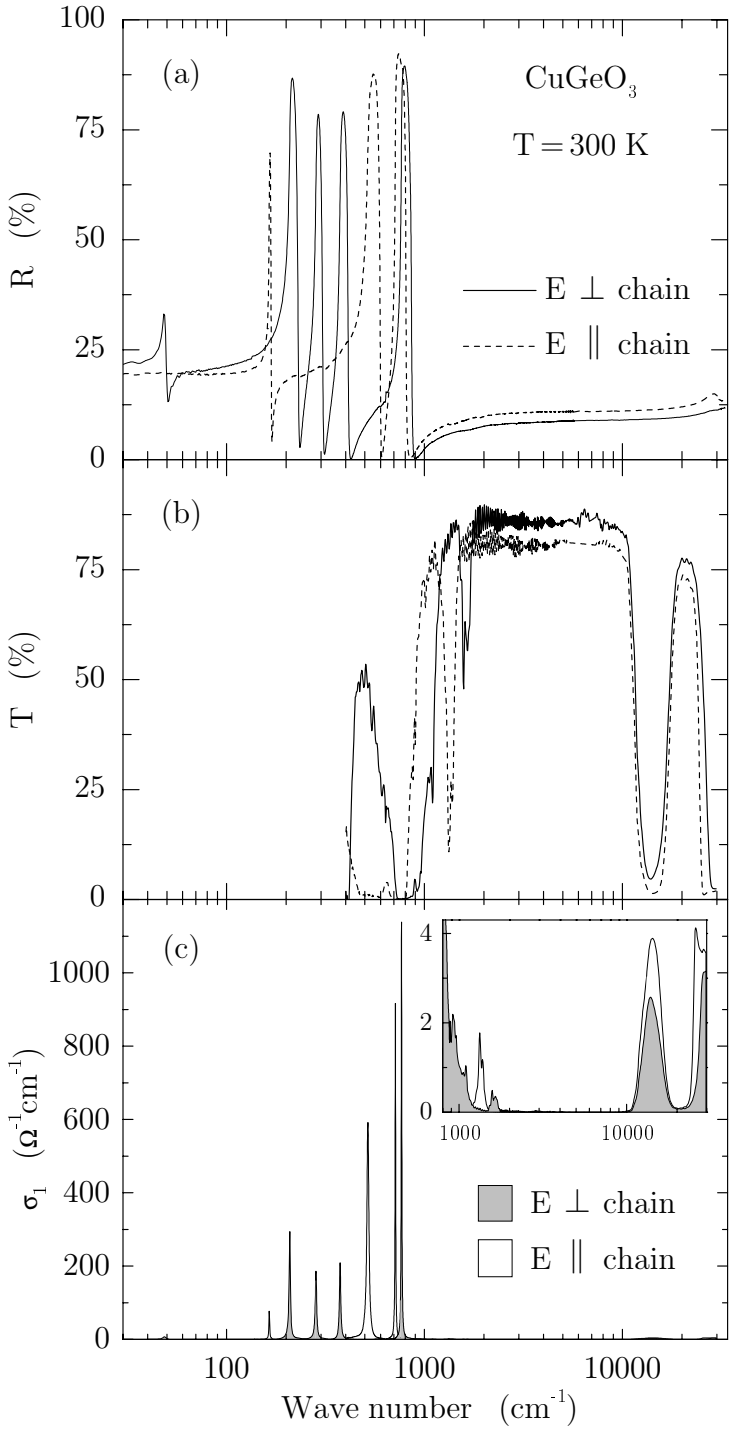

Figure 3.3: *Optical spectra of $CuGeO_3$ at 300 K for $E \parallel b$ (i.e., $\perp$ to the chain direction) and $E \parallel c$ (i.e., $\parallel$ the chain direction), in the frequency range going from 30 to 34 000 cm^{-1}. Panel (a), (b), and (c) show the results for reflectivity, transmission, and optical conductivity, respectively. In the inset of panel (c) an enlarged view of $\sigma_1(\omega)$ from 800 to 30 000 cm^{-1} is presented (note the very low absolute value of conductivity).*

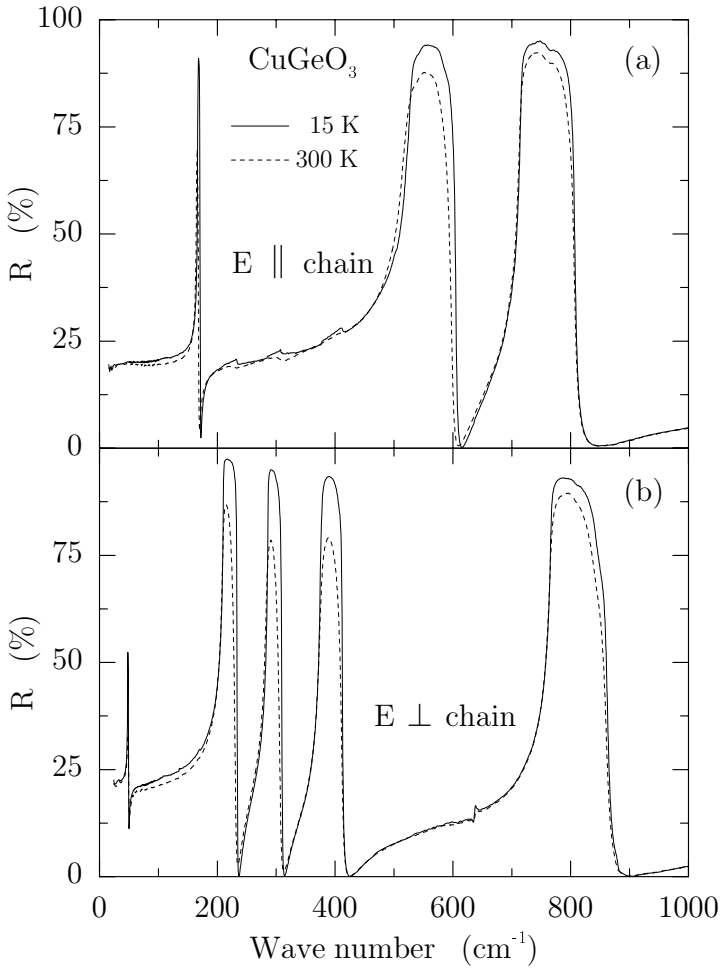

Figure 3.4: *Reflectivity of a single crystal of pure $CuGeO_3$, as a function of frequency, at two different temperatures (300 K and 15 K) in the undistorted phase. The spectra are shown for E parallel and perpendicular to the chain direction in panel (a) and (b), respectively.*

tiphonon processes. At ∼14 000 cm^{-1} (∼1.8 eV), for both orientations of the electric field, a very weak peak is present which has been shown to be due to phonon-assisted Cu *d-d* transitions [25]. Finally, the onset of the Cu-O charge-transfer excitations is observable at ∼27 000 cm^{-1}. Superimposed to it are some sharper features of probable excitonic nature.

3.3.1 Phonon Spectrum and Lattice Distortion

In this section we will discuss in detail the phonon spectrum of pure $CuGeO_3$, for both the high temperature undistorted phase and the low temperature dimerized SP phase. In particular, we will analyze the optical data in order to find possible zone-boundary folded

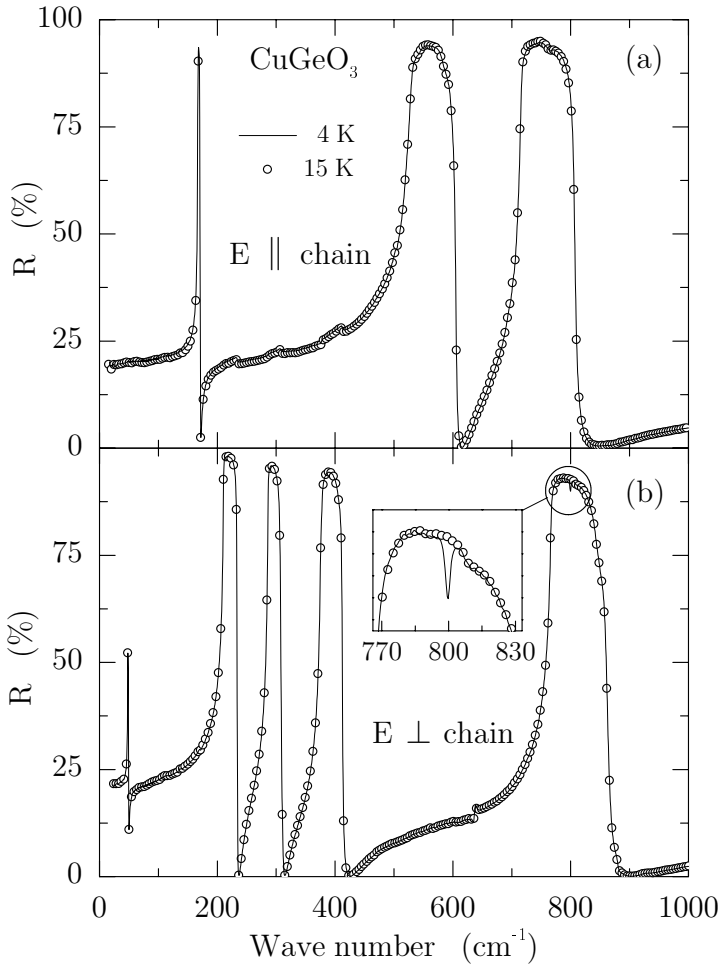

Figure 3.5: *Comparison between reflectivity spectra measured in the SP phase at 4 K (solid line) and just before the SP transition at 15 K (circles) on a pure single-crystal of $CuGeO_3$. For $E\|$chain (a) no difference is found across the phase transition whereas for $E\perp$ chain (b) a new feature appears at 800 cm^{-1} (as clearly shown in the inset).*

modes activated by the lattice distortion involved in the SP phase transition. The c and b-axis (*i.e.*, $E\,\|$ chain and $E\perp$chain, respectively) reflectivity spectra of $CuGeO_3$, in the undistorted phase, are presented in fig. 3.4, for two different temperatures higher than T_{SP}=14 K. The data are shown up to 1000 cm^{-1} which covers the full phonon spectrum. Three phonons are detected along the c axis ($\omega_{TO} \approx$167, 528 and 715 cm^{-1}, for T=15 K), and five along the b axis ($\omega_{TO} \approx$48, 210, 286, 376 and 766 cm^{-1}, for T=15 K). This is in agreement with what is expected on the basis of the group-theoretical analysis presented in section 3.1, (see eq. 3.5) for the space group *Pbmm* proposed for $CuGeO_3$ in the uniform phase [2]. The structure in fig. 3.4a between 200 and 400 cm^{-1} is due to a leakage of the polarizer and corresponds to the three modes detected along the b axis in the same frequency range. Similarly, the feature at approximately 630 cm^{-1} in fig. 3.4b is a leakage

of a mode polarized along the *a* axis [21]. However, the reason why this phonon has been detected in the *b*-axis reflectivity is not simply, as in the previous case, a leakage of the polarizer. It has to do with the finite angle of incidence $\theta = 11°$ of the radiation on the sample, and with the fact that *p*-polarized light was used to probe the optical response along the *b* axis. In fact, whereas for *s*-polarized light the electric field was parallel to the *b*-*c* plane, in *p* polarization there was a small but finite component of the electric vector perpendicular to the plane of the sample, which could then couple to the *a*-axis excitations (at least to those particularly intense). As a last remark, we would like to stress that the temperature dependence observable in the reflectivity spectra of fig. 3.4 mainly corresponds to the hardening and sharpening of the phonon lines, usually observable in a crystalline material upon reducing the temperature. However, a more extensive discussion of the temperature dependence of the phonon parameters over a broad temperature range will be presented in section 3.3.2, in relation to the soft-mode issue.

Cooling down the sample below the phase transition temperature T_{SP}=14 K, we can seek for changes in the phonon spectrum with respect to the result obtained at temperature just above T_{SP}. The *c* and *b*-axis reflectivity spectra measured at T=15 K (circles) and T=4 K (solid line) are compared in fig. 3.5. Note that the 15 K curves have been plotted with lower resolution, for the sake of clarity (and that the solid line is not a just a fit but it is the 4 K experimental result !). Whereas for $E \| c$ the spectra are exactly identical, a new feature, though very weak, is detected in the SP phase at 800 cm^{-1} for $E \| b$, as shown in the inset of fig. 3.5b. A careful investigation of temperatures ranging from 4 to 15 K (see fig. 3.6) clearly shows that this feature, that falls in the frequency region of high reflectivity for the B_{2u}-symmetry mode at 766 cm^{-1} and therefore shows up in reflectivity mainly for its absorption, is activated by the SP transition. It corresponds to a new absorption peak in conductivity, superimposed on a background due to the lorentzian tail of the close B_{2u} phonon (see inset of fig. 3.6).

By fitting the reflectivity spectra with Lorentz oscillators for all the optical phonons, it is possible to obtain the temperature dependence of the oscillator strength for the 800 cm^{-1} feature. The results are plotted in fig. 3.7, together with the peak intensity of a superlattice reflection measured by Harris *et al.* in an x-ray scattering experiment on a pure $CuGeO_3$ single crystal characterized, as our sample, by $T_{SP}\approx$13.2 K [26]. The data clearly show the second-order character of the phase transition. From the perfect agreement of the infrared and x-ray scattering results, and from the observation that the resonant frequency is not shifting at all with temperature, we can conclude that the peak at 800 cm^{-1} corresponds to a pure lattice excitation. It has to be a folded zone-boundary mode most probably related to the B_{2u} phonon observed at 766 cm^{-1}, which is mainly an oxygen vibration [21]. We can then estimate for the B_{2u} mode an energy dispersion, over the full Brillouin zone, of the order of 34 cm^{-1}=4.22 meV, at T=15 K. If magnetic degrees of freedom were involved (e.g., if this excitation were a magnon-plus-phonon process [27]), not only a decrease in intensity would be observable, but also a frequency shift to lower values, reflecting the closing of the magnetic gap for $T \to T_{SP}$ from below. In fact, on the basis of Cross and Fisher theory for the SP phase transition [4], the magnetic gap would scale as $\delta^{2/3}$ [where δ, $\sim(1-T/T_{SP})^{\beta}$ close to T_{SP}, denotes the generalize symmetry-

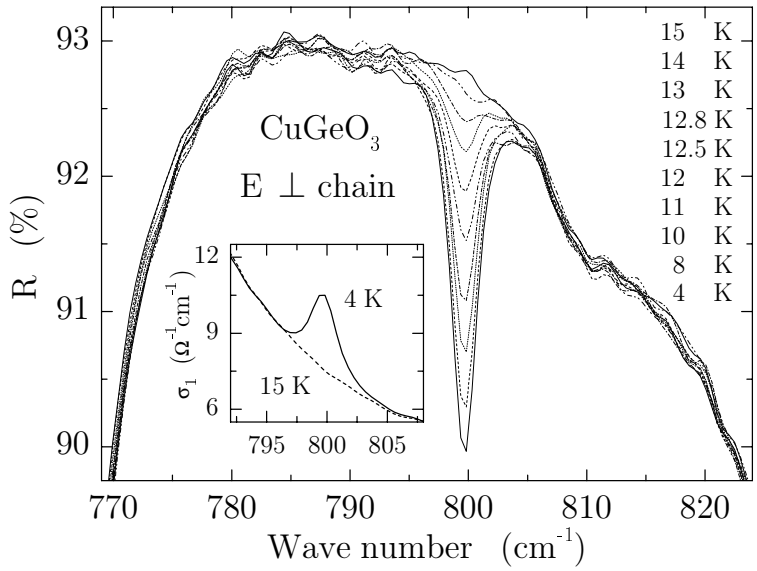

Figure 3.6: *Detailed temperature dependence of the 800 cm^{-1} line observed with $E \perp$ chain in the reflectivity spectra for $T<T_{SP}$. In the inset, where the dynamical conductivity calculated via Kramers-Kronig analysis is plotted, a new peak is clearly visible for T=4 K.*

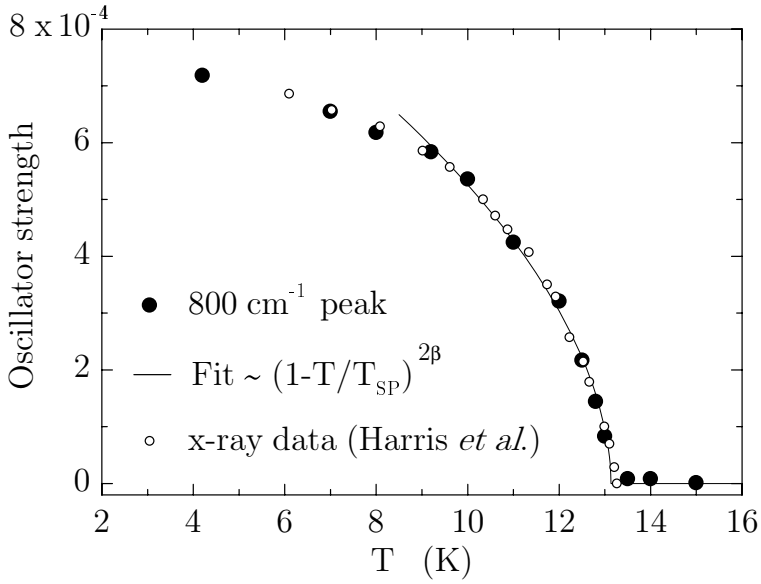

Figure 3.7: *Oscillator strength of the 800 cm^{-1} folded mode, observed for $E \perp$ chain on a pure $CuGeO_3$ single crystal, plotted vs. temperature. The x-ray scattering data of Harris et al. [26], and the fit to a power law in the reduced temperature are also shown.*

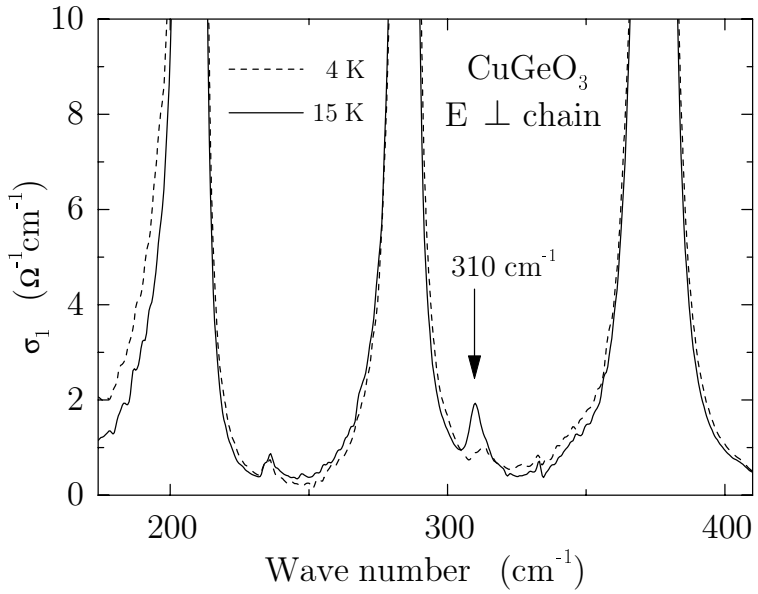

Figure 3.8: *Comparison between conductivity spectra measured in the SP phase at 4 K and just before the SP transition at 15 K, for $E \perp$ chain, on a pure single-crystal of $CuGeO_3$: A zone boundary folded mode appears, across the phase transition, at 310 cm^{-1}.*

breaking lattice distortion]. Moreover, its gradual closing has been directly observed in neutron and inelastic light scattering experiments [28, 29]. Because both the intensity of the superlattice reflections measured with x-ray or neutron scattering, and the intensity of the zone-boundary folded modes in an optical experiment are simply proportional to δ^2 [30], we can try to fit the temperature dependence of the oscillator strength for the 800 cm^{-1} SP-activated mode to the equation $\sim (1 - T/T_{SP})^{2\beta}$. As a result of the fit performed over a broad temperature range (see fig. 3.7), we obtained $\beta = 0.26 \pm 0.02$, in agreement with ref. 28. However, the best fit value of β is strongly dependent on the temperature range chosen to fit the data [31]. If only points very close (within one Kelvin) to T_{SP} are considered, the value $\beta = 0.36 \pm 0.03$ is obtained, as reported in ref. 32. At this point, in relation to the soft-mode issue in $CuGeO_3$ treated in section 3.3.2, we would like to mention that for the organic SP system TTF-$CuS_4C_4(CF_3)_4$, which shows a precursive 3D soft-phonon at the superlattice position, the value $\beta = 0.5$ was obtained [33]. It was argued by Cross and Fisher, in their original paper [4], that this soft-mode is responsible for the mean-field behavior, i.e. $\beta = 1/4$, in the TTF salt.

As we saw in fig. 3.5, only one phonon activated by the SP phase transition, of the many we actually expected, was directly observable in reflectivity spectra. However, by carefully checking the optical conductivity at 4 and 15 K, a second folded mode is found along the b axis at 310 cm^{-1} (see fig. 3.8). This line was not distinguishable in reflectivity because it coincides with ω_{LO} of the B_{2u}-symmetry phonon at 286 cm^{-1}. The reasons for not detecting all the phonons predicted from the group theoretical analysis (eq. 3.6) in reflectivity measurements, at $T < T_{SP}$, are probably the small values of the atomic dis-

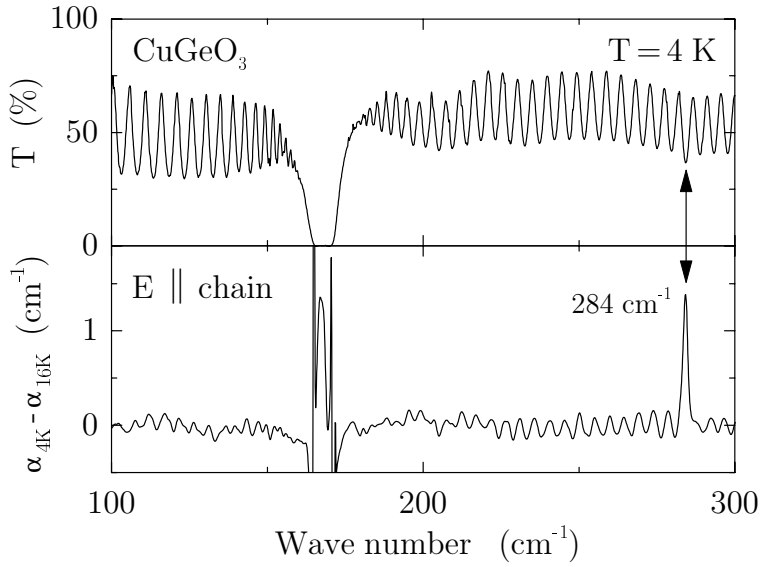

Figure 3.9: *Top panel: Transmission spectrum of a pure single-crystal of $CuGeO_3$ measured in the SP phase at 4 K with $E \| chain$. Bottom panel: The absorbance difference spectrum $\alpha_{4K} - \alpha_{16K}$ clearly shows an activated zone boundary mode at 284 cm^{-1}.*

placements involved in the SP transition (with a correspondingly small oscillator strength of zone-boundary modes), and/or possibly the small dispersion of the optical branches of some of the lattice vibrations. However, it is not surprising that the only activated modes have been detected along the b axis of the crystal. In fact, it is for this axis that for $T < T_{SP}$ a strong spontaneous thermal contraction has been observed [28], which can be responsible for a relative increase of the oscillator strength of the phonons polarized along the b axis, with respect to those polarized along the c axis. In order to probe the phonon spectrum of the dimerized phase with a more sensitive tool, transmission measurements on a 350 μm thick sample were performed in the far-infrared region. One more line was then detected at 284 cm^{-1} along the c axis, as shown in fig. 3.9. In the top panel a transmission spectrum acquired at 4 K is plotted in the frequency range 100-300 cm^{-1}. Fabry-Perot interference fringes are clearly visible, interrupted at $\sim$167 cm^{-1} by the strong absorption of the lowest energy B_{1u}-symmetry phonon. Moreover, at 284 cm^{-1} one can observe a slightly more pronounced minimum in the interference pattern. However, because of the weakness of this line, a real peak can be observed only in the absorbance difference spectrum (bottom panel of fig. 3.9). The spikes present at $\sim$167 cm^{-1} in the absorbance difference spectrum are due to the complete absorption of the light in that frequency range (top panel). As a last remark, we want to stress that the final assignment of the 310 and 284 cm^{-1} peaks to optical phonons activated by the SP transition was based, as for the one observed at 800 cm^{-1}, on their detailed temperature dependence (not shown). Unfortunately, because of the too low intensities, a careful quantitative analysis of their temperature dependent oscillator strength was not possible.

In conclusion, whereas our data on pure $CuGeO_3$ [18,19] confirm the structure proposed

for the high temperature undistorted phase [2], they do not give sufficient information to completely resolve the symmetry of the SP lattice distortion. On the other hand, we were able to detected signatures of the phase transition in the phonon spectrum, with enough accuracy to clearly show the second order character of the transition.

3.3.2 Phonon Parameters and Soft-Mode Issue

As far as the dynamical interplay between spins and phonons in $CuGeO_3$ is concerned, it is clear from the reflectivity spectra plotted in fig. 3.4 and 3.5 that a well-defined soft mode, driving the structural deformation in $CuGeO_3$, has not been detected in our measurements. However, as any dimerization must be related to normal modes away from the zone center, the softening of one or more modes, across the SP phase transition, should be expected at $k=(\pi/a,0,\pi/c)$, the actual propagation vector in $CuGeO_3$. Therefore, as optical techniques can probe the phonon branches only at the Γ point ($k=0$), the softening can, strictly speaking, be investigated only by neutron scattering. On the other hand, no detailed experimental neutron scattering investigation nor full lattice dynamical calculation were available, for the 30 phonon branches of $CuGeO_3$, when we started our work on this system. In this context, we tried to gain interesting insights from the temperature dependence of the phonon parameters obtained from the fit of the reflectivity data (see table 3.1). In fact, if the dispersion and the mixing of the branches are not too strong, one could hope that the presence of a soft mode at $k=(\pi/a,0,\pi/c)$ would result in an overall softening of the branch it belongs to. Therefore, our first attempt was to check if any of the optical phonons detected in our experiments was showing a red shift upon cooling the sample. In fig. 3.10 we can clearly observe that the B_{2u} mode (E $\perp$ chain) at 48 cm^{-1} is the only one showing an evident monotonic red shift from 300 to 15 K . Below T_{SP} this mode shows only a small blue shift. Also the behavior of the oscillator strength of this phonon is rather interesting: It grows continuously from 300 to 15 K (a $\sim$23% increase), and it shows a sudden drop of $\sim$15% across the phase transition. On the basis of these results, we could conclude that these particular phonon branch could have been a good candidate to show a real softening at the SP distortion vector in the Brillouin zone.

In order to check more directly the possible presence of a soft mode in $CuGeO_3$, we performed transmission measurements with a mm-wave transmission setup, equipped with a backward wave oscillator operating in the frequency range 3.6 - 6.0 cm^{-1} [34]. The measurements were done on a $\sim$1 mm thick sample of pure $CuGeO_3$ and, in order to relax the k-conservation rule and to obtain a result averaged over the all Brillouin zone, on Si and Mg substituted crystals, with approximately the same thickness of the pure one. In this way, we aimed to measure very accurately the transmission through the samples at one very low fixed frequency (5 cm^{-1}), as a function of temperature. If a mode would get soft, it would possibly result in a temperature dependent transmission showing a 'w-shape' centered at T_{SP}: Two minima in the absolute transmission, one on each side of T_{SP}. Unfortunately, we could not detect any change. Had we seen the expected 'w-shape' behavior of transmission, this would have been a reasonably strong indication of the existence of a soft mode in $CuGeO_3$; in the opposite case we cannot put forward any conclusion.

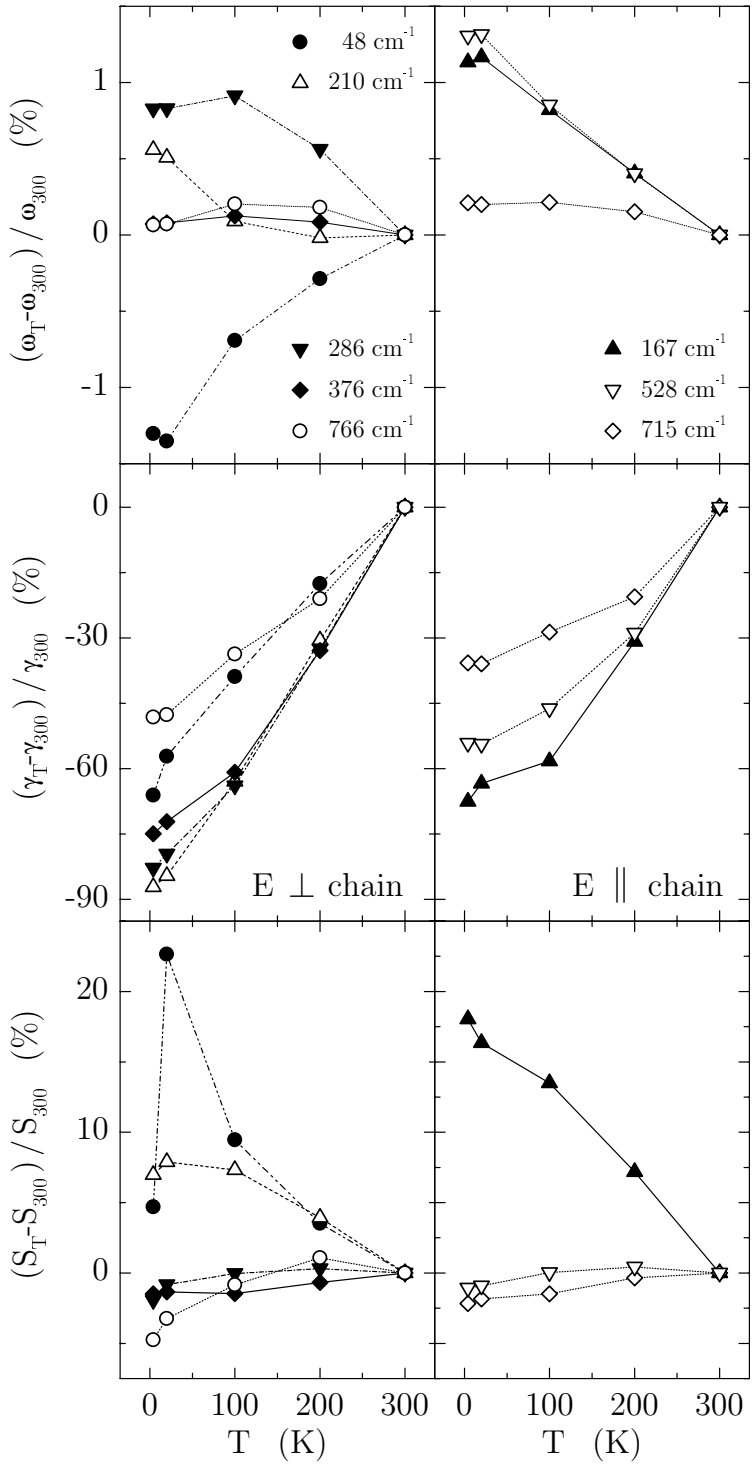

Figure 3.10: *Temperature dependence of the percentage change in resonant frequency, damping, and oscillator strength (from top to bottom) of the transverse optical phonons (of the undistorted phase), observed for $E\perp$ chain (left) and $E\|$chain (right) on the pure single-crystal of $CuGeO_3$.*

Mode	Parameters	4 K	15 K	100 K	200 K	300 K
	ω_{TO}	166.78	166.82	166.25	165.56	164.90
B_{1u}	γ	0.41	0.46	0.53	0.88	1.27
	S	0.348	0.343	0.335	0.316	0.295
	ω_{TO}	527.69	527.74	525.33	522.98	520.89
B_{1u}	γ	4.07	4.05	4.78	6.32	8.89
	S	1.900	1.903	1.921	1.929	1.921
	ω_{TO}	715.25	715.17	715.27	714.84	713.75
B_{1u}	γ	3.12	3.11	3.46	3.85	4.85
	S	0.636	0.638	0.640	0.648	0.650
	ω_{TO}	48.28	48.26	48.58	48.78	48.92
B_{2u}	γ	0.63	0.79	1.13	1.52	1.85
	S	0.286	0.335	0.299	0.282	0.273
	ω_{TO}	210.27	210.17	209.29	209.07	209.10
B_{2u}	γ	0.44	0.53	1.28	2.41	3.46
	S	1.717	1.732	1.723	1.669	1.605
	ω_{TO}	285.79	285.79	286.03	285.04	283.45
B_{2u}	γ	0.83	0.99	1.75	3.27	4.84
	S	0.765	0.773	0.780	0.782	0.780
	ω_{TO}	375.62	375.65	375.81	375.66	375.35
B_{2u}	γ	1.44	1.60	2.26	3.86	5.76
	S	0.596	0.597	0.596	0.601	0.605
	ω_{TO}	766.28	766.34	767.35	767.16	765.79
B_{2u}	γ	3.27	3.30	4.18	4.98	6.30
	S	0.677	0.689	0.705	0.718	0.711
	ω_{TO}	284.21	-	-	-	-
B_{1u} (SP)	γ	—	-	-	-	-
	S	—	-	-	-	-
	ω_{TO}	309.58	-	-	-	-
B_{2u} (SP)	γ	4.27	-	-	-	-
	S	2.8×10^{-3}	-	-	-	-
	ω_{TO}	799.75	-	-	-	-
B_{2u} (SP)	γ	2.32	-	-	-	-
	S	7.2×10^{-4}	-	-	-	-

Table 3.1: *Resonant frequency* ω_{TO} *(*cm^{-1}*), damping* γ *(*cm^{-1}*), and oscillator strength* S *of the optical phonons detected for* $E \| chain$ *(*B_{1u} *symmetry) and* $E \perp$ *chain (*B_{2u} *symmetry) on the pure single-crystal of* $CuGeO_3$*. The parameters have been obtained by fitting the phonon spectra with Lorentz oscillators, at different temperatures.*

The final word about this issue had to come, as expected, from neutron scattering measurements. And indeed, recently, it was clearly shown that the pre-existing soft mode, expected in the classical theories of the SP phase transition [4,5], is not there in the case of $CuGeO_3$ [35]. Neither is present the central peak usually observed in order-disorder phase transitions [30]. In fact, Braden *et al.* investigated the lattice dynamics of $CuGeO_3$ with inelastic neutron scattering combined with shell model lattice dynamical calculations [35]. They could identify the low-lying modes of the symmetry of the structural distortion characterizing the dimerized SP phase, and show that there is no soft mode behavior for these phonons at $k=(\pi/a,0,\pi/c)$, nor in any other point of the line $[x,0,x]$. Moreover, they found that the static SP distortion does not correspond to one single normal mode of the uniform phase, as usually expected for a continuous displacive transition [30], but it corresponds to the linear combination, in ratio of 3:2, of two out of four optical phonons allowed by symmetry. Of these two modes, one involves an appreciable Cu displacement (essential for the dimerization), the second is associated with the twisting of the CuO_2 ribbons (which is the second element of the distortion). Finally, they showed that none of the two belongs to a branch having, at $k=0$, an optically allowed symmetry [35].

As a consequence of these findings, it appears that the behavior of the phonon parameters for the B_{2u} mode at 48 cm^{-1} is simply 'accidental'. However, one may speculate, that the absence of a softening at $k=(\pi/a,0,\pi/c)$ implies that the phase transition is not driven by a softening of the phonon spectrum at $k=(\pi/a,0,\pi/c)$, but only by a change in electronic structure which in turn determines the dynamical charge of the ions and the interatomic force constants. In this scenario, the large change in oscillator strength of some of the vibrational modes observed in our optical data (see fig. 3.10), results from a change in ionicity, or, in other words, a transfer of spectral weight from the elastic degrees of freedom to electronic excitations. As far as the understanding of the SP phase transition in $CuGeO_3$ is concerned, now that the absence of a soft phonon is a well established experimental fact [35], a further discussion will be presented in section 3.5.

A last remark has to be made regarding the temperature dependence of the B_{2u} mode observed at 286 cm^{-1}. On the basis of optical reflectivity measurements [36], a softening of this phonon, upon going through the phase transition, was suggested. This is not confirmed by our results which show no considerable frequency shift for this resonance upon reducing the temperature from 15 to 4 K (see fig. 3.10). On the other hand a reduction of both the scattering rate and the oscillator strength is observed, which can explain the double-peak structure in the reflectance ratio R(20 K)/R(5 K) reported in ref. 36.

3.3.3 Magnetic Excitations

Inelastic neutron and light scattering experiments are very sensitive to magnetic excitations and, in the case of $CuGeO_3$, they have been very powerful tools in detecting the singlet-triplet magnetic gap [8,9], separated by a second gap from a continuum of magnon excitations [37–40], and a singlet bound-states within the two energy gaps [29,41]. On the other hand, optical spectroscopy is usually not the elective technique to study this kind of processes, unless a static (charged magnons [42,43]) or a dynamic (phonon assisted

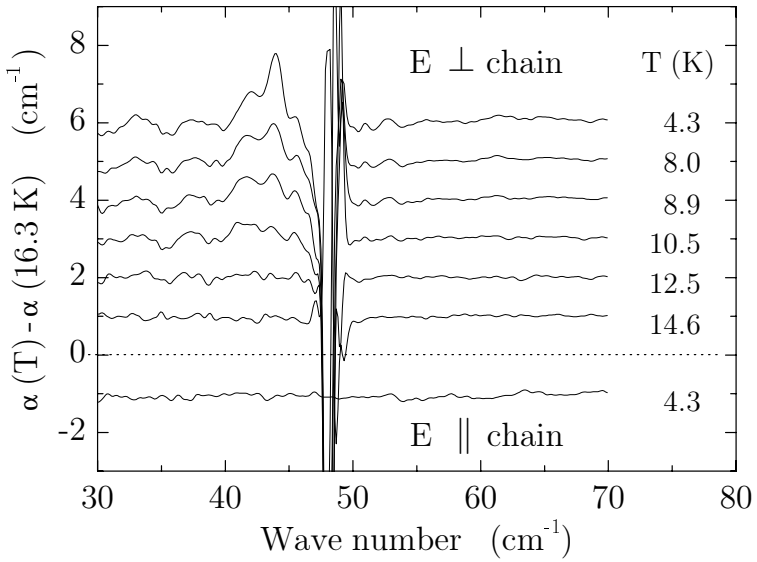

Figure 3.11: *Absorbance difference spectra for the pure single-crystal of $CuGeO_3$, with $E \perp$ chain (top) and $E \parallel$ chain (bottom). The spectra have been shifted for clarity.*

bi-magnons [27]) breaking of symmetry is present in the system under investigation (for a more detailed discussion see chapter 4). Moreover, in these two latter cases, only those excitations characterized by a total $\Delta S = 0$ can be probed, because of spin conservation. Therefore, a direct singlet-triplet excitation is, in principle, not detectable. However, such a transition has been observed at 44.3 cm^{-1} in an infrared transmission experiment where the singlet-triplet nature of the transition was demonstrated by the Zeeman splitting observed in magnetic field [44]. In a later theoretical paper [45], this line was interpreted as a magnetic excitation across the gap at the wave vector $(0,2\pi/b,0)$ in the Brillouin zone, activated by the existence of staggered magnetic fields along the direction perpendicular to the chains. Therefore, in a transmission experiment performed with polarized light incoming onto the b-c plane of the sample at normal incidence, this excitation would be detectable only for magnetic field of the radiation parallel to the b axis of the crystal ($\perp$ chain), i.e., E parallel to the c axis ($\parallel$ chain) [45]. In order to verify this interpretation, we measured the far-infrared transmission on a 350 μm thick pure single crystal of $CuGeO_3$, for both $E \perp$ chain and $E \parallel$ chain. The absorbance difference spectra are reported in fig. 3.11, where they have been shifted for clarity. Contrary to what expected following the interpretation given in ref. 45, for $E \parallel$ chain (fig. 3.11, bottom) no absorption is observed. However, for $E \perp$ chain (fig. 3.11, top) an absorption peak, showing the temperature dependence appropriate for an excitation activated by the SP phase transition, is present at approximately 44 cm^{-1}. One has to note that the feature at 48 cm^{-1} is produced by the low-energy B_{2u} phonon. In fact, because of the complete absorption of the light in that frequency range, spikes are obtained when absorbance difference spectra are calculated. The observed polarization dependence puts a strong experimental constraint on the possible microscopic mechanism giving rise to the singlet-triplet absorption peak. For a complete understand-

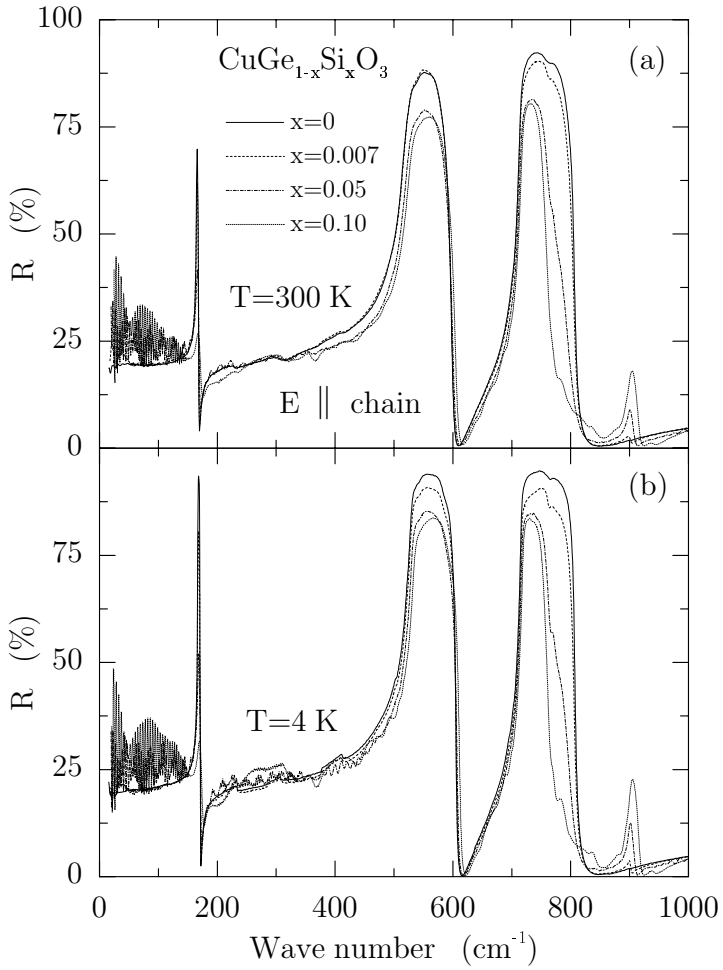

Figure 3.12: *C-axis reflectivity spectra of Si-doped single crystals of $CuGeO_3$, for different silicon concentrations, at two different temperatures: T=300 K (a), and T=4 K (b).*

ing, a full experimental investigation of the symmetry of this magnetic absorption process, by ,e.g., measuring transmission through the *a-b* and *a-c* planes for different orientations of the fields, is needed. A discussion of this not understood feature, in relation to other critical theoretical and experimental issues of the physics of $CuGeO_3$, will be presented in section 3.5.

3.4 Doped $CuGeO_3$

In this section we will present the optical spectroscopy data of several $Cu_{1-\delta}Mg_{\delta}GeO_3$ (with $\delta = 0, 0.01$), and $CuGe_{1-x}B_xO_3$ [with B=Si ($x = 0, 0.007, 0.05, 0.1$), and Al ($x = 0, 0.01$)] single crystals. In particular, we investigated, as we did for the pure material, the phonon spectrum as a function of temperature of Mg and Si substituted $CuGeO_3$, by means of reflectivity measurements in the far-infrared region (see section 3.4.1). The aim of this

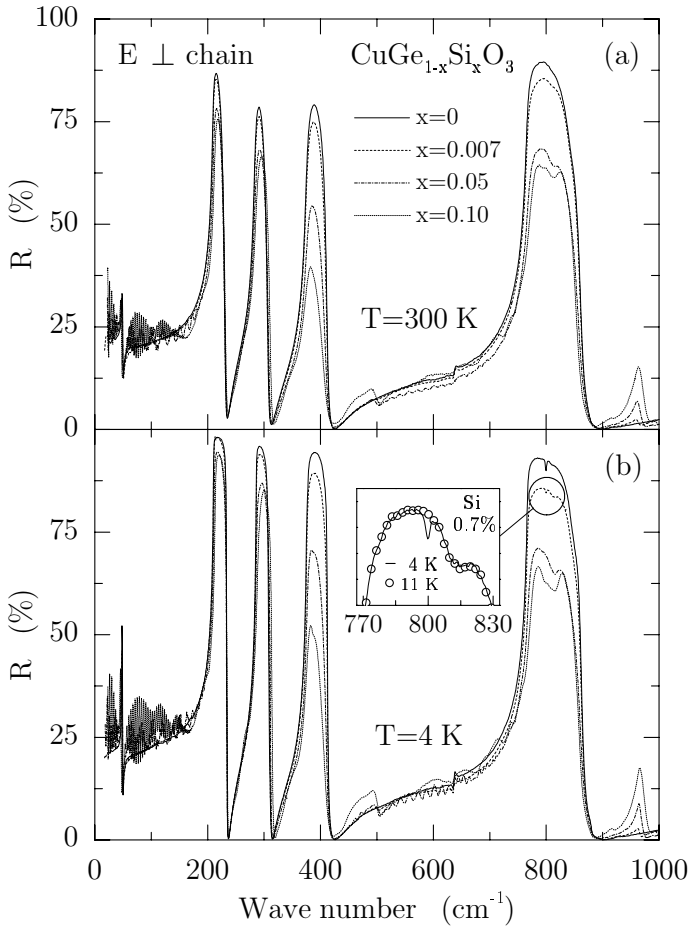

Figure 3.13: *B-axis reflectivity spectra of Si-doped single crystals of $CuGeO_3$, for different silicon concentrations, at two different temperatures: T=300 K (a), and T=4 K (b). The 800 cm^{-1} folded mode, activated by the SP transition, is still observable for 0.7% Si-doping by comparing (see inset) the 4 K (solid line) and the 11 K (circles) data.*

investigation was, first of all, to study the effect of doping on the SP phase transition; second, to verify the recent claims of Yamada and co-workers [46,47] who suggested that the structure originally proposed for $CuGeO_3$, in the high temperature undistorted phase [2], could be wrong (see section 3.4.1). Moreover, transmission measurements in the mid-infrared region were performed on all the samples, in order to detect possible electronic and/or magnetic excitation which could provide us with additional information about the interplay of spin and charge in this quasi-1D systems (see section 3.4.2).

3.4.1 Far-Infrared Reflection

The reflectivity data acquired on the Si doped samples for $E \parallel$ chain (c axis), and $E \perp$ chain (b axis), are shown in fig. 3.12 and 3.13, respectively. The spectra are similar to those we

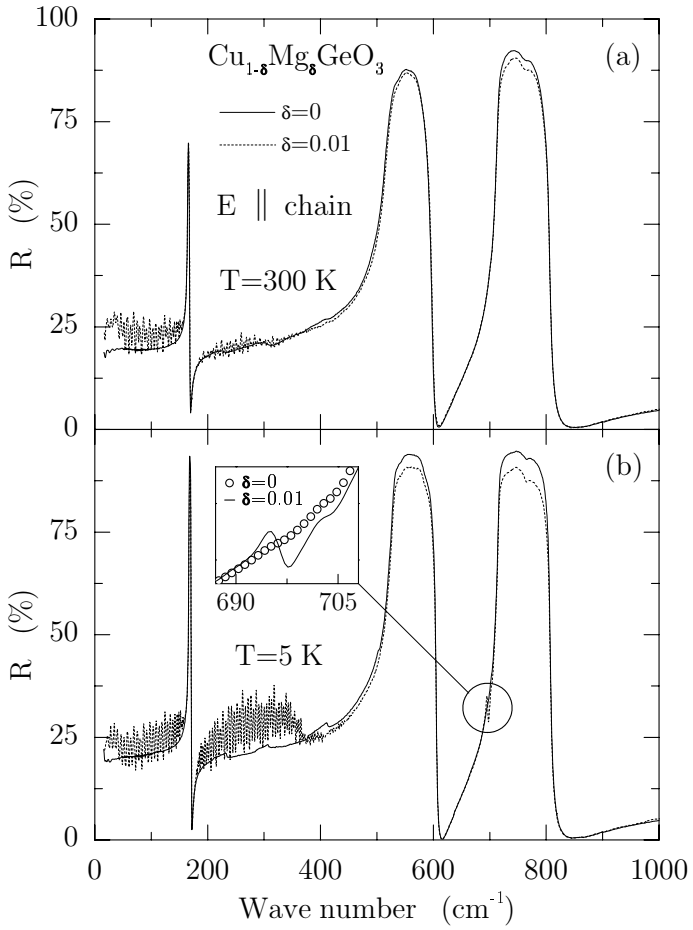

Figure 3.14: *C-axis reflectivity spectra of pure and 1% Mg-doped single crystals of $CuGeO_3$, at two different temperatures: T=300 K (a) and T=5 K (b). The inset shows an enlarged view of the frequency region around 700 cm^{-1} for the data obtained on the pure (circles) and Mg-doped (solid line) samples, at T=5 K. The additional peak observed for Mg doping is due to the mass difference between Cu and Mg and it is not related to the SP transition.*

already discussed for pure $CuGeO_3$. However, some new features, stronger in intensity the higher the Si concentration, are observable already at room temperature. Therefore, they are due to the substitution of Ge with the lighter Si and not directly related to the SP transition: New phonon peaks at 900 cm^{-1}, along the *c* axis (fig. 3.12), and at 500 and 960 cm^{-1}, along the *b* axis (fig. 3.13). Moreover, the much more complicated line shape and the considerable reduction of the oscillator strength of the high frequency phonons indicate: First, a strong Ge (Si) contribution to these modes, mainly due to O vibrations [21]. Second, that substituting Si for Ge has apparently a strong symmetry-lowering effect, a point which we will discuss again later in relation to the claim of Yamada *et al.* [46,47] about a possible lower symmetry, with respect to the one originally proposed by Völlenkle *et al.* [2], for the uniform structure of $CuGeO_3$. At temperatures lower than

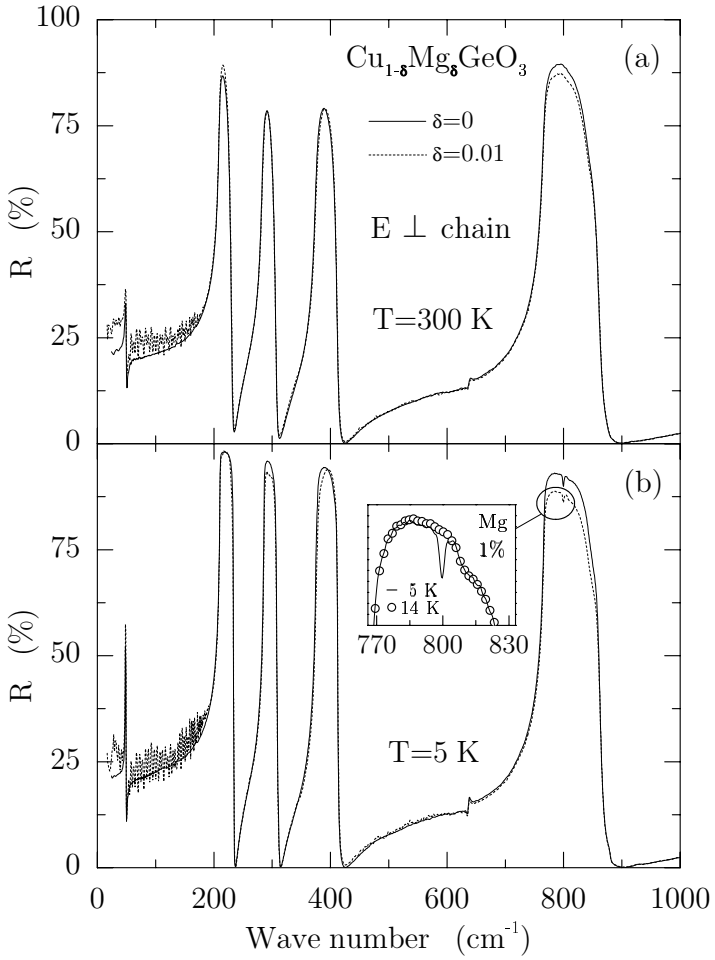

Figure 3.15: *B-axis reflectivity spectra of pure and 1% Mg-doped single crystals of $CuGeO_3$, at two different temperatures: T=300 K (a) and T=5 K (b). For the Mg-doped sample the 800 cm^{-1} folded mode, activated by the SP transition, is clearly observable in the inset, where the 5 K (solid line) and the 14 K (circles) data are presented.*

T_{SP} (fig. 3.13b), we can observe the folded mode at 800 cm^{-1} along the b axis, previously detected on pure $CuGeO_3$ (see section 3.4.1). However, it is found only for the lowest Si concentration, as shown in the inset of fig. 3.13b, where the 4 K and 11 K data are compared. We can conclude that up to 0.7% Si doping the SP transition is still present with T_{SP} <11 K, whereas for 5% and 10% Si concentrations no signature of the transition could be found in our spectra.

The results obtained on the 1% Mg-doped sample are plotted, together with the results obtained on pure $CuGeO_3$, in fig. 3.14 and fig. 3.15 for $E \parallel$ chain (c axis), and $E \perp$ chain (b axis), respectively. Clearly, Mg doping is affecting the optical response of $CuGeO_3$ less than Si doping does. A new phonon, due simply to the mass difference between Cu and Mg, is present in the c-axis spectra at 695 cm^{-1}, as clearly shown in the inset of fig. 3.14b,

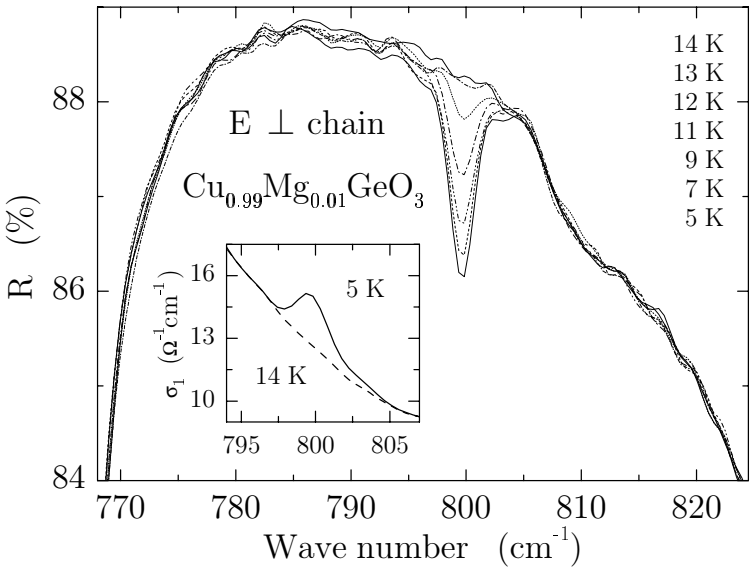

Figure 3.16: *Detailed temperature dependence of the 800 cm^{-1} activated mode observed with $E \perp$ chain in the reflectivity spectra of $Cu_{0.99}Mg_{0.01}GeO_3$, for $T<T_{SP}$. In the inset, where the dynamical conductivity calculated via Kramers-Kronig analysis is plotted, a new peak is clearly visible for T=5 K.*

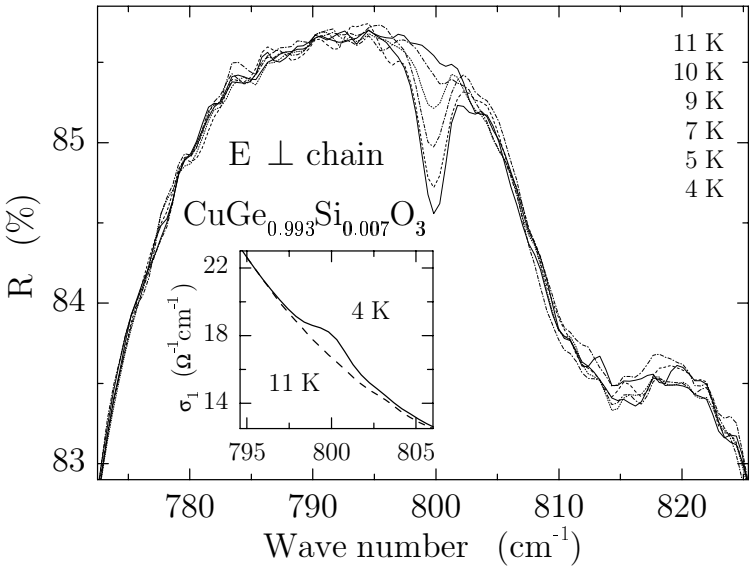

Figure 3.17: *Detailed temperature dependence of the 800 cm^{-1} activated mode observed with $E \perp$ chain in the reflectivity spectra of $CuGe_{0.993}Si_{0.007}O_3$, for $T<T_{SP}$. In the inset, where the dynamical conductivity calculated via Kramers-Kronig analysis is plotted, a new peak is clearly visible for T=4 K.*

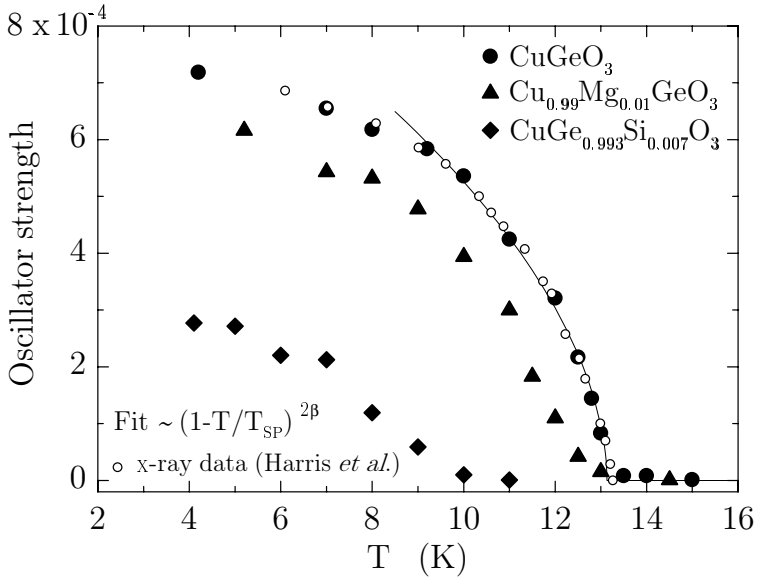

Figure 3.18: *Temperature dependence of the oscillator strength of the zone boundary folded mode observed, for $E \perp$ chain, at 800 cm^{-1} on pure, 1% Mg-doped, and 0.7% Si-doped $CuGeO_3$ single crystals. The x-ray scattering data of Harris et al. [26] and the fit to the power law described in section 3.3.1 are also plotted, for pure $CuGeO_3$.*

for T=5 K. Moreover, we clearly observe for $E \perp$ chain (see inset of fig. 3.15b), the 800 cm^{-1} zone boundary mode activated by the SP transition. On the one hand, for the 1% Mg-doped sample, T_{SP} seems to be lower than in pure $CuGeO_3$; on the other hand, the structural deformation is not as strongly reduced as in the 0.7% Si-doped sample, as can be deduced from the direct comparison between the insets of fig. 3.13b and fig. 3.15b.

In order to estimate more precisely the reduction the oscillator strength for the 800 cm^{-1} phonon, and eventually the decrease of T_{SP} with respect to what was observed on pure $CuGeO_3$, we made careful measurements for $T < T_{SP}$ on the 1% Mg and the 0.7% Si-doped samples (see fig. 3.16 and 3.17, respectively). In both cases we can observe, in the reflectivity spectra, the gradual disappearance of the activated phonon for $T \to T_{SP}$ from below and, in the optical conductivity (see insets of fig. 3.16 and 3.17), the additional peak present in the dimerized phase data, superimposed to the background of the B_{2u} phonon of the high symmetry phase. As for the pure material (section 3.3.1), by fitting the reflectivity spectra with Lorentz oscillators for the optical phonons, we could obtain the temperature dependence of the oscillator strength for the 800 cm^{-1} line. The results are plotted, for all the samples at once, in fig. 3.18. For pure $CuGeO_3$ we saw that our results for the oscillator strength of the activated optical phonon are in very good agreement with the peak intensity of a superlattice reflection measured by Harris *et al.* [26] (see fig. 3.18). Similarly, the data obtained on doped samples, compare nicely to those presented, for 0.7% Si doping, in ref. 48 and, for 1% Mg doping, to those reported in ref. 49 for an 0.9% Zn-doped sample (superlattice reflection data for Mg-doped $CuGeO_3$, obtained by neutron-

scattering, became available in the literature only very recently [50], however for a too high Mg concentration to be directly comparable to our results). It is not possible to perform the same fit for the data acquired on doped samples, as we did on the pure crystal, because they are characterized by an upturned curvature near T_{SP}, which can be explained in terms of a distribution of transition temperatures due to the disorder introduced upon doping the system [48]. However, for the 1% Mg and the 0.7% Si doped samples the estimates for T_{SP} of approximately 12.4 K and 9.3 K, respectively, can be obtained (fig. 3.18). Considering that usually, for pure $CuGeO_3$, $T_{SP} \approx 14.2$ (on our pure sample a slightly reduced value has been observed), we can conclude that Si is three times more effective in reducing T_{SP} than Mg. This result has recently been confirmed, on a more strong basis, by a very systematic and detailed investigation of the decrease of T_{SP} and of the occurrence of 3D AF order at lower temperature on several doped single crystals of $CuGeO_3$, by magnetic susceptibility measurements [51].

The difference between Mg and Si in influencing the phase transition can be understood considering what is the effect of these two different ways of doping on the magnetism of the system. The substitution of a Cu^{2+} ion by a non magnetic impurity, like Mg, effectively cuts the CuO_2 chain in two segments and, at the same time, breaks a singlet dimer. Therefore, a free S=1/2 Cu^{2+} spin is created for each Mg impurity. More subtle is the effect of the substitution of Ge with Si: As shown by Khomskii and co-workers [52,53], it has to do with the question why the Cu-Cu nn superexchange interaction in $CuGeO_3$ is AF in the first place. In fact, because the Cu-O(2)-Cu bond angle is $\gamma \approx 98°$, and because the Goodenough-Kanamory-Anderson rule [54] states that the 90° superexchange of two magnetic ions (via a ligand), with partially filled d shells, is (weakly) ferromagnetic, it is not that obvious why the nn superexchange is AF in $CuGeO_3$. Khomskii and co-workers [52,53] showed that the 8° deviation from the critical value of 90° is not sufficient for the superexchange to change sign. The AF interaction was shown to be a consequence of the side-group effect. In fact, because of the presence of Ge and, in particular, because of the Ge-O hybridization, the oxygen p_x and p_y orbitals are not equivalent any more. Therefore, the cancellation of the AF contributions to the Cu-Cu superexchange, via the ligand O, is no longer complete, resulting in a (weak) AF superexchange. When Si is introduced in the system at Ge place, one could at a first glance expect not too strong an effect because, contrary to the substitution of Cu with Mg, Si is not directly breaking a dimer. However, because Si is smaller than Ge, both the Si-O bond length [which is proportional the Cu-O(2)-Cu bond angle γ] and the Si-O hybridization are reduced [52, 53]. As a result, Si breaks the Cu-Cu superexchange interaction on the two neighboring CuO_2 chains adjacent to the Si^{4+} ion. What we just discussed explains why Si has to be at least twice as efficient as Mg in reducing T_{SP}. The reason why the experimentally observed influence is a factor of three larger, and not only a factor of two, is still not completely clear.

Let us now turn to discuss the doubts recently raised by Yamada and co-workers [46,47] about the structure of $CuGeO_3$ in the high-temperature undistorted phase. They showed that the results of electron paramagnetic resonance experiments [46] can be fully understood only taking into account spin-antisymmetric interaction, such as the Dzyaloshinsky-Moriya exchange interaction [55]. However, the antisymmetric exchange interaction is

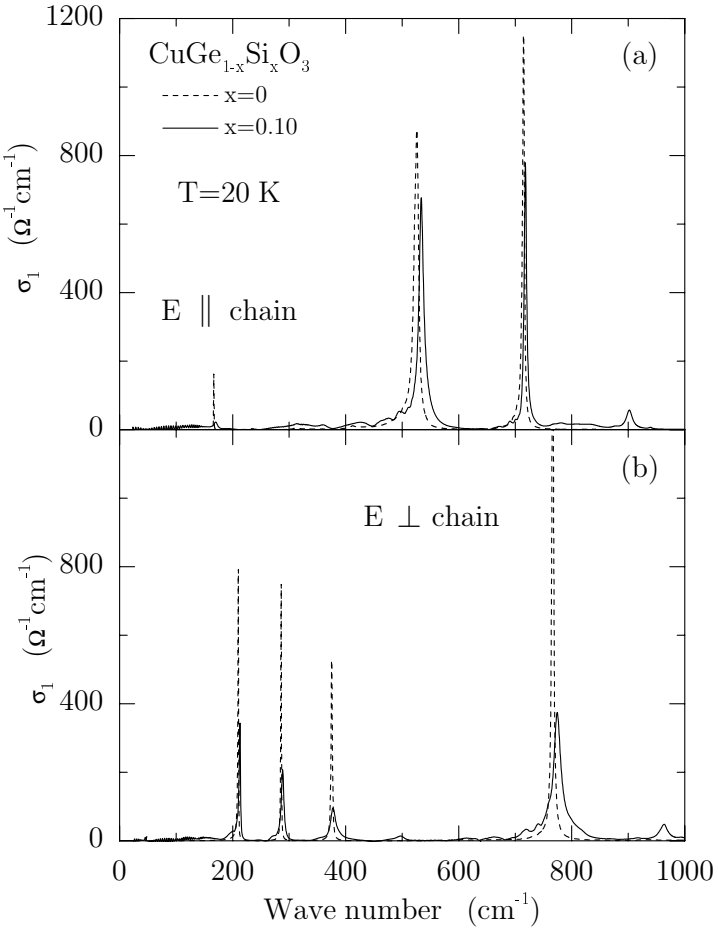

Figure 3.19: *Low temperature optical conductivity spectra, obtained by Kramers-Kronig analysis, of pure and 10% Si-doped $CuGeO_3$, for $E \parallel$ chain (a) and $E \perp$ chain (b). Note that in panel (b) the data on pure $CuGeO_3$ have ben clipped in order to use the same scale as in panel (a): in fact, the peak value of the phonon at 766 cm^{-1} is 2010 $\Omega^{-1}cm^{-1}$.*

strictly forbidden in the space group *Pbmm* because the midpoint in between two adjacent Cu^{2+} ions, along the CuO_2 chains, has inversion symmetry. To verify this findings, x-ray diffraction experiments were performed by Hidaka *et al.* [47], at room temperature, on pure single crystals grown by the floating-zone method, subsequently improved in their quality by a combined annealing and slow cooling process. As a result, new superlattice reflections were found, related to tilting and rotation of the GeO_4 tetrahedra in four different manners along the c axis, and in antiphase along the a axis. As a consequence, local distortions of the CuO_6 octahedra are induced, with a four times periodicity along the c axis. The space group was determined to be $P2_12_12_1$, with an eight times larger unit cell, i.e., $2a \times b \times 4c$, with respect to the one originally proposed by Völlenkle *et al.* [2]. According to Hidaka *et al.* [47], this additional deformation of the structure would be there also on non carefully annealed single crystals, but only on a short-range scale. Moreover,

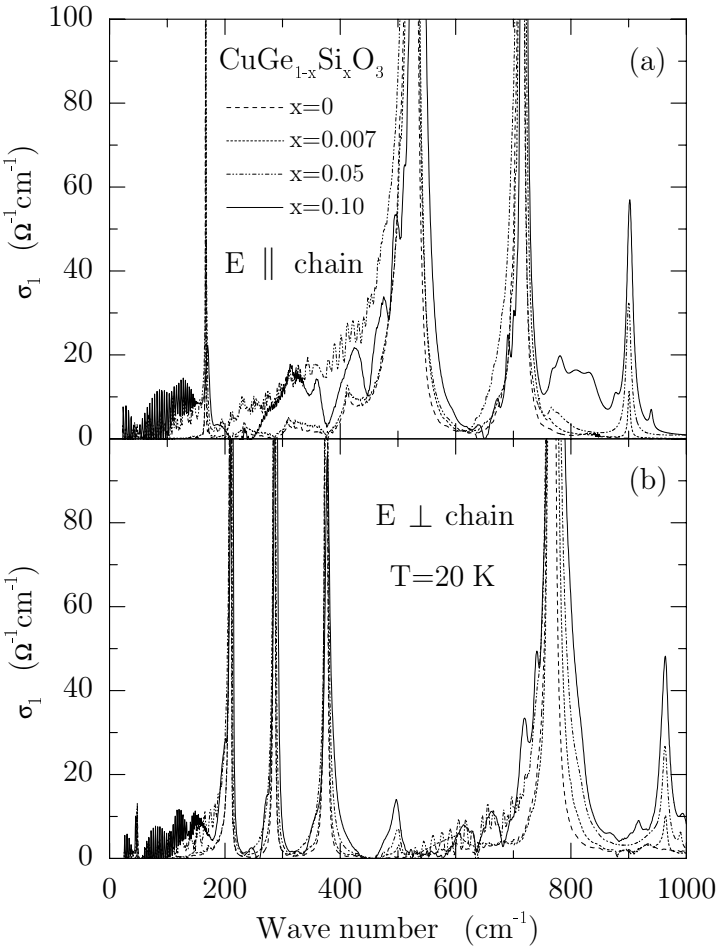

Figure 3.20: *Low temperature optical conductivity, obtained by Kramers-Kronig analysis, of pure and several Si-doped $CuGeO_3$ single crystals, for $E \parallel$ chain (a) and $E \perp$ chain (b).*

the newly proposed structure allows for the antisymmetric exchange interaction which was required to interpret the electron paramagnetic resonance results [46] on both annealed and as-grown samples, because the Dzyaloshinsky-Moriya exchange interaction depends only on the local symmetry around the nn spins on the c axis [55].

The results we just discussed [46, 47] could have strong consequences on the picture of the SP transition in $CuGeO_3$, because they imply the presence of four different values of the superexchange interaction at room temperature and, upon decreasing the temperature toward T_{SP}, strong fluctuations of the exchange interactions, induced by the increasing lattice instability. We will then try to see whether any conclusion (confirmation) can be drawn on the basis of our optical investigation of the phonon spectra, in both pure and doped $CuGeO_3$. In order to do that, we have first to calculate, by a group theoretical analysis, symmetry and number (obviously huge, for an eight times larger unit cell) of the lattice vibrations for the newly proposed space group $P2_12_12_1$ [47]. Skipping the details of the calculation, the irreducible representations of the optical vibrations of $CuGeO_3$ in the

high temperature phase, for the space group $P2_12_12_1$, is:

$$\begin{aligned}\Gamma'' = 56A(aa,bb,cc) + 55B_1(ab) + 63B_2(ac) + 63B_3(bc) \\ + 55B_1(E\|c) + 63B_2(E\|b) + 63B_3(E\|a)\ ,\end{aligned} \tag{3.7}$$

corresponding to 63, 63, and 55 optical active modes along the a, b, and c axes, respectively. As we already discuss in section 3.3.1, the number of phonons detected in the reflectivity spectrum of pure $CuGeO_3$ was in agreement with the results of the group theoretical analysis for the space group *Pbmm* proposed by Völlenkle *et al.* [2]. At the same time, as observed by Yamada and co-workers [46, 47], the additional distortion, characterizing the $P2_12_12_1$ space group, is present only on a short-range scale in as-grown samples, like the ones used in this experimental work. However, even on pure $CuGeO_3$, in fitting the reflectivity spectra with Lorentz oscillators for the optical phonons, we had to add, in order to be able to exactly reproduce the experimental data, a number of very weak and broad additional peaks, of unclear origin. In these context, more significant seem to be the results acquired on Si substituted $CuGeO_3$ single crystals. We already mentioned, commenting the reflectivity spectra, how strongly was the phonon spectrum affected by the presence of Si in the samples. This effect is even more evident when the optical conductivity spectra are considered. In fig. 3.19, the low temperature optical conductivity of pure and 10% Si-doped $CuGeO_3$, for $E \parallel$ chain (a) and $E \perp$ chain (b), is plotted. We can observe a reduction of oscillator strength and a broadening for all the lattice vibrations. Moreover, additional bands appear over the all range, as clearly shown in fig. 3.20, where the low temperature optical conductivity, for all the measured Si-doped samples, is presented. We can see that not only sharp peaks appear at 900 and 960 cm^{-1} along the c and b axes, respectively, as discussed at the beginning of this section. There is also, in fact, a large number of phonon bands, growing in intensity upon increasing the Si concentration, at both low and high frequencies. It is obviously not possible to check in detail whether we detected all the modes expected, on the basis of group theory, for the newly proposed space group $P2_12_12_1$ [46,47]: There are simply too many of them, in both theory (see eq. 3.7) and experiment (see fig. 3.20). Moreover, we have to take into account that, in general, the introduction of impurities in a crystal results in a relaxation of the k conservation rule. Therefore, states with $k \neq 0$ are projected back to the Γ point, and phonon bands averaged over the entire Brillouin zone can be measured in an optical experiment. However, we may speculate that Si, that has such a strong influence on T_{SP} via the side group effect [52, 53], could also be responsible for enhancing the underlying lattice distortion which was suggested to be already present in pure $CuGeO_3$, by Yamada and co-workers [46, 47]. In our opinion these results, although not conclusive, indicate that a symmetry lower than the one assumed until now could be a possible one. In particular, it should be taken into account as one of the possible explanations for the aspects still unresolved of the physics of $CuGeO_3$ (see section 3.5).

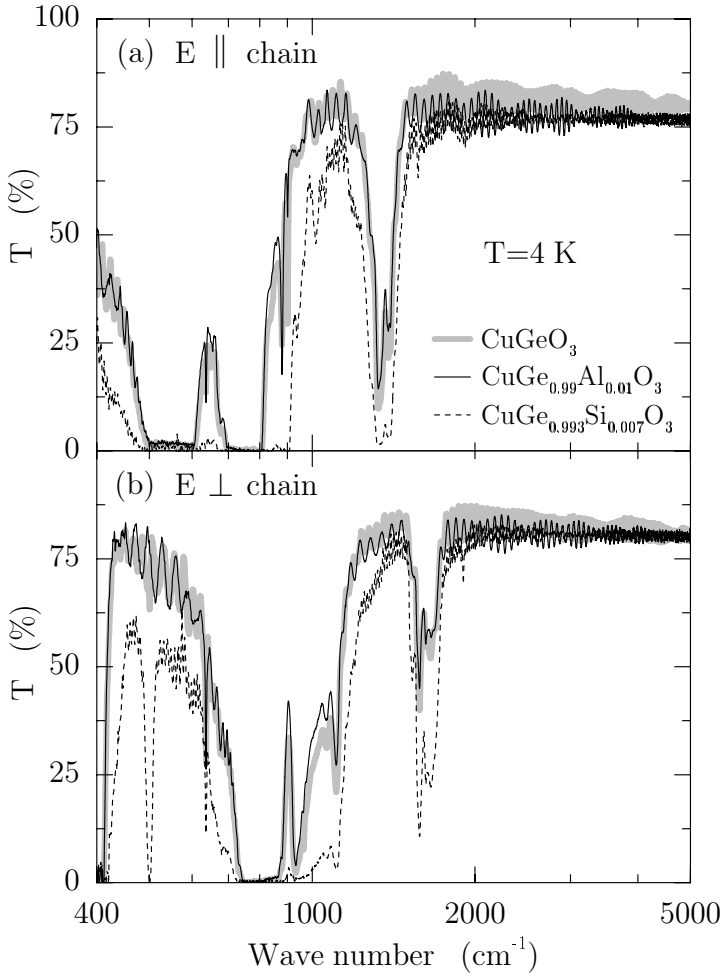

Figure 3.21: *Low temperature transmission spectra of pure, 1% Al, and 0.7% Si doped $CuGeO_3$, for $E \parallel$ chain (a) and $E \perp$ chain (b).*

3.4.2 Mid-Infrared Transmission

In this section we will discuss the optical data obtained by performing transmission experiments, in the range going from 400 to 8000 cm^{-1}, on several $Cu_{1-\delta}Mg_\delta GeO_3$ (with $\delta = 0, 0.01$), and $CuGe_{1-x}B_xO_3$ [with B=Si ($x = 0, 0.007, 0.05, 0.1$), and Al ($x = 0, 0.01$)] single crystals. In particular, by combining reflectivity and transmission results, we could calculate the optical conductivity by direct inversion of the Fresnel formula [23]. By this investigation, we aimed to study whether, in $CuGeO_3$, doping has an effect on the electronic and/or magnetic excitations similar to what has been observed on the underdoped parent compounds of high-T_c superconductors [56–58]. In fact, on the latter materials, chemical substitution introduces charge carriers in the 2D Cu-O planes, resulting in a disappearance of the gap and in the transfer of spectral weight into a Drude peak, for the in-plane optical response. Moreover, the so called 'mid-infrared' band, whose interpretation is still

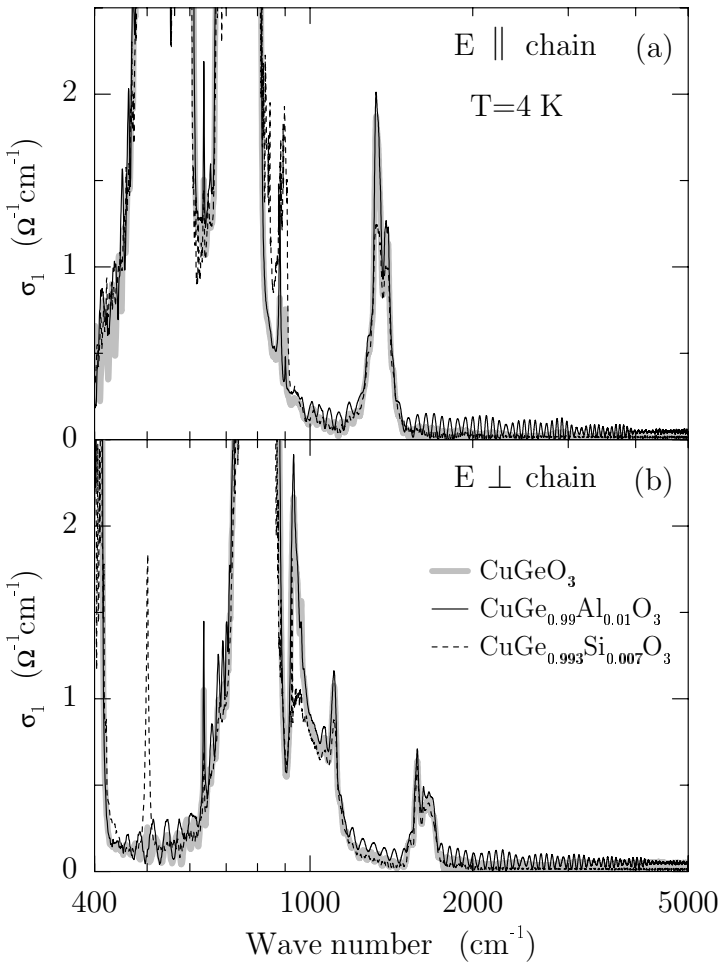

Figure 3.22: *Low temperature conductivity spectra, obtained by direct inversion of the Fresnel formula, of pure, 1% Al, and 0.7% Si doped $CuGeO_3$, for $E \parallel$ chain (a) and $E \perp$ chain (b). Note the very low value of $\sigma_1(\omega)$.*

controversial, is usually present in these systems [56–58].

The low temperature (4 K) transmission spectra of pure, 1% Al, and 0.7% Si doped $CuGeO_3$, for $E \parallel$ chain and $E \perp$ chain, are plotted in fig. 3.21a and 3.21b, respectively. Spectra at different temperatures above and below the phase transition were measured. However, the results are not shown because no particular temperature dependence was observed in cooling down the sample from room temperature to T_{SP}, nor across the phase transition. Similarly, the spectra for 1% Mg and 5 and 10% Si doped crystals are not presented because no additional information can be obtained from these results. As shown by fig. 3.21, the transmission through pure $CuGeO_3$, in this frequency region, is mainly characterized by the strong absorptions of the phonons of the high symmetry phase at 528 and 715 cm^{-1}, along the c axis, and at 376 and 766 cm^{-1}, along the b axis. In addition, many multiphonon bands are present, the most intense ones being at 1330 and 1580 cm^{-1}

along the c and b axes, respectively. The same features are observable on the doped samples where, however, more multiphonon bands are detected reflecting the presence of additional peaks in the single-phonon spectrum, already discuss in section 3.4.1 on the basis of reflectivity measurements. A last remark has to be made about the oscillations present in all the spectra of fig. 3.21. These are, as mentioned before, interference fringes due to Fabry-Perot resonances [23]; the different period of the interference pattern for the three crystals is simply due to the different thickness of the samples used in the experiments.

If we now consider the optical conductivity spectra plotted in fig. 3.22, it is clear that nothing else has been detected, in this frequency range, besides absorption processes purely related to lattice degrees of freedom. In particular, for all the sample, the conductivity is just zero from 2000 to 8000 cm^{-1}. From these results and from the fact that no signature of a Drude peak was observed in any of the doped samples in reflectivity experiments (see section 3.4.1), we conclude that no charge carriers are introduced in the $CuGeO_3$ by the different chemical substitutions we tried, nor magnetic/dielectric polarons (observed, e.g., in ultra low doped $YBa_2Cu_3O_6$ [57, 58]). One has to note that, in this sense, the most significant of the results we showed is the one obtained on Al substituted $CuGeO_3$ because in this case, contrary to Si substitution, Ge is replaced by an element with different valence.

3.5 Discussion

As shown in the course of this chapter, in our investigation of pure and doped $CuGeO_3$ with optical spectroscopy, we observed features which are not completely understandable on the basis of Cross and Fisher theory for the SP phase transition [4], and of the achieved picture of the SP transition in $CuGeO_3$. No pre-existing soft mode was detected, not only in our optical measurements, but especially in neutron scattering experiments [35]. Moreover, a direct singlet-triplet excitation across the magnetic gap, possibly at the wave vector $(0,2\pi/b,0)$ in the Brillouin zone, was detected in our transmission spectra. This excitation is, in principle, 'doubly' forbidden: In fact, because of symmetry considerations and of spin conservation we are restricted, in an optical experiment, to excitations characterized by $k=0$ and $\Delta S=0$. Finally, strong changes in the phonon spectrum were observed on Si-substituted samples, which might be explained in terms of the alternative space group $P2_12_12_1$, recently proposed for $CuGeO_3$ in the high temperature uniform phase [46, 47].

Many attempts have recently been made to improve the understanding of the SP phase transition in $CuGeO_3$. In particular, it has been shown that the adiabatic treatment of the 3D phonon system, characteristic for the Cross and Fisher theory [4], is not appropriate for the case of $CuGeO_3$, where the phonons contributing appreciably to the SP distortion have energies much higher that the magnetic gap [59, 60]. An alternative description of the SP transition, not based on the assumption of phononic adiabaticity, was developed by Uhrig [59]: Phonons are considered as the fast subsystem, responsible for the interchain coupling, and an effective dressed spin model is derived. As a result, the soft phonon is absent and the SP transition is characterized by growing domains of coherent dimerization, whose size diverges at T_{SP}. Alternatively, Gros *et al.* [60] showed that no inconsistency is present

in Cross and Fisher theory [4]: They concluded that, in Cross and Fisher framework, a soft phonon has to be present only if the bare phonon frequency satisfies the relation $\Omega_0 < 2.2\,T_{SP}$. For larger phonon frequencies only a central peak is expected at T_{SP}. However, this new collective excitation, which would consist of the linear superposition of a phonon with two magnons in a singlet state [60], has not been observed up to now. Moreover, it has been shown that for a detailed understanding of magnetic susceptibility [1,10] and magnetostriction [61,62] data and, at the same time, of the singlet and triplet excitation branches below the continuum [29,37], not only the 2D character of the system cannot be neglected [8,59], but also both the nn (J_1) and the nnn (J_2) magnetic exchange interactions have to be taken into account in $CuGeO_3$ [62–64]. The system would then be described by an alternating and frustrated AF 1D Heisenberg spin-chain model:

$$H = J \sum_j \left\{ \left[1 + \delta(-1)^i \right] \vec{S}_j \cdot \vec{S}_{j+1} + \alpha \vec{S}_j \cdot \vec{S}_{j+2} \right\} \ , \tag{3.8}$$

where δ is the static dimerization parameter and $\alpha = J_1/J_2$ is the frustration parameter. In particular, the value $\alpha = 0.354$ was obtained [62–64], which is significantly larger than the critical value sufficient for the formation of a spontaneous gap in the magnetic excitation spectrum, in absence of lattice dimerization, i.e., $\alpha_c = 0.241$ [65,66]. However, on the basis of this approach and, in particular, with the large value obtained for α, the amplitude of the dimerization δ, estimated by reproducing the singlet-triplet excitation gap [67,68], is substantially underestimated. In fact in this way, the very small value $\delta \simeq 0.012$ is obtained, whereas, from the combined analysis of the structural lattice distortion in the dimerized phase and of the magneto-elastic coupling in the uniform phase (from magnetostriction measurements), the value $\delta \simeq 0.04 - 0.05$ results [69]. Still retaining the value $\alpha = 0.354$, a consistent value for the lattice dimerization (i.e., of the order of 5%) is obtained from the analysis of the inelastic neutron scattering data if, instead of a static dimerization parameter δ, an explicit coupling between the spins and the three dimensional phonon system is introduced in the Hamiltonian given in eq. 3.8 [70].

In relation to the space group $P2_12_12_1$, recently proposed for $CuGeO_3$ in the high temperature phase [46,47], besides the optical data on Si-substituted samples we presented, very interesting are the inelastic neutron scattering results reported by Lorenzo *et al.* [71]. A second singlet-triplet (optical) branch was observed in pure $CuGeO_3$, with a gap value at the Γ point of ~ 5.8 meV. The spectral weight of this branch has been shown to be related to the presence of Dzyaloshinsky-Moriya antisymmetric exchange interaction [55] and, therefore, to the absence of a center of inversion between Cu^{2+} ions along the CuO_2 chains, feature characteristic of the space group $P2_12_12_1$ [47]. These results are not only showing that the structure generally assumed for $CuGeO_3$ in the uniform phase may be incorrect, but they are also suggesting a possible explanation for the singlet-triplet excitation we observed in transmission at ~ 44 cm$^{-1} \sim 5.5$ meV. In fact, such a transition, with approximately the right energy value, is now present at $k = 0$ and not only at the wave vector $(0,2\pi/b,0)$, which is not accessible in an optical experiment. The final constraint $\Delta S = 0$, which is not satisfied for this excitation, could be possibly explained as a consequence of spin-orbit interaction, which relaxes the spin conservation rule.

3.6 Conclusions

In this chapter we have been discussing the temperature dependent optical response of pure and doped $CuGeO_3$, in the frequency range going from 20 to 32 000 cm^{-1} [18, 19]. We could detect, in the phonon spectra, zone boundary folded modes activated by the SP phase transition. Following the temperature dependence of these modes we were able to determine the second order character of the phase transition and to study the effect of doping on T_{SP}: In particular, we showed that the substitution of Ge with Si is three times more efficient, than the one of Cu with Mg, in reducing T_{SP}. This was explained, following Khomskii and co-workers [52, 53], as a consequence of the side-group effect. Moreover, in the transmission spectra we detected a direct singlet-triplet excitation, across the magnetic gap, which is in principle optically forbidden in the space group *Pbmm* generally assumed for $CuGeO_3$ in the high temperature phase. The optical activity of this excitation and the strong changes in the phonon spectra of Si-substituted samples might be explained in terms of the alternative space group $P2_12_12_1$, recently proposed for $CuGeO_3$ in the high temperature uniform phase [46, 47].

References

[1] M. Hase, I. Terasaki, and K. Uchinokura, Phys. Rev. Lett. **70**, 3651 (1993).

[2] H. Völlenkle, A. Wittmann, and H. Nowotny, Monatsh. Chem. **98**, 1352 (1967).

[3] E. Pytte, Phys. Rev. B **10**, 4637 (1974).

[4] M.C. Cross, and D.S. Fisher, Phys. Rev. B **19**, 402 (1979).

[5] L.N. Bulaevskii, A.I. Buzdin, and D.I. Khomskii, Solid State Commun. **27**, 5 (1978).

[6] M.C. Cross, Phys. Rev. B **20**, 4606 (1979).

[7] For a review, see J.P. Boucher, and L.P. Regnault, J. Phys. I **6**, 1939 (1996).

[8] M. Nishi, O. Fujita, and J. Akimitsu, Phys. Rev. B **50**, 6508 (1994).

[9] O. Fujita, J. Akimitsu, M. Nishi, and K. Kakurai, Phys. Rev. Lett. **74**, 1677 (1995).

[10] J.P. Pouget, L.P. Regnault, M. Aïn, B. Hennion, J.-P. Renard, P. Veillet, G. Dhalenne, and A. Revcolevschi, Phys. Rev. Lett. **72**, 4037 (1994).

[11] K. Hirota, D.E. Cox, J.E. Lorenzo, G. Shirane, J.M. Tranquada, M. Hase, K. Uchinokura, H. Kojima, Y. Shibuya and I. Tanaka, Phys. Rev. Lett. **73**, 736 (1994).

[12] M. Braden, G. Wilkendorf, J. Lorenzana, M. Aïn, G.J. McIntyre, M. Behruzi, G. Heger, G. Dhalenne, and A. Revcolevschi, Phys. Rev. B **54**, 1105 (1996).

[13] M. Hase, I. Terasaki, K. Uchinokura, M. Tokunaga, N. Miura, and H. Obara, Phys. Rev. B **48**, 9616 (1993).

[14] T. Lorenz, U. Ammerahl, T. Auweiler, B. Büchner, A. Revcolevschi, and G. Dhalenne, Phys. Rev. B **55**, 5914 (1997).

[15] J.W. Bray, H.R. Hart, L.V. Interrante, I.S. Jacobs, J.S. Kasper, G.D. Watkins, and S.H. Wee, Phys. Rev. Lett. **35**, 744 (1975).

[16] I.S. Jacobs, J.W. Bray, H.R. Hart, L.V. Interrante, J.S. Kasper, G.D. Watkins, D.E. Prober, and J.C. Bonner, Phys. Rev. B **14**, 3036 (1976).

[17] S. Huizinga, J. Kommandeur, G.A. Sawatzky, B.T. Thole, K. Kopinga, W.J.M. de Jonge, and J. Roos, Phys. Rev. B **19**, 4723 (1979).

[18] A. Damascelli, D. van der Marel, F. Parmigiani, G. Dhalenne, and A. Revcolevschi, Phys. Rev. B **56**, R11 373 (1997).

[19] A. Damascelli, D. van der Marel, F. Parmigiani, G. Dhalenne, and A. Revcolevschi, Physica B **244**, 114 (1998).

[20] D.L. Rousseau, R.P. Bauman, and S.P.S. Porto, J. Raman Spectrosc. **10**, 253 (1981).

[21] Z.V. Popović, S.D. Dević, V.N. Popov, G. Dhalenne, and A. Revcolevschi, Phys. Rev. B **52**, 4185 (1995).

[22] A. Revcolevschi, and G. Dhalenne, Adv. Mater. **5**, 657 (1993).

[23] M.V. Klein, and T.E. Furtak, *Optics* (John Wiley & Sons, New York, 1983).

[24] I. Terasaki, R. Itti, N. Koshizuka, M. Hase, I. Tsukada, and K. Uchinokur, Phys. Rev. B **52**, 295 (1995).

[25] M. Bassi, P. Camagni, R. Rolli, G. Samoggia, F. Parmigiani, G. Dhalenne, and A. Revcolevschi , Phys. Rev. B. **54**, R11 030 (1996).

[26] Q.J. Harris, Q. Feng, R.J. Birgeneau, K. Hirota, G. Shirane, M. Hase, and K. Uchinokura, Phys. Rev. B **52**, 15 420 (1995).

[27] J. Lorenzana, and G.A. Sawatzky, Phys. Rev. Lett. **74**, 1867 (1995).

[28] Q.J. Harris, Q. Feng, R.J. Birgeneau, K. Hirota, K. Kakurai, J.E. Lorenzo, G. Shirane, M. Hase, K. Uchinokura, H. Kojima, I. Tanaka, and Y. Shibuya, Phys. Rev. B **50**, 12 606 (1994).

[29] G. Els, P.H.M. van Loosdrecht, P. Lemmens, H. Vonberg, G. Güntherodt, G.S. Uhrig, O. Fujita, J. Akimitsu, G. Dhalenne, and A. Revcolevschi, Phys. Rev. Lett. **79**, 5138 (1997).

[30] A.D. Bruce, and R.A. Cowley, *Structural Phase Transitions* (Taylor & Francis, London, 1981).

[31] M.D. Lumsden, B.D. Gaulin, and H. Dabkowska, Phys. Rev. B **57**, 14 097 (1998).

[32] M.D. Lumsden, B.D. Gaulin, H. Dabkowska, and M.L. Plumer, Phys. Rev. Lett. **76**, 4919 (1996).

[33] D.E. Moncton, R.J. Birgeneau, L.V. Interrante, and F. Wudl, Phys. Rev. Lett. **39**, 507 (1977).

[34] For a detailed description of the backward wave oscillator and its use in (sub)mm spectroscopy on solids, see G. Kozlov, and A. Volkov, "Coherent Source Submillimeter Wave Spectroscopy" in *Millimeter Wave Spectroscopy on Solids*, G. Grüner ed. (Springer Verlag, 1995).

[35] M. Braden, B. Hennion, W. Reichardt, G. Dhalenne, and A. Revcolevschi, Phys. Rev. Lett. **80**, 3634 (1998).

[36] G. Li, J.L. Musfeldt, Y.J. Wang, S. Jandl, M. Poirier, A. Revcolevschi, and G. Dhalenne, Phys. Rev. B **54**, R15 633 (1996).

[37] M. Aïn, J.E. Lorenzo, L.P. Regnault, G. Dhalenne, A. Revcolevschi, B. Hennion, and Th. Jolicoeur, Phys. Rev. Lett. **78**, 1560 (1997).

[38] M. Arai, M. Fujita, M. Motokawa, J. Akimitsu, and S.M. Bennington, Phys. Rev. Lett. **77**, 3649 (1996).

[39] H. Kuroe, T. Sekine, M. Hase, Y. Sasago, K. Uchinokura, H. Kojima, I. Tanaka, and Y. Shibuya, Phys. Rev. B **50**, R16 468 (1994).

[40] P.H.M. van Loosdrecht, J.P. Boucher, and G. Martinez, G. Dhalenne, and A. Revcolevschi, Phys. Rev. Lett. **76**, 311 (1996).

[41] P.H.M. van Loosdrecht, J. Zeman, G. Martinez, G. Dhalenne, and A. Revcolevschi, Phys. Rev. Lett. **78**, 487 (1997).

[42] A. Damascelli, D. van der Marel, M. Grüninger, C. Presura, T.T.M. Palstra, J. Jegoudez, and A. Revcolevschi, Phys. Rev. Lett. **81**, 918 (1998).

[43] A. Damascelli, D. van der Marel, J. Jegoudez, G. Dhalenne, and A. Revcolevschi, Physica B, in press (1999).

[44] P.H.M. van Loosdrecht, S. Huant, G. Martinez, G. Dhalenne, and A. Revcolevschi, Phys. Rev. B **54**, R3730 (1996).

[45] G.S. Uhrig, Phys. Rev. Lett. **79**, 163 (1997).

[46] I. Yamada, M. Nishi, and J. Akimitsu, J. Phys. **8**, 2625 (1996).

[47] M. Hidaka, M. Hatae, I. Yamada, M. Nishi, and J. Akimitsu, J. Phys. **9**, 809 (1997).

[48] L.P. Regnault, J.-P. Renard, G. Dhalenne, and A. Revcolevschi, Europhys. Lett. **32**, 579 (1995).

[49] Y. Sasago, N. Koide, K. Uchinokura, M.C. Martin, M. Hase, K. Hirota, and G. Shirane, Phys. Rev. B **54**, R6835 (1996).

[50] H. Nakao, M. Nishi, Y. Fujii, T. Masuda, I. Tsukada, K. Uchinokura, K. Hirota, and G. Shirane, cond-mat/9811324 (23 November 1998).

[51] B. Grenier, J.-P. Renard, P. Veillet, C. Paulsen, G. Dhalenne, and A. Revcolevschi, Phys. Rev. B **58**, 8202 (1998).

[52] W. Geertsma, and D. Khomskii, Phys. Rev. B **54**, 3011 (1996).

[53] D. Khomskii, W. Geertsma, and M. Mostovoy, Czech. J. Phys. **46**, 3239 (1996).

[54] J. Goodenough, *Magnetism and the Chemical Bond* (John Wiley & Sons, New York, 1963).

[55] T. Moriya, Phys. Rev. **120**, 91 (1960).

[56] For a review, see M.A. Kastner, R.J. Birgeneau, G. Shirane, and Y. Endoh, Rev. Mod. Phys. **70**, 897 (1998), and references therein.

[57] M. Grüninger, Ph.D. Thesis, University of Groningen, in preparation (1999).

[58] M. Grüninger, D. van der Marel, A. Damascelli, A. Zibold, H.P. Geserich, A. Erb, M. Kläser, Th. Wolf, T. Nunner, and T. Kopp, Physica C, in press (1999).

[59] G.S. Uhrig, Phys. Rev. B **57**, R14 004 (1998).

[60] C. Gros, and R. Werner, Phys. Rev. B **58**, R14 677 (1998).

[61] B. Büchner, U. Ammerahl, T. Lorenz, W. Brenig, G. Dhalenne, and A. Revcolevschi, Phys. Rev. Lett. **77**, 1624 (1996).

[62] T. Lorenz, B. Büchner, P.H.M. van Loosdrecht, F. Schönfeld, G. Chouteau, A. Revcolevschi, and G. Dhalenne, Phys. Rev. Lett. **81**, 148 (1998).

[63] K. Fabricius, A. Klümper, U. Löw, B. Büchner, T. Lorenz, G. Dhalenne, and A. Revcolevschi, Phys. Rev. B **57**, 1102 (1998).

[64] G. Bouzerar, A.P. Kampf, and G.I. Japaridze, Phys. Rev. B **58**, 3117 (1998).

[65] G. Castilla, S. Chakravarty, and V.J. Emery, Phys. Rev. Lett. **75**, 1823 (1995).

[66] K. Okamoto, and K. Nomura, Phys. Lett. A **169**, 433 (1993).

[67] J. Riera, and A. Dobry, Phys. Rev. B **51**, 16 098 (1995).

[68] G. Bouzerar, A.P. Kampf, and F. Schönfeld, cond-mat/9701176 (23 January 1997).

[69] B. Büchner, H. Fehske, A.P. Kampf, and G. Wellein, cond-mat/9806022 (2 June 1998).

[70] G. Wellein, H. Fehske, and A.P. Kampf, Phys. Rev. Lett. **81**, 3956 (1998).

[71] J.E. Lorenzo, L.P. Regnault, J.P. Boucher, B. Hennion, G. Dhalenne, and A. Revcolevschi, preprint (1998).

Chapter 4

Charged Magnon Model

In the last few years insulating quasi two-dimensional (2D) S=1/2 quantum antiferromagnets (AF) and their one-dimensional (1D) analogs have attracted a lot of attention because of their relevance to the understanding of high-T_c superconductivity: The spin dynamics can be studied in detail in these systems by inelastic neutron and Raman scattering. However, it has been shown both experimentally and theoretically [1–6] that also infrared optical spectroscopy can be a very useful probe. For example, in the 2D-system La_2CuO_4 (1D-system Sr_2CuO_3) where two-magnon (two-spinon) excitations are in principle not optically active because of the presence of a center of inversion that inhibits the formation of any finite dipole moment, phonon-assisted magnetic excitations were detected in the mid-infrared region [1,4]. These magneto-elastic absorption processes are optically allowed because the phonon there involved is effectively lowering the symmetry of the system.

In this chapter we will focus our attention on systems where a breaking of symmetry is present because of charge ordering. We will show that, in this case, magnetic excitations are expected to be directly optically active and detectable in an optical experiment as *charged bi-magnons*: Double spin-flip excitations carrying a finite dipole moment. We will do that investigating the spin-photon interaction in a single two-leg ladder with a charge disproportionated ground state. We will then discuss the applicability of this simple analysis to real quasi-1D and 2D systems: On the basis of this model we can interpret qualitatively and quantitatively, as we will show in detail in chapter 5, the optical conductivity spectra of α'-NaV_2O_5 [7,8]. Moreover, we will briefly discuss the relevance of this model to the stripe phase of copper oxides superconductors [9] and of other strongly correlated oxides [10].

4.1 Single Two-Leg Ladder

4.1.1 Model Hamiltonian

In this section we discuss the single two-leg ladder depicted in fig. 4.1, where $t_\perp$ and $t_\parallel$ are the hopping parameters for the rungs and the legs, respectively, $d_\perp$ is the length of a rung, and -$\Delta/2$ and +$\Delta/2$ are the on-site energies for the left and the right leg of the ladder,

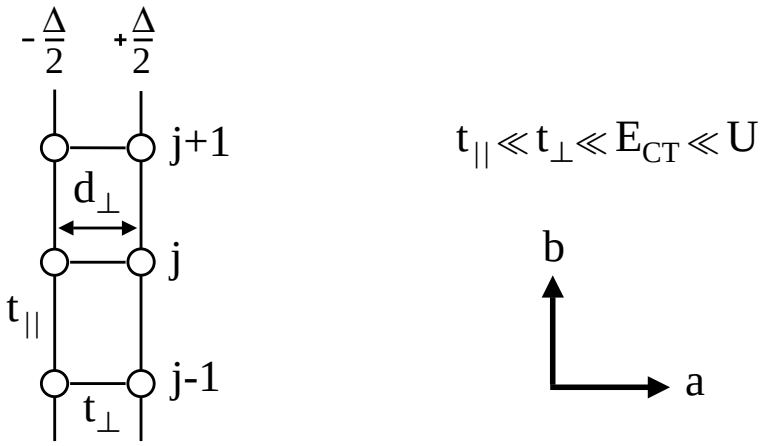

Figure 4.1: *Sketch of the single two-leg ladder discussed in this chapter. The circles represent the ionic sites having on-site energies -Δ/2 and +Δ/2 on the left and on the right leg of the ladder, respectively. The relevant parameters of the system are indicated: $t_\perp$ and $t_\parallel$ are the hopping parameters for the rungs and the legs, respectively, $d_\perp$ is the length of a rung, and j is the rung index. Also indicated is the relation, assumed throughout the discussion, between the different energy scales of the model.*

respectively. We work at quarter filling, i.e., one electron per rung. The total Hamiltonian H_T of the system is:

$$
\begin{aligned}
H_T &= H_0 + H_\perp + H_\parallel \\
\\
H_0 &= U \sum_j \{ n_{jR\uparrow} n_{jR\downarrow} + n_{jL\uparrow} n_{jL\downarrow} \} + \Delta \sum_j n_{jC} \\
H_\perp &= t_\perp \sum_{j,\sigma} \left\{ L^\dagger_{j,\sigma} R_{j,\sigma} + H.c. \right\} \\
H_\parallel &= t_\parallel \sum_{j,\sigma} \left\{ R^\dagger_{j,\sigma} R_{j+1,\sigma} + L^\dagger_{j,\sigma} L_{j+1,\sigma} + H.c. \right\} \ ,
\end{aligned}
\tag{4.1}
$$

where $L^\dagger_{j,\sigma}$ ($R^\dagger_{j,\sigma}$) creates an electron with spin σ on the left-hand (right-hand) site of the jth rung, U is the on-site Hubbard repulsion, $n_{jR\uparrow} n_{jR\downarrow}$ ($n_{jL\uparrow} n_{jL\downarrow}$) is counting the double occupancies on the right-hand (left-hand) site, $n_{jC} = (n_{jR} - n_{jL})/2$ is the charge displacement operator, and Δ is the potential energy difference between the two sites. Considering only H_0 at quarter filling one immediately realizes that Δ is not only breaking the left-right symmetry of the system (for the symmetric ladder $\Delta = 0$), but it is also introducing a long range charge ordering with one electron per site on the left leg of the ladder. Working in the limit $t_\perp \gg t_\parallel$ we can consider each rung as an independent polar molecule (with one electron) described by the Hamiltonian H_{j0}+$H_{j\perp}$. The two solutions are lob-sided bonding and antibonding wave functions $|\tilde{L}\rangle = u|L\rangle + v|R\rangle$, and $|\tilde{R}\rangle = u|R\rangle - v|L\rangle$,

with:

$$u = \frac{1}{\sqrt{2}}\sqrt{1+\frac{\Delta}{E_{CT}}}\ , \qquad\qquad v = \frac{1}{\sqrt{2}}\sqrt{1-\frac{\Delta}{E_{CT}}}\ , \tag{4.2}$$

where $E_{CT}=\sqrt{\Delta^2+4t_\perp^2}$ is the splitting between these two eigenstates. The excitation of the electron from the bonding to the antibonding state is an optically active transition with a degree of charge transfer (CT) from the left to the right site which is the larger the bigger is Δ. It is possible to calculate the integral of the real part of the optical conductivity $\sigma_1(\omega)$ for this excitation, quantity that can be very useful in the analysis of optical spectra. Starting from the general expression derived in chapter 1:

$$\int_0^\infty \sigma_1(\omega)d\omega = \frac{\pi q_e^2}{\hbar^2 V}\sum_{n\neq g}(E_n-E_g)\ |\langle n|\sum_i \mathbf{x}_i|g\rangle|^2\ , \tag{4.3}$$

where V is the volume, q_e is the electron charge and i is the site index, and noticing that for one rung $\langle\tilde{R}|\mathbf{x}_i|\tilde{L}\rangle=-d_\perp t_\perp/E_{CT}$, we obtain the following expression, which is exact for one electron on two coupled tight-binding orbitals:

$$\int_{CT}\sigma_1(\omega)d\omega = \pi q_e^2 N d_\perp^2 t_\perp^2 \hbar^{-2} E_{CT}^{-1}\ , \tag{4.4}$$

where N is the volume density of the rungs. Comparing eq. 4.4 and the expression for E_{CT} with the area and the energy position of the CT peak observed in the experiment, we can extract both $t_\perp$ and Δ.

In the ground state of the Hamiltonian $H_0+H_\perp$, each electron resides in a $|L\rangle$ orbital, with some admixture of $|R\rangle$. Let us now introduce the coupling of the rungs along the legs, considering $H_\parallel$ and a small fragment of the ladder with only two rungs. We have now to take into account the spin degrees of freedom: If the two spins are parallel, the inclusion of $H_\parallel$ has no effect, due to the Pauli-principle. If they form a $S=0$ state, the ground state can gain some kinetic energy along the legs by mixing in states where two electrons reside on the same rung. We start from the singlet ground state for the two rungs:

$$|\tilde{L}_1\tilde{L}_2\rangle = \frac{1}{\sqrt{2}}\left\{|\tilde{L}_{1\uparrow}\tilde{L}_{2\downarrow}\rangle - |\tilde{L}_{1\downarrow}\tilde{L}_{2\uparrow}\rangle\right\}\ , \tag{4.5}$$

with eigenvalue $E_{L_1L_2}=-E_{CT}$, and we study the effect of $H_\parallel$ using a perturbation expansion in $t_\parallel/E_{CT}$, to the second order. However, $H_\parallel|\tilde{L}_1\tilde{L}_2\rangle$ does not coincide with any of the singlet eigenstates of the system consisting of two electrons on one rung with the Hamiltonian $H_{j0}+H_{j\perp}$. Therefore, in order to obtain the exchange coupling constant $J_\parallel$ between two spins on neighboring rungs, we have first to calculate the set of spin-singlet eigenstates for the two electrons on one rung, and then to evaluate the fractional parentages of $H_\parallel|\tilde{L}_1\tilde{L}_2\rangle$ with respect to that set.

The Hilbert subspace of two-electron spin-singlet states is spanned by the vectors:

$$\begin{aligned} |\,L_jL_j\rangle &= L^\dagger_{j,\uparrow}L^\dagger_{j,\downarrow}|0\rangle \\ |L_jR_j\rangle &= \frac{1}{\sqrt{2}}\left\{L^\dagger_{j,\uparrow}R^\dagger_{j,\downarrow} - L^\dagger_{j,\downarrow}R^\dagger_{j,\uparrow}\right\}|0\rangle \\ |R_jR_j\rangle &= R^\dagger_{j,\uparrow}R^\dagger_{j,\downarrow}|0\rangle\ . \end{aligned} \tag{4.6}$$

On this basis the Hamiltonian of the jth rung is:

$$H_{j0}+H_{j\perp} = \begin{bmatrix} U-\Delta & \sqrt{2}t_\perp & 0 \\ \sqrt{2}t_\perp & 0 & \sqrt{2}t_\perp \\ 0 & \sqrt{2}t_\perp & U+\Delta \end{bmatrix}\ . \tag{4.7}$$

A significant simplification of the problem occurs in the limit of a large U, which moreover elucidates the physics of exchange processes between a pair of dimers in an elegant and simple way. We therefore take the limit where $U\to\infty$. The solutions for $\Delta=0$ (ref. 11 by M.J. Rice) are the (anti)-symmetric linear combinations of $|L_jL_j\rangle$ and $|R_jR_j\rangle$ with energy U, and $|L_jR_j\rangle$ with energy $E_{LR}=-4t_\perp^2/U\to 0$. The triplet states have energy 0. For a general value of Δ (still obeying $\Delta\ll U$) the only *relevant* eigenstate for the calculation of the exchange processes between neighboring dimers is $|L_jR_j\rangle$, with energy $E_{LR}=0$. The other two states with energy of order U are projected out in this limit.

We can now go back to the problem of two rungs with one electron per rung, and consider the hopping along the legs treating $H_\parallel$ as a small perturbation with respect to $H_0+H_\perp$. We proceed by calculating the corrections to $|\tilde{L}_1\tilde{L}_2\rangle$ by allowing a finite hopping parameter $t_\parallel$ between the rungs. Using lowest order perturbation theory, the ground state energy of a spin-singlet is:

$$E_{g,S=0} = -E_{CT} - \langle\tilde{L}_1\tilde{L}_2|H_\parallel\frac{1}{H_0+H_\perp+E_{CT}}H_\parallel|\tilde{L}_1\tilde{L}_2\rangle\ . \tag{4.8}$$

We proceed by calculating the coefficients of fractional parantage by projecting $H_\parallel|\tilde{L}_1\tilde{L}_2\rangle$ on the two-electron single eigenstates of a single rung:

$$H_\parallel|\tilde{L}_1\tilde{L}_2\rangle = \sqrt{2}\,t_\parallel\sum_{j=1,2}\left\{u^2|L_jL_j\rangle + v^2|R_jR_j\rangle + \sqrt{2}\,uv\,|L_jR_j\rangle\right\}\ . \tag{4.9}$$

Calculating the second order correction to $E_{L_1L_2}$ for the S=0 state, in the limit where $U\to\infty$, and realizing that the correction for the S=1 spin configuration is zero, we obtain the exchange coupling constant $J_\parallel$:

$$J_\parallel = \frac{8\,t_\parallel^2\,t_\perp^2}{[\Delta^2+4\,t_\perp^2\,]^{\frac{3}{2}}}\ . \tag{4.10}$$

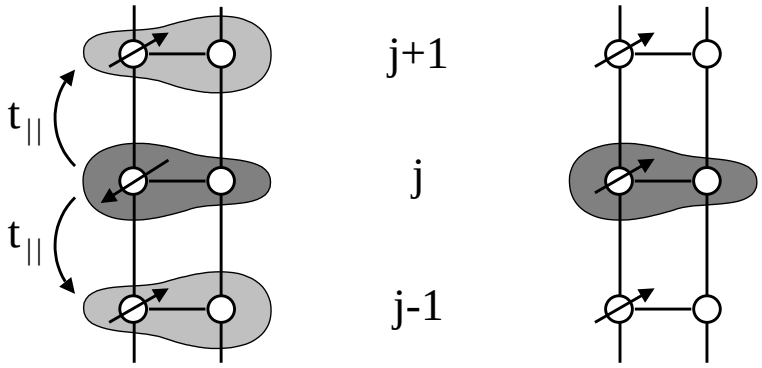

Figure 4.2: *Pictorial description of the electric dipole moment associated with a single spin-flip in the asymmetrical two-leg ladder. If spins are antiparallel (left-hand side), the charge of the jth electron is asymmetrically distributed not only over the jth rung but also on the nn rungs (with opposite asymmetry), because of the virtual hopping. If we flip its spin (right-hand side), the jth electron is confined to the jth rung, resulting in a reduced charge density on the right leg of the ladder. Therefore, there is a net dipole displacement (along the rung direction) of the antiparallel spin configuration compared to the parallel one.*

4.1.2 Interaction Hamiltonians and Effective Charges

Let us now consider three rungs of the ladder (see fig. 4.2) to understand the role of spin-flip excitations in this system. Because of the energy gain $J_{\parallel}$, in the ground state we have antiparallel alignment of the spins (fig. 4.2, left-hand side). The jth electron is described by the lob-sided bonding wave function $|\tilde{L}_j\rangle$ and, because of the virtual hopping to the nearest-neighbor (nn) rungs, by states where two electrons reside on the same rung. Working in the limit $U \to \infty$ these states have one electron in the $|L\rangle$ and one in the $|R\rangle$ state on the same rung. Therefore, the charge of the jth electron is asymmetrically distributed not only over the jth rung (dark grey area in fig. 4.2, left) but also on the nn rungs (light grey area in fig. 4.2, left). However, in the latter case most of the charge density is localized on the right leg of the ladder. If we flip the spin of the jth electron (fig. 4.2, right-hand side) no virtual hopping is possible any more to the nn rungs because of the Pauli principle. The electron charge distribution is now determined only by the lob-sided wave function $|\tilde{L}_j\rangle$ (dark grey area in fig. 4.2, right). As a result, there is a net dipole displacement of the antiparallel spin configuration compared to the parallel one: The spin-flip excitations carry a finite dipole moment parallel to the rung direction (a axis). This dipole moment can couple to the electric field of the incident radiation in an optical experiment, and result in what we refer to as *charged bi-magnon excitations*. One may remark, at this point, that only double spin flips can be probed in an optical experiment because of spin conservation. However, what we just discuss for a single spin flip can be extended to the situation where two spin flips on two different rungs are considered.

The coupling to light with $\vec{E} \,\|\, \vec{a}$ (rung direction) can now be included using the dipole

approximation. The only effect is to change the potential energy of the $|R\rangle$ states relative to the $|L\rangle$ states. In other words, we have to replace Δ with $\Delta+q_e d_\perp E_a$, where E_a is the component of the electric field along the rung. The coupling to the CT transition on the rungs is given by the Hamiltonian:

$$H_{CT} = q_e d_\perp E_a n_C = q_e d_\perp E_a \sum_j n_{jC} \ . \tag{4.11}$$

The Hamiltonian for the spin-photon coupling can be obtained taking the Taylor expansion of $J_\parallel$ with respect to E_a, and retaining the term which is linear in the electric field. Noticing that $dE_a = d\Delta/q_e d_\perp$, we have:

$$H_S = q_m d_\perp E_a h_S = q_m d_\perp E_a \sum_j \vec{S}_j \cdot \vec{S}_{j+1} \ , \tag{4.12}$$

where $q_m = \frac{1}{d_\perp}\frac{\partial J_\parallel}{\partial E_a} = q_e \frac{\partial J_\parallel}{\partial \Delta}$ is the effective charge involved in a double spin-flip transition, and $h_S = \sum_j \vec{S}_j \cdot \vec{S}_{j+1}$. Working in the limit $U \to \infty$, this effective charge reduces to:

$$q_m = q_e \frac{3J_\parallel \Delta}{\Delta^2 + 4t_\perp^2} \ , \tag{4.13}$$

where $J_\parallel$ is given by eq. 4.10. One has to note that for a symmetrical ladder, where $\Delta = 0$, the effective charge q_m vanishes, and the charged magnon effect disappears: The peculiar behavior of the spin flips we just described is an exclusive consequence of the broken left-right symmetry of the ground state. On the other hand, the bonding-antibonding transition would still be optically active. However, the bonding-antibonding energy splitting would be determined only by $t_\perp$, i.e., $E'_{CT} = 2t_\perp$. At this point we like to speculate on the role played by Δ in determining not only the optical activity of the double spin-flip excitations but also the insulating (metallic) nature of the system along the leg direction. For $\Delta = 0$ and for strong on-site Coulomb repulsion U, the energy cost to transfer one electron from one rung to the neighboring one is $E'_{CT} = 2t_\perp$. Therefore, the system is insulating for $4t_\parallel < E'_{CT} = 2t_\perp$ and metallic in the opposite case. If we now start from a metallic situation $4t_\parallel \geq E'_{CT} = 2t_\perp$, switching on Δ we can realize the condition $4t_\parallel < E_{CT} = \sqrt{\Delta^2 + 4t_\perp^2}$ which would result in a metal-insulator transition and, at the same time, in optical activity for the charged bi-magnons.

4.1.3 Spectral Weights

In this section we will attempt to estimate what would be, in an optical experiment, the relative spectral weights for the CT and the charged bi-magnon excitations of the single two-leg ladder. In particular, we want to show that these quantities can be expressed in terms of properly defined correlation functions. Considering the integral of the optical

conductivity, eq. 4.3, and the interaction Hamiltonians H_{CT} and H_S, we can write:

$$\begin{aligned}\int_{CT}\sigma_1(\omega)d\omega &= \frac{\pi q_e^2 d_\perp^2}{\hbar^2 V}\sum_{n\neq g}(E_n-E_g)\,|\langle n|n_C|g\rangle|^2 \\ \int_{S}\sigma_1(\omega)d\omega &= \frac{\pi q_m^2 d_\perp^2}{\hbar^2 V}\sum_{n\neq g}(E_n-E_g)\,|\langle n|h_S|g\rangle|^2 \quad .\end{aligned} \tag{4.14}$$

Let us now first concentrate on the CT excitation which is a simpler problem because, as we already discussed in section 4.1.1, on each rung we are dealing with one electron on two coupled tight-binding orbitals $|\tilde{L}\rangle$ and $|\tilde{R}\rangle$. Therefore, only one energy term $(E_n-E_g)=E_{CT}$ has to be considered in the previous equation. We can then write:

$$\begin{aligned}&\sum_{n\neq g}(E_n-E_g)\,|\langle n|n_C|g\rangle|^2 = E_{CT}\left\{\sum_n |\langle n|n_C|g\rangle|^2 - |\langle g|n_C|g\rangle|^2\right\} = \\ &= E_{CT}\left\{\langle g|n_C^2|g\rangle - |\langle g|n_C|g\rangle|^2\right\} = E_{CT}\left\{\langle n_C^2\rangle - \langle n_C\rangle^2\right\} \ ,\end{aligned} \tag{4.15}$$

where we took into account that the expectation value of n_C over the ground state is a real number. In the end, we obtain:

$$\int_{CT}\sigma_1(\omega)d\omega = \frac{\pi q_e^2 d_\perp^2}{4\hbar^2 V}E_{CT}\,g_C(T) \ , \tag{4.16}$$

where we have introduced the correlation function:

$$g_C(T) = 4\langle\langle n_C^2\rangle - \langle n_C\rangle^2\rangle_T \ . \tag{4.17}$$

For the ground state of the N independent rungs per unit volume $|g\rangle=\prod_j|\tilde{L}_j\rangle$, we can calculate $g_C=N[N-(N-1)4u^2v^2-N(v^2-u^2)^2]$. Because $(v^2-u^2)^2=1-4u^2v^2$, it follows that $g_C=N(2uv)^2$. From this result we see that $g_C=0$ if the two sites on a rung are completely independent: $u=1$ and $v=0$, for $t_\perp=0$ and $\Delta\neq 0$. On the other hand, g_C will have its maximum value $g_C=N$ when the rungs form homo-polar molecules: $u=v=1/\sqrt{2}$, for $t_\perp\neq 0$ and $\Delta=0$. Noticing that $1/(2uv)^2=1+(\Delta/2t_\perp)^2$ one can see that eq. 4.16 and eq. 4.4 correspond exactly to the same result.

In performing a similar quantitative analysis for the spin-flip excitations in the single two-leg ladder, we have to consider the elementary excitations of the 1D S=1/2 Heisenberg (HB) AF, system which does not have long range magnetic order at any temperature due to its 1D character. It was claimed by des Cloizeaux and Pearson [12] that the set of lowest excited states are one-magnon triplet (S=1) states, described by the dispersion relation:

$$\epsilon_1(q) = \frac{\pi}{2}J\,|\,sin\,q\,|\ , \qquad\qquad -\pi\leq q\leq\pi \ . \tag{4.18}$$

In addition to that, the exact calculations by Yamada [13] revealed the existence of a continuum of excited triplet states extending from the lower boundary given by eq. 4.18 to the upper boundary given by:

$$\epsilon_2(q) = \pi J\,|\,sin\,\frac{q}{2}\,|\ , \qquad\qquad -\pi\leq q\leq\pi \ . \tag{4.19}$$

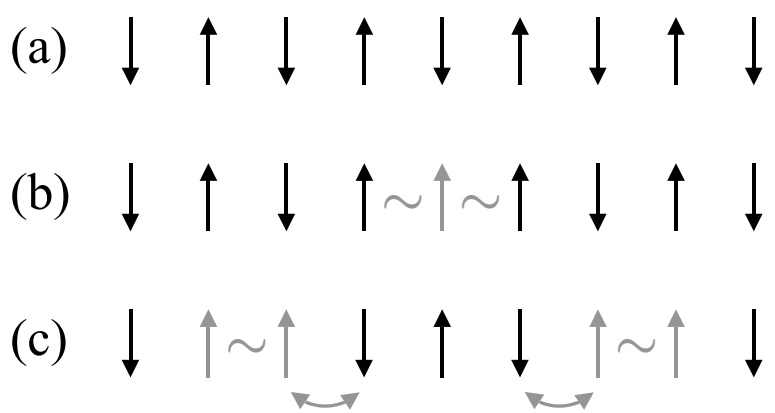

Figure 4.3: *Pictorial representation of the decay of a single spin-flip excitation (one magnon) into two spinons, in a 1D AF system. Starting from a Néel ordered 1D chain (a), a one magnon (S=1) excitation is created (b). Because of quantum fluctuations, spins are interchanged and two spinons (S=1/2) are eventually formed (c).*

Moreover, a second continuum of singlet (S=0) states would be degenerate with the triplet continuum, at least in the thermodynamic limit $N \to \infty$ [14]. Within this picture, the existence of the continuum can be understood as a consequence of the quantum fluctuations represented by the terms $(S_i^+ S_{i+1}^- + S_i^- S_{i+1}^+)$ in the HB Hamiltonian, which make a one-magnon excitation a not well defined quasiparticle in a 1D system. This concept can be explained in a pictorial way starting from the 1D chain of antiparallel spins sketched in fig. 4.3a (one has to be aware of the fact that we are using a starting point which, strictly speaking, is not valid because there is no long range Néel order in the ground state). In fig. 4.3b one magnon S=1 excited state is created and two wrong magnetic bonds are introduced in the system. Because of the quantum fluctuations, spins can be interchanged and the initial S=1 excitation decays in two S=1/2 excitations, referred to as spinons. These are domain walls between AF ordered segments of the 1D chain, corresponding to two wrong magnetic bonds (fig. 4.3c).

It has been shown by Faddeev and Takhtajan [15] that the true elementary excitations of the 1D HB AF are indeed the doublets of S=1/2 spinon excitations depicted in fig. 4.3c. Each spinon is described by the dispersion relation:

$$\epsilon'(k) = \frac{\pi}{2} J sin\, k \ , \qquad 0 \leq k \leq \pi \ . \tag{4.20}$$

The two-spinon continuum, with a total spin S=1 or S=0, is defined by $\epsilon'(q) = \epsilon'(k_1) + \epsilon'(k_2)$, where $q = k_1 + k_2$, and k_1 and k_2 are the momenta of the spinons (see fig. 4.4). The lower boundary is found for $k_1 = 0$ and $k_2 = q$ (or the other way around), i.e. $\epsilon'_1(q) = \frac{\pi}{2} J sin\, q$; and the upper one for $k_1 = k_2 = q/2$, i.e. $\epsilon'_2(q) = \pi J sin(q/2)$.

In the case we are presently discussing, we are dealing with double spin flips generated by the interaction Hamiltonian H_S. What is then relevant is the four-spinon continuum defined by $\epsilon'(q) = \sum_i \epsilon'(k_i)$, where $q = \sum_i k_i$, and the index i refers to the four spinons. Of

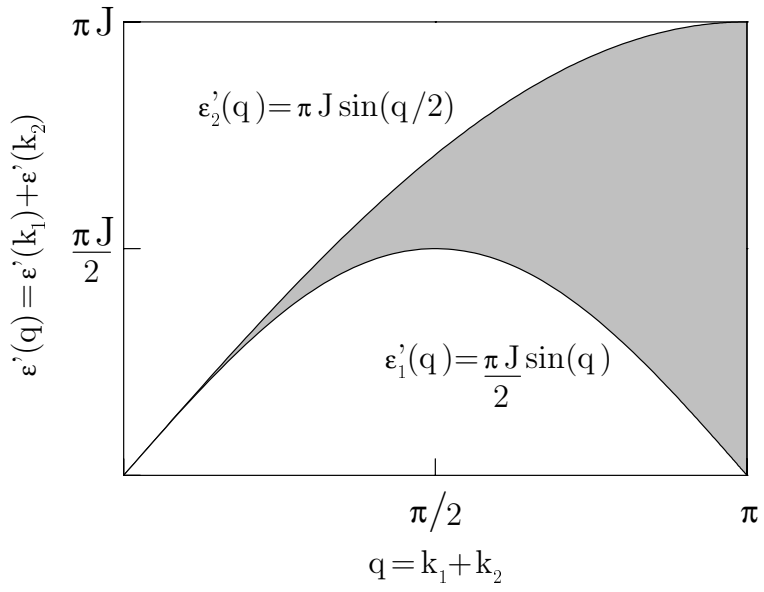

Figure 4.4: *Continuum of the two-spinon excitations for the 1D S=1/2 HB AF plotted versus the total momentum q of the two spinons. Indicated are the lower and upper boundaries of the two-spinon continuum given by $\epsilon_1'(q)$ and $\epsilon_2'(q)$, respectively.*

this excitation spectrum we would actually probe in an optical experiment only the $q=0$ (or equivalently $q=2\pi$) states, with total spin S=0. These states form a continuum at $q=0$ ($q=2\pi$) extending from $\epsilon_1'(0)=0$ to $\epsilon_2'(0)=2\pi J$. In fact, because eq. 4.20 has its maximum $\epsilon'_{max}=\pi J/2$ for $k=\pi/2$, four spinons with the same $k=\pi/2$ will correspond to the $q=2\pi$ ($q=0$) excited state with the highest possible energy: $\epsilon_2'(0)=4\epsilon'_{max}=2\pi J$.

If we now go back to eq. 4.14, we see that the evaluation of the integrated optical conductivity for the spin excitations is problematic because it requires a detailed analysis of the matrix elements for the states within the four-spinon continuum, at $q=0$. However, we can simplify the problem by means of a very crude approximation, and obtain the result which, although not rigorous, yet is meaningful for a comparison with the experiment. Let us replace in eq. 4.14 the quantity $(E_n - E_g)$ with the average energy value of the four spinon continuum: $E_S = \pi J_{\parallel}$. In this way, as in the case of the CT excitations, we can write:

$$\int_S \sigma_1(\omega) d\omega = \frac{\pi q_m^2 d_\perp^2}{4\hbar^2 V} E_S \, g_S(T) \ , \tag{4.21}$$

where $g_S(T)$ is the spin-correlation function defined as:

$$g_S(T) = 4\langle \langle h_S^2 \rangle - \langle h_S \rangle^2 \rangle_T \ . \tag{4.22}$$

One has to note that a non zero value of g_S requires that the total Hamiltonian H_T and the interaction Hamiltonian H_S do not commute with each other. This condition would be realized including, in H_T or in h_S, *nnn* interaction terms which would, unfortunately,

complicate the problem considerably. However, a finite value of g_S is obtained also in case of an AF broken symmetry of the ground state. We can then estimate an upper limit for g_S starting from a long range Néel ordered state, i.e. $|g\rangle = \prod_j |\tilde{L}_{2j,\uparrow}\tilde{L}_{2j+1,\downarrow}\rangle$. Over this ground state we can calculate $g_S = N$. On the other hand, for a random orientation of spins we would obtain $g_S = 0$. The real spin configuration of the system is of course something in between these two extreme cases and the value of g_S depends on the details of the many-body wave function of the spins. In particular, it depends on the probability of having fragments of three neighboring spins ordered antiferromagnetically. Therefore, g_S is higher the lower is the temperature and reaches for $T \to 0$ its maximum value which would be strictly smaller than $g_S = N$ in a truly 1D system. In relation to the interpretation of the optical conductivity data of α'-NaV_2O_5 within the charged magnon model (see chapter 5), it is important to note that, in a dimerized singlet (or triplet) configuration of the single two-leg ladder, we have $g_S = 0$.

In conclusion, the intensity of the spin fluctuations relative to the CT excitations in terms of effective charges, for the single two-leg ladder system, is given by the relation:

$$\frac{\int_S \sigma_1(\omega)d\omega}{\int_{CT} \sigma_1(\omega)d\omega} = \frac{q_m^2 g_S E_S}{q_e^2 g_C E_{CT}} \ . \tag{4.23}$$

Moreover, on the basis of the analysis presented above, we can state that the maximum limiting value for this quantity, in the limit $U \to \infty$ and with $J_\parallel$ given by eq. 4.10, is:

$$\frac{\int_S \sigma_1(\omega)d\omega}{\int_{CT} \sigma_1(\omega)d\omega} \leq \frac{9\pi}{32} \frac{\Delta^2 J_\parallel^4}{t_\parallel^2 t_\perp^4} \ . \tag{4.24}$$

4.2 Conclusions

The model we have been discussing in this chapter has been developed explicitly to interpret, qualitatively and quantitatively, the peculiar optical conductivity spectra we measured on single crystals of α'-NaV_2O_5 [7, 8]. The experimental results and their detailed analysis will be the subject of chapter 5. Here we want to stress that this very simplified model based on a single two-leg ladder at quarter filling, where only the parameter $t_\perp$, $t_\parallel$, Δ, and U have been taken into account in Hamiltonian H_T, is applicable to the case of α'-NaV_2O_5 because of the quasi one-dimensionality of this material. In fact, the basic building blocks of the crystal structure of α'-NaV_2O_5 are linear chains of alternating V and O ions, oriented along the b axis [16]. These chains are grouped into sets of two, forming a two-leg ladder (as in fig. 4.1), with the rungs oriented along the a axis. The rungs are formed by two V ions, one on each leg of the ladder, bridged by an oxygen ion. Only one V d electron per rung is present (quarter filling). The V-O distances along the rungs are shorter than along the legs, implying a stronger bonding along the rung ($t_\perp \gg t_\parallel$). In the a-b plane the ladders are shifted half a period along the b axis relative to their neighbors, and the coupling between the ladders is weak (quasi one-dimensionality).

In chapter 5 we will show that in the optical spectra of α'-NaV_2O_5 there are indeed features ascribable to charged bi-magnon excitations. However, our opinion is that the

importance of the charged magnon model goes beyond the understanding of the excitation spectrum of just this particular system. We expect this model (obviously in a more general and rigorous form), to be relevant to many of the strongly correlated electron systems, where the interplay of spin and charge plays a crucial role in determining the low energy electrodynamics.

At this point we would like to speculate that a specific case where charged magnon excitations could be observed is the stripe phase of copper oxides superconductors [9] and of other strongly correlated oxides [10]. In fact, even though the magnetism is quasi 2D in these systems, in the stripe phase a symmetry-breaking quasi 1D charge ordering takes place, which could result in optical activity for the charged magnons. For instance, in the optical conductivity spectra reported in the literature for $La_{1.67}Sr_{0.33}NiO_4$ below the charge ordering transition [17], it is possible to observe some residual conductivity inside the energy gap, whose nature has not been completely understood so far. Without further experimental and theoretical investigations it is of course not possible to make a strong claim. However, the reported features are suggestive of charged magnon excitations. In fact, for the value of J obtained from the two-magnon Raman scattering on this material [18], direct two-magnon optical absorption is expected in the same energy range (i.e., from zero to $\sim$0.2 eV) where the residual structure has been experimentally observed [17].

Pushing the speculation to its limit, one could imagine that even the local breaking of symmetry introduced by a single impurity in an AF could result in optical activity for pure spin-flip excitations [19, 20]. One particular system where this situation is probably realized is Zn-substituted $YBa_2Cu_3O_6$, where Zn is introduced in the CuO_2 planes. As we already discussed, in the cuprate parent compounds direct bi-magnon optical absorption is not allowed due to the inversion symmetry; only phonon-assisted magnetic excitations are optically active, whenever the involved phonon is lowering the symmetry of the system. In fact, phonon assisted bi-magnon excitations in the mid-infrared region were detected on both $YBa_2Cu_3O_6$ and $YBa_2Cu_{2.85}Zn_{0.15}O_6$ by our group [20, 21]. But on the sample with Cu substituted by Zn it is possible to observe, in the optical conductivity spectra, various features with frequencies coincident with those of pure double spin-flip excitations and, therefore, most probably ascribable to charged bi-magnon absorption processes [20, 21].

References

[1] J.D. Perkins, J.M. Graybeal, M.A. Kastner, R.J. Birgeneau, J.P. Falck, and M. Greven, Phys. Rev. Lett. **71**, 1621 (1993).

[2] J. Lorenzana, and G.A. Sawatzky, Phys. Rev. Lett. **74**, 1867 (1995).

[3] J. Lorenzana, and G.A. Sawatzky, Phys. Rev. B **52**, 9576 (1995).

[4] H. Suzuura, H. Yasuhara, A. Furusaki, N. Nagaosa, and Y. Tokura, Phys. Rev. Lett. **76**, 2579 (1996).

[5] J. Lorenzana, and R. Eder, Phys. Rev. B **55**, R3358 (1997).

[6] For a review, see M.A. Kastner, R.J. Birgeneau, G. Shirane, and Y. Endoh, Rev. Mod. Phys. **70**, 897 (1998), and references therein.

[7] A. Damascelli, D. van der Marel, M. Grüninger, C. Presura, T.T.M. Palstra, J. Jegoudez, and A. Revcolevschi, Phys. Rev. Lett. **81**, 918 (1998).

[8] A. Damascelli, D. van der Marel, J. Jegoudez, G. Dhalenne, and A. Revcolevschi, Physica B, in press (1999).

[9] J.M. Tranquada, B.J. Sternlieb, J.D. Axe, Y. Nakamura, and S. Uchida, Nature **375**, 561 (1995).

[10] C.H. Chen, S-W. Cheong, and A.S. Cooper, Phys. Rev. Lett. **71**, 2461 (1993).

[11] M.J. Rice, Solid State Comm. **31**, 93 (1979).

[12] J. des Cloizeaux, and J.J. Pearson, Phys. Rev. **128**, 2131 (1962).

[13] T. Yamada, Progr. Theor. Phys. Jpn. **41**, 880 (1969).

[14] J.C. Bonner, B. Sutherland, and P. Richards, AIP Conf. Proc. **24**, 335 (1975).

[15] L.D.Faddeev, and L.A. Takhtajan, Phys. Lett. A **85**, 744 (1981).

[16] P.A. Carpy, and J. Galy, Acta Cryst. B **31**, 1481 (1975).

[17] T. Katsufuji, T. Tanabe, T. Ishikawa, Y. Fukuda, T. Arima, and Y. Tokura, Phys. Rev. B **54**, R14230 (1996).

[18] K. Yamamoto, T. Katsufuji, T. Tanabe, and Y. Tokura , Phys. Rev. Lett. **80**, 1493 (1998).

[19] A. Damascelli, M. Grüninger, and D. van der Marel, in preparation.

[20] M. Grüninger, Ph.D. Thesis, University of Groningen, in preparation (1999).

[21] M. Grüninger, D. van der Marel, A. Damascelli, A. Zibold, H.P. Geserich, A. Erb, M. Kläser, Th. Wolf, T. Nunner, and T. Kopp, Physica C, in press (1999).

Chapter 5

Optical Spectroscopy of α'-NaV_2O_5

After many years of intensive experimental and theoretical work on $CuGeO_3$ (see chapter 3), another inorganic compound, α'-NaV_2O_5, has been attracting the attention of the scientific community working on low-dimensional spin systems, in general, and on the spin-Peierls (SP) phenomenon, in particular. In fact, in 1996 the isotropic activated behavior of the magnetic susceptibility has been observed at low temperatures on α'-NaV_2O_5 [1]. Moreover, superlattice reflections, with a lattice modulation vector $k=(\pi/a, \pi/b, \pi/2c)$, were found in an x-ray scattering experiment [2], and a spin gap Δ=9.8 meV was observed, at the reciprocal lattice point $(2\pi/a, \pi/b, 0)$, with inelastic neutron scattering [2]. The SP picture was then proposed to explain the low temperature properties of this compound, with a SP transition temperatures T_{SP}=34 K [1]. In this context, α'-NaV_2O_5 seemed to be a particularly interesting material, as far as the full understanding of the SP phenomenon is concerned, because on the basis of the structural analysis reported by Carpy and Galy in 1975, suggesting the noncentrosymmetric space group $P2_1mn$ [3], it was assumed to be described by the one-dimensional (1D) spin-1/2 Heisenberg model better than $CuGeO_3$. In fact, for the latter compound it has been established both experimentally [4] and theoretically [5] that the 2D character of the system cannot be neglected.

On the other hand, on the basis of additional experimental results later obtained, the interpretation of the phase transition in α'-NaV_2O_5 is still controversial. First of all, the reduction of T_{SP} upon increasing the intensity of an externally applied magnetic field, expected for a true SP system, has not been observed [6,7]. For instance, Büchner *et al.* [6], performing low temperature magnetization and specific heat measurements in magnetic field $H \leq 14\,\mathrm{T}$, obtained $\Delta T_{SP}(H) = T_{SP}(0) - T_{SP}(14\,\mathrm{T}) \approx 0.15$ K, i.e., almost a factor of 7 smaller that what expected on the basis of Cross and Fisher theory [8,9]. Furthermore, they claimed that the entropy reduction experimentally observed, across the phase transition, is considerably larger than the theoretical expectation for a 1D AF Heisenberg chain with only spin degrees of freedom and $J = 48$ meV (i.e., value obtained for α'-NaV_2O_5 from magnetic susceptibility measurements [1]). In order to explain these findings, degrees of freedom additional to those of the spin system should be taken into account, contrary to the interpretation of a magnetically driven phase transition [6].

This already quite puzzling picture became even more complicated when the crystal

structure and the symmetry of the electronic configuration of α'-NaV_2O_5, in the high temperature phase, were investigated in detail. In fact, on the basis of x-ray diffraction measurements we found [10], in agreement with other groups [11, 12], that the symmetry of this compound at room temperature is better described by the centrosymmetric space group $Pmmn$ than by the originally proposed $P2_1mn$ [3]. On the other hand, the intensities and polarization dependence of the electronic excitations detected in our optical spectra gave a direct evidence for a broken-parity electronic ground state [13, 14], in apparently better agreement with the noncentrosymmetric space group $P2_1mn$ originally proposed by Carpy and Galy [3]. As we will see in the course of the chapter, the solution of this controversy and the assessment of the symmetry issue are of fundamental importance for the understanding of the electronic and magnetic properties of the system and, ultimately, of the phase transition.

In presenting the results of our investigation on α'-NaV_2O_5, we will indeed start from the discussion of the symmetry of the high temperature phase on the basis of x-ray diffraction measurements [10]. Then we will analyze the data obtained with optical spectroscopy at different temperatures above and below T_{SP} (throughout the chapter, we will refer to the transition temperature as T_{SP} for simplicity, even though the interpretation of the transition is still controversial). In particular, we will concentrate on:

- Analysis of the temperature dependent phonon spectra, in relation to the x-ray diffraction data, in order to: First, learn more about the symmetry of the material in both high and low temperature phase. Second, detect signatures of the lattice distortion and study the character of the phase transition.

- Detailed study of the very peculiar electronic and magnetic excitation spectra. In particular, we will show that we could detect a low frequency continuum of excitations which, on the basis of the model developed in chapter 4, we ascribe to 'charged bimagnons', i.e., direct two-magnon optical absorption processes [13, 14].

Finally (section 5.5), we will discuss the relevance of our findings to the understanding of the nature of the phase transition in α'-NaV_2O_5. In particular we will try to assess whether the picture of a charge ordering transition, accompanied by the opening of a magnetic gap, is a valid alternative to the originally proposed SP description of the phase transition in α'-NaV_2O_5. In fact, this alternative interpretation has been recently put forward [15–19], on the basis of temperature dependent nuclear magnetic resonance (NMR) data [15].

5.1 Room-Temperature Crystal Structure

The interpretation of the phase transition at 34 K as a SP transition [1] is based on the noncentrosymmetric space group $P2_1mn$ originally proposed for α'-NaV_2O_5, in the high temperature phase, by Carpy and Galy [3]. Following their crystallographic analysis, the structure can be constructed from double-rows (parallel to the b axis) of edge sharing pyramids, one facing up and the other down, with respect to the a-b plane (see fig. 5.1).

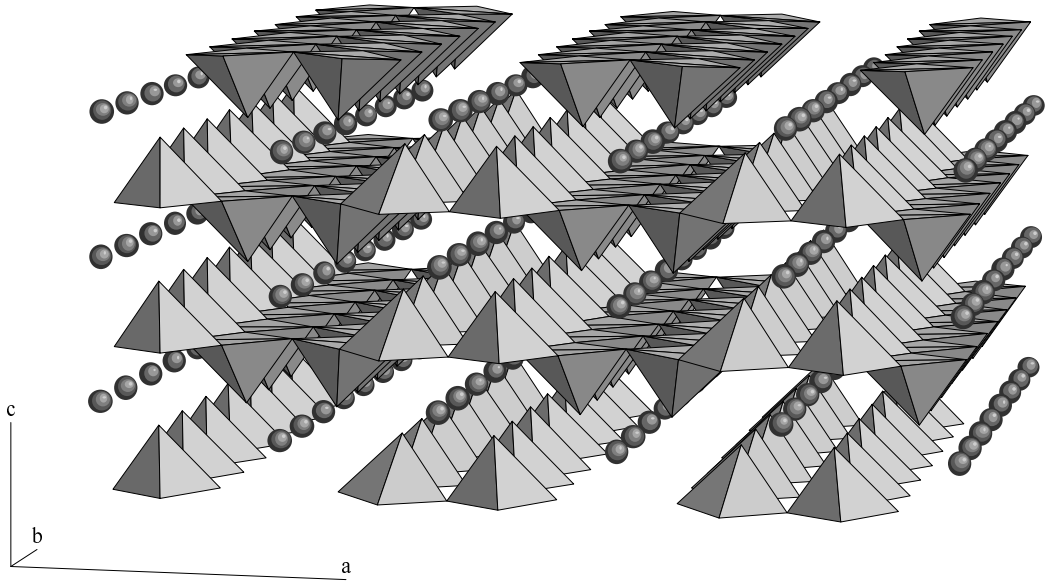

Figure 5.1: *High temperature crystal structure of α'-NaV_2O_5: The square pyramids around V ions [V-0(1), V-0(2), V-0(3)×3] and the rows of Na ions are shown.*

These double rows are connected by sharing corners, yielding a planar material. The planes are stacked along the c axis, with the Na in the channels of the pyramids. In the a-b plane (see fig. 5.2), we can then identify linear chains of alternating V and O ions, oriented along the b axis. These chains are grouped into sets of two, forming a ladder, with the rungs oriented along the a axis. The rungs are formed by two V ions, one on each leg of the ladder, bridged by an O ion. The V-O distances along the rungs are shorter than along the legs, implying a stronger bonding along the rung. In the a-b plane the ladders are shifted half a period along the b axis relative to their neighbors. The refinement of Carpy and Galy [3], based on photographic data, in the noncentrosymmetric space group $P2_1mn$, allows for two inequivalent V positions in the asymmetric unit. These sites were interpreted as different valence states, V^{4+} and V^{5+}, represented by dark and light gray balls, respectively, in fig. 5.2. In this structure it is possible to identify well-distinct 1D magnetic V^{4+} (S=1/2) and non-magnetic V^{5+} (S=0) chains running along the b axis of the crystal, and alternating each other along the a axis. This configuration would be responsible for the 1D character (Bonner-Fisher-like [20]) of the high temperature susceptibility [21] and for the SP transition, possibly involving dimerization within the V^{4+} chains [1]. Moreover, due to the details of the crystal structure, only one of the three t_{2g} orbitals of V^{4+}, i.e., the d_{xy} orbital, is occupied [12]. As a result, the insulating character of α'-NaV_2O_5, which has been observed in DC resistivity measurements [22, 23], would be an obvious consequence of having a 1D 1/2-filled Mott-Hubbard system. However, the structure determination reported by Carpy and Galy [3] yielded atomic coordinates with a pseudo inversion center at (0.259, 0.25, 0.11) [24]. Therefore, we have undertaken a structure redetermination to investigate the (centro)symmetry.

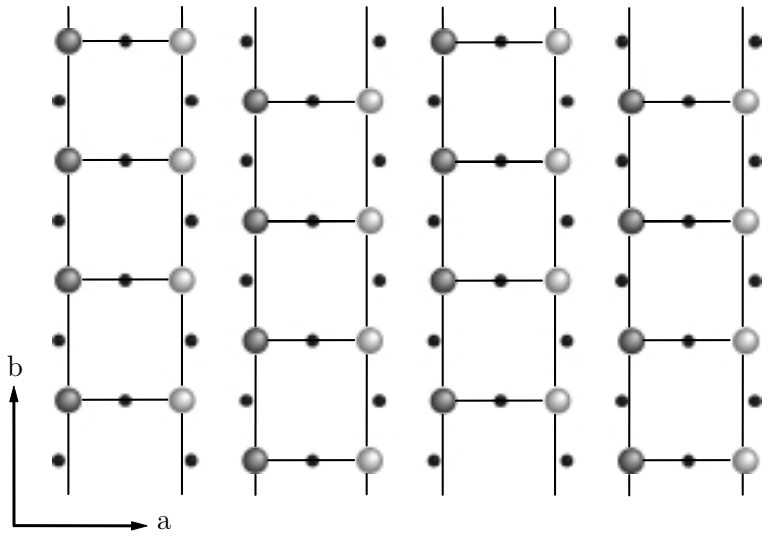

Figure 5.2: *Two-leg ladder structure formed by O and V ions in the a-b plane of α'-NaV_2O_5. Black dots are O ions; dark and light gray balls are V^{4+} and V^{5+} ions, respectively, arranged in 1D chains in the space group $P2_1mn$ proposed by Carpy and Galy [3].*

5.1.1 X-Ray Diffraction Analysis

The experimental details of our structure redetermination [10] are reported in table 5.1, whereas the fractional atomic coordinates and some selected geometric parameters are given in table 5.2 and 5.3, respectively. The ORTEP (Oak Ridge Thermal-Ellipsoid Plot Program) drawing with displacement ellipsoids at the 50% probability level of α'-NaV_2O_5 is presented in fig. 5.3, where several VO_5 square pyramids are shown. Our results suggest a structure very similar to the one proposed by Carpy and Galy [3] [a small difference was the somewhat more symmetric eight-fold coordination of Na (with Na-O distances 2.4325(11)-2.6038(9) Å) than in the refinement of Carpy and Galy (2.43-2.90 Å)]. On the other hand, one major difference was found, namely, the presence of a center of inversion in the unit cell. Therefore, we think that our structure determination is a proof for the centrosymmetric space group *Pmmn*. In particular, this result suggests the existence of only one kind of V per unit cell, with an average valence for the V ions of +4.5.

This finding has important implications on the understanding of the electronic and magnetic properties of α'-NaV_2O_5. In fact, we have now to think in the framework of a 1/4-filled two-leg ladder system: It is still possible to recover an insulating ground state assuming that the *d* electron, supplied by the two V ions forming a rung of the ladder, is not attached to a particular V site but is shared in a V-O-V molecular bonding orbital along the rung [12]. In this way, we are effectively back to a 1D spin system (a two-leg ladder with one spin per rung in a symmetrical position). However, in case of a SP phase transition, singlets would have to be formed by electrons laying in molecular-like orbitals and a rather complicated distortion pattern would have to take place: Not simply the dimerization within a real 1D chain (as, e.g., in $CuGeO_3$), but a deformation of the

Crystal data	
α'-NaV_2O_5	Mo $K\bar{\alpha}$ radiation
M_r=204.87	λ=0.71073 Å
Orthorhombic	Unit cell parameters
Pmmn (origin: choice 2)	from 22 reflections
a=11.311(1) Å	θ=14.57-22.37°
b=3.610(1) Å	μ=4.77 mm^{-1}
c=4.800(1) Å	T=295 K
V=196.00(7) $Å^3$	Rectangular plate
Z=2	0.20×0.15×0.013 mm
D_x=3.471 Mg m^{-3}	Black
D_m not measured	Crystal source: by synthesis
Data collection	
Enraf-Nonius CAD-4F diffractometer	R_{int}=0.0232
$\omega/2\theta$ scans	θ_{max}=39.96°
Absorption correction:	h= -20→20
gaussian by integration (Spek, 1983)	k=0→6
T_{min}=0.6010; T_{max}=0.9381	l=0→8
1472 measured reflections	3 standard reflections
701 independent reflections	frequency: 180 min
650 reflections with $I>2\sigma(I)$	intensity decay: 1.0%
Refinement	
Refinement on F^2	$(\Delta/\sigma)_{max}$=0.001
$R(F)$=0.0151	$\Delta\rho_{max}$=0.675 e $Å^{-3}$
$wR(F^2)$=0.0386	$\Delta\rho_{min}$= -0.429 e $Å^{-3}$
S=1.126	Extinction correction: SHELXL
701 reflections	Extinction coefficient: 0.067(4)
28 parameters	Scattering factors from
$w=1/[\sigma^2(F_0^2)+(0.0189P)^2]$	*International Tables for*
where $P=(F_0^2+2F_c^2)/3$	*Crystallography* (Vol. C)

Table 5.1: *Experimental details regarding the investigated α'-NaV_2O_5 single crystal, the data collection, and the refinement of the x-ray diffraction data.*

plaquettes, formed by four V ions, within a ladder.

Our evidence for the centrosymmetric space group $Pmmn$ is the very low $R(F)$-value of 0.015, and the fact that no lower value of $R(F)$ can be obtained when omitting the inversion center. The noncentrosymmetric space group $P2_1mn$ reported by Carpy and Galy [3] is, in our opinion, the result of the limited data set of 117 reflections, and of the photographic-data quality. Nevertheless, it is worthwhile to assess the validity of very small distortions yielding lower symmetry. Therefore, we considered a refinement in the polar 'equivalent' of $Pmmn$, i.e., the noncentrosymmetric space-group $P2_1mn$, in greater detail. The refinement converged to $wR(F^2)$=0.0512 for 1355 reflections with $F_0^2 \geq 0$ and 50 parameters, and $R(F)$=0.0201 for 1245 reflections obeying $F_0 \geq 4.0\,\sigma(F_0)$. The analysis shows that the standard deviations of the atomic positions in the polar refinement are approximately a factor of 10 larger than in the centrosymmetric refinement. This indicates much shallower minima in the least-squares refinement, caused by large correlation between atomic coordinates related by the pseudo-inversion-center. Similarly, the least-squares refinement protocol yields a substantial number (15) of large (> 0.90) correlation-coefficients between various parameters. Most of the equivalent bonds in $Pmmn$ are, in $P2_1mn$, still almost equal. The largest difference in interatomic distances between formerly equivalent bonds is found for V-O(1). The bond length of 1.8259(6) Å in $Pmmn$ splits into 1.7966(63) Å and 1.8543(63) Å in $P2_1mn$, i.e., a displacement of 0.0289 Å from the average value of 1.8254. One can interpret this measure of noncentrosymmetry of 0.029 Å in two ways.

The common 'crystallographic' interpretation considers the noncentrosymmetry as an artifact. We found that V and O's have all anisotropic temperature ellipsoids. One can mimic this by making the space group noncentrosymmetric and using a more isotropic temperature factor. Obviously, this causes large correlation between parameters in the least-squares procedure. Furthermore, one should keep in mind that the calculated standard deviations are based on random fluctuations, and are significantly underestimated when correlation is important. Therefore, this interpretation assigns a much higher probability to the centrosymmetric space group $Pmmn$.

An alternative interpretation is to use the statistics not to distinguish between the symmetries, but to quantify the maximum deviations from centrosymmetry in order to asses, e.g., the magnitude of the transition dipole moment. Our analysis shows that the reported standard deviations for the atomic positions are based on the underlying symmetry. This allows 0.029 Å deviations from centrosymmetry, about five times larger than the estimated standard deviation in the interatomic bond length, and should therefore be considered significant.

We conclude that our data are evidence for the centrosymmetric space group $Pmmn$. Deviations from centrosymmetry are restricted to values not larger than 0.03 Å. The Flack x parameter is often used to indicate noncentrosymmetric structures. However, its value of 0.41(7) indicates at most twinning in case of a noncentrosymmetric structure, and this would still lead to a centrosymmetric 'space-average'. Furthermore, we have to stress that x-ray diffraction measurements are sensitive mainly to charge distribution of core electrons and not of valence electrons. Therefore, if a breaking of symmetry in the distribution of the V d electrons were present on a local scale (as suggested by the optical conductivity

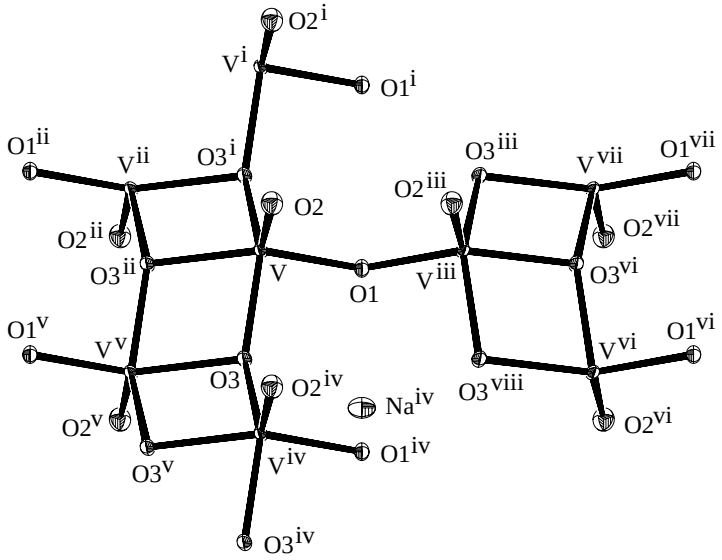

Figure 5.3: *ORTEP drawing with displacement ellipsoids at the 50% probability level of α'-NaV_2O_5 showing several VO_5 square pyramids. The symmetry codes of the V and O sub-labels are: (i) $x, 1+y, z$; (ii) $-x, \frac{1}{2}+y, 1-z$; (iii) $\frac{1}{2}-x, \frac{3}{2}-y, z$; (iv) $x, -1+y, z$; (v) $-x, -\frac{1}{2}+y, 1-z$; (vi) $\frac{1}{2}+x, 1-y, 1-z$; (vii) $\frac{1}{2}+x, \frac{1}{2}+y, 1+z$; (viii) $\frac{1}{2}-x, \frac{1}{2}-y, z$.*

	x	y	z	U_{eq}
V	0.09788(1)	3/4	0.60781(3)	0.0073(1)
O1	1/4	3/4	0.48050(2)	0.0094(2)
O2	0.11452(7)	3/4	0.94197(17)	0.0151(2)
O3	0.07302(6)	1/4	0.48769(16)	0.0097(1)
Na	1/4	1/4	0.14080(15)	0.0170(2)

Table 5.2: *Fractional atomic coordinates and equivalent isotropic parameters ($Å^2$) defined as: $U_{eq} = (1/3)\sum_i \sum_j U^{ij} a^i a^j \mathbf{a}_i \cdot \mathbf{a}_j$.*

V-O1	1.8259(6)	V-O3^i	1.9156(6)
V-O2	1.6150(9)	V-O3^{ii}	1.9867(9)
V-O3	1.9156(6)		
O1-V-O2	102.86(4)	O3-V-O3^i	140.87(3)
O1-V-O3	92.15(2)	O3-V-O3^{ii}	77.74(2)
O1-V-O3^i	92.15(2)	O3^i-V-O3^{ii}	77.74(2)
O1-V-O3^{ii}	147.11(4)	V-O1-V^{iii}	140.89(6)
O2-V-O3	108.42(2)	V-O3-V^{iv}	140.87(4)
O2-V-O3^i	108.42(2)	V-O3-V^v	102.26(2)
O2-V-O3^{ii}	110.03(4)	V^{iv}-O3-V^v	102.26(2)

Table 5.3: *Selected geometric parameters (Å,°), with the same symmetry codes as in fig. 5.3.*

data we will present in section 5.4), but without the long range order required by the noncentrosymmetric space group $P2_1mn$ proposed by Carpy and Galy [3], it would not be detectable in an x-ray diffraction experiment. Once again, x-rays would just see the 'space-average' given by the centrosymmetric space group $Pmmn$.

5.1.2 Group Theoretical Analysis

As discussed in the previous section, on the basis of our x-ray diffraction analysis [10] the symmetry of α'-NaV_2O_5, in the high temperature phase, is better described by the centrosymmetric space group $Pmmn$ than by the noncentrosymmetric $P2_1mn$ originally proposed by Carpy and Galy [3]. An additional way to assess the symmetry issue is to investigate the Raman and infrared phonon spectra, comparing the number of experimentally observed modes to the number expected for the two different space groups on the basis of a group-theoretical analysis. Obviously, a large number of modes has to be expected because each unit cell contains two formula units, corresponding to 48 degrees of freedom, which will be reflected in 48 phonon branches.

In the centrosymmetric space group $Pmmn$ the site groups in the unit cell are: C_{2v}^z for the 2 Na and the 2 O(1) atoms, and C_s^{xz} for the 4 V, the 4 O(2) and the 4 O(3). Following the nuclear site group analysis method extended to crystals [25], the contribution of each occupied site to the total irreducible representation of the crystal is:

$$\begin{aligned} \Gamma_{\mathrm{Na+O(1)}} &= 2[A_g + B_{1u} + B_{2g} + B_{2u} + B_{3g} + B_{3u}] \ , \\ \Gamma_{\mathrm{V+O(2)+O(3)}} &= 3[2A_g + A_u + B_{1g} + 2B_{1u} + 2B_{2g} + B_{2u} + B_{3g} + 2B_{3u}] \ . \end{aligned} \tag{5.1}$$

Subtracting the silent modes ($3A_u$) and the acoustic modes (B_{1u}+B_{2u}+B_{3u}), the irreducible representation of the optical vibrations, for the centrosymmetric space group $Pmmn$, is:

$$\begin{aligned} \Gamma = {} & 8A_g(aa,bb,cc) + 3B_{1g}(ab) + 8B_{2g}(ac) + 5B_{3g}(bc) \\ & + 7B_{1u}(E\|c) + 4B_{2u}(E\|b) + 7B_{3u}(E\|a) \ , \end{aligned} \tag{5.2}$$

corresponding to 24 Raman (A_g,B_{1g},B_{2g},B_{3g}) and 18 infrared (B_{1u},B_{2u},B_{3u}) active modes.

In the analysis for the noncentrosymmetric space group $P2_1mn$, we have to consider only the site group C_s^{yz} for all the atoms in the unit cell: 2 Na, 2 V(1), 2 V(2), 2 O(1), 2 O(2), 2 O(3), 2 O(4), and 2 O(5). Therefore, the total irreducible representation is:

$$8 \times \Gamma_{C_s^{yz}} = 8 \times [2A_1 + A_2 + B_1 + 2B_2] \ . \tag{5.3}$$

Once again, subtracting the acoustic modes $A_1 + B_1 + B_2$ (there is no silent mode in this particular case), the irreducible representation of the optical vibrations, for the noncentrosymmetric space group $P2_1mn$, is:

$$\Gamma' = 15A_1(aa,bb,cc;E\|a) + 8A_2(bc) + 7B_1(ab;E\|b) + 15B_2(ac;E\|c) \ , \tag{5.4}$$

corresponding to 45 Raman (A_1,A_2,B_1,B_2) and 37 infrared (A_1,B_1,B_2) active modes.

As a final result, we see that the number of optical vibrations, expected on the basis of group theory, is very different for the two space groups. Moreover, whereas in the case of $Pmmn$ the phonons are exclusively Raman or infrared active, for $P2_1mn$, because of the lack of inversion symmetry, there is no more distinction between *gerade* and *ungerade* and certain modes are in principle (group theory does not say anything about intensities) detectable with both techniques.

5.2 Optical Spectroscopy: Experimental

We investigated the optical properties of α'-NaV_2O_5 in the frequency range going from 30 to 32 000 cm^{-1}. High-quality single crystals were grown by high temperature solution growth from a vanadate mixture flux, as described in reference [26]. The crystals, with dimensions of 1, 3, and 0.3 mm along the a, b, and c axes, respectively, were aligned by conventional Laue diffraction, and mounted in a liquid He flow cryostat to study the temperature dependence of the optical properties between 4 and 300 K. Reflectivity measurements, in near normal incidence configuration ($\theta = 11°$), were performed on two different Fourier transform spectrometers: A Bruker IFS 113v, in the frequency range going 20 - 7000 cm^{-1}, and a Bomem DA3, between 6000 and 32 000 cm^{-1}. Polarized light was used, in order to probe the optical response of the crystals along the a and b axes. The absolute reflectivity was obtained by calibrating the data acquired on the samples against a gold mirror, from low frequencies up to 15 000 cm^{-1}, and an aluminum mirror for higher frequencies. The optical conductivity was calculated from the reflectivity data using Kramers-Kronig relations [27].

5.3 Optical Spectroscopy: Results

Let us now, as an introduction to what we will discuss in detail in the following sections, describe briefly the main features of the optical spectra of α'-NaV_2O_5, over the entire frequency range we covered with our experimental systems. In fig. 5.4 we present reflectivity and conductivity data of α'-NaV_2O_5 at 300 K for $E \parallel a$ (i.e., $\perp$ to the chain direction) and $E \parallel b$ (i.e., $\parallel$ the chain direction), in the frequency range going from 30 to 17 000 cm^{-1}. We can observe a very rich and peculiar excitation spectrum, characterized by strong anisotropy for direction parallel and perpendicular to the V-O chains.

For $E \parallel$ chain, the far-infrared region ($\omega < 800$ cm^{-1}) is characterized by strong optical phonon modes, with no background conductivity, as expected for an ionic insulator. At higher frequencies a strong electronic absorption is present (peaking at ~ 9000 cm^{-1}), directly observable in both reflectivity and conductivity. Moreover, in the mid-infrared region (between 800 and 5000 cm^{-1}) we detected a very weak continuum of excitations, as shown by the finite value of the conductivity (see inset of fig. 5.4b) and by the reflectivity which is continuously raising in that frequency range (fig. 5.4a).

On the other hand, for $E \perp$ chain, a weak broad band of optical absorption, additional to the phonon modes, was detected in the far-infrared region. This is directly recognizable

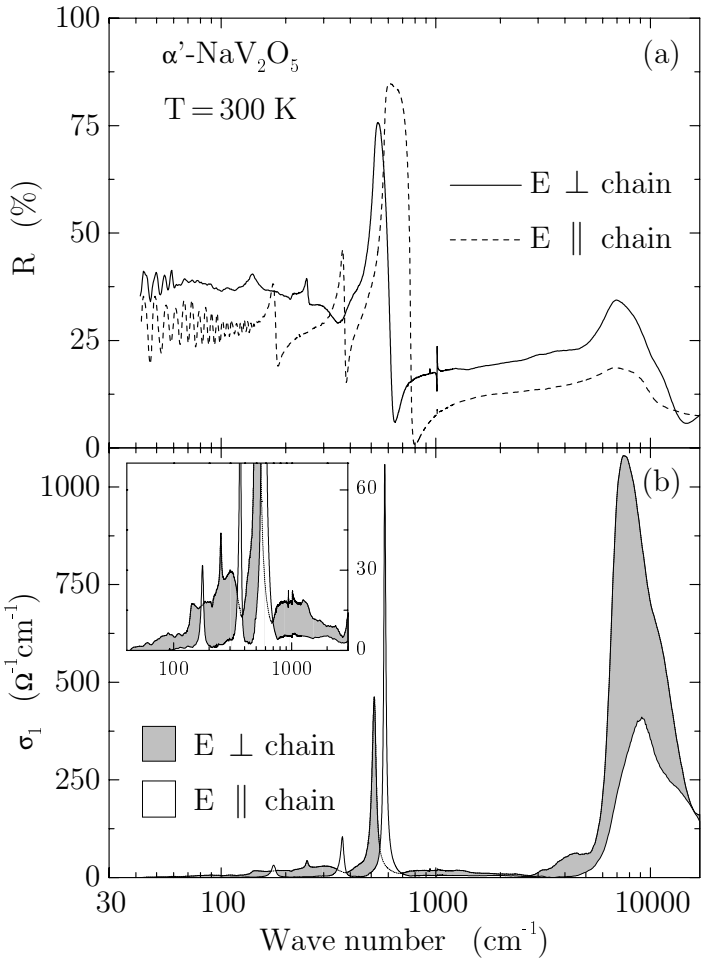

Figure 5.4: *Optical spectra of α'-NaV_2O_5 at 300 K for $E \| a$ (i.e., $\perp$ to the chain direction) and $E \| b$ (i.e., $\|$ the chain direction), in the frequency range going from 30 to 17000 cm^{-1}. Panel (a), and (b) show the results for reflectivity, and optical conductivity, respectively. In the inset of panel (b) an enlarged view of $\sigma_1(\omega)$ from 40 to 3000 cm^{-1} is presented.*

in the reflectivity spectrum (fig. 5.4a): In fact, reducing the frequency of the incoming light, contrary to what observed for $E \|$ chain, we can observe an overall increase in reflectivity which masks the contribution due to the sharp phonon lines. At the same time, the interference fringes, due to Fabry-Perot resonances [28], which were dominating the optical reflectivity below 140 cm^{-1} for $E \|$ chain, are almost completely suppressed for $E \perp$ chain, indicating a stronger absorption for the latter polarization. In the optical conductivity, a continuum, with a broad maximum in the far infrared (see inset of fig. 5.4b), extends from very low frequencies up to the electronic excitation at $\sim$7500 $cm^{-1} \sim$ 1 eV, which is now much more intense than the similar one detected for $E \|$ chain. Moreover, along the direction perpendicular to the V-O chains, we can observe an additional shoulder in the conductivity spectrum, between 3000 and 5000 cm^{-1}.

Finally, for both polarizations, an absorption edge (not shown), corresponding to the onset of charge-transfer transitions, was detected at ~ 3 eV, in agreement with ref. 29.

5.3.1 Phonon Spectrum of the High Temperature Phase

In this section we will concentrate on the phonon spectrum of the high temperature undistorted phase of α'-NaV_2O_5. Alternatively to the discussion we already presented in section 5.1, based on the x-ray diffraction data, we will now try to assess the symmetry issue by comparing the number and the symmetry of the experimentally observed optical vibrations to the results obtained via the group theoretical analysis for the two different space groups proposed, for α'-NaV_2O_5, in the undistorted phase [3, 10]. In fig. 5.5 we present the reflectivity spectra for E perpendicular and parallel to the V-O chains (i.e., along the a and b axes, respectively), up to 1000 cm^{-1}, which covers the full phonon spectrum for these two crystal axes. In this respect, different is the case of the c axis: Along this direction a phonon mode was detected at ~ 1000 cm^{-1}, as we will show in section 5.3.3 while discussing the results reported in fig. 5.10. In fig. 5.5 the data are shown for $T = 100$ K, temperature which is low enough for the phonons to be sufficiently sharp and therefore more easily detectable. At the same time, it is far from T_{SP}, so that we can clearly identify the phonon spectrum of the undistorted phase without having any contribution from the one of the low temperature distorted phase.

In the reflectivity spectra (see fig. 5.5), three pronounced phonon modes are observable for $E \parallel$ chain ($\omega_{TO} \approx 177$, 371, and 586 cm^{-1}, at 100 K), and three for $E \perp$ chain ($\omega_{TO} \approx 137$, 256, and 518 cm^{-1}, at 100 K). It has to be mentioned that the feature at 213 cm^{-1} along the a axis, which looks like an antiresonance, is a leakage of a c-axis mode [30] due to the finite angle of incidence of the radiation on the sample (θ=11°), and to the use of p-polarization (therefore with a finite $E \| c$ component) to probe the a-axis optical response. Analyzing in detail the spectra few more lines are observable, as shown in the insets of fig. 5.5. Along the b axis a fourth phonon is present at 225 cm^{-1}: Being the sample a 300 μm thick platelet characterized by some transparency in this frequency region, Fabry-Perot interferences with a sinusoidal pattern are measurable [28]. At 225 cm^{-1} the pattern is not regular anymore, indicating the presence of an absorption process at this particular frequency. From the temperature dependence, it can be assigned to a lattice vibration. Similarly, three more phonons are detected along the a axis at 90, 740 and 938 cm^{-1}.

In conclusion, 6 a-axis and 4 b-axis phonons were detected on α'-NaV_2O_5, in the high temperature undistorted phase. The resonant frequencies of these vibrational modes are summarized, for two different temperatures, in table 5.4. These results compare better with the group theoretical analysis for the centrosymmetric space group $Pmmn$ (see eq. 5.2), which gave 7 and 4 vibrational modes for E$\|a$ and E$\|b$, respectively, than with the analysis for the noncentrosymmetric $P2_1mn$. In fact, in the latter case 15 and 7 phonons ought to be expected (see eq. 5.4). Therefore, in agreement with the result of our x-ray structure redetermination [10], also the optical investigation of the phonon spectra indicates the centrosymmetric space group $Pmmn$ as the most probable one for α'-NaV_2O_5, at temperatures larger than T_{SP}.

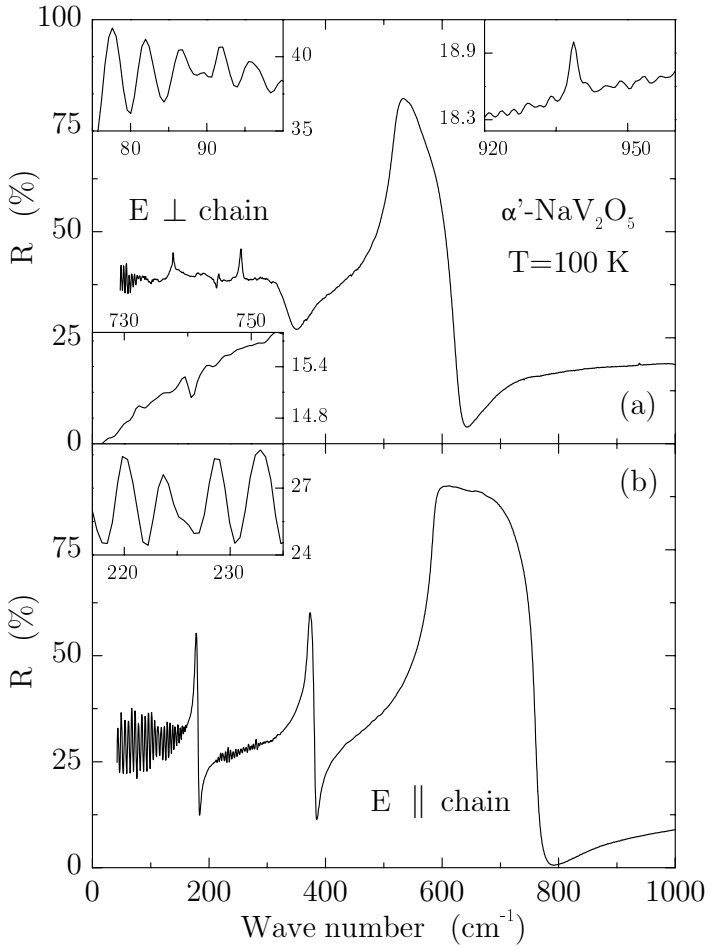

Figure 5.5: *Reflectivity of a single crystal of α'-NaV_2O_5 in the undistorted phase, at 100 K, as a function of frequency. The spectra are shown for E perpendicular and parallel to the chain direction in panel (a) and (b), respectively. An enlarged view of the frequency regions, where very weak optical phonons were detected, is given in the insets.*

However, $P2_1mn$ is, in principle, not completely ruled out as a possible space group on the basis of phonon spectra observed with optical spectroscopy. In fact, group theory gives information only about the number of phonons that one could expect but not about their resonant frequencies and, in particular, their effective strength, which, in the end, determines whether a mode is detectable or not. The only really conclusive answer would have been to detect more modes than those allowed by symmetry for the space group *Pmmn*. In the present situation, it may be possible that the correct space group is still the non-centrosymmetric $P2_1mn$ and that some of the phonon modes have escaped detection because the frequency is too low for our setup or due to a vanishing oscillator strength. In this respect, we have to stress that, indeed, the oscillator strength of the additional modes expected for the noncentrosymmetric $P2_1mn$ would have to be small because, as we learned from the x-ray diffraction analysis, if a deviation from centrosymmetry is present, it is

Polarization	T (K)	ω_{TO} (cm^{-1})					
$E \parallel$ a	4	91.12	139.15	255.49	517.30	740.62	938.21
	100	89.67	136.81	255.82	517.74	740.49	938.49
$E \parallel$ b	4	177.46	224.67	373.91	587.20		
	100	177.18	225.20	371.02	585.88		

Table 5.4: *Resonant frequencies of the optical vibrational modes characteristic of the undistorted phase of α'-NaV_2O_5, obtained by fitting the optical phonons with Fano line shapes.*

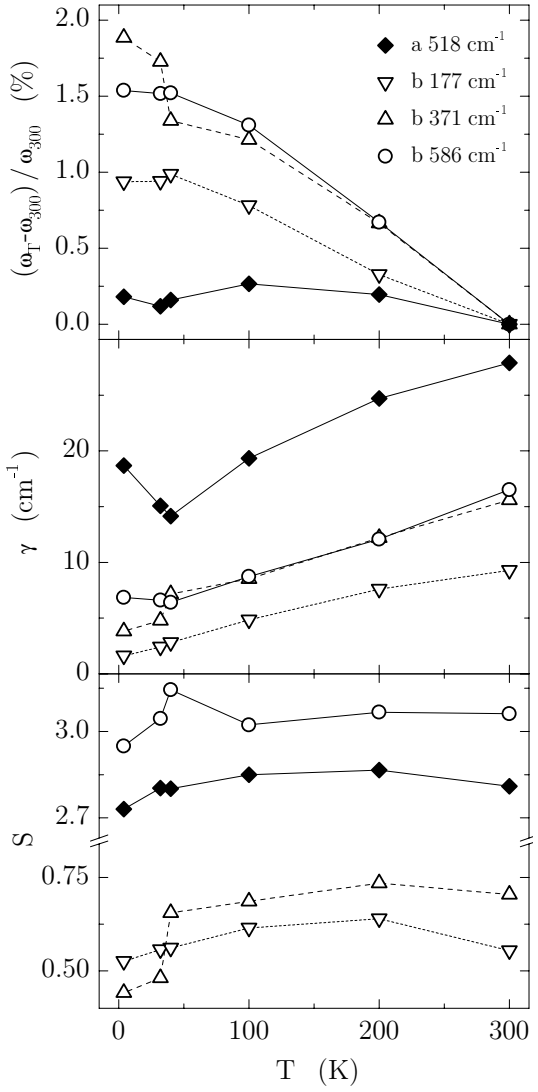

Figure 5.6: *Temperature dependence of the percentage change in resonant frequency, of the damping, and of the oscillator strength (obtained by fitting the vibrational modes with Fano line shapes), for the most intense optical phonons of the undistorted phase of α'-NaV_2O_5.*

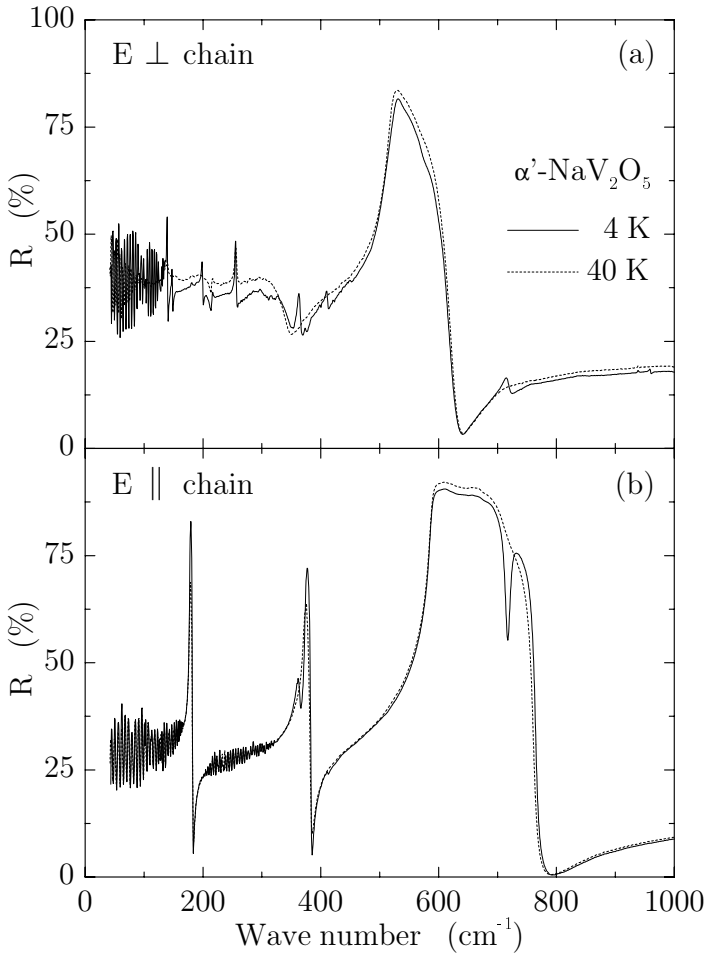

Figure 5.7: *Reflectivity spectra of α'-NaV_2O_5 measured for $E\perp$ chain (a) and $E\|$chain (b) below (4 K) and just above (40 K) the phase transition. Along both axes of the crystal, new phonon lines activated by the phase transition are observable for $T<T_{SP}=34$ K.*

smaller than 0.03 Å. In addition, we have been performing a lattice dynamical calculation for both space groups which shows that, removing the center of inversion and changing the valence of the V ions (i.e., from the uniform $V^{4.5+}$ for all sites to an equal number of V^{4+} and V^{5+} sites), the number of modes characterized by a finite value of the oscillator strength does not increase, even if a strictly long range charge ordering in 1D chains of V^{4+} and of V^{5+} ions is assumed.

It has to be mentioned that, during the last year, many independent investigations of the Raman and infrared phonon spectra, on α'-NaV_2O_5, were reported [13, 29–37]. Of course, there was not immediately a perfect agreement between all the different results and, e.g., phonon lines detected by one group were not always confirmed by others. As a matter of fact, in the first experimental studies of lattice vibrations [29, 31], the optical spectra there presented were interpreted as an evidence for the noncentrosymmetric space group $P2_1mn$. At this stage, we believe that the results of our investigation [13], performed on

high quality single crystals, give a very complete picture of the optical vibrational modes of α'-NaV_2O_5, in the undistorted phase, for $E\|a$ and $E\|b$ (see table 5.4). Moreover, our results were completely confirmed by those obtained by Smirnov *et al.* [30,32] (who could measure also the c-axis phonon spectrum), on samples of different origin.

Before moving to the analysis of the phonon spectra characteristic of the low temperature distorted phase of α'-NaV_2O_5, we would like to discuss the temperature dependence, from 4 to 300 K, of the lattice vibrations which are already present in the uniform phase. In order to extract, from the experimental results, information about their parameters, we had to fit the data using Fano line shapes for the phonon peaks [38]. In fact, most of them, in particular along the a axis, are characterized by a strong asymmetry, indicating an interaction with the underlaying low frequency continuum. In this case the symmetrical Lorentz line shape was not suitable and the asymmetrical Fano profile had to be used: The latter model contains an additional parameter which takes care of the degree of asymmetry of an excitation line, due to the coupling between that discrete state and an underlaying continuum of states (for a more detailed discussion of the Fano model see chapter 2).

The results for the percentage change in resonant frequency, the damping, and the oscillator strength of the most intense optical phonons of the undistorted phase of α'-NaV_2O_5, are plotted in fig. 5.6, between 4 and 300 K. One can observe that some of the modes show a sudden change in their parameters between 40 and 32 K, i.e., upon reducing the temperature below $T_{SP} = 34$ K. In particular, the oscillator strength of the phonons at 371 and 586 cm^{-1}, along the b axis, decreases across the phase transition, suggesting either a transfer of spectral weight to zone boundary folded modes activated by the phase transition or to electronic degrees of freedom. We will see later, in the course of the chapter, that for the chain direction the reduction of the phonon oscillator strength will be compensated mainly by the strength gained by the zone boundary folded modes activated by the phase transition. On the other hand, for $E \perp$ chain, the change in spectral weight of the electronic excitations will appear to be particularly important.

5.3.2 Phonon Spectrum of the Low Temperature Phase

Upon cooling down the sample below T_{SP}=34 K, significant changes occur in the optical phonon spectra, as one can see in fig. 5.7 where we present the reflectivity spectra of α'-NaV_2O_5 measured, for $E \perp$ chain (a) and $E \parallel$ chain (b), below (4 K) and just above (40 K) the phase transition. Contrary to the case of $CuGeO_3$ (see section 3.3), where we could clearly observe in reflectivity only a single, very weak additional phonon [39, 40], 10 new lines are detected for $E \perp$ chain ($\omega_{TO} \approx$ 101, 127, 147, 199, 362, 374, 410, 450, 717, and 960 cm^{-1}), and 7 for $E \parallel$ chain ($\omega_{TO} \approx$ 102, 128, 234, 362, 410, 718, and 960 cm^{-1}), some of them showing a quite large oscillator strength. The stronger intensity of the lines, with respect to the case of $CuGeO_3$, suggests larger lattice distortions in α'-NaV_2O_5, on going through the phase transition. The resonant frequencies (at T=4 K) of all the detected zone boundary folded modes are summarized in table 5.5. The observation of many identical or almost identical frequencies for both axes, which is an important information for a full understanding of the structural distortion, is an intrinsic property

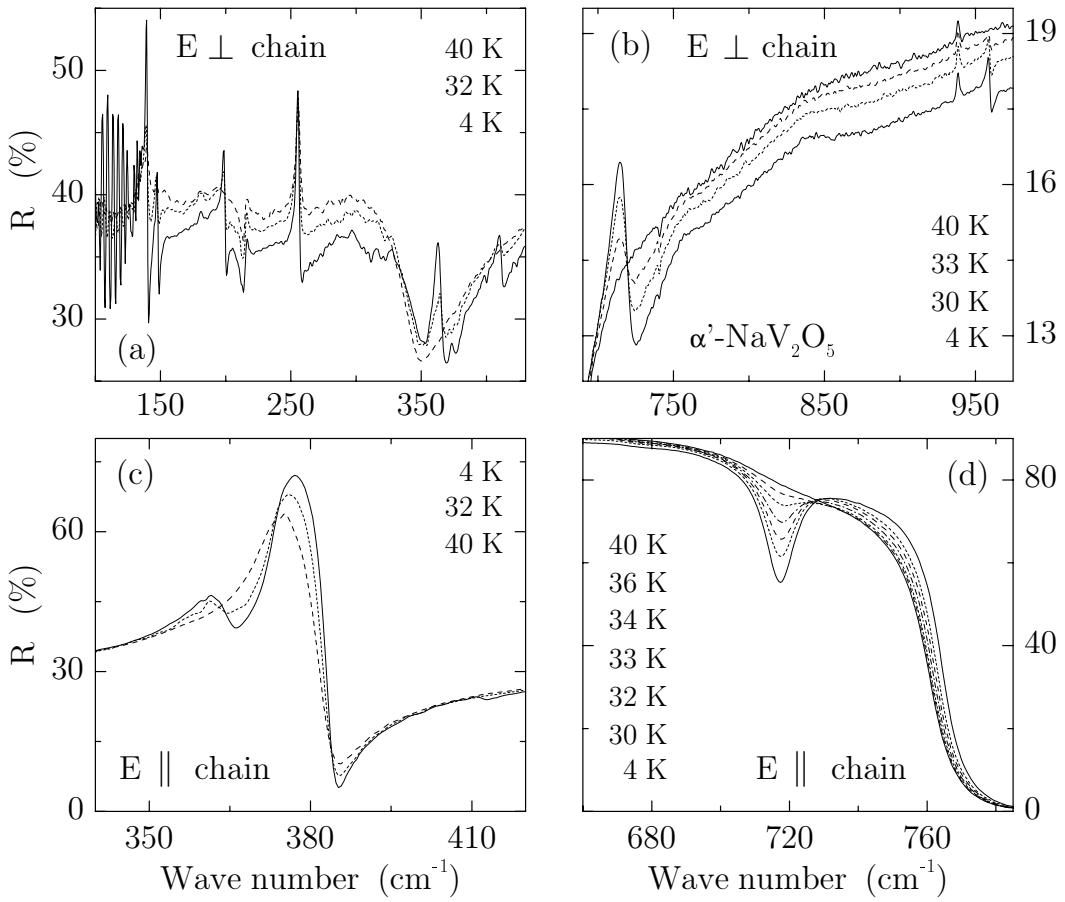

Figure 5.8: *Detailed temperature dependence of some of the zone boundary folded modes observed in the reflectivity spectra, for $T<T_{SP}$, with $E\perp$ chain (a,b) and $E\|$chain (c,d).*

of the low temperature phase. Experimental errors, like polarization leakage or sample misalignment, are excluded from the well-defined anisotropic phonon of the undistorted phase. A more detailed discussion of this point will be presented in section 5.3.3, in relation to the reflectivity data reported in fig. 5.10.

An enlarged view of few of the frequency regions where the zone boundary folded modes were detected, is given in fig. 5.8. We can observe the gradual growing of the these modes, whose oscillator strength increases the more the temperature is reduced below T_{SP}=34 K. Moreover, the reflectivity data acquired for $E\perp$ chain [panel (a) in fig. 5.7 and panels (a) and (b) in fig. 5.8] show that also the underlaying continuum as a considerable temperature dependence. In fact, the reflectivity is decreasing, over the entire frequency range, upon reducing the temperature from 40 to 4 K. In particular, in fig. 5.8a, we can see that very pronounced interference fringes, due to Fabry-Perot resonances [28], appear at 4 K at frequencies lower than 136 cm^{-1}, indicating a particularly strong reduction of the absorption in that frequency region. This effect is, in our opinion, related to the opening of the magnetic gap in the excitation spectrum, and will be discussed in great detail in

Polarization	ω_{TO} (cm^{-1})										
$E \parallel$ a (SP)	101	127	147	199	—	362	374	410	450	717	960
$E \parallel$ b (SP)	102	128	—	—	234	362	—	410	—	718	960

Table 5.5: *Resonant frequencies, at 4 K, of the zone boundary folded modes detected on α'-NaV_2O_5 in the low temperature distorted phase, with $E \perp$ chain and $E \parallel$ chain.*

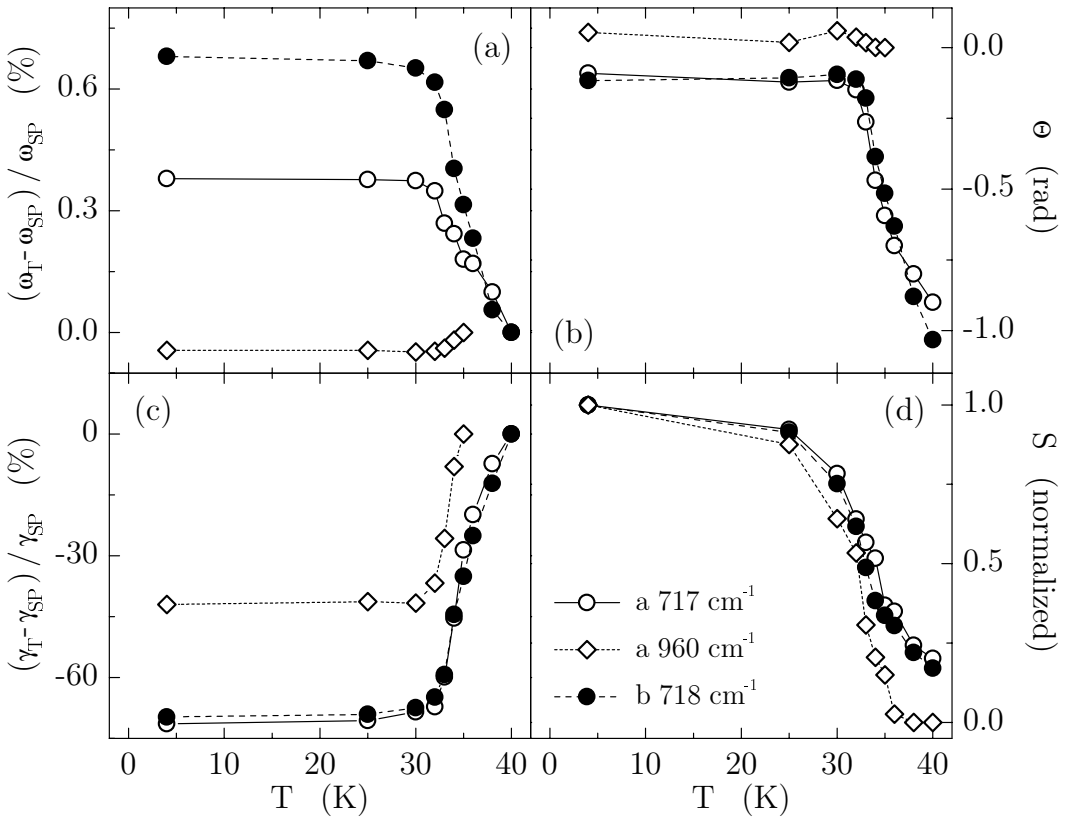

Figure 5.9: *Temperature dependence of the percentage change in resonant frequency (a) and damping (c), of the normalized oscillator strength (d), and of the Fano asymmetry parameter (b), for the folded phonons observed below the phase transition at 717 and 960 cm^{-1} along the a axis, and at 718 cm^{-1} along the b axis, on α'-NaV_2O_5.*

section 5.3.4.

Of all the detected folded modes, for experimental reasons (i.e., higher sensitivity of the detector and therefore higher accuracy of the results in this frequency range), we carefully investigated the ones at 718 ($E \parallel a,b$) and 960 cm^{-1} ($E \parallel a$), for several temperatures between 4 and 40 K. We fitted these phonons to a Fano profile because the 718 cm^{-1} modes show an asymmetrical line-shape. The results of the percentage change in resonant frequency and damping, of the normalized oscillator strength, and of the Fano asymmetry parameter are plotted versus temperature in the different panels of fig. 5.9. As in chapter 2, we use here an asymmetry parameter Θ (rad) redefined in such a way that the larger the value of Θ, the stronger is the asymmetry of the line: A Lorentz line-shape is eventually recovered for Θ=0 [41].

Let us now start by commenting on the results obtained for the oscillator strength: In fig. 5.9d we see that S has a similar behavior for the three different lines. However, the 960 cm^{-1} peak vanishes at T_{SP} whereas the two 718 cm^{-1} modes have still a finite intensity at T=40 K and, as a matter of fact, disappear only for $T > 60$-70 K. At the same time, the line-shape of the 960 cm^{-1} mode is perfectly lorentzian at all temperatures, whereas the two other phonons show a consistently increasing asymmetry for $T > 32$ K. Also the increase in resonant frequency (fig. 5.9a) and the reduction of the damping (fig. 5.9c) are much more pronounced for the two 718 cm^{-1} modes. From these results we conclude that the second-order character of the phase transition is nicely shown by the behavior of S for the 960 cm^{-1} folded mode. On the other hand, pretransitional fluctuations manifest themselves in the finite intensity of the 718 cm^{-1} modes above T_{SP}, and in the extremely large value of Θ and γ for these lines ($\gamma \sim 35$ cm^{-1} at 40 K). In other words, the lattice distortion is already taking place in the system, at temperature much higher than T_{SP}, but with a short range character, whereas a coherent long range distortion is realized only below the phase transition temperature. In this respect, it is worth mentioning that similar pretransitional fluctuations, below 70 K, have been observed also in the course of a study of the propagation of ultrasonic waves along the chain direction of α'-NaV_2O_5 [42], and, very recently, in x-ray diffuse scattering measurements [43].

5.3.3 Symmetry of the Lattice Distortion

We saw in the previous section that many of the folded zone boundary phonon modes, activated by the phase transition, show the same resonant frequency for $E \| a$ and $E \| b$ (see table 5.5), even though they are characterized by a different oscillator strength along the two different axes (e.g., $S \sim 0.021$ for $E \| a$ and $S \sim 0.014$ for $E \| b$, for the 718 cm^{-1} modes at 4 K). This is quite a surprising result because the phonon spectrum of the undistorted high temperature phase has a well defined anisotropy, at any temperature, with different resonant frequencies for vibrations polarized along the a and b axes (see table 5.4). Similar anisotropy should then be present below the phase transition if the system is still orthorhombic, even for the folded modes.

To further check these findings, we performed reflectivity measurements on a single crystal of α'-NaV_2O_5, at the fixed temperature of 6 K, rotating the polarization of the

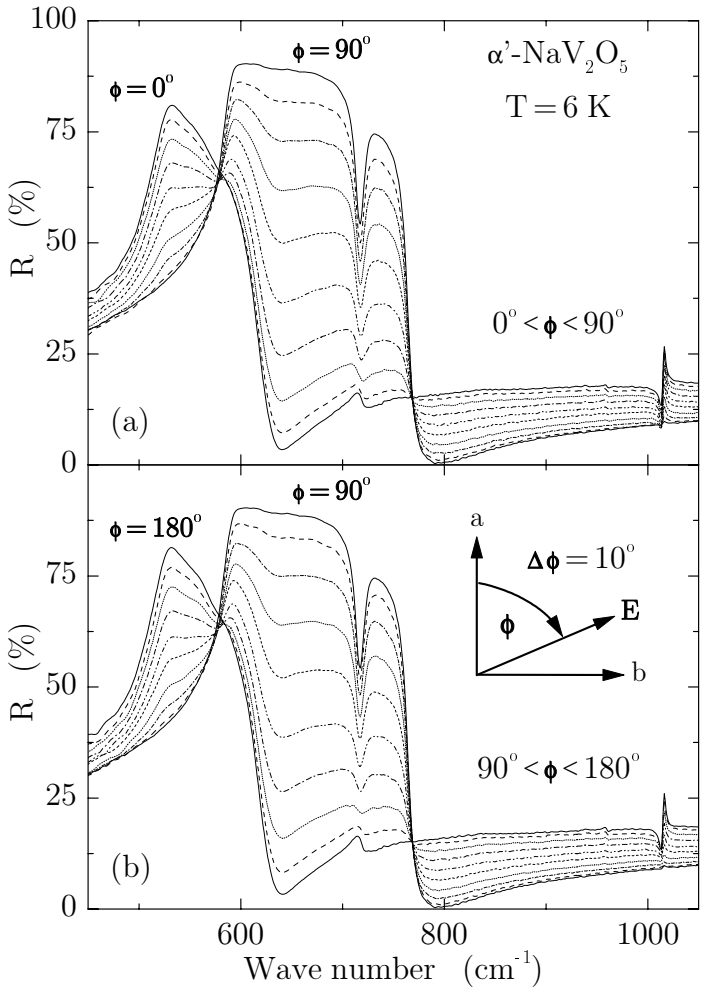

Figure 5.10: *Reflectivity spectra of α'-NaV_2O_5 measured, at 6 K, for different orientations of the electric field of the light with respect to the sample axes (as sketched in panel b, with $\Delta\phi$=10°). The values ϕ=0°,180° correspond to $E\perp$ chain, and ϕ=90° to $E\|$chain.*

incident light of an angle ϕ (see fig. 5.10). The sample was aligned in such a way to have the electric field of the light parallel to the a axis of the crystal, for $\phi = 0°$ and 180°, and parallel to the b axis, for $\phi = 90°$. For these polarizations of the light the obtained results are, obviously, identical to those presented in fig. 5.7. However in fig. 5.10 the data are shown in a different frequency range, extending up to 1050 cm^{-1}. We can then observe at $\sim$1000 cm^{-1} along the a axis, which again was probed with p-polarized light, the antiresonance due to the leakage of a c-axis phonon [30]. Starting from $\phi = 0°$ and turning the polarization in steps $\Delta\phi = 10°$, we observe a gradual decrease of the a axis contribution and, at the same time, an increase of the b axis contribution to the total reflectivity. Moreover, the set of curves plotted in fig. 5.10 satisfy the following relations:

$$R(45°) + R(-45°) = R(0°) + R(90°) \ , \tag{5.5}$$

$$R(\phi) = R(0°)cos^2(\phi) + R(90°)sin^2(\phi) \ . \tag{5.6}$$

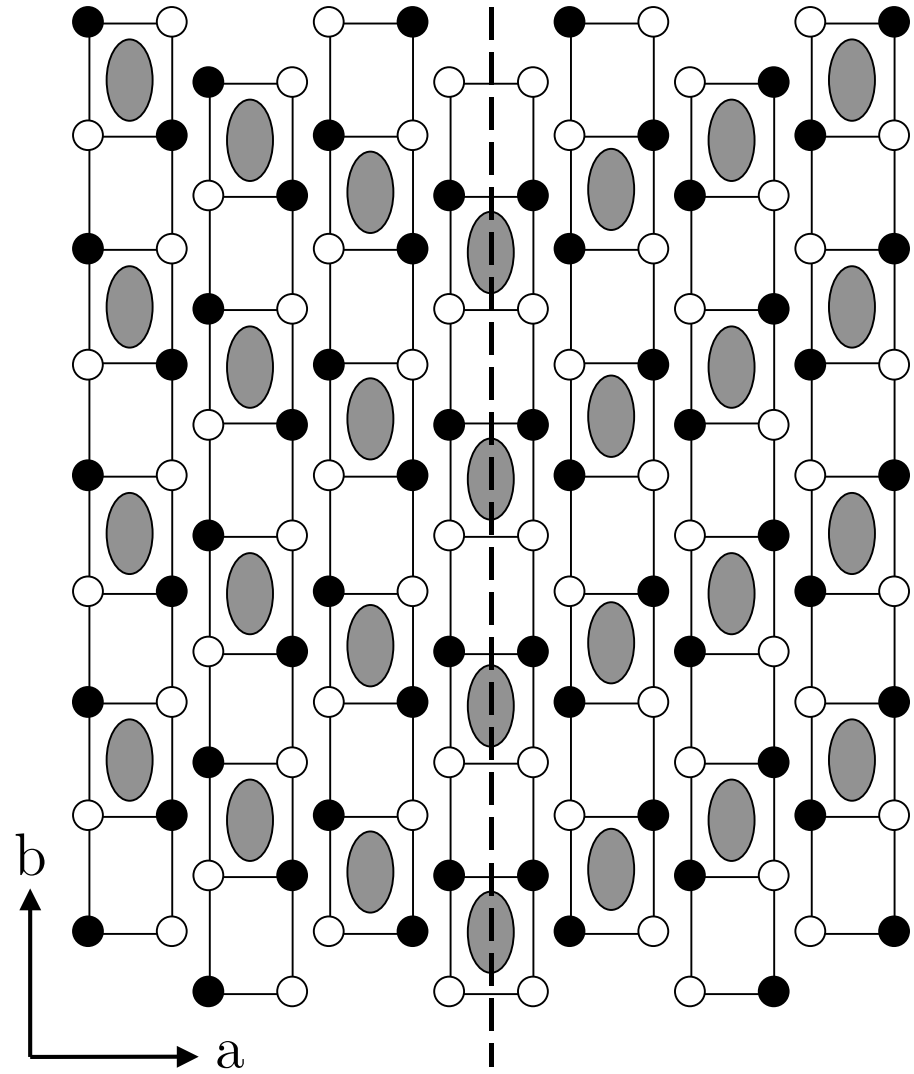

Figure 5.11: *Possible charge ordering pattern in α'-NaV_2O_5, in the low temperature phase. The grey ellipsoids represent the electronic charge involved in the formation of singlets, within the ladders, over every second plaquette formed by four V ions. On adjacent ladders, the charge is assumed to define a diagonal long-range singlet-pattern, as shown in the left-hand side of the figure. In this configuration, two different kinds of V ions are identifiable: V ions adjacent to empty plaquettes (white circles) and V ions adjacent to plaquettes containing a singlet (black circles), arranged in zig-zag patterns on each ladder. If domains with different orientation for the diagonal long-range singlet-pattern are presents in the system, the zig-zag ordering of the different kind of V ions is destroyed in correspondence of a domain wall (dashed line).*

This suggests that the system, even in the distorted phase, has the optical axes along the crystal directions a, b, and c (on the contrary, for a triclinic structure there would be no natural choice of the optical axes). However, the low temperature folded mode at 718 cm^{-1} can be observed for all possible orientations of the electric field of the incident radiation (see fig. 5.10). Because identical resonance frequencies, along the a and the b axes of the crystal, were observed for six of the folded zone boundary modes, we cannot believe in an accidental coincidence.

A possible explanation for the observed effect is the following: We know that in the low temperature phase a non-magnetic ground state is realized, and true singlets are present in α'-NaV_2O_5. The most probable situation is that the singlets are formed, within the ladders, over the plaquettes defined by four V ions. In this case, as shown in fig. 5.11, within one ladder there is an alternation of 'empty' plaquettes and plaquettes containing a singlet (represented by the grey area in fig. 5.11). Let us now assume that in adjacent ladders the charge is arranged in such a way as to result in a diagonal long-range singlet-pattern, as shown in the left-hand side of fig. 5.11. This picture is consistent with the doubling of the lattice constant observed, along the a axis, in low temperature x-ray scattering experiments [2]. Moreover, two different kinds of V ions are identifiable which could possibly explain the results obtained in low temperature NMR experiments [15] (for a more detailed discussion see section 5.5). In fact, there are V ions adjacent to empty plaquettes (white circles) and V ions adjacent to plaquettes containing a singlet (black circles), arranged in zig-zag patterns on each ladder. At this stage, the low temperature phonon spectra should still be characterized by a well defined anisotropy, with distinct eigenfrequencies for different polarizations of the electric field of the incoming radiation. However, there is no reason for the polarization of the folded zone boundary modes to be precisely along the a or the b axes. In fact, they could be polarized with a certain angle with respect to the crystal axes (e.g., along directions parallel and perpendicular to the diagonal long-range singlet-pattern). If domains are present in the system, with opposite orientation for the diagonal long-range singlet-pattern (left and right hand sides of fig. 5.11), each domain will still be characterized by a phonon spectrum with a well defined polarization, as just discussed. However, in presence of such domains the phonon spectra measured in the experiments correspond to an average over many domains with the two possible orientations randomly distributed. As a result, almost no anisotropy is found for light polarized along a and b axes of the crystal.

5.3.4 Optical Conductivity

Very interesting information and a deeper understanding of the symmetry of α'-NaV_2O_5 are obtained from the detailed analysis of the optical conductivity data, in particular when the electronic excitations are considered and compared to the result relative to $CuGeO_3$ (see fig. 5.12). On the latter compound we observed sharp phonon lines below 1000 cm^{-1} [39], multiphonon absorption at $\sim$1500 cm^{-1}, very weak [note the low values of $\sigma_1(\omega)$ in the inset of fig. 5.12a] phonon-assisted Cu d-d transitions at $\sim$14 000 cm^{-1} [44], and the onset of the Cu-O charge-transfer (CT) excitations at $\sim$27 000 cm^{-1}. On α'-NaV_2O_5, besides

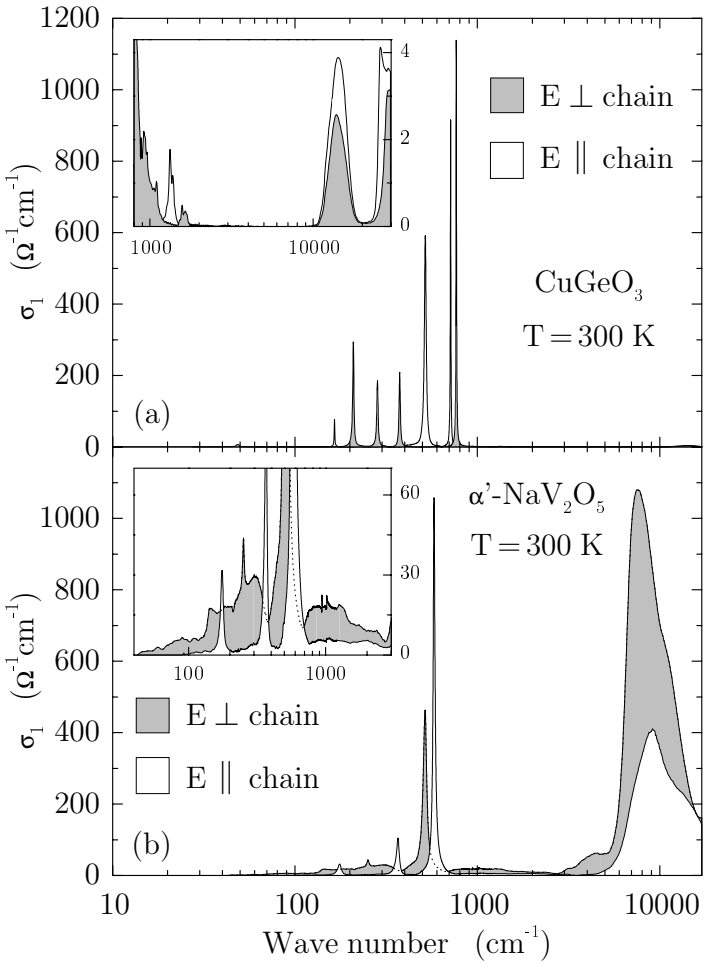

Figure 5.12: *Optical conductivity of $CuGeO_3$ (panel a) and of α'-NaV_2O_5 (panel b), at 300 K, for E parallel and perpendicular to the Cu-O or to the V-O chains. Inset of panel a: enlarged view of $\sigma_1(\omega)$, for $CuGeO_3$, from 800 to 30 000 cm^{-1}. Inset of panel (b): enlarged view of $\sigma_1(\omega)$, for α'-NaV_2O_5, from 40 to 3000 cm^{-1}.*

the phonon lines in the far-infrared region, we detected features that are completely absent in $CuGeO_3$: A strong absorption peak at $\sim$8000 cm^{-1} and, in particular for $E \perp$ chain, a low-frequency continuum of excitations (see inset of fig. 5.12b). Our main goal is to interpret the complete excitation spectrum for α'-NaV_2O_5, trying, in this way, to learn more about the system on a microscopic level. In order to do that, we have first to identify possible candidates for the excitation processes observed in the experimental data.

On the basis of intensity considerations, the peak at $\sim$8000 cm^{-1} $\sim$1 eV, in the optical conductivity of α'-NaV_2O_5, has to be ascribed to an optically allowed excitation. Contrary to the case of the absorption detected at $\sim 14\,000$ cm^{-1} on $CuGeO_3$, it cannot be interpreted just as a *d-d* exciton on the transition metal ion (i.e., V in the case of α'-NaV_2O_5). In fact, this kind of transition is in principle optically forbidden and only weakly allowed in the

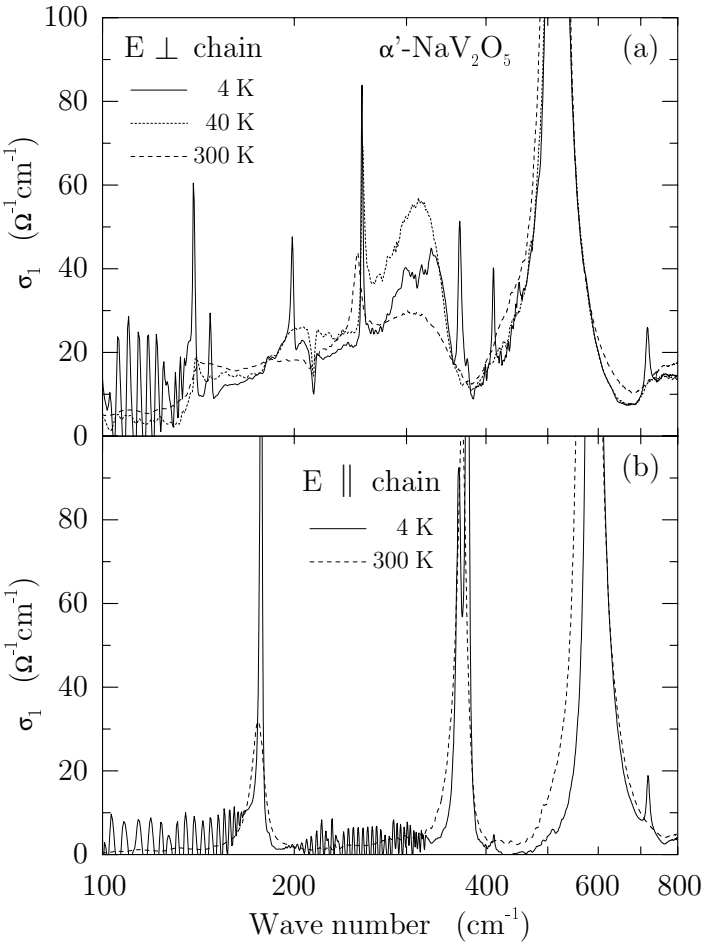

Figure 5.13: *Optical conductivity spectra of α'-NaV_2O_5 measured for $E\perp$ chain (a) and $E\|$chain (b), below and above the phase transition. Along both axes of the crystal new phonon lines, activated by the phase transition, are present for $T<T_{SP}=34$ K. Moreover, for $E\perp$ chain, the temperature dependence of the low frequency continuum is observable.*

presence of a strong parity-broken crystal field or electron-phonon coupling. We have now to recall one of the main consequences of the structural analysis which suggested as a most probable space group, for α'-NaV_2O_5 in the undistorted phase, the centrosymmetric *Pmmn*: The existence of only one kind of V per unit cell, with an average valence of +4.5. Taking into account that the hopping parameter along the rungs $t_\perp$, is approximately a factor of two larger than the one along the legs of the ladder $t_\parallel$ [45, 46], all the other hopping amplitudes being much smaller (including the nearest-neighbor t_{xy}), α'-NaV_2O_5 can be regarded as a 1/4-filled two-leg ladder system, with one V *d*-electron per rung shared by two V ions in a molecular bonding orbital [12]. In this context, the most obvious candidate for the strong optical absorption observed at 1 eV is the on-rung bonding-antibonding transition, with a characteristic energy given by $2t_\perp$. However, on the basis of LMTO band structure calculation [45] and exact diagonalization calculation applied to finite size

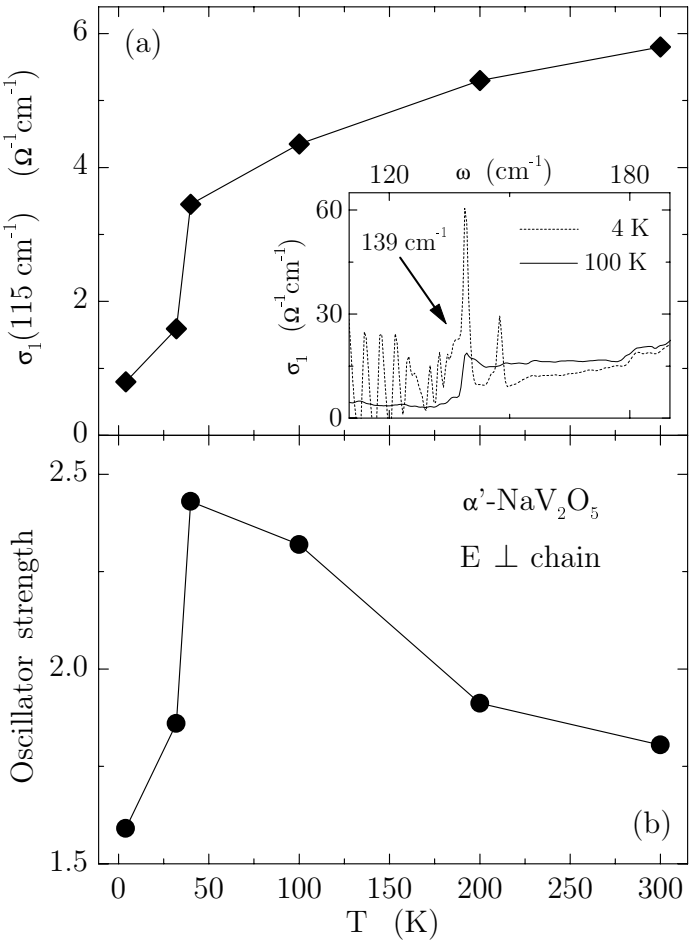

Figure 5.14: *Panel (a): Temperature dependence of the optical conductivity at the frequency value 115 cm^{-1}, for $E \perp$ chain. The values are obtained from Kramers-Kronig analysis, for $T > T_{SP}$, and by fitting the interference fringes in reflectivity, for $T < T_{SP}$. In the inset, an enlarged view of $\sigma_1(\omega)$, from 110 to 190 cm^{-1}, is given. Panel (b): Oscillator strength of the low frequency electronic continuum, for $E \perp$ chain, plotted versus temperature.*

clusters [46], $t_\perp$ was estimated to be $\sim$0.30-0.35 eV, which gives a value for the bonding-antibonding transition lower than the experimentally observed 1 eV. This energy mismatch, together with the strong dependence of the intensity of the 1 eV peak on the polarization of the light, are important pieces of information and will be discussed further in section 5.4.

Let us now turn to the infrared continuum detected for $E \perp$ chain (see inset of fig. 5.12b). We already showed , discussing the low temperature reflectivity data (see fig. 5.7 and 5.8), that this broad band of optical absorption has a considerable temperature dependence: The overall reflectivity was decreasing upon reducing the temperature and, for $T < T_{SP}$, Fabry-Perot resonances [28] appear at frequencies lower than 136 cm^{-1}, indicating a particularly strong reduction of the optical absorption in that frequency region. These effects become even more evident when we consider the low temperature optical

conductivity calculated from the reflectivity data via Kramers-Kronig transformations (see fig. 5.13). However, we have to keep in mind that performing this kind of calculation, we will obtain unphysical oscillations for the optical conductivity in the frequency regions where reflectivity is dominated by interference fringes.

In fig. 5.13b we can observe that, for $E \parallel$ chain, not much is happening besides the sharpening of the phonon lines and the appearance of the zone boundary folded modes. On the other hand, for $E \perp$ chain we can observe, in addition to the folded modes for $T < T_{SP}$, first the increase of the continuum intensity upon cooling down the sample from 300 to 40 K and, subsequently, a reduction of it from 40 to 4 K. In the frequency region below the phonon peak at 139 cm^{-1}, whereas a reduction is observable in going from 300 to 40 K, not much can be said about the absolute conductivity of the 4 K data, because of the presence of fringes.

In order to evaluate the low temperature values of conductivity more precisely, we can fit the interference fringes directly in reflectivity. In fact, fitting the period and the amplitude of them, we have enough parameters to calculate right away the real and imaginary part of the index of refraction and, eventually, the dynamical conductivity σ_1 [27]. The so obtained values are plotted versus the temperature in fig. 5.14a. The data for 100, 200, and 300 K were obtained via Kramers-Kronig transformations, whereas those for 4 and 32 K from the fitting of the interferences in the range 105-125 cm^{-1}. The 40 K point, as at that temperature very shallow fringes start to be observable, was calculated with both methods, which show a rather good agreement in this case. As a results we can observe (see fig. 5.14a) a pronounced reduction of σ_1, across the phase transition, corresponding to the opening of a gap in the optical conductivity.

It is difficult to evaluate precisely the gap size because of the phonon at 139 cm^{-1} (see inset of fig. 5.14a). However, we can estimate a lower limit for the gap of about 17 ± 3 meV (136 cm^{-1}). At this point, the important information is that the value of the gap in the optical conductivity is approximately twice the spin gap value observed with inelastic neutron scattering experiments [2] and magnetic susceptibility measurements [47], for T< 34 K. This finding indicates that the infrared broad band of optical absorption has to be related to electronic degrees of freedom. Moreover, because the range of frequency coincides with the low-energy-scale spin excitations, the most likely candidates for this continuum are excitations involving two spin flips.

In relation to what we just discussed, it is interesting to note the effect, of the opening of a gap in the optical conductivity, on the phonon located at 139 cm^{-1}. This can be clearly identified in the inset of fig. 5.14a, where an enlarged view of $\sigma_1(\omega)$ at low frequency is given, for 100 and 4 K. At 100 K this mode is characterized by a very pronounced anomaly of its line shape. As a matter of fact, fitting this phonon with a Fano line shape we obtained for the asymmetry parameter the value $\Theta = -1.7$ rad, indicating a strong coupling to the continuum. However at 4 K, once the gap is open and the intensity of the underlying continuum has decreased, a sharp and rather symmetrical line shape is recovered.

An additional information we can extract from the conductivity spectra is the value of the integrated intensity, and its temperature dependence, for the infrared broad band of optical absorption detected on α'-$NaV_2O_5$for $E \perp$ chain. The oscillator strength, obtained

by integrating $\sigma_1(\omega)$ (with phonons subtracted) up to ~ 800 cm^{-1}, is displayed in fig. 5.14b. It increases upon cooling down the sample from room temperature to T_{SP}, and rapidly decreases for $T < T_{SP}$. The possible meaning of this behavior will be further discussed in the next section.

As a last remark, it is important to mention that low temperature measurements of the dielectric constant, in the microwave frequency range, were recently performed, on α'-NaV_2O_5, by different groups [48,49]. The reported results show no anomaly, across the phase transition, for the real part of the dielectric constant along the b axis. On the other hand, along the a axis, an anomalous behavior, i.e., a pronounced decrease below T_{SP}, was found. The observed behavior, as a matter of fact, is in very good agreement with the temperature dependence of the oscillator strength of the low frequency continuum present, in the optical spectra, along the a axis (fig. 5.14b). One has to note that the comparison is meaningful because the contribution of all the possible optical excitations to the static dielectric constant is just given by their oscillator strengths. The very good agreement of the different results proves, as already suggested by the authors of ref. 48 and 49, that the change in the very low frequency dielectric constant is related to electronic (magnetic) degrees of freedom.

5.4 Charged Bi-Magnons

In the previous section we identified possible candidates for the 1 eV excitation (on-rung bonding-antibonding transition) and for the low frequency continuum detected on α'-NaV_2O_5 for $E \perp$ chain (double spin flips). However, we also stressed that, for a symmetrical 1/4-filled two leg ladder system, the bonding-antibonding transition would be at $2t_\perp \sim 0.7$ eV and not at the experimentally observed value of 1 eV. Moreover, also intensity and polarization ($E \perp$ chain) of the continuum cannot be understood assuming the complete equivalence of the V sites required by the space group *Pmmn*. In fact, because of the high symmetry, no dipole moment perpendicular to the V-O chains would be associated with a double spin flip process. Therefore, no optical activity, involving magnetic degrees of freedom, would be detectable. Even phonon-assisted spin excitations (where the role of the involved phonon is just to lower the symmetry of the system [50–52]) could not be a possible explanation for the observed spectra: The energy is too low for this kind of processes.

A possible solution to these problems is to assume a charge disproportionation on each rung of the ladders without, however, any particular long range charge ordering (see fig. 5.15). The latter is, in fact, most probably excluded by the x-ray diffraction results and by the phonon spectra of α'-NaV_2O_5 in the undistorted phase. It is worth mentioning that the assumption of charge disproportionation has been recently confirmed by calculations of the optical conductivity by exact-diagonalization technique on finite size clusters [53]. Only in this way it was possible to reproduce the frequency position of the 1 eV peak, and the anisotropy observed in the experiment between a and b axes (see fig. 5.12). We can now try to interpret the optical data on α'-NaV_2O_5 in the framework of the model developed

in chapter 4.

Let us start from the analysis of the absorption band at 1 eV. We model the jth rung, formed by two V ions, with the Hamiltonian:

$$H_j = t_\perp \sum_\sigma \left\{ L^\dagger_{j,\sigma} R_{j,\sigma} + R^\dagger_{j,\sigma} L_{j,\sigma} \right\} + \Delta n_C + U \left\{ n_{jR\uparrow} n_{jR\downarrow} + n_{jL\uparrow} n_{jL\downarrow} \right\} \ , \qquad (5.7)$$

where $L^\dagger_{j,\sigma}$ ($R^\dagger_{j,\sigma}$) creates an electron with spin σ on the left-hand (right-hand) V site of the jth rung, U is the on-site Hubbard repulsion, $n_C = \sum_j (n_{jR} - n_{jL})/2$ is the charge displacement operator, and Δ is the potential energy difference between the two V sites on the rung. Here Δ has the role of a charge disproportionation parameter: For the symmetric ladder $\Delta = 0$. For a single electron per rung, the two solutions are lob-sided bonding and antibonding wave functions $|\tilde{L}\rangle = u|L\rangle + v|R\rangle$, and $|\tilde{R}\rangle = u|R\rangle - v|L\rangle$, where $1/(2uv)^2 = 1 + (\Delta/2t_\perp)^2$. The splitting between these two eigenstates, $E_{CT} = \sqrt{\Delta^2 + 4t_\perp^2}$, corresponds to the photon *energy* of the optical absorption. We see that, if $\Delta \neq 0$, the experimental value of 1 eV can be reproduced.

A second crucial piece of information is provided by the *intensity* of the absorption. We can calculate the integrated intensity of the 1 eV peak and then take advantage of the expression derived in chapter 4 (see eq. 4.3 and 4.4), which is exact for one electron on two coupled tight-binding orbitals:

$$\int_{CT} \sigma_1(\omega) d\omega = \pi q_e^2 N d_\perp^2 t_\perp^2 \hbar^{-2} E_{CT}^{-1} \ , \qquad (5.8)$$

where q_e is the electron charge, N is the volume density of the rungs, and $d_\perp$=3.44 Å is the distance between the two V ions on the same rung. This way we calculated from the spectra $|t_\perp| \approx 0.3$ eV, value which is, as a matter of fact, in very good agreement with those obtained from LMTO band structure calculation [45] and exact diagonalization calculation applied to finite size clusters [46]. Combining this number with $E_{CT} = 1$ eV, we obtain $\Delta \approx 0.8$ eV. The corresponding two eigenstates have 90 % and 10 % character on either side of the rung. Therefore the valence of the two V-ions is 4.1 and 4.9, respectively. The optical transition at 1 eV is essentially a charge transfer (CT) excitation from the occupied V $3d$ state at one side of the rung to the empty $3d$ state at the opposite side of the same rung.

Let us now turn to the infrared continuum detected for $E \perp$ chain. The presence of *two* V states ($|L\rangle$ and $|R\rangle$) per spin, along with the broken left-right parity of the ground state on each rung, gives rise to a fascinating behavior of the spin flips (described, in a pictorial way, in fig. 5.15): Consider a small fragment of the ladder with only two rungs, with one spin per rung. Each rung is described by the Hamiltonian defined above. Let us assume that in the ground state of this cluster each spin resides in a $|L\rangle$ orbital, with some admixture of $|R\rangle$. We can now include the coupling of the two rungs along the legs, using:

$$t_\parallel \sum_\sigma \left\{ R^\dagger_{1,\sigma} R_{2,\sigma} + L^\dagger_{1,\sigma} L_{2,\sigma} + R^\dagger_{2,\sigma} R_{1,\sigma} + L^\dagger_{2,\sigma} L_{1,\sigma} \right\} \ . \qquad (5.9)$$

If the two spins are parallel, the inclusion of this term has no effect, due to the Pauli-principle. If they form an $S=0$ state, the ground state gains some kinetic energy along the legs by mixing in states where two electrons reside on the same rung. In the limit $U\to\infty$, these states have one electron in the $|L\rangle$ and one in the $|R\rangle$ state on the same rung (see chapter 4). As a result, there is a net dipole displacement of the singlet state compared to the triplet state: *The spin-flip excitations carry a finite electric dipole moment.* Using a perturbation expansion in $t_\parallel/E_{CT}$, and working in the limit $U\to\infty$, the exchange coupling constant between two spins on neighboring rungs becomes (see chapter 4):

$$J_\parallel = \frac{8t_\parallel^2 t_\perp^2}{[\Delta^2+4t_\perp^2]^{3/2}} \ . \tag{5.10}$$

The coupling to infrared light with $E\perp$chain can now be included using the dipole approximation. The only effect is to change the potential energy of the $|R\rangle$ states relative to the $|L\rangle$ states. We have then to replace Δ with $\Delta+q_e d_\perp E_a$, where E_a is the component of the electric field along the rung. By expanding $J_\parallel$ we obtain the spin-photon coupling:

$$H_S = q_m d_\perp E_a h_S = q_m d_\perp E_a \sum_j \vec{S}_j\cdot\vec{S}_{j+1} \ , \tag{5.11}$$

where $q_m = q_e\frac{3J_\parallel\Delta}{\Delta^2+4t_\perp^2}$ is the effective charge involved in a double spin-flip transition. For a symmetrical ladder, where $\Delta=0$, the effective charge vanishes, and the charged magnon effect disappears. In that case higher-order processes like the phonon assisted spin-excitations, considered by Lorenzana and Sawatzky [50–52], can still contribute. These are probably responsible for the weak mid-infrared continuum in the $E\parallel$chain spectra (see fig. 5.12b and, in particular, its inset).

Taking the values of $t_\perp$ and Δ calculated from the optical data and $|t_\parallel|\approx 0.2\,$eV [54], for the exchange coupling constant we obtain $J_\parallel\approx 30$ meV. It is significant that the value we obtained from the optical data, is comparable to those reported in the literature, on the basis of magnetic susceptibility measurements, which range from 38 [47] to 48 meV [1]. Moreover, for the effective charge of the bi-magnon excitation process we obtain $q_m/q_e=0.07$. Using the correlation functions defined in chapter 4:

$$g_S(T) = 4\langle\langle h_S^2\rangle - \langle h_S\rangle^2\rangle_T \ . \tag{5.12}$$

$$g_C(T) = 4\langle\langle n_C^2\rangle - \langle n_C\rangle^2\rangle_T \ . \tag{5.13}$$

we can express the intensity of the spin-fluctuations relative to the CT excitations in terms of the effective charge:

$$\frac{\int_S \sigma_1(\omega)d\omega}{\int_{CT}\sigma_1(\omega)d\omega} = \frac{q_m^2 g_S E_S}{q_e^2 g_C E_{CT}} \ . \tag{5.14}$$

In chapter 4 we showed that $g_C=N(2uv)^2$ and for the present parameters, $g_C\simeq 0.4N$. E_S is the average energy of the infrared spin fluctuation spectrum. From the discussion given

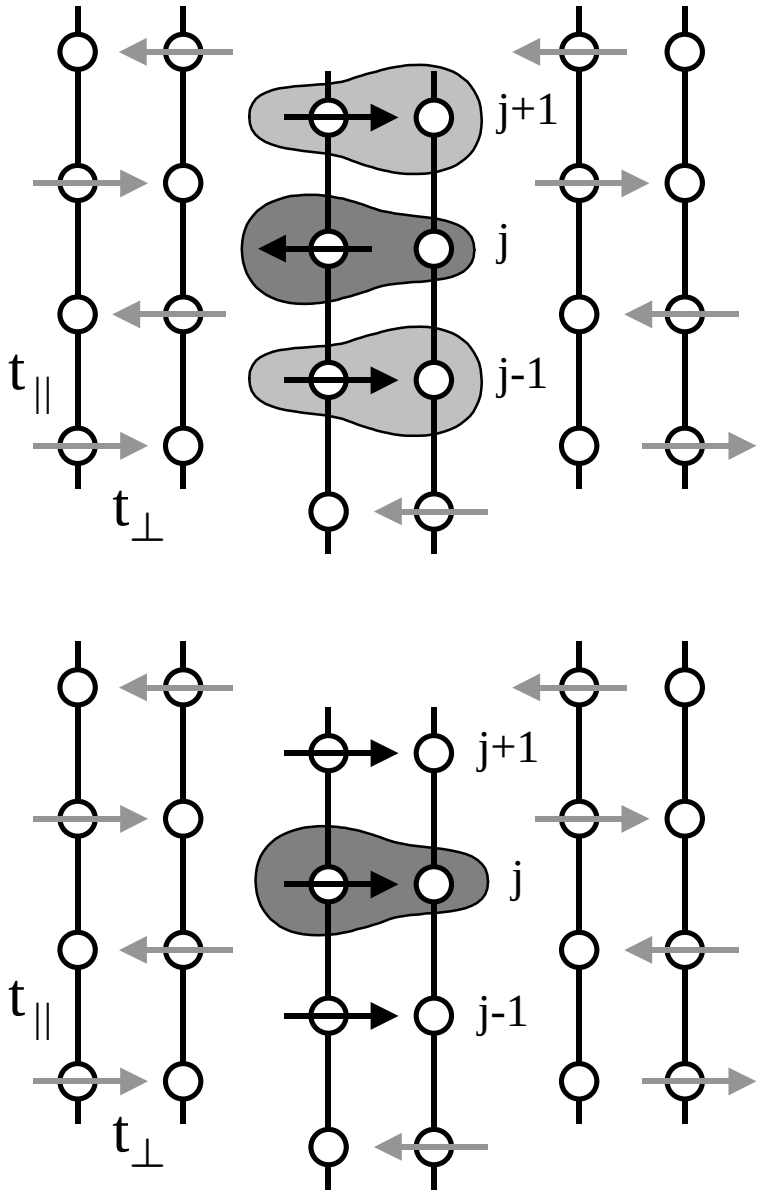

Figure 5.15: *Pictorial description of the electric dipole moment associated with a single spin-flip in α'-NaV_2O_5, when a local breaking of symmetry in the electron distribution on each rung is assumed. If three neighboring antiparallel spins are laying on the same leg of the ladder (top), the charge of the jth electron is asymmetrically distributed not only over the jth rung but also on the nn rungs (with opposite asymmetry), because of the virtual hopping $t_{\|}$. If we flip its spin (bottom), the jth electron is confined to the jth rung, resulting in a reduced charge density on the right leg of the ladder. Therefore, there is a net dipole displacement (along the rung direction) of the antiparallel spin configuration compared to the parallel one.*

in chapter 4 and from the value of $J_{\parallel}$ obtained from the analysis of the optical conductivity, E_S can be estimated to be of the order of 0.1 eV. The spin-correlation function g_S depends on the details of the many-body wave function of the spins. For an antiferromagnetic chain with long range Néel order $g_S = N$, whereas for a random orientation of the spins it is zero. In between it depends on the probability of having fragments of three neighboring spins ordered antiferromagnetically. Hence the maximum relative intensity in eq. 5.14 is $\sim$0.0014 (an expression for the maximum limiting value of this quantity was given in chapter 4, eq. 4.24). The experimental value is $\sim$0.0008 at T=300 K, in good agreement with the numerical estimate. Note that a finite value of g_S requires either terms in the Hamiltonian which do not commute with h_S, or an antiferromagnetic broken symmetry of the ground state.

We can now try to interpret the temperature dependence of the spin-fluctuation continuum presented in fig. 5.14b. We saw that the oscillator strength increases upon cooling down the sample from room temperature to $T_{\rm SP}$, and rapidly decreases for $T < T_{\rm SP}$. Within the discussion given above, this increase marks an increase in short range antiferromagnetic correlations of the chains. Below the phase transition, nearest neighbor (nn) spin-singlet correlations become dominant, and g_S is suppressed.

In conclusion, by a detailed analysis of the optical conductivity, we provided a direct evidence for a local breaking of symmetry in the electronic charge distribution over the rungs of the ladders in α'-NaV_2O_5, in the high temperature undistorted phase. Moreover, we showed that a direct two-magnon optical absorption process is responsible for the low frequency continuum observed perpendicularly to the V-O chains.

5.5 Discussion

As we discussed in the course of this chapter, the interpretation of the phase transition in α'-NaV_2O_5 is still controversial. On the one hand, the SP picture was suggested by preliminary magnetic susceptibility [1] and inelastic neutron scattering measurements [2]. On the other, x-ray diffraction redeterminations of the crystal structure of the compound, in the high temperature undistorted phase [10–12], showed that the dimerization within well defined 1D magnetic chains is not very probable in α'-NaV_2O_5. Moreover, the magnetic field dependence of $T_{\rm SP}$, expected for a true SP system on the basis of Cross and Fisher theory [8, 9], has not been observed [6, 7].

Additional information came recently from NMR experiments [15]: Above $T_{\rm SP}$, only one kind of V site (magnetic) was clearly detected, whereas no signature of nonmagnetic V^{5+} was found. However, another set of magnetic V sites which are invisible in the NMR spectrum could not be ruled out [15]. On the other hand, below the phase transition, two inequivalent sets of V sites were detected and assigned to V^{4+} and V^{5+}. These results were then interpreted as an indication of the charge ordering nature of the phase transition, in α'-NaV_2O_5 [15]. Subsequently, many theoretical studies have been addressing this possibility [16–19]. The main point to be explained is why a charge ordering would automatically result in the opening of a spin gap (with the same transition temperature). Among all

the models, the more interesting seem to be those were a 'zig-zag' charge ordering on the ladders is realized. In this case, the ordering would immediately result in a nonmagnetic ground state, due to the formation of spin singlets on nn V sites belonging to two different ladders [16] or, alternatively, to the modulation of $J_{\|}$ within a single ladder [18].

In the discussion of our spectra of the optical conductivity, we showed that the infrared continuum, observed perpendicularly to the V-O chains direction, could be attributed to direct optical absorption of double spin-flip excitations. However, in order to have optical activity for these processes and, at the same time, to explain the frequency position and the polarization dependence of the on-rung bonding-antibonding transition at 1 eV, we had to assume a charge disproportionation between the two V sites on a rung. This assumption seems to contrast the results of the x-ray diffraction analysis [10] and of NMR measurements [15]. As far as the former is concerned, it is obvious that if the charge disproportionation does not have a long range character it would not be detectable in an x-ray diffraction experiment, but would still result in optical activity of charged bi-magnon excitations. Regarding the disagreement with the NMR results [15], we saw that the existence of another kind of V sites could not be completely excluded in the NMR spectrum [15]. Furthermore, in comparing the optical to the NMR data, there could also be a problem with the different time scales of the two experimental techniques (i.e., 'fast' and 'slow' for optics and NMR, respectively). Therefore, if there are fluctuations in the system, the experimental results could be different.

From the analysis of the optical conductivity, we cannot really say which is the more appropriate picture for the low temperature transition in α'-NaV_2O_5. We saw that, indeed, the electronic and/or magnetic degrees of freedom are playing a leading role across the phase transition. This is shown, e.g., by the strong temperature dependence of the infrared spin fluctuation spectrum which, in turn, determines the anomalous behavior of the microwave dielectric constant [49]. However, the reduction of the oscillator strength of the infrared continuum for $T < T_{SP}$, which we discussed as a consequence of nn spin-singlet correlations becoming dominant below T_{SP}, could also result from a zig-zag charge ordering on the ladders. In this case, as for the perfectly symmetrical 1/4-filled ladder, the optical activity of double spin flips would simply vanish.

In our opinion, for a better understanding of the phase transition, the pretransitional fluctuations observed with optical spectroscopy [13], ultrasonic wave propagation [42], and x-ray diffuse scattering [43], have to be taken into account. They probably reflect the high degree of disorder present in the system above the phase transition, which is also shown by the local and 'disordered' charge disproportionation necessary to interpret the optical conductivity. In this context, a charge ordering transition, where more degrees of freedom than just those of the spins are involved, seems plausible. It would also explain the experimentally observed entropy reduction, which appeared to be larger than what expected for a 1D AF Heisenberg chain [6].

Finally, also the degeneracy of the zone boundary folded modes, activated by the phase transition, could be an important piece of information. However, at this stage of the investigation of the electronic and magnetic properties of α'-NaV_2O_5, very important insights could come from the x-ray diffraction determination of the low temperature structure.

Probably, only at that point it will be possible to fit all the different results together and come up with the final interpretation of the phase transition.

5.6 Conclusions

In this chapter we have been discussing the high and low temperature properties of α'-NaV_2O_5. We studied the symmetry of the material, in the high temperature undistorted phase, on the basis of x-ray diffraction results, and of the phonon spectra detected in reflectivity measurements. We found that the system is described by the centrosymmetric space group *Pmmn*, within an accuracy of 0.03 Å.

On the other hand, by a detailed analysis of the optical conductivity, we provided direct evidence for a charged disproportionated electronic ground-state, at least on a locale scale: An asymmetrical charge distribution on each rung, without any long range order. We showed that, because of the locally broken symmetry, spin-flip excitations carry a finite electric dipole moment, which is responsible for the detection of charged bi-magnons in the optical spectrum for $E \perp$ chain, i.e., direct two-magnon optical absorption processes.

By analyzing the optically allowed phonons at various temperatures below and above the phase transition, we concluded that a second-order change to a larger unit cell takes place below 34 K, with a fluctuation regime extending over a very broad temperature range.

References

[1] M. Isobe, and Y. Ueda, J. Phys. Soc. Jpn. **65**, 1178 (1996).

[2] Y. Fujii, H. Nakao, T. Yosihama, M. Nishi, K. Nakajima, K. Kakurai, M. Isobe, Y. Ueda, and H. Sawa, J. Phys. Soc. Jpn. **66**, 326 (1997).

[3] P.A. Carpy, and J. Galy, Acta Cryst. B **31**, 1481 (1975).

[4] M. Nishi, O. Fujita, and J. Akimitsu, Phys. Rev. B **50**, 6508 (1994).

[5] G.S. Uhrig, Phys. Rev. Lett. **79**, 163 (1997).

[6] B. Büchner, private communication.

[7] W. Schnelle, Yu. Grin, and R.K. Kremer, Phys. Rev. B **59**, 73 (1999).

[8] M.C. Cross, and D.S. Fisher, Phys. Rev. B **19**, 402 (1979).

[9] M.C. Cross, Phys. Rev. B **20**, 4606 (1979).

[10] A. Meetsma, J.L. de Boer, A. Damascelli, J. Jegoudez, A. Revcolevschi, and T.T.M. Palstra, Acta Cryst. C **54**, 1558 (1998).

[11] H.G. von Schnering, Yu. Grin, M. Kaupp, M. Somer, R.K. Kremer, and O. Jepsen, Z. Kristallogr. **213**, 246 (1998).

[12] H. Smolinski, C. Gros, W. Weber, U. Peuchert, G. Roth, M. Weiden, and C. Geibel, Phys. Rev. Lett. **80**, 5164 (1998).

[13] A. Damascelli, D. van der Marel, M. Grüninger, C. Presura, T.T.M. Palstra, J. Jegoudez, and A. Revcolevschi, Phys. Rev. Lett. **81**, 918 (1998).

[14] A. Damascelli, D. van der Marel, J. Jegoudez, G. Dhalenne, and A. Revcolevschi, Physica B, in press (1999).

[15] T. Ohama, H. Yasuoka, M. Isobe, and Y. Ueda, Phys. Rev. B **59**, 3299 (1999).

[16] H. Seo, and H. Fukuyama, J. Phys. Soc. Jpn. **67**, 2602 (1998).

[17] P. Thalmeier, and P. Fulde, Europhys. Lett. **44**, 242 (1998).

[18] M. Mostovoy, and D. Khomskii, cond-mat/9806215 (18 June 1998).

[19] J. Riera, and D. Poilblanc, Phys. Rev. B **4**, 2667 (1999).

[20] J.C. Bonner, and M.E. Fisher, Phys. Rev. A **135**, 610 (1964).

[21] F. Mila, P. Millet, and J. Bonvoisin, Phys. Rev. B **54**, 11 925 (1996).

[22] M. Isobe, and Y. Ueda, Physica B **262**, 180 (1997).

[23] J. Hemberger, M. Lohmann, M. Nicklas, A. Loidl, M. Klemm, G. Obermeier, and S. Horn, Europhys. Lett. **42**, 661 (1998).

[24] Y. La Page, J. Appl. Cryst. **20**, 264 (1987); J. Appl. Cryst. **21**, 983 (1988).

[25] D.L. Rousseau, R.P. Bauman, and S.P.S. Porto, J. Raman Spectrosc. **10**, 253 (1981).

[26] M. Isobe, C. Kagami, and Y. Ueda, J. Crystal Growth **181**, 314 (1997).

[27] F. Wooten, *Optical Properties of Solids* (Academic Press, New York, 1972).

[28] M.V. Klein, and T.E. Furtak, *Optics* (John Wiley & Sons, New York, 1983).

[29] A. Golubchik, M. Isobe, A.N. Ivlev, B.N. Mavrin, M.N. Popova, A.B. Sushkov, Y. Ueda, and A.N. Vasil'ev, J. Phys. Soc. Jpn. **66**, 4042 (1997).

[30] D. Smirnov, J. Leotin, P. Millet, J. Jegoudez, and A. Revcolevschi, Physica B, in press (1999).

[31] M.N. Popova, A.B. Sushkov, A.N. Vasil'ev, M. Isobe, and Y. Ueda, JETP Lett. **65**, 743 (1997).

[32] D. Smirnov, P. Millet, J. Leotin, D. Poilblanc, J. Riera, D. Augier, and P. Hansen, Phys. Rev. B **57**, R11 035 (1998).

[33] Z.V. Popović, M.J. Konstantinović, R. Gajić, V. Popov, Y.S. Raptis, A.N. Vasil'ev, M. Isobe, and Y Ueda, J. Phys. Condens. Matter **10**, 513 (1998).

[34] M. Fischer, P. Lemmens, G. Güntherodt, M. Weiden, R. Hauptmann, C. Geibel, and F. Steglich, Physica B **244**, 76 (1998).

[35] P. Lemmens, M. Fischer, G. Els, G. Güntherodt, A.S. Mishchenko, M. Weiden, R. Hauptmann, C. Geibel, and F. Steglich, Phys. Rev. B **58**, 14 159 (1998).

[36] H. Kuroe, H. Seto, J. Sasaki, T.Sekine, M. Isobe, and Y. Ueda, J. Phys. Soc. Jpn. **67**, 2881 (1998).

[37] M.N. Popova, A.B. Sushkov, S.A. Golubchik, B.N. Mavrin, V.N. Denisov, B.Z. Malkin, A.I. Iskhakova, M. Isobe, and Y. Ueda, cond-mat/9807369 (28 July 1998).

[38] U. Fano, Phys. Rev. **124**, 1866 (1961).

[39] A. Damascelli, D. van der Marel, F. Parmigiani, G. Dhalenne, and A. Revcolevschi, Phys. Rev. B. **56**, R11 373 (1997).

[40] A. Damascelli, D. van der Marel, F. Parmigiani, G. Dhalenne, and A. Revcolevschi, Physica B **244**, 114 (1998).

[41] A. Damascelli, K. Schulte, D. van der Marel, and A.A. Menowsky, Phys. Rev. B **55**, R4863 (1997).

[42] P. Fertey, M. Poirier, M. Castonguay, J. Jegoudez, and A. Revcolevschi, Phys. Rev. B **57**, 13 698 (1998).

[43] S. Ravy, J. Jegoudez, and A. Revcolevschi, Phys. Rev. B **2**, R681(1999).

[44] M. Bassi, P. Camagni, R. Rolli, G. Samoggia, F. Parmigiani, G. Dhalenne, and A. Revcolevschi , Phys. Rev. B. **54**, R11 030 (1996).

[45] P. Horsch, and F. Mack, Eur. Phys. J. B **5**, 367 (1998).

[46] S. Nishimoto, and Y. Ohta, J. Phys. Soc. Jpn. **67**, 2996 (1998).

[47] M. Weiden, R. Hauptmann, C. Geibel, F. Steglich, M. Fischer, P. Lemmens, and G. Güntherodt, Z. Phys. B **103**, 1 (1997).

[48] Y. Sekine, N. Takeshita, N. Môri, M.Isobe, and Y.Ueda, preprint (1998).

[49] A.I.Smirnov, M.N.Popova, A.B.Sushkov, S.A.Golubchik, D.I.Khomskii, M.V.Mostovoy, A.N.Vasil'ev, M.Isobe, and Y.Ueda, cond-mat/9808165 (27 October 1998).

[50] J. Lorenzana, and G.A. Sawatzky, Phys. Rev. Lett. **74**, 1867 (1995).

[51] J. Lorenzana, and G.A. Sawatzky, Phys. Rev. B **52**, 9576 (1995).

[52] J. Lorenzana, and R. Eder, Phys. Rev. B **55**, R3358 (1997).

[53] S. Nishimoto, and Y. Ohta, J. Phys. Soc. Jpn. **67**, 3679 (1998).

[54] W.A. Harrison, *Electronic Structure and the Properties of Solids* (Dover Publications, New York, 1989).

Summary

This thesis work illustrates the results obtained on a number of solid crystalline materials using optical spectroscopy. This experimental technique consists of shining light of different frequencies onto the sample under investigation, and of observing which frequencies are absorbed by the material itself. The experiments were performed in the frequency range extending from the far infrared to the ultra violet (i.e., from 4 meV to 4 eV). Linearly polarized light was used, therefore characterized by a well defined direction of oscillation for the electric field of the radiation, in order to probe the possible anisotropy of the samples. In this way we could investigate the lattice vibrational modes (detectable in a solid in the far-infrared region), and the electronic and/or magnetic excitation spectra. Additional information was obtained by performing the optical experiments while varying the temperature of the samples between 4 and 300 K. From the detailed analysis of the temperature dependent experimental data, we could learn about the crystal structure of the different systems, and their electronic and magnetic properties like, e.g., ground state configuration, electron-phonon coupling, and spin-charge interplay.

As far as the compounds discussed in this thesis are concerned (transition metal monosilicides, $CuGeO_3$, and α'-NaV_2O_5), the common feature is that they all belong to the class of *strongly correlated electron systems*, i.e., compounds whose properties are dominated by strong electron-electron correlations. This is the case when the on-site electron-electron repulsion U is much larger than the energies associated with the overlap of atomic orbitals belonging to different atoms. Because these energies are characterized, in a solid, by the width W of the energy band under consideration, a large U/W ratio is expected in systems involving well-localized electrons like the $4f$ and $5f$ electrons of the rare earths and the actinides, respectively, but also the d electrons of the transition metals (TM).

The importance of electron-electron correlations in influencing the basic properties of a compound can be understood considering the example of CoO. This oxide, if treated within the independent-electron approximation (i.e., writing the total wavefunction of the N-electron system in the form of an antisymmetrized product of single-electron wavefunctions), is expected to be metallic, with an odd number of electrons per unit cell and a partially filled d band. In reality, as a consequence of strong correlations, which are suppressing charge fluctuations and therefore the electrical conductivity, CoO is an insulator.

More in general, strong electron-electron correlations can give rise to a large variety of peculiar phenomena, the most famous being probably high-temperature superconductivity, heavy-fermion and Kondo-insulating behavior, and colossal magnetoresistance. For

the description of these collective phenomena, and for the development of appropriate microscopic models, it is useful to investigate the elementary excitations of these materials. In fact, the excitations between the ground state and the lowest excited states reflect the interplay between quantum magnetism and low energy charge degrees of freedom, a fingerprint of strong electron-electron correlations.

In the course of this thesis work we investigated a number of TM mono-silicides and, among them, in particular FeSi which shows Kondo-insulating behavior at low temperature. Moreover, we studied quasi-one-dimensional (1D) systems in which electron-electron correlations, together with the low dimensionality, give rise to fascinating phenomena like the spin-Peierls (SP) phase transition ($CuGeO_3$), and the direct optical absorption for spin-flip excitations (α'-NaV_2O_5).

Infrared Spectroscopy Study of Phonons Coupled to Charge Excitations in FeSi

We investigated the optical response of FeSi, CoSi, and MnSi. Whereas on CoSi and MnSi we observed a metallic behavior at any temperature, on FeSi we could follow the opening of a gap of the order of 70 meV, upon reducing the temperature below 100 K.

By analyzing in detail the phonon spectra we could determine the dynamical (or transverse effective) charge of the TM atoms and Si, for each temperature: The large value $e_T^* \approx 4e$ was obtained on all compounds. For a purely ionic insulator this is also the actual charge of the ions. However, because the TM atoms and Si have practically the same electronegativity and electron affinity, strong ionicity is not expected from a chemical point of view in this class of materials. On the other hand, for a covalent compound with resonating bonds a finite value of the transverse effective charge results from a dynamical charge redistribution associated with the ionic motion due to an optical phonon. We showed that the large value of the transverse effective charge, along with the resonance behavior of the phonon parameters, observed on FeSi when the gap sweeps through the phonon-frequency, provides strong evidence for a moderate coupling between the vibrational degrees of freedom and low energy electron-hole excitations in these systems ($\lambda \approx 0.1$, in FeSi).

Based on the discussion of the infrared spectra presented in this thesis and of published transport data, we provided a qualitative model for the electronic structure of the TM mono-silicides. The main conclusion is that six electrons per transition metal atom are engaged in chemical bonds to the Si sublattice. The remaining electrons of the TM atoms (e.g., two for FeSi) occupy a doubly degenerate quasi-atomic d-state, and obey Hund's rules: In FeSi, the two localized d electrons result in a local moment $S = 1$ on the Fe site. The conduction band supports two weakly bound itinerant electrons (mainly of Si $3p$ character) which in the case of FeSi, at sufficiently low temperatures, compensate the local moment loosing their itinerant character, by forming what is called a Kondo singlet ($S = 0$). This framework provides a basis for understanding the observed range of chemical stability of these compounds (from CrSi to NiSi), and the physical properties of FeSi.

Infrared Signatures of the Spin-Peierls Transition in $CuGeO_3$

$CuGeO_3$ is considered as a quasi-1D system because weakly-coupled 1D CuO_2 chains, running parallel to each other, can be identified in this material. Each Cu^{2+} ion is in a d^9 electronic configuration which corresponds to a spin $S = 1/2$ on each Cu site. These magnetic moments interact antiferromagnetically: For each spin it is more favorable to be antiparallel (rather than parallel) with respect to the two neighboring spins.

In 1993, $CuGeO_3$ was recognized as the first inorganic compound showing a SP phase transition: A lattice distortion that occurs together with the formation of a nonmagnetic ground state ($S = 0$), and the opening of a finite energy gap in the magnetic excitation spectrum. This magneto-elastic transition is driven by the magnetic energy gain due to dimerization of the antiferromagnetic exchange between the spin 1/2 moments of the Cu^{2+} ions, which overcompensates the elastic energy loss resulting from the deformation of the lattice. In the SP ordered phase (i.e., for $T < T_{SP} = 14$ K), the Cu^{2+} magnetic moments form singlet dimers along the chains, and spin triplet excitations are gapped.

Because the phase transition involves a lattice distortion and, therefore, a change of the symmetry of the crystal, the phonon spectrum is expected to change across the transition. Therefore, we have been investigating the temperature dependent optical spectra of pure and doped $CuGeO_3$ concentrating, in particular, on the lattice vibrational modes. As a matter of fact, we could detect new optical phonon modes activated by the SP phase transition, and reflecting the lower symmetry of the system for $T < T_{SP}$. Following the temperature dependence of these modes we were able to determine the second order character of the phase transition and to study the effect of doping on T_{SP}: In particular, we showed that the substitution of Ge with Si is three times more efficient, than the one of Cu with Mg, in reducing T_{SP}. This result was discussed in relation to the difference, between Mg and Si doping, in affecting the magnetism of the system.

Furthermore, we detected a direct singlet-triplet excitation, across the magnetic gap, which is in principle optically forbidden on the basis of the crystal structure generally assumed, for $CuGeO_3$, in the high temperature phase. The optical activity of this excitation and the strong changes observed in the phonon spectra of Si-substituted samples might be explained in terms of an alternative crystal structure, recently proposed for $CuGeO_3$.

Direct Two-Magnon Optical Absorption in α'-NaV_2O_5: "Charged" Magnons

After $CuGeO_3$, another inorganic compound, α'-NaV_2O_5, has been attracting the attention of the scientific community working on low-dimensional spin systems, in general, and on the SP phenomenon, in particular. In fact, in 1996 the SP picture was proposed to explain the low temperature properties of α'-NaV_2O_5, with a transition temperature T_{SP}=34 K. The basic building blocks of the crystal structure are linear chains of alternating V and O ions. These chains are grouped into sets of two, resulting in a two-leg ladder with rungs formed by two V ions, one on each leg of the ladder, bridged by an oxygen ion. Only one V d electron per rung is present (i.e., $S = 1/2$). Because the coupling between the ladders is weak, also α'-NaV_2O_5 has a quasi-1D character.

As in the case of $CuGeO_3$, by analyzing the optically allowed phonons at various temperatures below and above the phase transition, we concluded that a second-order change to a larger unit cell takes place below 34 K, as expected for a SP transition. On the other hand, on the basis of specific heat measurements in high magnetic field recently reported, the interpretation of the phase transition in α'-NaV_2O_5 is still controversial. In particular, the reduction of T_{SP} upon increasing the intensity of the externally applied magnetic field, which is typical for a true SP system, has not been observed.

This already quite puzzling picture became even more complicated when the crystal structure and the symmetry of the electronic configuration of α'-NaV_2O_5, in the high temperature phase, were investigated in detail. In fact, on the basis of x-ray diffraction measurements we found, in agreement with other groups, that the symmetry of this compound at room temperature is better described by the centrosymmetric space group $Pmmn$ than by the originally proposed $P2_1mn$. On the other hand, the intensities and polarization dependence of the electronic excitations detected in our optical spectra were not understandable in terms of a centrosymmetric space group.

We showed that a consistent interpretation of both x-ray diffraction results and optical conductivity data requires a charge disproportionated electronic ground-state, at least on a local scale, i.e., an asymmetrical charge distribution of the V d electron on each rung, without any long range order. We found that the presence of only one V d electron per rung, along with the broken left-right parity of the ground-state, gives rise to a fascinating behavior of the spin flips in α'-NaV_2O_5: Spin-flip excitations carry a finite electric dipole moment, which is responsible for the detection of *charged bi-magnons* in the optical spectra, i.e., direct two-magnon optical absorption processes.

Finally, we discussed the relevance of these findings to other quasi 1D and quasi 2D strongly correlated electron systems, where the interplay of spin and charge plays a crucial role in determining the low energy electrodynamics. The possibility to observe bi-magnon excitations directly, in optical spectroscopy, may become extremely useful in the study of, e.g., magnetic excitations near defects and phase-antiphase boundaries. Moreover, we expect that further study of this effect in other materials will provide important clues to the notorious mid-infrared bands in many doped strongly correlated antiferromagnetic materials, such as the high-temperature superconductors.

Samenvatting

Dit proefschrift bevat de resultaten van optische metingen aan een aantal monsters van vaste stoffen. Optische spectroscopie is een experimentele methode waarbij licht van verschillende frequenties op het te onderzoeken monster geschenen wordt, waarna wordt gekeken welke frequenties door het monster worden geabsorbeerd. De metingen zijn gedaan in een frequentie gebied dat zich uitstrekt van het Verre Infrarood tot het Ultraviolet (van 4 meV tot 4 eV). Hierbij werd lineair gepolariseerd licht gebruikt, wat gekarakteriseerd wordt door een welomschreven polarisatie richting (het elektrisch veld heeft precies één oscillatie richting). Dit is nodig om mogelijke anisotrope eigenschappen van het monster te kunnen bepalen. Op deze manier was het mogelijk voor ons om zowel de roostertrillingen of fononen (deze fononen bevinden zich ruwweg in het Verre Infrarood) alsmede de elektronische en/of magnetische excitaties van de monsters te meten. Extra informatie werd verkregen door de temperatuur van het monster tijdens de metingen te variëren van 4 tot 300 Kelvin. Middels een gedetailleerde analyse van deze temperatuurafhankelijke spectra kregen we een beter zicht op de kristalstructuur van de verschillende bestudeerde stoffen en hun magnetische en elektronische eigenschappen (zoals bijvoorbeeld de grondtoestand, de koppeling tussen elektronen en fononen, en de interactie tussen spins en lading).

De bindende factor tussen de materialen die beschreven worden in dit proefschrift (overgangsmetaal-monosiliciden, $CuGeO_3$, en α'-NaV_2O_5) is dat ze allen deel uit maken van de klasse der *sterk gecorreleerde elektronen systemen*, dit betekend dat al hun eigenschappen beheerst worden door de sterke onderlinge wisselwerking van elektronen. Dit gebeurt wanneer de afstoting U tussen elektronen die zich op hetzelfde roosterpunt bevinden veel sterker is dan de winst in energie tengevolge van de overlap van atomaire orbitalen gelokaliseerd op verschillende roosterpunten. Deze energie wordt in de vaste stoffen beschreven door de breedte in energie W van de aldus ontstane energiebanden. Voor materialen die (gedeeltelijk) bestaan uit elementen met sterk gelokaliseerde elektronenbanen, zoals de $4f$ en de $5f$ elektronen in respectievelijk de zeldzame aarden en de actiniden, maar ook tot op zekere hoogte de d elektronen in de overgangs metalen (OM) wordt derhalve verwacht dat de ratio U/W veel groter is dan één.

Het belang van deze elektron-elektron correlaties en de manier waarop ze de intrinsieke eigenschappen van een materiaal beïnvloeden, kunnen we uitleggen aan de hand van een voorbeeld: CoO. Wanneer we dit materiaal beschrijven in termen van een zogeheten onafhankelijk elektronmodel, waarin de elektron-elektron correlaties buiten beschouwing gelaten worden (dit betekent dat de totale golffunctie van een systeem met N elektro-

nen bestaat uit het geantisymmetriseerde produkt van de afzonderlijke golffuncties van de elektronen) is de uitkomst dat CoO metallisch is, met een oneven aantal elektronen per eenheidscel en een gedeeltelijk gevulde d band. In de praktijk blijkt echter dat als gevolg van de sterke correlaties de geleidbaarheid onderdrukt wordt en CoO een isolator is.

Meer in het algemeen kan men stellen dat sterke onderlinge elektron interactie in diverse vaste stoffen de verklaring is voor een groot aantal eigenaardige eigenschappen. De meest bekende verschijnselen zijn waarschijnlijk die van hoge temperatuur supergeleiding, 'zware fermionen', Kondo-isolatoren en kolossale magneto-weerstand. Om tot een goede microscopische beschrijving van deze materialen te kunnen komen is het van belang om de fundamentele excitaties van deze materialen te bestuderen. Vooral de laag-energetische excitaties van de grondtoestand naar de eerste aangeslagen toestanden geven een goed beeld van het samenspel van quantum magnetisme en de toegestane ladingsexcitaties en zijn daarmee een directe vingerafdruk van de elektron-elektron correlaties.

Gedurende de afgelopen vier jaar hebben we een aantal OM monosiliciden bestudeerd, in het bijzonder FeSi, dat zich bij lage temperaturen als een Kondo-isolator gedraagt, en vervolgens materialen uit een klasse van quasi-ééndimensionale (1D) systemen, waarin de sterke onderlinge wisselwerking tezamen met de lage dimensionaliteit van deze systemen resulteerden in fascinerende effecten als de spin-Peierls (SP) fase overgang ($CuGeO_3$) en de directe waarneming van spin-flip excitaties in het optische spectrum (α'-NaV_2O_5).

Fononen Gekoppeld aan Ladingsexcitaties in FeSi

We hebben de optische eigenschappen van FeSi, CoSi en MnSi bestudeerd. Het blijkt dat CoSi en MnSi metallisch zijn bij elke door ons onderzochte temperatuur, terwijl in FeSi de laagfrequente geleidbaarheid afneemt als functie van afnemende temperatuur tot zich bij 4 K een energiekloof heeft gevormd van ongeveer 70 meV in de optische geleidbaarheid.

Door nauwkeurig de fononpieken te analyseren, konden we de dynamische (of transversale effectieve) lading van de OM en Si atomen bepalen, bij elke temperatuur. We vonden hiervoor een relatief grote waarde ($e_T^* \approx 4e$) in al deze materialen. Voor puur ionogene stoffen is deze lading meteen ook de valentie van de ionen. Maar, voor de OM-siliciden is sterke ioniciteit niet erg waarschijnlijk omdat de elektronegativiteit en elektronaffiniteit van de OM en de Si atomen ongeveer gelijk zijn. Voor covalente materialen echter wordt een grote waarde voor e_T^* uitgelegd als dynamische ladingsherverdeling tengevolge van de interactie met een optisch fonon. Dit heet in het kort 'resonerende bindingen'. Verder hebben we laten zien dat de hoge waarde voor de effectieve lading, samen met het resonante gedrag van de fononparameters, zoals in FeSi wanneer de energiekloof door de fononfrequentie heengaat, erop duidt dat er een gematigd sterke koppeling ($\lambda \approx 0.1$, in FeSi) bestaat tussen de fononen en de laag-energetische elektron-gat excitaties in deze stoffen.

Gebaseerd op deze uitkomst van onze experimenten en reeds gepubliceerde transportmetingen, hebben we vervolgens een kwalitatief model voorgesteld voor de elektronische structuur van de OM-monosilicides. Het voornaamste punt hierin is dat er 6 elektronen per overgangs metaalatoom betrokken zijn bij de bindingen met het Si subrooster. De overgebleven elektronen van de OM atomen (2 in het geval van FeSi) bezetten een dubbel

ontaarde quasi-atomaire d-toestand, waarin ze zich houden aan de regels van Hund: in FeSi vormen de twee gelokaliseerde d elektronen een totale lokale spin $S=1$ op de positie van het Fe atoom. De OM-Si geleidingsband bevat twee semi-vrije elektronen (voornamelijk met Si $3p$ karakter) die in het geval van FeSi, bij voldoende lage temperaturen, het lokale spin moment compenseren, waarbij ze hun vrije karakter verliezen en een zogenaamd Kondo singlet vormen ($S=0$). Dit model geeft een aanzet tot het beter begrijpen van de chemische stabiliteit van deze reeks (van CrSi tot NiSi) van materialen en de fysische eigenschappen van FeSi in het bijzonder.

Aanwijzingen voor een Spin-Peierls Overgang in het Infrarood in $CuGeO_3$

$CuGeO_3$ wordt over het algemeen beschouwd als een quasi-ééndimensionaal systeem vanwege de aanwezigheid van zwak gekoppelde parallelle 1D CuO_2 ketens. Elk Cu^{2+} ion bevindt zich in een d^9 toestand, wat inhoudt dat er op elke Cu positie een spin $S=1/2$ zit. Deze magnetische momenten hebben een antiferromagnetische wisselwerking met elkaar: dit betekent dat de spins zich het liefst antiparallel opstellen ten opzichte van hun buurman.

In 1993 werd in $CuGeO_3$ als eerste anorganische materiaal, een SP fase overgang waargenomen. Een SP fase overgang bestaat uit een roostervervorming waarbij zich tegelijkertijd een non-magnetische grondtoestand ($S=0$) formeert, en er een kloof ontstaat in het magnetische excitatiespectrum. Deze magneto-elastische overgang is rendabel doordat de winst in magnetische energie voortkomend uit de dimerisatie van twee antiferromagnetisch gekoppelde spins op naburige Cu ionen groter is dan het verlies aan elastische energie tengevolge van de roostervervorming. Voor temperaturen lager dan de overgangstemperatuur ($T < T_{\rm SP} = 14$ K) vormen de Cu ionen zich paarsgewijs tot spin-singlet dimeren in de CuO_2 keten, tussen deze nieuwe grondtoestand en de eerste aangeslagen toestand (spin-triplet) bevindt zich een energiekloof.

Omdat de fase overgang gepaard gaat met een roostervervorming, en dus een verandering in de symmetrie van het kristal, verwacht men dat het fononspectrum van het materiaal zal veranderen beneden $T_{\rm SP}$. Om dit te testen hebben we de temperatuurafhankelijkheid van de optische spectra bestudeerd van zowel puur als gedoteerd $CuGeO_3$, waarbij we voornamelijk hebben gelet op de trillingen van het rooster. En inderdaad, beneden $T_{\rm SP}$ hebben we nieuwe optische fononen aangetroffen die de lagere symmetrie van het systeem weerspiegelen. Door nauwkeurig het gedrag van deze nieuwe fononen als functie van temperatuur te bestuderen konden we vaststellen dat de fase overgang van de tweede orde moet zijn en wat het effect is van dotering op de overgangstemperatuur: hier vonden we dat de vervanging van Ge door Si drie keer zo effectief is in het verlagen van $T_{\rm SP}$ als de vervanging van Cu door Mg. Dit resultaat kan worden verklaard doordat Mg een ander effect heeft op de magnetische eigenschappen van het systeem dan Si.

Bovendien hebben we in de spectra de directe excitatie van de spin-singlet grondtoestand naar de spin-triplet toestand gezien, hoewel deze in principe optisch verboden zou moeten zijn, gelet op de kristalstructuur die men voor $CuGeO_3$ heeft voorgesteld. De optische activiteit van deze excitatie kan echter misschien verklaard worden wanneer een ándere kristalstructuur voor $CuGeO_3$ genomen wordt, die recentelijk is voorgesteld.

Directe Twee-Magnon Optische Absorptie in α'-NaV_2O_5: "Geladen" Magnonen

Na $CuGeO_3$ ontstond er binnen de wetenschappelijke wereld belangstelling voor een andere anorganische stof: α'-NaV_2O_5. In 1996 meldde men dat het SP model de eigenschappen van α'-NaV_2O_5 bij lage temperaturen kon verklaren, met een overgangstemperatuur van T_{SP}=34 K. De basiseenheden in de kristalstructuur van α'-NaV_2O_5 zijn rechte ketens van afwisselend V en O ionen. Deze ketens zijn gegroepeerd in setjes van twee, en vormen zo een ladder waarbij de sporten gevormd worden door de twee V ionen met een O ion in hun midden. Per sport is er één V d elektron beschikbaar (dus $S=1/2$). Omdat de koppeling tussen de ladders erg zwak is, is ook dit een quasi-ééndimensionaal systeem.

Net zoals bij $CuGeO_3$, konden we aan de hand van de temperatuurafhankelijkheid van de fononen, vaststellen dat er een tweede orde fase overgang plaatsvindt bij 34 K naar een toestand met een grotere eenheidscel. Dit is in overeenstemming met het SP model. Maar, recente soortelijke warmte metingen in hoge magneetvelden hebben juist aangetoond dat het bij α'-NaV_2O_5 niet gaat om een SP overgang: de verwachte daling van T_{SP} bij sterkere magneetvelden is door hun niet gezien.

Dit op zich al gecompliceerde plaatje werd nog ingewikkelder toen men de kristalstructuur en de symmetrie van de elektronische configuratie van de kamertemperatuur fase van α'-NaV_2O_5 nauwkeuriger ging bekijken. Uit Röntgendiffractiespectra concludeerde men dat de symmetrie bij kamertemperatuur beter beschreven wordt door de centrosymmetrische ruimtegroep $Pmmn$ dan door de aanvankelijk voorgestelde groep $P2_1mn$. In onze optische spectra echter is het niet mogelijk om de intensiteit en de polarisatieafhankelijkheid van de elektronische excitaties te beschrijven met als uitgangspunt een centrosymmetrische groep.

Wij hebben laten zien dat een consistente beschrijving van zowel de Röntgendiffractiespectra alsmede de optische geleidbaarheid bereikt kan worden als men voor de grondtoestand aanneemt dat de elektronen asymmetrisch verdeeld zijn, op tenminste een lokaal niveau, d.w.z. een asymmetrische ladingsverdeling van het vanadium d elektron over de sport van de ladder, maar zonder een specifieke ordening over een grotere afstand. Het feit dat er slechts één d elektron is per sport, plus de gebroken ladingssymmetrie op elke sport leidde ons tot de voorspelling dat de spin-flip excitaties in α'-NaV_2O_5 zich anders zullen gedragen dan gewoonlijk: de spin-flip excitaties moeten een eindig elektrisch dipoolmoment met zich mee dragen. Daardoor kunnen deze *geladen bi-magnonen* direct worden waargenomen in een optische meting: de twee-magnon excitatie is optisch toegestaan.

Als laatste bespreken we het belang van deze bevindingen in het kader van andere quasi 1D en quasi 2D sterk gecorreleerde elektronsystemen, waarin het onderlinge samenspel van spins en lading een cruciale rol speelt in het bepalen van de laag-energetische elektrodynamische eigenschappen. De mogelijkheid om directe bi-magnon excitaties te kunnen zien in een optische meting, kan uiterst nuttig zijn bij het bestuderen van bijvoorbeeld magnetische excitaties nabij defecten en fase-antifase grenzen in het kristal. Sterker nog, wij verwachten dat een verdere bestudering van dit effect in andere materialen belangrijke aanwijzingen kan geven omtrent de beruchte midinfrarood banden in andere sterk gecorreleerde antiferromagnetische materialen, zoals de hoge temperatuur supergeleiders.

Acknowledgements

Meeting Dick van der Marel was just a coincidence. At that time I was working in the field of nonlinear optics and I had never heard of him. Then again, he had never heard of me either! Now, after the four years that I spent working with him, I can indeed say that this coincidence was a very lucky one. I really appreciate his way of both doing research and guiding the students in their projects. As an experimental physicist, his aim is not only to obtain relevant *'experimental facts'*, but also to understand them on a deep theoretical and intellectual level. As a supervisor, he is constantly inspiring and confronting his students, but, at the same time, he grants them all the freedom they wish. In other words, thanks Dick for what I learned from you, for your contagious enthusiasm, and for the great time we had together. I hope that these four years will be the basis of a long friendship and fruitful future collaborations.

Working in Groningen has been a special experience also because of the high level scientific environment. I had the opportunity to interact with scientists who have vast knowledge and experience, like George Sawatzky, Daniel Khomskii, and Thom Palstra. I would like to thank George Sawatzky for the interest he always showed in my work and, in particular, for the series of evening lectures he gave for Ph.D. students. It was extremely useful and pleasant being there: I never saw anybody else able to talk about solid state physics in such a fascinating way. I am very grateful to Daniel Khomskii for the careful reading of my manuscript but, above all, for the 'daily discussions' we had, which were extremely important for me when entering the realm of low dimensional spin systems. He is indeed a theoretician who knows how to talk to experimentalists. I am particularly grateful to Thom Palstra for the intense collaboration we had on the project of α'-NaV_2O_5. His alternative experimental approach and the occasional 'divergence of opinions' have been extremely precious and stimulating.

Obviously, not only the 'big shots' made Groningen such a pleasant place for me. The number of people is much larger and, among them, I would like to thank, first of all, Cor Bos, the godfather of our 'Cor-related experimental systems'. His technical and much more than technical assistance was irreplaceable. Secondly, I would like to express my gratitude to Auke Meetsma and Jan de Boer, who tried hard to turn me into a crystallographer; Henk Bron, who polished and 'smoked' most of my samples; and Frans van der Horst, who was never tired of having to enlarge my *quota* on our work-station.

Special thanks to Maxim Mostovoy, a brilliant theoretician and an even more brilliant (and patient) teacher. I really enjoyed our frequent discussions.

And now, the people of my group, who I could write a book about. Markus Grüninger, the *German paranimf*: We shared everything, life inside and outside the lab, the experience of having a son (I mean, you had yours and I had mine!)...not to mention our tough discussions (the one we had at the bottom of the Grand Canyon was great!). Thanks Markus, I'm sure our friendship will not be just a four year experience. Johan Feenstra: thanks Johan, you also are a *tremendous* friend, even though we did not really share everything: I'm sorry, but I was not brave enough to eat a *kroket* together with you. However, I was very pleased to see how much you did appreciate my *risotto* and, remember, you will always be welcome. Anna-Maria Janner: What can I say? We already told each other everything, and in Italian! One remark: Life has indeed changed in our office since you left - it's just so quiet! Thanks Anna-Maria, and when Johan comes to our place for a *risotto*, don't be shy and join him! Karina Schulte: I really enjoyed working with you when you were my student and later when you became my k-space teacher. Most important of all, we had a great time: You, me and the Bomem. *Dank je*, Karina, for the translation of the *Samenvatting*, along with all the 'Dutch mail' that, strangely enough, I was receiving every day. One last thing, *toti toti*! Let me now continue by thanking people in a more concise way: Jeroen van der Eb (see you in Stanford?), Diana Dulic (see you and Walter in Sardinia?), Artem Tsvetkov (*spasibo, tovaristch*: We had a short but good time together), Cristian Presura (who is taking good care of my samples), Hajo Molegraaf (who took care of the layout of the front cover), Ronald Hesper (and his brilliant car), Mark James (who took care of considerably improving the English here and there), Jae H. Kim and Jürgen Schützmann (my personal FTIR trainers, together with Clay Paays from Bomem), and the 'Italian Mafia': Salvatore Altieri and Alberto Morpurgo (*se vedemo, testine di silicio*). Although he doesn't belong to the Solid State Physics Lab of the University of Groningen, I would also like to thank Fabio Fiorani, the *Italian paranimf*: thanks Fabio, for being such a great *contrappeso* for so many years!

During my Ph.D research I had the opportunity to interact with many people outside the University of Groningen. First of all, a big thank you goes to the people who grew the beautiful and large single crystals used in this experimental investigation: A.A. Menovsky for the transition-metal mono-silicide samples, and J. Jegoudez, G. Dhalenne, and A. Revcolevschi for the $CuGeO_3$ and α'-NaV_2O_5 samples.

I am indebted to M. Fäth, J. Aarts, and J.A. Mydosh for their intense cooperation on the FeSi project (with a continuous exchange of 'unpublished' data), and to V. Vescoli and L. Degiorgi for numerous discussions and for providing me with their optical data on RuSi. I also enjoyed fruitful discussions with P.H.M. van Loosdrecht, D. Smirnov, J. Leotin, B. Büchner, T. Mizokawa, J.E. Lorenzo, P. Lemmens, G.S. Uhrig, and M. Braden.

I would like to take this opportunity to acknowledge M.J. Rice and G. Aeppli for their careful reading of this manuscript, and for their constructive remarks. Furthermore, I would like to express my gratitude to M.J. Rice for the several 'private communications' on theoretical aspects of this research project.

The last thank you goes to Fulvio Parmigiani, who supervised my undergraduate thesis project and suggested to me to come to Groningen for my Ph.D. research. Since then, he has never stopped giving me good advice, and unlimited scientific and moral support.

At this point some people may wonder:

Isn't this guy going to thank all those friends not scientifically involved in his thesis work ?

And what about his parents, who made everything possible in the first place ??

And, even more surprisingly, isn't he going to thank his beloved wife Barbara, who let him go to The Netherlands for his Ph.D. after only two weeks of marriage, who one year later managed to find an occupation in Groningen and moved over there so that they could live together, who gave birth to their son Matteo, who was waiting for him to come home from the lab all those nights and weekends, who always encouraged him, and who even accepted to be put on the front cover of his thesis ???

Don't worry, I will do that, but in real life !!!

List of Publications

- A. Damascelli, G. Gabetta, A. Lumachi, L. Fini, and F. Parmigiani.
Multiphoton Electron Emission from Cu and W: an Angle-Resolved Study.
Physical Review B **54**, 6031 (1996).

- A. Damascelli, K. Schulte, D. van der Marel, M. Fäth, and A.A. Menovsky.
Optical Phonons in the Reflectivity Spectrum of FeSi.
Physica B **230-232**, 787 (1997).

- A. Damascelli, K. Schulte, D. van der Marel, and A.A. Menovsky.
Infrared Spectroscopic Study of Phonons Coupled to Charge Excitations in FeSi.
Physical Review B (Rapid Communications) **55**, R4863 (1997).

- A. Damascelli, D. van der Marel, F. Parmigiani, G. Dhalenne, and A. Revcolevschi.
Infrared Signatures of the Spin-Peierls Transition in $CuGeO_3$.
Physical Review B (Rapid Communications) **56**, R11 373 (1997).

- A. Damascelli, D. van der Marel, F. Parmigiani, G. Dhalenne, and A. Revcolevschi.
Infrared Reflectivity of Pure and Doped $CuGeO_3$.
Physica B **244**, 114 (1998).

- D. van der Marel, A. Damascelli, K. Schulte, and A.A. Menovsky.
Spin, Charge and Bonding in Transition Metal Mono-Silicides.
Physica B **244**, 138 (1998).

- A. Damascelli, D. van der Marel, M. Grüninger, C. Presura, T.T.M. Palstra, J. Jegoudez, and A. Revcolevschi.
Direct Two-Magnon Optical Absorption in α'-NaV_2O_5: "Charged" Magnons.
Physical Review Letters **81**, 918 (1998).

- A.A. Tsvetkov, D. van der Marel, K.A. Moler, J.R. Kirtley, J.L. de Boer, A. Meetsma, Z.F. Ren, N. Koleshnikov, D. Dulic, A. Damascelli, M. Grüninger, J. Schützmann, J.W. van der Eb, H.S. Somal, and J.H. Wang.
Global and Local Measures of the Intrinsic Josephson Coupling in $Tl_2Ba_2CuO_6$ as a Test of the Interlayer Tunneling Model.
Nature **395**, 360 (1998).

- A. Meetsma, J.L. de Boer, A. Damascelli, J. Jegoudez, A. Revcolevschi, and T.T.M. Palstra.
  Inversion Symmetry in the Spin-Peierls Compound α'*-*NaV_2O_5.
  Acta Crystallographica C **54**, 1558 (1998).

- A. Damascelli, D. van der Marel, J. Jegoudez, G. Dhalenne, and A. Revcolevschi.
  The Symmetry Problem in α'*-*NaV_2O_5.
  Physica B, in press (1999).

- M. Grüninger, D. van der Marel, A. Damascelli, A. Zibold, H.P. Geserich, A. Erb, M. Kläser, Th. Wolf, T. Nunner, and T. Kopp.
  Charged Magnons and Magneto-Elastic Polarons in the MIR Spectrum of $YBa_2Cu_3O_6$.
  Physica C, in press (1999).

- A.A. Tsvetkov, D. Dulic, D. van der Marel, A. Damascelli, G.A. Kaljushnaia, J.I. Gorina, N.N. Senturina, B. Willemsen, N.N. Kolesnikov, Z.F. Ren, J.H. Wang, A.A. Menovsky, and T.T.M. Palstra.
  Systematics of c-axis Phonons in the Tl and Bi Based Cuprate Superconductors .
  Submitted to Physical Review B (1999).

Happy End

During the four years I spent in Groningen working on my Ph.D., I tried many and many times to explain to people, not belonging to the 'Physics Flying Circus', what my work was all about. In particular, we usually went through a rather reproducible series of questions and answers (to be completely honest, I was often questioning myself in a similar way). Below, I would like to go through these questions once more:

What are you working on?

Once this question has been formulated, I take a deep breath, I see all my life passing before my eyes like in a movie, and then I start talking. In the simplest possible way. After a little while we all feel we are dealing with a major communication problem here. With hindsight, my interrogators realize this was not such a clever question, in the first place. After all, what I am exactly doing is not so important to them. The essential point is:

Is it useful?

With this question people usually mean whether the things I am doing, independently of how am I doing them, will eventually result in any practical application that could improve the quality of life. Unfortunately, I have to answer that I do not think so. Not even in the very far future. But I do not miss the opportunity to stress how interesting these experimental studies are from the point of view of 'fundamental research'. However, the disappointment at this point is usually so deep that people reply:

That's what we are paying you for?!

You can imagine that this could easily be the end of our conversation and, probably, of my job: People could completely disagree with the use the government is making of their tax contributions and decide not to finance academic activities any longer. Fortunately, this is usually not the case, at least not in The Netherlands. About Italy, I am not that sure.

Stellingen

behorende bij het proefschrift
Optical Spectroscopy of Quantum Spin Systems
van Andrea Damascelli

1. In the transition-metal mono-silicides vibrational degrees of freedom are coupled to low-energy electron-hole excitations: "Charged Phonons".
   Chapter 2 of this thesis

2. Spin-flip excitations can carry a finite electric dipole moment: "Charged Magnons".
   Chapter 4 and 5 of this thesis

3. In reflectivity spectra an optical phonon does not always have to look like a peak.

4. The nonexistence of phonon softening at T_{SP} in $CuGeO_3$ is an experimental fact.
   M. Braden et al., Phys. Rev. Lett. 80, 3634 (1998)

5. The expression *'this is an experimental fact'* means a lot of work for theoreticians.

6. Fluid dynamics can be successfully applied to the study of plant organ growth.

7. Leonardo da Vinci said: *'It is not enough to believe what you see, you must also understand what you see'*. For completeness, I would personally like to add: *'...But you will never understand what you see, if you do not believe it first'*.

8. $\tau\grave{o}\ \delta\rho\tilde{\alpha}\nu\ \pi\alpha\theta\epsilon\tilde{\iota}\nu$: To act implies suffering.
   $\pi\tilde{\alpha}\theta\epsilon\iota\ \mu\acute{\alpha}\theta o\varsigma$: Suffering leads to knowledge.
   Aeschylus

9. The water cycle is well known to everybody: Water falls on the earth in form of rain, snow or hail. It collects in streams, lakes and rivers, finally reaching the ocean. This water then evaporates forming clouds and, eventually, falls again and the cycle repeats. What is not known to the majority of the people is that 'most' of this water falls on The Netherlands.

10. The tradition of Sinterklaas is wonderful for kids. But what an exhausting job for the Zwarte Pieten!